Title	The Effects of Stepped Slopes on the Hydraulic Performance of Submerged Breakwaters
Author(s)	Suwannarat, Watusiri
Citation	大阪大学, 2023, 博士論文
Version Type	VoR
URL	https://doi.org/10.18910/92969
rights	
Note	

Doctoral Dissertation

The Effects of Stepped Slopes on the
Hydraulic Performance of Submerged
Breakwaters

Watusiri Suwannarat

June 2023

Graduate School of Engineering,
Osaka University

Ph.D. Thesis

The Effects of Stepped Slopes on
the Hydraulic Performance of Submerged Breakwaters

(潜堤表面上の階段状斜面が消波性能に及ぼす影響)

By

Watusiri Suwannarat

A Thesis Submitted in Partial Fulfillment of the Requirements for
the Degree of Doctor of Engineering

The International Program of Maritime and Urban Engineering,
The Division of Global Architecture,
The Department of Civil Engineering,
Osaka University, Japan

The Research is Supervised by

Professor, Dr. Susumu Araki

Department of Civil Engineering, Osaka University
2023

I

ACKNOWLEDGEMENTS

First and foremost, I would like to express my sincere thanks to Prof. Dr. Susumu Araki, my advisor, for his guidance throughout my postgraduate experience. I appreciate all his kind guidance and support. Without his advice, this dissertation would not be accomplished.

Moreover, I also sincerely appreciate joining the land development and management engineering laboratory at Osaka University, which was headed by Prof. Shin-Ichi Aoki. It also was such a pleasure to be advised by Prof. Aoki. Any suggestions and constructive comments are important guidelines for this research.

I also gratefully acknowledge the Japanese Government Scholarship (Ministry of Education, Culture, Sports, Science and Technology: MEXT) for funding my studies. Without the scholarship, I might not have been able to study in Japan.

I also would like to thank to Asst. Prof. Yuya Sasaki, Mrs. Yoko Endo and all the members in our laboratory for their help throughout the last three years. I also sincerely thanks to Dr. Kukulege Bhathisha Akalanla Silva, my senior, who recommended this laboratory and lead me to follow the higher education.

Last but not least, I would like to thank my beloved family and friends for their encouragement and strong support in every part of my life.

ABSTRACT

In the last few decades, submerged breakwaters have been increasingly used as a potential coastal protection and beach control device. Because of the desirable consequences, a submerged crest under the water surface provides better water circulation between onshore and offshore, which improves the water quality nearby shoreline. A low-crest structure also provides multiple benefits such as a low construction cost, coastal erosion reduction, an overtopping reduction and etc. This type of structure also associates with low wave reflection which provides a minimal impact on ship navigation. Besides a significant amount of wave transmission and reflection, a submerged breakwater also preserves the ecosystem and maintains pleasing esthetics, which greatly supports the tourism industry in the coastal area. Whereas, in the fact that a submerged breakwater is not powerful as an emerged breakwater. Therefore, to overcome and achieve more efficiency for wave energy dissipation, several structural geometries have been examined and investigated on the hydraulic performance of submerged breakwaters in many studies.

In this thesis, studies on the influences of a stepped slope on the submerged structure are conducted in computational fluid dynamics (CFD) software, OpenFOAM®, which are investigated under several conditions of waves and structural geometries.

Firstly, Chapter 1 provides the introduction of the research study by introducing the general background and motivation of the structure development.

Chapter 2 mentions related theories and previous research studies about waves, submerged breakwaters and the influences of structural geometries on the ability of wave energy dissipation to acknowledge and indicate the research gap of stepped submerged breakwaters.

Chapter 3 explains research methodology in the numerical model. The processes of numerical simulation are clearly described in detail and also illustrated the specification of model setup and the results of model validation.

Chapter 4 reports the results of numerical simulation to examine the performances of wave energy dissipation. The hydraulic performances of submerged breakwaters were evaluated by the coefficients of wave transmission, wave reflection and wave energy dissipation.

Chapter 5 describes the behavior of wave attenuation through submerged breakwaters. The abilities of wave dissipation were analyzed based on wave breaking and turbulence models, which were illustrated from the viewpoint of the instantaneous wave profiles and the magnitude

of turbulent kinetic energy.

Chapter 6 presents the risk-based assessment of scour around submerged breakwaters, which were analyzed by shear stress computation and turbulence characteristics at the seabed. The influences of structural geometries on scour risks were mainly considered and compared.

Finally, Chapter 7 aims to provide conclusions with a concise and comprehensive overview of the research. The contents and the results of the study on the hydraulic performances of submerged breakwaters are emphasized. In addition, some recommendations for future numerical simulation works are also provided.

CONTENTS

LIST OF FIGURES

LIST OF TABLES

CHAPTER 1
INTRODUCTION

Chapter 1

INTRODUCTION

This chapter consists of three main sections. Firstly, motivation from the doubt on the structural development of submerged breakwaters is introduced, which is followed by the purposes of the research study. The outline of the thesis is presented at the end of this chapter.

1.1. MOTIVATION

In the last few decades, submerged breakwaters or low-crested structures have been increasingly used as coastal protection in many countries. Because of a submerged crest under the water surface, the low-crest structures provide better water circulation between onshore and offshore, which improves the water quality nearby coastline. A low-crest structure also provides multiple benefits such as a low construction cost, coastal erosion reduction, an overtopping reduction and etc. (Carevic et al., 2009). This type of structure also associates with low wave reflection which provides a minimal impact on ship navigation. Moreover, submerged structures also provide a cleaner ocean view that greatly supports the tourism industry in coastal areas (Johnson et al., 2005). For these reasons, interest in the development of submerged breakwater as an alternative wave energy dissipation has gradually increased.

In Thailand, there are around 2,815 kilometers of coastline including the Gulf of Thailand Coast and the Andaman Sea Coast. The coastline in the Gulf of Thailand is around 1,878 kilometers and in the Andaman Sea is around 937 kilometers. The coastal zones are characterized by the geologic nature of landforms as rocky coasts, tidal flats, marshes, sandy beaches and developed coastal areas, which are shown in Figure 1.1. (Department of mineral resources, 2016).

Coastal erosion is a main problem for Thailand in both Gulf of Thailand and the Andaman Sea. Figures 1.2. and 1.3. show the coastal erosion problems in Pattaya Beach and in the southern part of Thailand. The impacts of incoming wave attack the land and roadways along the shorelines, and these damages continuously happen every year. Department of Marine and Coastal Resources of Thailand (2013) revealed that strong erosion occurs along the coastline with an average rate of 5 meters per year. There are many causes of coastal erosion such as coastal development activities for the tourism industry, the decreasing of upstream sediment

supply due to dams and upland deterioration, climatic change during the dynamic of natural coastal process and improper land-use activities along the coast. In order to protect against damage from the impact of incoming waves, there are two main types of coastal protection in Thailand that are soft solution and hard solution. Soft solutions are used such as beach nourishment, dune nourishment, mangrove afforestation and beach setback. Some of the hard structures have been constructed such as breakwaters, seawalls and groynes. However, there are many areas that are not successful in solving the problem due to disagreement among the inhabitant in the coastal areas and a high construction cost for hard structures. The tourism industry on shorelines is one of the biggest important economies, therefore many inhabitants are strongly against constructing a hard structure on shorelines and would like to preserve the beautiful areas for several activities. In order to deal with coastal erosion prevention and preserve clear landscapes in the sea areas, submerged breakwaters or low-crest structures are one of the hard structures that would be considered to deal with both two main issues in Thailand.
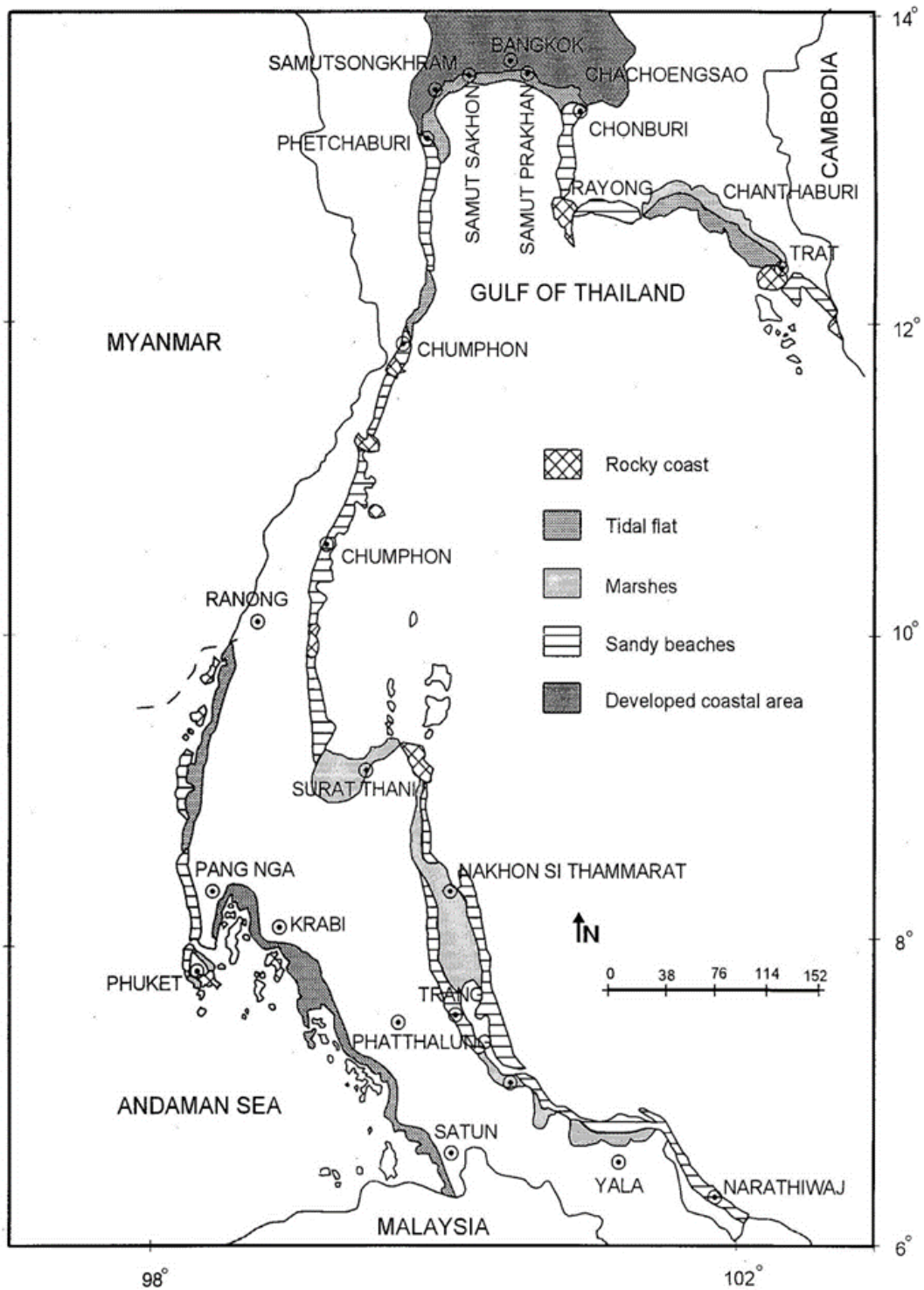
Figure 1.1. Types of Coastal Zone in Thailand

(Department of mineral resources, 2016)

Figure 1.2. The damage of waves on the shoreline in Thailand

Figure 1.3. Coastal Erosion in Southern Thailand

Submerged breakwaters are not powerful as an emerged breakwater. Therefore, many research studies on the efficiency of the submerged breakwater have been investigated and developed these days. To overcome and achieve more efficiency for wave energy dissipation, several shapes of structures have been examined. In general, an appropriate proportion of structural geometry and the submergence depth are the main key points in determining the capability of the submerged breakwater. In order to find out an optimized and effective shape for low-crest structures, various designs on structures have also been considered in many studies (e.g., Cho et al., 2001; Jiang et al., 2017; Gomes et al., 2020; Ahmed et al., 2021).

5

A stepped slope is also one of the designs that have been applied in coastal engineering over the last 100 years, as can be seen as revetments for coastal protection. A comprehensive literature review on hydraulic model tests related to stepped revetment with a focus on wave overtopping, wave run-up and scour development was introduced by Karpen and Schlurmann (2016). On the strength of the stepped slope, the performance of the steps has also been examined for submerged structures lately. The literature reviews for stepped submerged breakwaters are also mentioned in Chapter 2 of this thesis.

However, in most of the previous studies, the effects of stepped slopes have only been considered in terms of wave transmission with a fixed shape of structural geometries. Therefore, in order to have more understanding and comprehension of the ability of wave dissipation, the main purpose of this research is to investigate the performances of stepped slopes on a low-crest structure, which is tested under various parameters such as the different stepped sized, breakwater crest widths, submergence ratios and wave conditions. Besides the efficiency of stepped submerged breakwaters, the behaviors of wave interaction with structures are also illustrated in a graphic diagram based on numerical simulations.

1.2.   RESEARCH PURPOSES

As it is mentioned under Section 1.1., a submerged breakwater is not powerful as an emerged breakwater. In order to overcome and achieve more efficiency in wave energy dissipation, a new shape of the structure is examined by applying a stepped slope in this research.

Normally, an appropriate proportion of structural design and the submergence depth are important parameters in determining the capability of the submerged breakwater. In this research, to find out an optimized and develop the new shape of low-crest structures, the effect of a stepped slope on submerged structures is investigated under several conditions of waves and structural geometries. The different stepped sizes and structure's crest widths are analyzed for the performance of submerged breakwaters. Focusing on the ability of wave energy dissipation, the performances of stepped submerged breakwaters are investigated from the viewpoint of the wave transmission coefficient (K_t), wave reflection coefficient (K_r) and wave energy dissipation rates (K_d). The wave interaction on the stepped submerged breakwater is also analyzed under several wave conditions such as wave heights (*H)*, wave periods (*T*), water depths (*d*), and wavelengths (*L*). Moreover, the ability of the stepped submerged structures on wave dissipation is also compared with the conventional breakwaters (smooth slope and vertical structure).

In order to gain more insight into the hydraulic properties of structures, the behaviors of wave propagation around submerged breakwaters are also illustrated in this study. The characteristics of wave breaking over low-crest structures and the interaction of waves on a stepped slope are considered for the wave flow conditions. The turbulence characteristics of flow-causing scour are presented to compare in terms of different structural geometries, submergence depths and porosities of structures.

By studying the efficiency of submerged breakwaters based on hydrodynamics, various cases of wave interaction with structures are simulated in the numerical model. A set of numerical simulations is carried out in a two-dimensional model by the open-source code fluid dynamics project, OlaFlow, which is developed within OpenFOAM® software. A set of wave generations in a numerical model is validated by a wave theory (Stoke 2nd Order Wave Theory). The numerical results are also compared with the previous physical and analytical studies.

1.3.   STRUCTURE OF THE THESIS

A review of related literature is provided in Chapter 2, which mainly consists of general wave theory, wave attenuation on submerged breakwater and the effect of structural geometry of low-crest structure on wave energy dissipation.

Chapter 3 intensively introduces the numerical methodology. The general backgrounds of all related software and solver are mentioned with an equation in the model. The processes of numerical simulation are also explained, which consist of numerical model setup, the details of mesh generation, numerical model validation and the processes of structural model creation.

The results and discussion of this research are divided into two parts. The performance of stepped submerged breakwaters on wave energy dissipation is provided in Chapter 4. The method of calculation and data analysis are mentioned in this chapter. The results are discussed on the efficiency of wave transmission, wave reflection and wave energy dissipation.

In Chapter 5, the behavior of wave interaction on the submerged breakwater is presented from the viewpoint of wave flow conditions, wave breaking over the structures, turbulence characteristic of flow on the seabed and the comparison of flow through permeable and impermeable structures.

Finally, a summary of the study and conclusions of the research are given in Chapter 6, which also mentions the points of recommendation for future research.

CHAPTER 2
LITERATURE REVIEW

Chapter 2

LITERATURE REVIEW

The second chapter mentions the related literature reviews in this research. The general wave theory is introduced in the first section, which is followed by wave interactions with submerged breakwaters. The effect of structural geometry on wave dissipation is presented in the last section, which collects the related studies of the conventional breakwater and stepped submerged breakwater.

2.1. GENERAL WAVE THEORY

In this section, the general wave theory is introduced with the basic definitions of waves. The properties of waves are mentioned with the definitions and theories of waves, which are followed by wave transformation and wave breaking.

2.1.1. THE PROPERTY OF WAVE

Waves in the ocean are caused by a disturbance on the surface water, which can be caused by winds, ships, or other disturbances such as a landslide or an underwater earthquake. Mostly, waves are formed by the force of the wind blowing across the ocean that transfers the energy passing through the surface water. Waves are undulation forms that move in a circular motion. The wave energy propagation can be dissipated by the wave-breaking process due to the approaching the shallow water or the coastal structures (Bascom, 1980).

This section introduces the basic definitions of wave mechanics, which are explained by the parameters of the wave profile in Figure 2.1 (Sawaragi, 1995). Waves in the ocean are generally formed under the assumption of an incompressible and inviscid fluid. The individual waves are assumed as long-crested that are part of an infinite train of repeating waves. Wavelength (L) defines the distance between wave crests. Wave height (H) is defined as the difference between the elevation of the crest and trough of an individual wave, which can determine the amplitude of waves (a) as $a=H/2$. The water depth (h) is the distance between the bottom and the still water level. η is defined as the water surface profile. The time of wave traveling under one wavelength is defined as wave period (T). In the case of a regular wave with a periodic in time

and space, the wave speed or wave celerity (*c*) can be defined as *c=L/T*, which is the speed of the wave moving across the water surface.
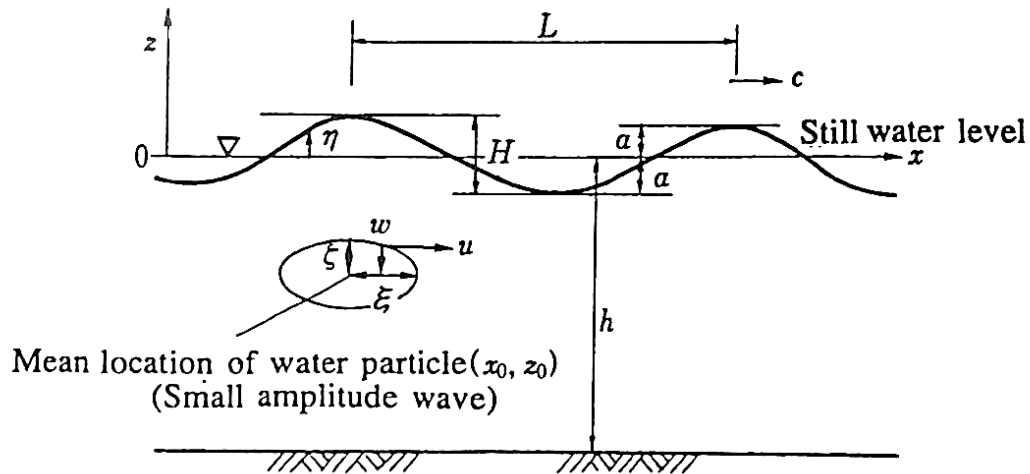
Figure 2.1. Spatial wave profile (Sawaragi, 1995)

In the development of wave theory, the continuity equation of an incompressible fluid can be expressed in terms of fluid velocity, which is defined in equation 2.1.

$$\frac{\partial u}{\partial x} + \frac{\partial v}{\partial y} + \frac{\partial w}{\partial z} = 0 \tag{2.1}$$

The small-amplitude wave theory is also known as "Linear wave theory", which can be widely used in the estimation of wave properties (Dean and Dalrymple, 1991; Sorensen, 1993). The equations of primary small amplitude wave theory are shown in Table 2.1, which is mathematically described regarding very shallow, shallow and deep water waves.

10

Table 2.1 Small-amplitude wave theory (Sawaragi, 1995)

Wave properties	Very shallow water wave $h/L < 1/25$	Shallow water wave $1/25 < h/L < 1/2$	Deepwater wave $h/L > 1/2$
Wave profile, η	$\eta = \frac{1}{2}H\cos(kx - \sigma t) = \frac{1}{2}H\cos\theta$		
Wave celerity, c	$c = \sqrt{gh}$	$c = \frac{gT^2}{2\pi}\tan h\left(\frac{2\pi h}{L}\right)$	$c = \frac{gT}{2\pi}$
Wavelength, L	$L = T\sqrt{gh}$	$L = \frac{gT^2}{2\pi}\tan h\left(\frac{2\pi h}{L}\right)$	$L = \frac{gT^2}{2\pi}$
Particle velocity Horizontal component, u	$u = \frac{H}{2}\sqrt{\frac{g}{h}}\cos\theta$	$u = \frac{H}{2}\frac{gT}{L}\frac{\cosh[2\pi(z+h)/L]}{\cosh\left(\frac{2\pi h}{L}\right)}\cos\theta$	$u = \frac{\pi H}{T}e^{\frac{2\pi z}{L}}\cos\theta$
Particle velocity Vertical component, w	$w = \frac{H\pi}{T}\left(1 + \frac{z}{h}\right)\sin\theta$	$w = \frac{H}{2}\frac{gT}{L}\frac{\sinh[2\pi(z+h)/L]}{\cosh\left(\frac{2\pi h}{L}\right)}\sin\theta$	$w = \frac{\pi H}{T}e^{\frac{2\pi z}{L}}\sin\theta$
Water pressure, p	$p = \rho g(\eta\text{-}z)$	$p = \rho g\eta\frac{\cosh[2\pi(h+z)/L]}{\cosh\left(\frac{2\pi h}{L}\right)} - \rho gz$	$p = \rho g\eta\, e^{\frac{2\pi z}{L}} - \rho gz$

According to Table 2.1, the small-amplitude wave theory can estimate the paths of individual water particles in water waves, which is schematically shown in Figure 2.2 for deepwater, shallow water waves and very shallow water waves. In deepwater, the circular motion magnitude of water particles decreases with the elevation below the free surface. In the intermediate or shallow water and very shallow water waves, the amplitude of the elliptical motion reduces with the increased water depth.
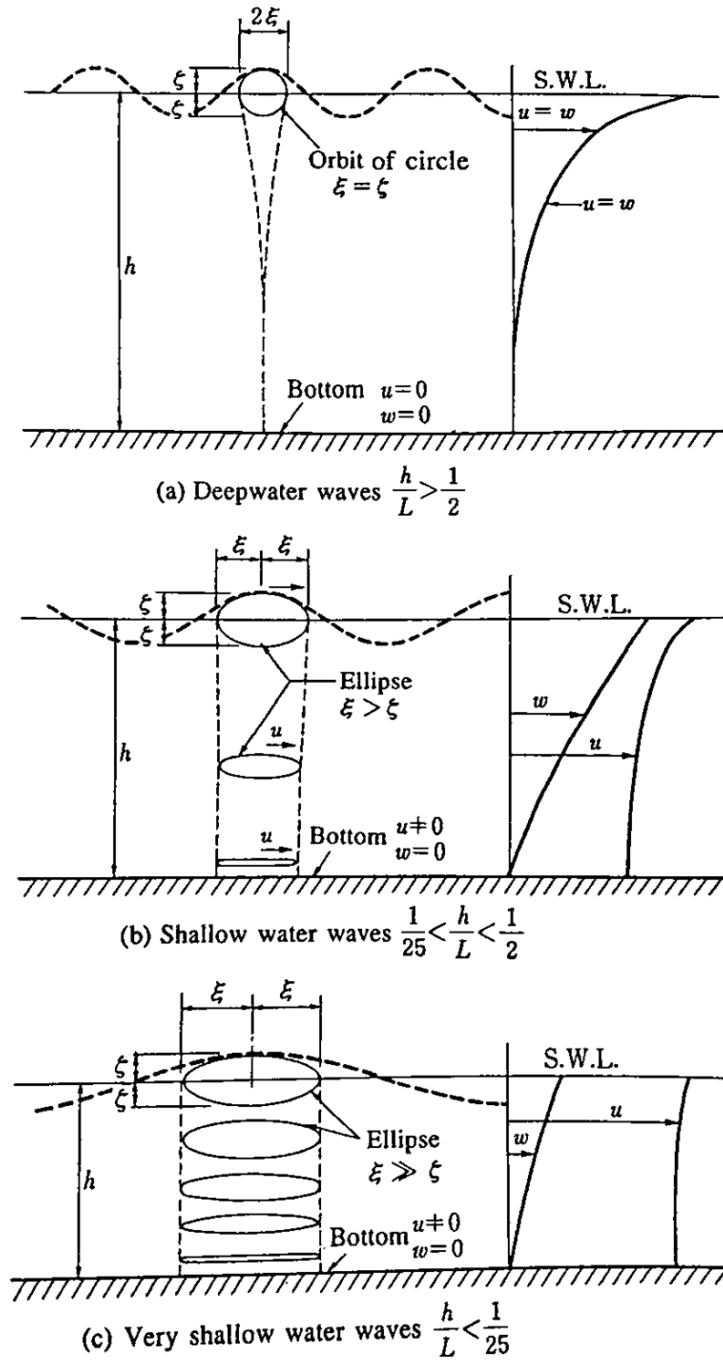
Figure 2.2. Particle orbits in small-amplitude wave theory (Sawaragi, 1995)

2.1.2. WAVE TRANSFORMATION AND WAVE BREAKING

Wave breaking emerges under the waves reaching a critical state, which is influenced by a significant effect such as a seabed configuration, shapes of coastal structures, a disturbance of the water surface, etc. The wave-breaking process can be described that the wave period of the

12

individual waves constantly remaining through the transformations until breaking with the changeable wave directions and wave heights. Wave transformations include the processes of reflection, dissipation, diffraction and shoaling by approaching to a shoreline or hitting a structure. In general, the breaking wave can be defined based on the wave steepness (*H/L*) and a limiting water depth. Many mathematical models have been developed to define a wave breaking under the wave steepness property, which were defined for a progressive wave, standing wave and partial standing wave (Michell, 1893; Miche, 1944; Penny and price 1952; Yamada, 1957; Kishi, 1959; Wiegel, 1964). The breaker types of waves are classified into four different types in Figure 2.3, which are spilling breaker, plunging breaker, surging breaker and collapsing breaker types.
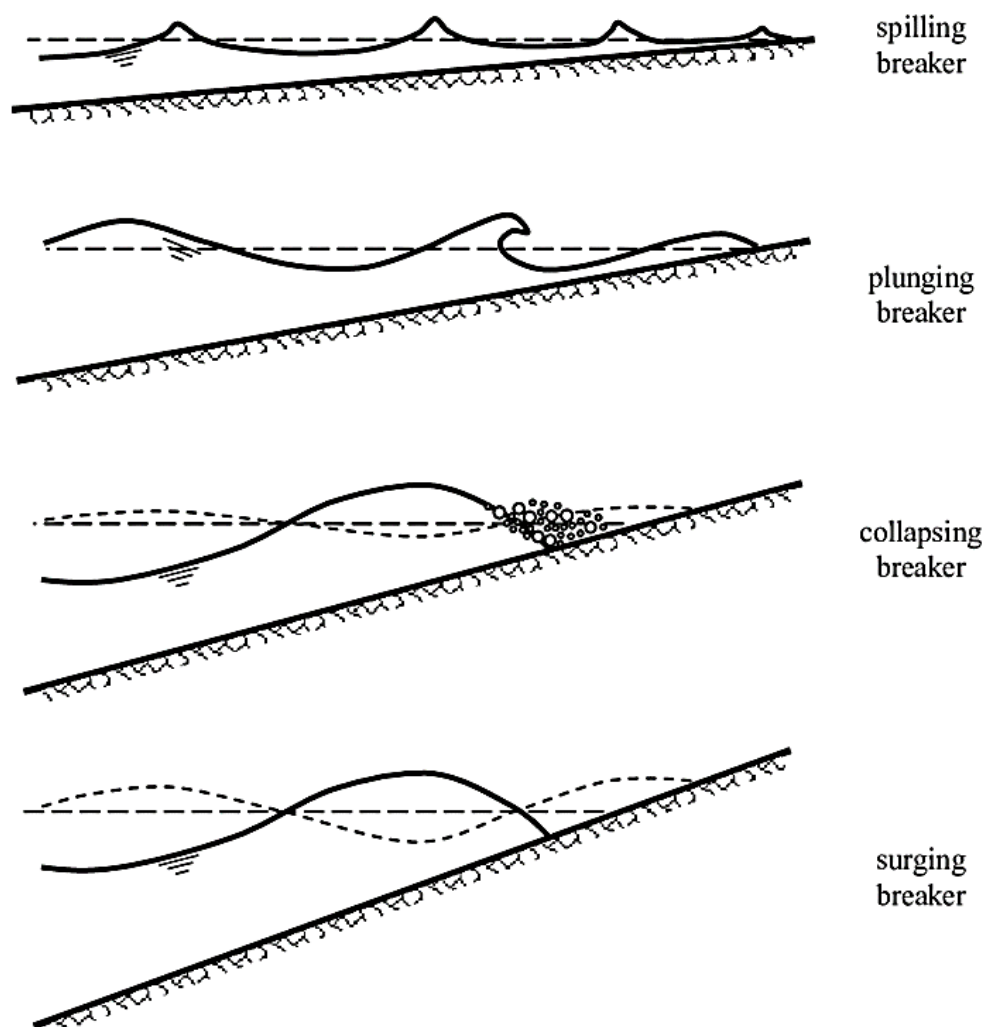
Figure 2.3. Types of breaking waves (Bay, 2005)

2.2. WAVE INTERACTIONS WITH SUBMERGED BREAKWATERS

In this section, the general background of submerged breakwaters is described on the purposes, the wave interaction with structures and the processes of wave attenuation through structures. Moreover, the effects of structural geometries on wave energy dissipation are presented with the several related studies, which are described in terms of the conventional shapes and the stepped slope on submerged breakwaters.

2.2.1. GENERAL BACKGROUND OF SUBMERGED BREAKWATERS

Breakwaters play an important role in coastal protection which are constructed as wave damage prevention and beach control devices. In the last few decades, submerged breakwaters have been increasingly used as potential coastal protection because of the desirable consequence. This special type of breakwater is built with its crest submerged under the water surface. Based on this advantage, submerged breakwaters provide the exchange of wave flow between onshore and offshore, which supports improving water quality nearby the shoreline. Moreover, besides a significant amount of wave reflection and transmission, this type of breakwater also preserves the ecosystem and maintains pleasing esthetics, which exactly supports the tourism industry in a coastal area.

The main functions of submerged breakwaters include wave breaking, wave dissipation and allowing some wave transmission over the structure. The definition sketch of submerged breakwater is shown in Figure 2.4. In terms of comparison with emerged breakwaters, the advantages of low-crest breakwaters are less damage around the structure, low construction cost, a gentler impact on sand accumulation, minimizing erosion, providing a good quality of water based on effective water circulation, etc. An example of a submerged breakwater that is constructed in a coastal area is shown in Figure 2.5.
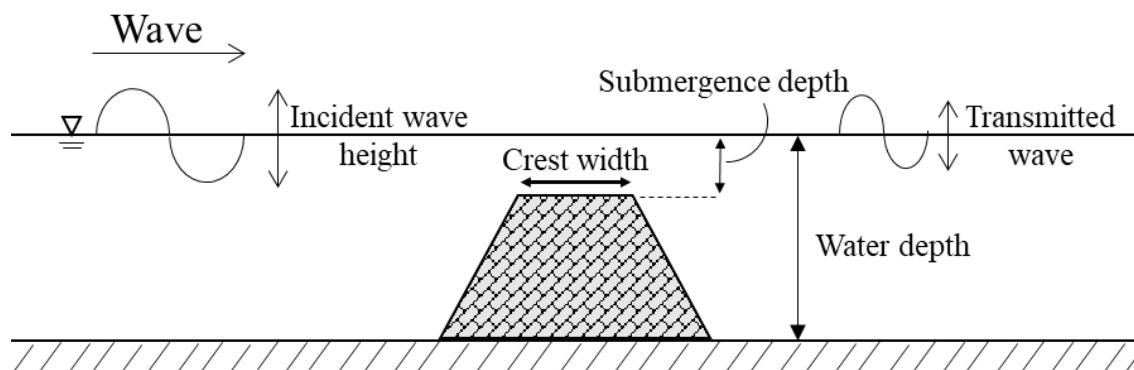
Figure 2.4. Definition sketch for submerged breakwater

14
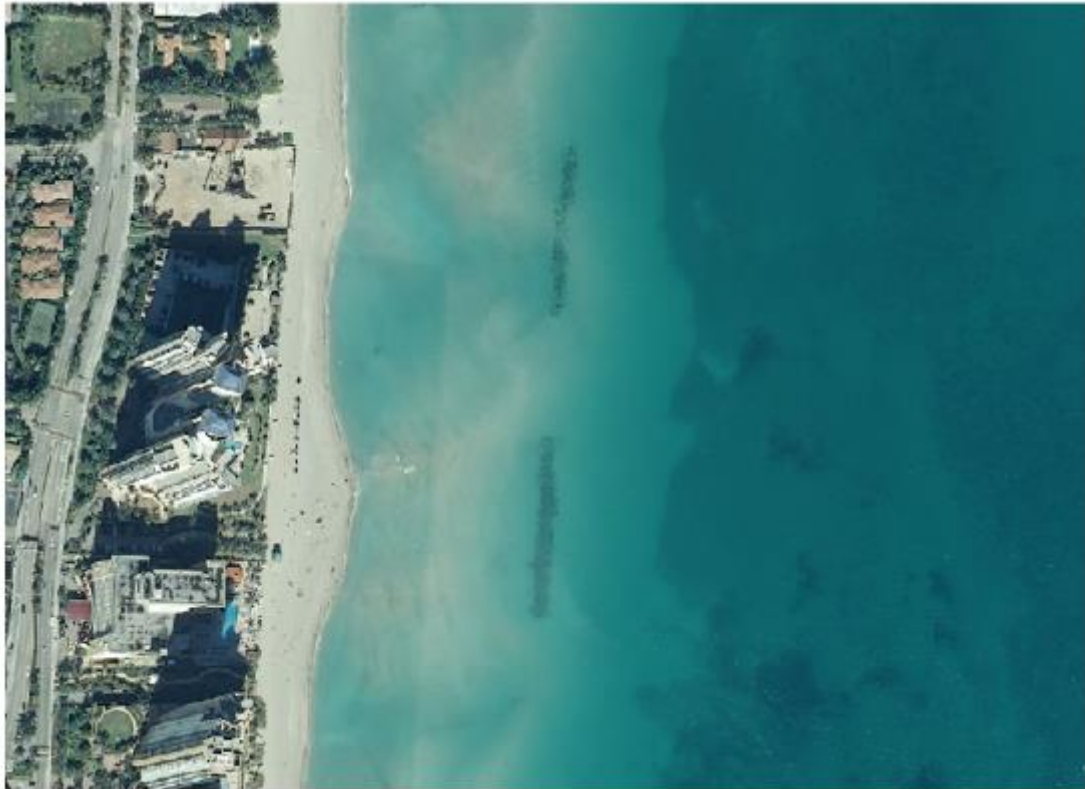
Figure 2.5. The submerged breakwaters in Sunny Isles, USA (Bosboom and Stive, 2023)

2.2.2. THE EFFECT OF STRUCTURAL GEOMETRY ON WAVE DISSIPATION OF SUBMERGED BREAKWATERS

As it is mentioned under Section 1.1., a submerged breakwater is not powerful as an emerged breakwater. In order to overcome and achieve more efficiency in wave energy dissipation, a new shape of the structure is examined in this research, which is applied by the stepped slope on submerged breakwaters. The performances of various geometries on structures are examined and compared with the performances of conventional breakwaters. Many kinds of research on the influence of structural shapes on the efficiency of submerged breakwaters have been revealed in decades.

2.2.2.1. CONVENTIONAL BREAKWATER

The studies on the efficiency and the review of conventional breakwaters are briefly described in this part, which have been considered on the normal flat slope of trapezoidal shapes and rectangular shapes. An example of the investigation of conventional breakwaters is mentioned in the following.

15

(a) Dong et al (2018) revealed the studies on the effects of the slope gradient of a fully permeable submerged breakwater. The study was conducted in a two-dimensional wave field, which was simulated in a numerical model. The model is able to consider the wave propagating through a porous media with inertial, linear and nonlinear resistance terms. In this study, the developed model was validated with the experimental results. The influences of different slopes on the conventional breakwater were analyzed in terms of wave transmission, reflection and energy dissipation

(b) The performances of impermeable trapezoidal submerged breakwater were experimentally investigated by Mahmoudi et al (2017). The experiment was conducted under regular waves, which was tested with three submergence depths and different wave groups. The efficiencies of this conventional breakwaters were analyzed on the coefficients of wave transmission and wave reflection. In terms of results and discussion, various empirical equations were included in this study.

(c) Ibrahim et al (2018) revealed a collection of a short review on submerged breakwaters, which was described the general performances between submerged and emerged breakwaters. Moreover, this paper also mentioned the several existed low crest breakwaters, which included a perforate concrete block, geosynthetic tubes and reef balls[TM] breakwaters. Some special breakwaters in Malaysia also were presented in this paper, which included the artificial mangrove root system (ArMS) submerged breakwater, geotextile tubes and wave breaker coral restoration (WABCORE).

2.2.2.2. STEPPED SUBMERGED BREAKWATER

In this part, the related studies of the stepped submerged breakwater in the last few decades are collected and reviewed, which are mentioned in the following.

(a) The comparison of the performance between smooth and stepped slopes on a submerged breakwater was studied by Lokesha et al (2015). The influences of relative breakwater width, relative depth of submergence of the breakwater and roughness of breakwater front slope on wave transmission are analyzed in this study, which was conducted in a two-dimensional wave flume.

The experiments were tested in a 700 cm length, 30 cm width and 54 cm height of wave flume with a flap type of wave generator and wave absorber on either end. The submerged breakwater models are made of wood material with smooth and stepped front slopes. A set of experiments was conducted for three different heights (h= 26 cm, 28 cm and 31 cm) and three different widths (B= 10 cm, 20 cm and 30 cm) of the model. The experimental models are subjected to four different wave heights (H= 3 cm, 5 cm, 7 cm and 9 cm) and five different wave periods (T= 0.55 s, 0.65 s, 0.75 s, 0.85 s and 0.95 s) of regular waves in a constant water depth of 31 cm.

In this experimental study, the hydrodynamic performance of submerged breakwater was analyzed in terms of the wave transmission coefficient, which was examined based on the ratio of transmitted wave height (H_t) to the incident wave height (H_i).

The results of this experimental study can be concluded that the total averaged reductions in the transmission coefficient for stepped slopes of R_c/H_i =0, R_c/H_i = -3.10 ~ -1.40, R_c/H_i = -4.64 ~ -2.39 are 17.61%, 13.9% and 10.29%, respectively which are compared to submerged breakwater with smooth front slope. Effective wave attenuation can be obtained by applying a stepped slope or increasing roughness on structures. However, based on the results of this investigation, the study reveals that the effect of a stepped slope can be used in the design of submerged breakwater for a medium wave transmission of dissipating wave energy.

(b) The investigation of the effect of submerged breakwater configurations on wave attenuation performance was studied by Lachmi et al (2017). The effects of different structural configurations were tested by physical modeling. A series of experiments were conducted to investigate the efficiency of wave attenuation in terms of the wave transmission coefficient, which was examined with the wave steepness (H_i/L), relative breakwater width (B/L), and the relative breakwater draft (h/d).

A series of experiments were carried out in a 10 m length, 0.32 m width and 0.48 m depth wave flume with a furnished wave generator and wave absorber. The breakwater models were made of multiple pipes with different configurations. The breakwater configurations were arranged based on the different sizes of cylindrical diameters (4.2 cm, 6.0 cm, 9.2 cm and 11.4 cm). The maximum width (B) and height (h) of the models were 0.308 m and 11.4 cm, respectively. The experiments were examined under regular waves of five different wave periods (T= 0.8 s, 1.0 s, 1.2 s, 1.4 s and 1.6 s) and two water depths (d= 11.4 cm and 15 cm). The range of wave steepness (H_i/L) varied between 0.008 – 0.065 with different relative water depths (h/d= 0.76 and 1.00).

In this experimental study, the results can be concluded that wave transmission was largely affected by the relative water depth (h/d). Whereas, there were fewer affected by wave steepness (H_i/L) and the relative breakwater width (B/L). However, the design with the front stepped slope was the best in wave attenuation which fully provided the optimized wave transmission in among of their designed tests. The stepped front slope was concluded as the recommended design for submerged breakwaters in this study.

(c) The influence of a rectangular barrier with different configurations on wave energy reduction was examined by El-Saie Yasser Mohamed (2018). For economical solution of submerged breakwaters have been effectively use, this study aims to investigate the ability of a rectangular barrier as the defense of shoreline. The experimental study was conducted under different water levels, submergence depths and wave heights. The rectangular steps on breakwater were tested as single and group of models, which considered the performances of structure from the viewpoint of wave transmission and the percentage of energy reduction.

The physical modeling was carried out in two-dimensional wave flume with a 12 m length, 0.5 m width and 0.6 m depth. The rectangular barrier was tested with a different height of models ($Y_1 = 15$ cm, $Y_2 = 20$ cm and $Y_3 = 25$m). The experiments were conducted with five water depths ($d_w = 25$ cm, 27.5 cm, 30 cm, 32.5 cm and 35 cm), five submergence depths ($d_s = 10$ cm, 12.5 cm, 15 cm, 17.5 cm and 20 cm).

The results of this study can be concluded that the efficiency of the submerged barrier increases with an increase of structure height and thickness. The three rows with different heights of breakwater provide more effective in wave energy reduction. Wave steepness was directly affected to the ability of energy dissipation, therefore increasing of wave steepness can lead to increase the effective results. The increasing of submergence ratio (d_s/d_w) led to decrease the percentage of wave energy reduction.

(d) The effect of seaward slopes on reef breakwaters with smooth and stepped slopes was investigated by Srineash and Murali (2019). This research examined wave transmission with porous and non-porous models, which was carried out in the numerical simulation, REEF3D. The wave interaction with reef breakwater was concentrated to cover a wide range of relative submergence depths.

The performance of permeable and impermeable for smooth and stepped submerged breakwater were carried out in numerical model. The numerical wave tank was created with

18

the total length of 30 m with the function of wave generation and wave absorption zone. A series of wave was generated based on the Stoke 2nd order theory. Two wave probes method by Goda and Suzuki (1976) was used to measure wave height. The efficiency of wave energy attenuation was considered from the viewpoint of wave transmission coefficient.

The results of the performance of the smooth and stepped reef breakwaters for varying seaward slopes and depth of submergence shown that the effect of seaward slope was observed to be negligible. Moreover, the effect due to the change between smooth and stepped slope was noticed to have negligible effects. The porous breakwater was noted to perform well on wave transmission which was compared with non-porous structure. Based on the variation of wave dissipation between permeable and impermeable models, wave attenuation decreases with the reduction of submergence.

(e) The efficiency of a stepped submerged breakwater in cases of slotted and without slotted was investigated by Sarhan (2020). The significant cases of submergence ratio, structural and hydraulic parameters of stepped submerged breakwater were considered on the performance of wave transmission.

The interaction of regular waves with stepped submerged breakwaters was conducted in two-dimensional experiments of 19 m length, 1 m height and 1 m height of wave flume. The performances of structures were presented as the function of wave transmission coefficient which was tested in a wide range of wave heights and wave periods.

The results of this study can be concluded that slotted-stepped submerged breakwater was more effective than without slotted in case of no submergence ratio. In terms of higher submergence ratio, stepped submerged breakwater with slotted was better than solid one when the crest width was bigger than the water depth.

(f) Wave dissipation in relation to the vortices propagation induced by a solitary-like wave over submerged breakwaters was investigated by Li et at., 2020. A series of experiments were conducted to visualize the occurrence of eddies and a related phenomenon of the range expansion of vortices around a single and composite set of rectangular and undulating submerged breakwaters.

The model experiments were carried out in a two-dimensional wave flume, which was 5 m length, 0.08 m width and 0.2 m depth. A solitary wave generator was set at the left end and a

fixed vertical baffle was installed to reduce a reflected wave at the right end of flume. A set of submerged breakwaters was composed of four different heights of blocks, which was arranged in an ascending step from upstream to downstream. A high-speed digital camera was used to record the changes in the waveform.

The experimental results showed that the sum of the relative vortex energy generated behind the composite submerged breakwater was greater than the case of a single set of models. Moreover, the rectangular submerged breakwater sets provided stronger effects on the energy dissipation of the solitary-like wave.

(g) Abdullah et al (2021) revealed the investigation of wave transmission behind a submerged wave breaker coral restorer (WABCORE). The submerged WABCORE model was arranged into a trapezoidal shape with a stepped slope and the holes in the model.

A two-dimensional analysis was carried out in experiment to examine the hydrodynamic phenomena through capturing the patterns of wave surface profiles, wave attenuation and flow velocity. Moreover, a three-dimensional computational modelling by CFD on hydrodynamic performance was simulated for a comprehensive insight into the wave transmission characteristic. The performance of wave transmission was considered with various relative significant incident wave height, relative structural crest width, water depths and wave steepness. A series of experiments were conducted in two-dimensional wave flume, which was 50 m length, 1.5 m width and 2 m height. A submerged WABCORE model was 0.91 m length, 1.46 m width and 0.5 m height with 0.03 porosity.

CHAPTER 3
NUMERICAL SIMULATION

Chapter 3

NUMERICAL SIMULATION

The third chapter explains the processes of numerical simulation. Firstly, the outline concept of the numerical simulation is introduced with the flowchart, which is followed by the introduction of numerical simulation software and the solver in this research. The details of the mathematical formula are mentioned that refer to the related equations and methods of calculation. For the numerical model setup, the model parameters, mesh generation processes and the details of structural modeling are also clarified in this section. At the end of this section, the processes of numerical validation are explained in detail, which also presents the results of the model validation.

3.1.　NUMERICAL SIMULATION FLOWCHART

The overall processes of numerical simulation are introduced in this section, which is illustrated in Figure 3.1. In the first place, the 30 submerged breakwater models for different submergence depths, varied sizes of crest widths and steps were created in FreeCAD software. FreeCAD is an open-source parametric 3D modeling that is able to design and sketch a model with any size of an object. In order to export the geometry from FreeCAD to calculate in OpenFOAM®, the models are exported as STL files that will be able to generate a mesh into specific shapes.
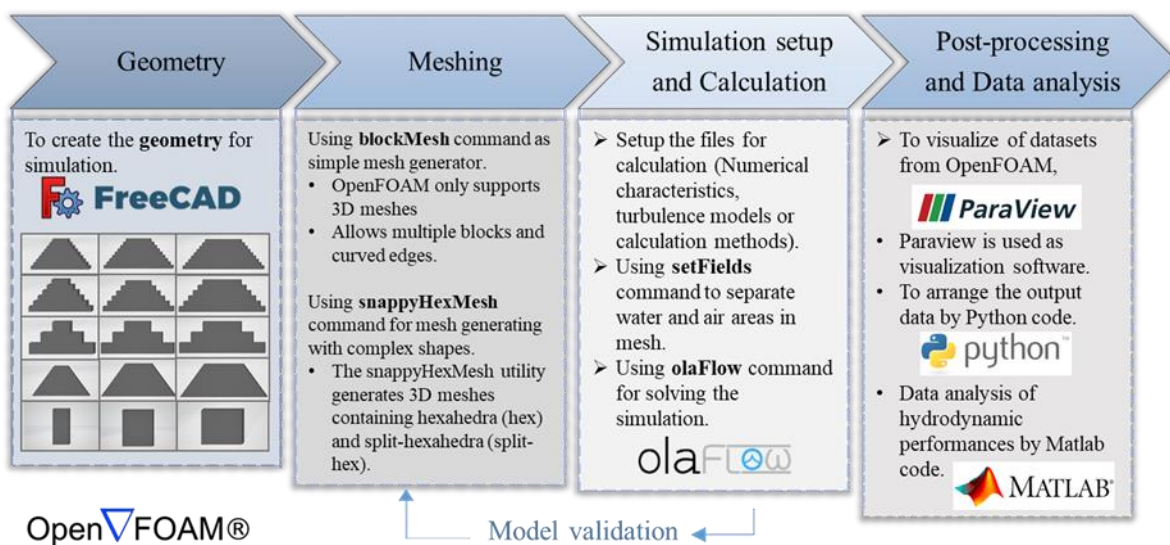
Figure 3.1. The numerical simulation flowchart

22

In Computational Fluid Dynamics (CFD) simulation, mesh generation is needed to process a mesh for flow simulation inside a cell or an element. The blockMesh utility is a simple mesher of OpenFOAM®, which is used to create background meshes for numerical simulation. In order to shape the generated mesh with blockMesh into a geometrical definition based on a prepared STL file, the snappyHexMesh is used in the shaping process.

To do field initialization, the setFields utility is used to define the phase fractions of water and air in the domain, which is processed with the setFieldsDict file. In order to run a simulation in parallel, the geometry needs to be decomposed into individual geometries for each MPI process. The decomposePar utility is commonly used to decompose a domain and subsequently distribute the fields. For running a simulation, the olaFlow command is used for solving the calculation. The reconstructPar utility is used to reassemble the mesh and the results, which is the reverse of the decomposePar.

OpenFOAM® is supplied with a post-processing of paraFoam utility that uses ParaView software to visualize the data sets from OpenFOAM®. In this study, in order to arrange the output of numerical simulation data, python code was used to compile an output file. In addition, data analysis of the hydrodynamic performances was computed by Matlab code.

3.2. INTRODUCTION TO OPENFOAM®

OpenFOAM® (Open Field Operation And Manipulation) is a collection of open-source codes for the development of numerical solvers, which is mainly developed in C++ language. The program is primarily developed to solve the solution of continuum mechanics problems, most importantly including computational fluid dynamics (CFD) that is supplied with pre-processing and post-processing utility. The overall structure of OpenFOAM® is presented in Figure 3.2.
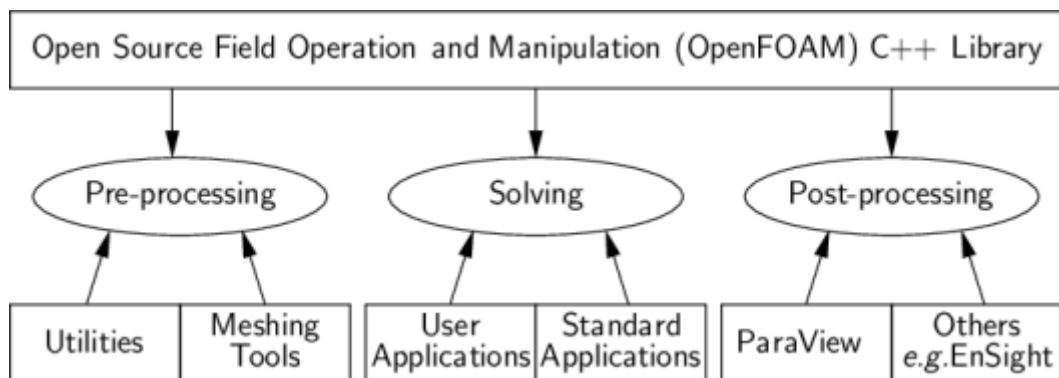
Figure 3.2. Overview of OpenFOAM® structure (OpenCFD, Ltd., 2023)

23

The libraries with C++ code for solving a complex problem (e.g., fluid flow, turbulence simulation, chemical reactions, combustion, etc.) are included in OpenFOAM®, which are featured applications for pre-and post-processing. Mesh generation tool (e.g., blockMesh, snappyHexMesh) and a setting field value are procured as pre-processing. Being an open-source code is capable to add new functionalities and modify the solving process by changing the source code. In solving processes, the toolboxes or solvers can be applied to solve the numerical solving in OpenFOAM®. In this study, the problems were solved by applying the open-source code fluid dynamics project, OlaFlow, which has been continuously developed from IHFoam (Higuera P., 2013). Because of processing with C++ code, adding third part programs to visualize the results is used for post-processing. ParaView® is an open-source multiple-platform application for interactive and scientific visualization that is used to visualize the data based on OpenFOAM®.

The basic directory structure to run an application for OpenFOAM® is shown in Figure 3.3. The minimum set of files consists of three main directories, which are '0' directory, 'constant' directory and 'system' directory.
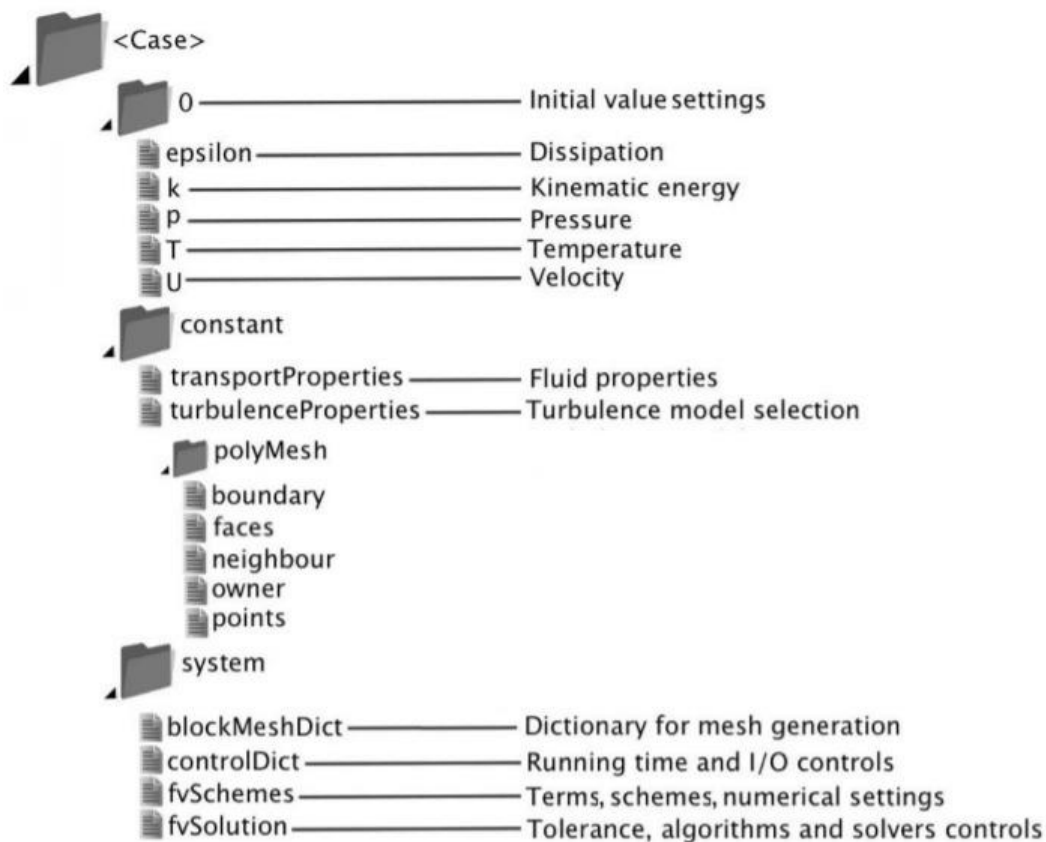
Figure 3.3. Case directory structure (SimCenter, 2020)

24

The '0' directory consists of initial conditions to run the simulation, such as the condition setting for velocity, kinematic energy, alpha water, pressure, etc. The 'constant' directory usually includes the constant properties of the simulation project such as the material properties, turbulence properties, structural geometries, etc. For the 'system' directory, the parameters set in the model associated with the solution procedure is included in this folder. The control file for timing information, write format, or the optional libraries can be modified in this directory.

3.3. OLAFLOW SOLVER

OlaFlow is an open-source code fluid dynamic project that is the toolbox for the numerical simulation of wave dynamics. The open-source project was conceived as a continuation work in Higuera's thesis (Higuera P., 2015) which has been continuously developed from IHFoam solver (2014-2016), OlaFoam (2016-2017) and OlaFlow (2017-now).

The program solves the three-dimensional Volume Averaged Reynolds Averaged Navier Stokes equations (VARANS) which are a modified version of RANS. The VARANS equation is the technique that characterizes the mean flow inside porous media, disregarding the complex porous geometry by considering each medium as homogeneous. The schematic process to obtain the VARANS equations is mentioned in Chapter 2.

The OlaFlow solver uses the Volume of Fluid (VOF) technique to present the two incompressible phases of water and air. The solver also includes various turbulence model that is included by means of different approaches (RANS, LES, DNS). The pressure-velocity equations are solved by two-step methods, PIMPLE which was derived from PISO (Pressure Implicit with Splitting of Operators) and SIMPLE (Semi-Implicit Method for Pressure-Linked Equations). The details of the free surface tracking technique, the turbulence model and the solving procedure of PIMPLE are presented in section 3.4.

OlaFlow includes a set of boundary conditions for wave generation and wave absorption at the boundaries. Based on the advantage of this feature, a damping zone or a relaxation zone does not need to be created with this solver, which can provide a faster simulation and save significant computational costs. This feature of including wave generation and absorption is one of the strengths of the OlaFlow solver. The domain characterization of OlaFlow and other wave models is shown in Figure 3.4. The solver allows the generation of regular waves (Stokes I, II and V, cnoidal and streamfunction regular waves) and irregular waves. The active wave absorption is utilized at the inlet and outlet boundaries based on a shallow water theory, which is supplied for the reflected wave prevention in the models.
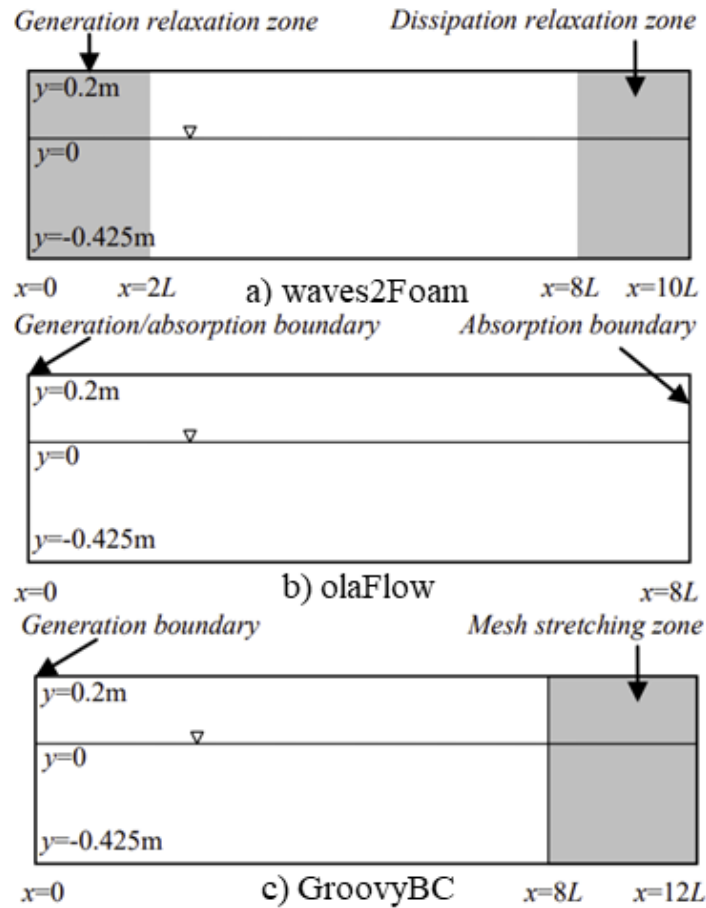
Figure 3.4. Domain characterization a) waves2Foam b) olaFlow c) GroovyBC

(Conde, 2019)

3.4. MATHEMATICAL FORMULATION OF NUMERICAL MODEL

The related mathematic equations and calculation methods of the numerical model are mentioned in this section. Firstly, the governing equations are presented, which is followed by the volume of fluid (VOF) method. Then, the turbulence modeling is explained in detail. At the end of this section, the solving procedure of the numerical solver is presented by the step of model work.

3.4.1. GOVERNING EQUATIONS

In the finite volume methods, the governing partial differential equations are recast in a conservative form, then solved over discrete control volumes. The variables used in the development of the governing equations in the OlaFlow solver are mentioned in this section, which is presented in terms of the RANS and VARANS equations (Higuera P., 2015).

(a) RANS equation

The RANS equations include the continuity and mass conservation equation which are the governing mathematical expression of velocity and pressure. The assumption of incompressible fluids has been used, which is applicable to most coastal engineering practical problems. The conservation of mass and momentum are presented in equations (3.1) and (3.2), respectively.

$$\nabla U = 0 \tag{3.1}$$

$$\frac{\partial \rho U}{\partial t} + \nabla \cdot (\rho U U) - \nabla(\mu_{eff} \nabla U) =$$
$$-\nabla p * -g \cdot X \nabla \rho + \nabla U \cdot \nabla \mu_{eff} + \sigma k_c \nabla \sigma \tag{3.2}$$

where ρ is the density, U is the velocity vector, $p*$ is the pseudo-dynamic pressure, g is the acceleration of gravity and X is the position vector. The last term on the right is the effect of surface tension that σ is the surface tension coefficient and k_c is the curvature of the interface which is calculated in equation (3.3). α is the indicator function that is mentioned in section 3.4.2. μ_{eff} is the efficient dynamic viscosity. It takes into account the molecular dynamic viscosity plus the turbulent effects, which is calculated from equation (3.4). v_{turb} is the turbulent kinetic viscosity.

$$k_c = \nabla \frac{\nabla \alpha}{|\nabla \alpha|} \tag{3.3}$$

$$\mu_{eff} = \mu + \rho v_{turb} \tag{3.4}$$

(b) VARANS equations

The VARANS equations are mainly used to physically characterize the flow inside a porous media, which are modified from the RANS equations. Some physical parameters such as the porosity (ϕ) and mean nominal diameter (D_{50}) are added to define the mean (volume-averaged) inside the porous materials. The continuity and momentum conservation equations are

27

presented in equations (3.5) and (3.6), respectively. According to VARANS equations, the equations are simultaneously applied outside a porous media that the porosity is equal to 1 in the free flow region.

$$\frac{\partial(u_i)}{\partial x_i} = 0 \tag{3.5}$$

$$\frac{1+C}{\emptyset}\frac{\partial\rho(u_i)}{\partial t} + \frac{1}{\emptyset}\frac{\partial}{\partial x_j}\left[\frac{1}{\emptyset}\rho(u_i)(u_j)\right] =$$
$$-\frac{\partial(p*)^f}{\partial x_i} - g_j X_j \frac{\partial\rho}{\partial x_i} + \frac{1}{\emptyset}\frac{\partial}{\partial x_j}\left[\mu_{eff}\frac{\partial(u_i)}{\partial x_j}\right] + F_i^{ST}$$
$$-\alpha\frac{(1-\emptyset)^3}{\emptyset^3}\frac{\mu}{D_{50}^2}(u_i) - \beta(1+\frac{7.5}{KC})\frac{1-\emptyset}{\emptyset^3}\frac{\rho}{D_{50}}\sqrt{(u_j)(u_j)(u_i)} \tag{3.6}$$

Equations (3.5) and (3.6) are solved by a two-step method (predictor-corrector), which used to be solved by PISO (Pressure Implicit with Splitting of Operators) algorithm in the original versions of OpenFOAM® (Issa, 1986). The current solving procedure in the last version of OpenFOAM® is solved by PIMPLE, which is the mixture algorithms of PISO and SIMPLE (Semi-Implicit Method for Pressure-Linked Equations). The PIMPLE technique is described in section 3.4.4.

3.4.2. VOLUME OF FLUID METHOD (VOF)

In OpenFOAM®, the volume of fluid (VOF) method represent two incompressible phases of water and air. This method is also mainly used for tracking the interface between water and air, which was presented by Hirt and Nichols (1981). Two incompressible phases of water and air are represented by the volume fraction of fluid in each grid cell, which is indicated by the indicator field, α.

In this method, the value of $\alpha=1$ stands for a complete full of water in a mesh cell. An empty mesh cell is indicated as $\alpha=0$. For the water surface tracking, $0<\alpha<1$ is indicated as the interface area between water and air. The tracking free surface by volume fraction of fluid in a grid cell is shown in Figure 3.5. The expression that tracks the fluid movement is started as an advection equation (3.7). Where, α is the volume fraction of fluid and U is the velocity field composed of u, v and w.

28

$$\frac{\partial \alpha}{\partial t} + \nabla \cdot U\alpha = 0 \tag{3.7}$$

0	0	0	0	0	0	0	0	0	0	0	0	0	0
0	0	0	0	0	0	0	0	0	0	0	0	0	0
0	0	0	0	0	0.25	0.85	0.94	0.87	0.21	0	0	0	0
0	0	0	0.13	0.73	1	1	1	1	1	0.28	0	0	0
0.58	0.62	0.88	1	1	1	1	1	1	0.33	0	0	0	0
1	1	1	1	1	1	1	1	1	0.33	0	0	0	0
1	1	1	1	1	1	1	1	1	1	0.9	0.76	0.7	0.69
1	1	1	1	1	1	1	1	1	1	1	1	1	1

Figure 3.5. The volume fraction of fluid in each grid cell

(Nguyen-Thi et al., 2021)

To calculate any properties of the fluid in each cell, the local fluid property is expressed as a weighted function. For example, the phase fraction of fluid can be determined by the density inside each cell of the mesh which is computed by equation (3.8). Where ρ is the density inside a cell, ρ_{water} is the density of water and ρ_{air} is the density of air.

$$\rho = \alpha\rho_{water} + (1 - \alpha)\rho_{air} \tag{3.8}$$

To reduce the significant errors of physical fluid properties, some restrictions apply to the phase fraction function (Jasak and Weller, 2002). A sharp interface in the model needs to be maintained and the volume fraction needs to be bounded between 0 and 1. An artificial compression term $(\nabla \cdot U_c\alpha(1 - \alpha))$ is applied instead of a compressing differencing scheme. In addition, the normal direction to the interface is only compressed with the flow $(\frac{\nabla\alpha}{|\nabla\alpha|})$. The final expression is shown in equation (3.9).

$$\frac{\partial \alpha}{\partial t} + \nabla \cdot U\alpha + \nabla \cdot U_c \alpha (1 - \alpha) = 0 \qquad (3.9)$$

3.4.3. TURBULENCE MODELLING

In this study, k-ω SST is used to define the turbulence simulation. K-ω SST is the turbulence model that combines the features of k-ε, k-ω models (Menter, 1994). The main advantage of k-ω SST is to separate the zones in each model yield by applying a set of blending functions. Because of the limitation of the k-ε model that cannot represent a boundary layer and flow separation correctly, whereas k-ω is used for those purposes.

The k-ω SST model is developed to combine these two features, which is able to provide a good result as k-ε for the free flow region and k-ω for the model with a boundary layer. Two equation models of k-ε and k-ω SST are expressed mathematically in equations (3.10) and (3.11). Where k represents the turbulent kinetic energy and ω represents the turbulent frequency scale. D_k and D_ω are the diffusion coefficients. β_k and β_ω are the dissipation coefficients. F_k and F_ω are the production terms and $CD_{k\omega}$ the cross-diffusion term between k-ε and k-ω.

$$\frac{\partial k}{\partial t} + u \cdot \nabla k - \nabla \cdot (D_k \nabla k) + \beta_k k = F_k \qquad (3.10)$$

$$\frac{\partial \omega}{\partial t} + u \cdot \nabla \omega - \nabla \cdot (D_\omega \nabla \omega) - (1 - F_1)CD_{k\omega} + \beta_\omega \omega = F_\omega \qquad (3.11)$$

3.4.4. SOLVING PROCEDURE

OlaFlow is an open-source project that has been continuously developed from the IHFOAM solver. The flow chart of the full procedure for solving each time step is shown in Figure 3.6, in which TFSL stands for Theoretical Free Surface Level.
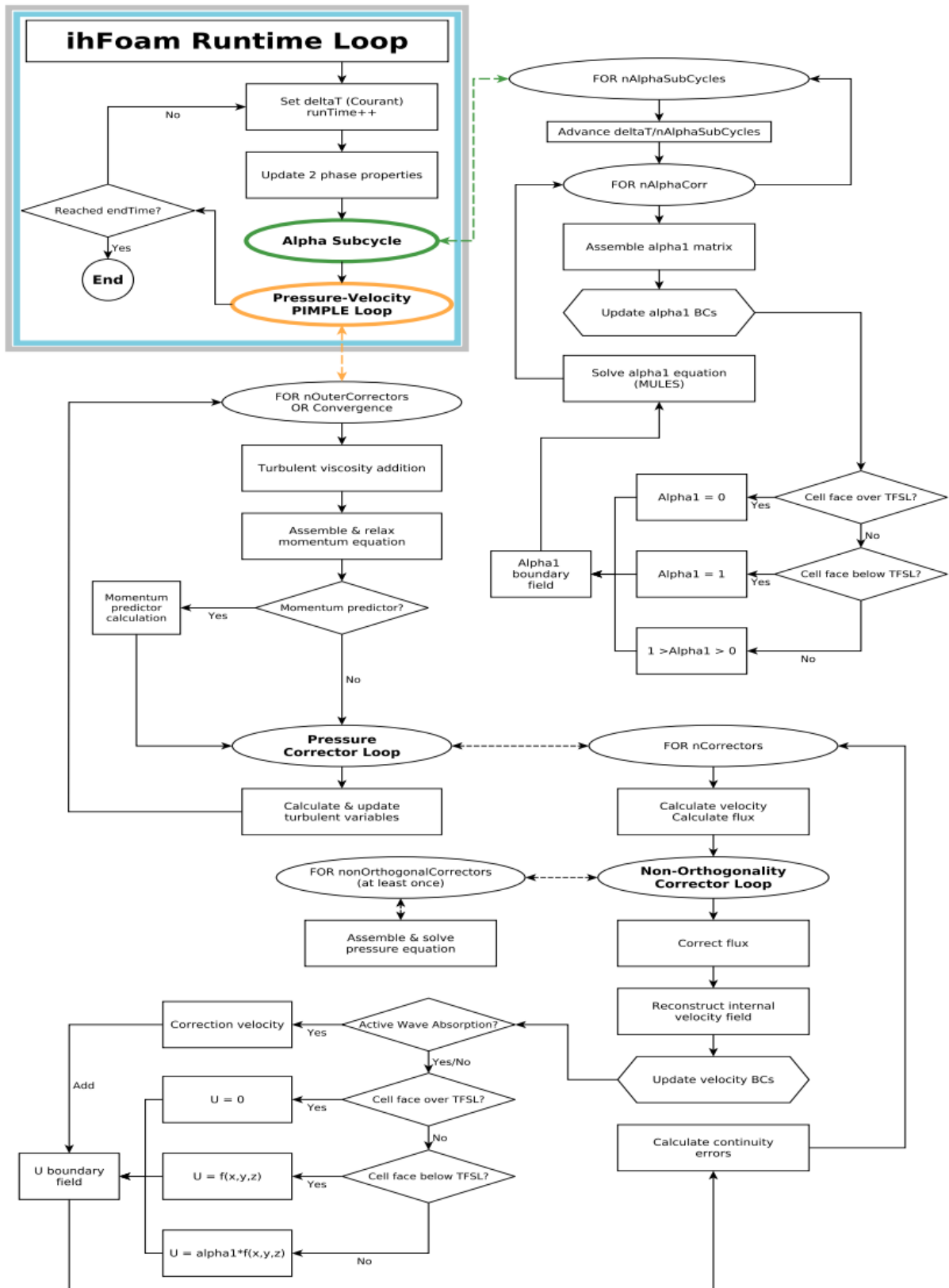
Figure 3.6. IHFOAM solving flow chart (Higuera P., 2015)

Since pressure and velocity are included in the numerical simulation, the solution of pressure-velocity equations is solved by a two-step method which is called PIMPLE. This solution is derived from PISO algorithm (Pressure Implicit with Splitting of Operators) and SIMPLE algorithm (Semi-Implicit Method for Pressure-Linked Equations), in particular the iterative loops and under-relaxation. PIMPLE is a two-step method (predictor-corrector), which can be explained as workflow in the following subtopics (Higuera P., 2015).

(a) Discretization of the momentum equation

The momentum equation is shown in equation (3.12) which is represented in a matrix form. Where M is the coefficient matrix that represents the implicit terms. U_* and P_* are the unknown velocity and pseudo-dynamic pressure, respectively. T_U is the coefficient matrix of the explicit terms. U is velocity. $T_U U$ stands for the velocity-dependent source terms and T_I is the source term (does not depend on velocity) that includes the surface tension and buoyancy effects.

$$MU_* = -\nabla P_* + T_U U + T_I \qquad (3.12)$$

(b) Relaxation of momentum equation

This technique operates to improve the stability of the simulation, especially for steady-state problems, which is inherited from the SIMPLE algorithm. The modifications of the coefficient matrix M and source T_U are performed to apply the under-relaxation mechanism limits.

(c) Momentum predictor

The momentum predictor is shown in equation (3.13) by applying the pressure (P) and velocity (U) field from the previous time step (n).

$$MU_* = -\nabla P_n + T_U U_n + T_I \qquad (3.13)$$

(d) Pressure equation solution and velocity corrector

To simplify the solving process, the PIMPLE method is used to involve a convenient decomposition of the equations. Finally, the velocity is improved to be solenoidal in the last step.

3.5. NUMERICAL MODEL SETUP

The two-dimensional hydraulic model tests were conducted in a numerical wave flume with a length of 40 m, a depth of 1.2 m and a width of 0.05 m. The schematic sketch of the numerical model is shown in Figure 3.7.

The numerical models were set with a wave generation boundary at the inlet and a wave absorption boundary at the outlet. The top of the model was set as an atmosphere boundary. A flatted floor with no slip was set at the bottom of the numerical wave flume. In this study, the investigation of wave interaction with submerged structures was considered in two dimensions, therefore front and back of numerical wave flume were set as empty boundaries. A specific submerged structure was fixed 10 m away from the inlet.
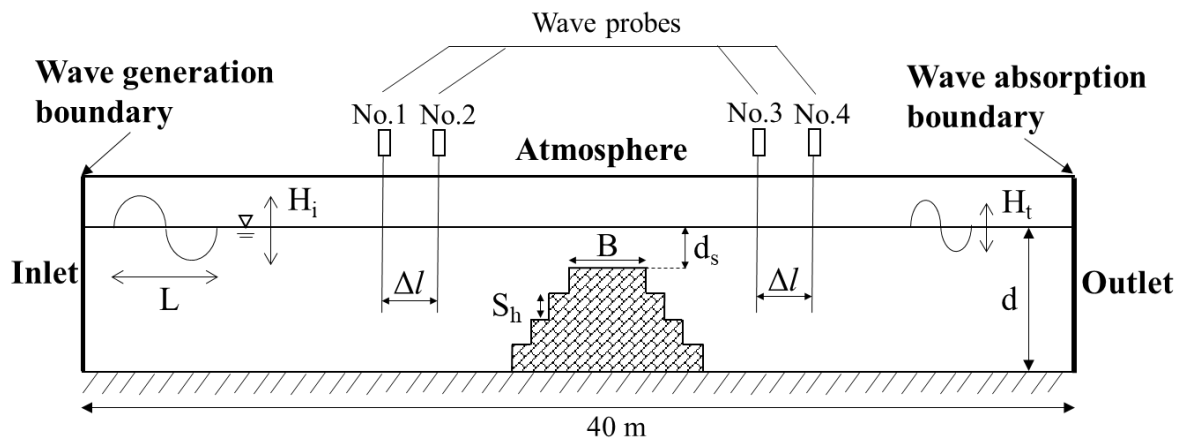
Figure 3.7. The schematic sketch of the numerical model

In order to estimate the characteristics of an incident wave, a transmitted wave and a reflected wave, the method of Goda and Suzuki (1976) was used to separate waves in this study. The water surface elevation is an interface area between water and air, which was calculated based on the Volume of Fluid (VOF) method. Probes No.1 and 2 were located in front of a structure, while probes No.3 and 4 are located behind the structure to collect the water elevation in the numerical model. The appropriate distance between each two wave probes is given in equation (3.14).

$$0.05 \leq \Delta l \, / \, L \geq 0.45 \qquad (3.14)$$

The efficiencies of the stepped slope on a submerged structure were examined and compared with the conventional breakwaters (smooth trapezoidal and vertical breakwaters). The influences of stepped slope on submerged structures are presented in a range of stepped heights, S_h, from $0 \leq d\text{-}d_s$. The structure with a non-stepped slope ($S_h = 0$ m) is represented as a smooth slope, which is followed by an expanded stepped height to the biggest stepped height as a vertical structure ($S_h = 0.54$ m). The structural geometries of the models are shown in Figure 3.8.
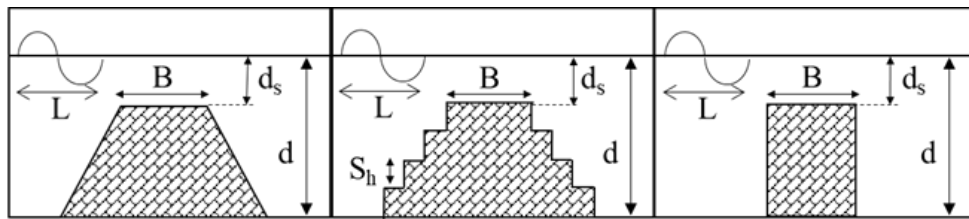
Figure 3.8. Geometries of the submerged structures

3.5.1. BOUNDARY CONDITIONS

In OlaFlow, the package includes a set of boundary conditions to generate and absorb waves at the boundaries. Based on this advantage, a damping or relaxation zone does not need to be created in the model, which can provide a faster calculation in numerical simulation. The available wave theories are included in an inlet boundary that is conducted by a waveDict file. Wave theories, wave periods, wave heights and other wave properties can be defined for wave generation. Moreover, wave absorption boundaries are set at the outlet to prevent wave reflection. In order to describe the hydraulic parameters in each boundary, the boundary conditions of the numerical model are shown in Table 3.1. Alpha water (α) is used to determine the volume fraction of water, air and the interface area between water and air. U is the velocity of the fluid field and k is used to determine the turbulent kinetic energy field in the model.

Table 3.1. Boundary condition setup in OpenFOAM®

Boundary	Alpha water (α)	Velocity (U)	Turbulent kinetic energy (k)
Inlet	waveAlpha	waveVelocity	inletOutlet
Outlet	zeroGradient	waveAbsorption2DVelocity	inletOutlet

Table 3.1. Boundary condition setup in OpenFOAM® (Cont'd)

Boundary	Alpha water (α)	Velocity (U)	Turbulent kinetic energy (k)
Atmosphere	inletOutlet	pressureInletOutletVelocity	inletOutlet
Bottom	zeroGradient	noslip	kqRWallFunction
Front	empty	empty	empty
Back	empty	empty	empty

According to Table 3.1, the implementation of boundary conditions is set in each boundary domain. The waveAlpha and waveVelocity are set to provide a phase fraction field of wave surface and velocity at the inlet boundary, which is conducted for wave generation at the inlet by waveDict file. The zeroGradient is used for the outlet and bottom boundary of the alpha water field, which allows surface tension between the wall and the interface area of the water-air to be ignored. For the top of the model, the boundary condition is set as an atmosphere that combines the stability of inflow and outflow according to the internal flow. The inletOutlet condition is used for an atmosphere of alpha water field, also inlet, outlet and atmosphere for turbulent kinetic energy. The boundary condition for wave absorption applicable of the *U* field is controlled with the waveAbsorption2DVelocity condition. The pressureInletOutletVelocity condition is used for the atmosphere boundary of the U field. The behavior of velocity along a wall is set by the noslip condition, which forces the velocity at the wall to be zero. For inlet, outlet and atmosphere boundaries of turbulent kinetic energy are set as calculated conditions, which are computed based on the turbulence equation. The kqRWallFunction provides a pure zero-gradient boundary condition on a wall. In this study, the numerical simulation is carried out in a two-dimensional model, the conditions of front and back are set as empty boundaries.

3.5.2. NUMERICAL PARAMETERS

In this study, three different crest widths of the stepped submerged breakwaters (0.25 m, 0.45 m and 0.65 m) and 0.54 m height of the models were tested with a regular wave. In order to investigate the effects of wave interaction with a stepped slope on the breakwater, five different step sizes were considered in this numerical simulation. Stepped submerged breakwaters were subjected to regular wave conditions under various wave periods and wave heights. The numerical setup parameters are concluded in Table 3.2. The other important solver and scheme settings in simulations are given in Table 3.3.

Table 3.2. The numerical setup parameters for stepped submerged breakwater

Parameters	Ranges
Water depth, d [m]	0.60, 0.80
Wave period, T [s]	1.5, 2.0
Wave length, L [m]	2.99 to 4.85
Wave height, H [m]	0.03, 0.09
Breakwater height, h [m]	0.54
Breakwater crest width, B [m]	0.25, 0.45, 0.65
Breakwater step height, h_s [m]	0.06, 0.09, 0.18
Breakwater step width, b_s [m]	0.05, 0.08, 0.20

Table 3.3. Solver and Scheme setting

ControlDict	Values/Schemes
application	olaFlow
adjustTimeStep	Yes
maxCo	0.45
maxAlphaCo	0.45
fvSchemes	**Values/Schemes**
ddt ($\frac{\partial}{\partial t}$)	Euler
Grad (∇U, $\nabla \alpha$)	Gauss linear
div(rhoPhi,U) ($\nabla \cdot (\rho \phi U)$)	Gauss limitedLinearV 1
div(phi,alpha) ($\nabla \cdot (\phi \alpha)$)	Gauss vanLeer
div(phirb,alpha) ($\nabla \cdot (\rho \phi_{rb} U)$)	Gauss interfaceCompression
div(phi,k) ($\nabla \cdot (\phi k)$)	Gauss upwind
div(phi,epsilon) ($\nabla \cdot (\phi \varepsilon)$)	Gauss upwind
div(phi,omega) ($\nabla \cdot (\phi \omega)$)	Gauss upwind
laplacian (∇^2)	Gauss linear corrected
interpolation	linear
snGrad	corrected
fvSolution	**Values/Schemes**
alpha.water.* (solver, tolerance, relTol)	smoothSolver, 1e-8, 0
pcorr.* (solver, tolerance, relTol)	PCG/DIC, 1e-5, 0
p_rgh (solver, tolerance, relTol)	PCG/DIC, 1e-7, 0
U (solver, tolerance, relTol)	smoothSolver, 1e-6, 0
k|epsilon|omega	smoothSolver, 1e-8, 0

3.5.3. WAVEMAKER IN NUMERICAL MODEL

OlaFlow solver allows the generation of regular and irregular waves based on several wave theories. The regular waves in the solver package consist of Stokes I, II, III and V, Cnoidal and streamfunction waves. Boussinesq solitary, Grimshaw solitary and irregular (random) waves are also included for wave generation.

In this study, a well-known diagram of the relative water depth and the wave steepness by Le Méhauté (1976) was considered to identify the applicable wave theory, which is shown in Figure 3.9. For the variables in this chart, H stands for wave height, d is water depth, g is gravitational acceleration and T is wave period. Stokes wave theory is a periodic wave that is valid for the high steepness of waves operating in transitional to deep water depth. Cnoidal wave theory is a long periodic wave that is operated in shallow and transitional water. The shape of the cnoidal wave has shaper crests and flatter troughs than Stokes wave. Solitary wave theory is widely used for shallow and transition water. A solitary wave is a non-periodic wave, which has a single crest above water level.

Based on the range of wave conditions in this study, the Stokes second order wave theory was applicable for simulation. The second order Stokes wave equation of free surface position was given by Dean and Dalrymple (1991), which is introduced in equation (3.15). Where η is surface elevation, H is the height of wave between crest and trough, k_n is the angular wave number, $k_n=2\pi/L$, ω is the angular frequency, $\omega=2\pi/T$, T is wave period, d is water depth and t is time.

$$\eta = \frac{H}{2}\cos(k_n x - \omega t)$$

$$+\frac{H^2 k_n}{16}\frac{\cosh(k_n d)}{\sin h^3(k_n d)}(2 + \cos d(2k_n d))\cos 2(k_n x - \omega t) \tag{3.15}$$
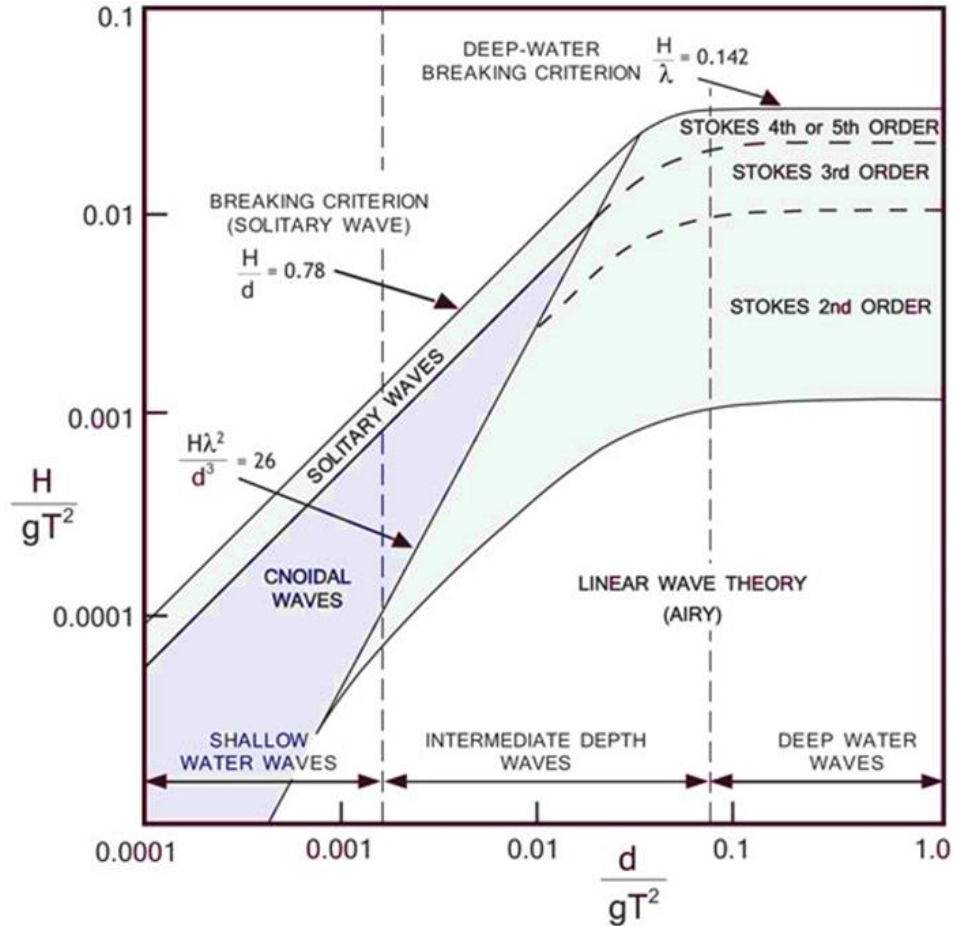
Figure 3.9. Wave theories range of applicability (Le Méhauté, 1976)

3.6. MESH GENERATION

In computational fluid dynamics (CFD) modeling, a grid cell or an element is created to fill the volume of flow simulation inside each grid cell. Mesh generation is the first step to prepare the background meshes for numerical simulation. Then, mathematical equations can be applied to calculate in each cell of the mesh. Therefore, generating a high-quality mesh is very important to obtain reliable solutions and high accuracy of numerical stability.

This section describes a simple mesh generation and mesh creation with high quality based on a complex shape, which is presented in blockMesh utility and snappyHexMesh utility.

3.6.1. BLOCKMESH

In OpenFOAM®, a mesh is generated from a dictionary file in software named blockMeshDict. The main principle of blockMesh utility is capable to decompose the domain geometry into a

38

set of block (one or three dimensions). An example of the dissection of domain geometry is shown in Figure 3.10. Each mesh block of geometry consists of 8 vertices and 12 edges with a fixed order.
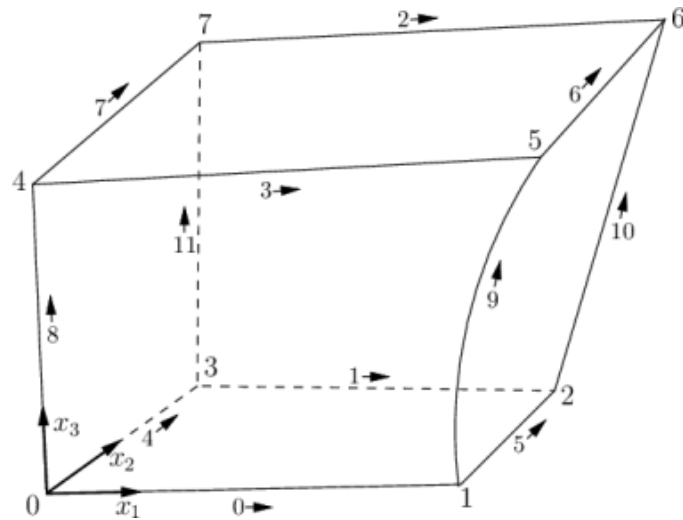
Figure 3.10. The dissection of domain geometry in blockMesh utility
(OpenCFD, Ltd., 2023a)

In this study, the background mesh of numerical simulation was generated to be a numerical wave flume, which is shown in Figure 3.11. The mesh was created into a 40 m long, 1.2 m deep and 0.05 m wide of numerical wave flume, which was divided for the fine grids size of Δx=0.02 m, Δy=0.025 m and Δz=0.1 m.
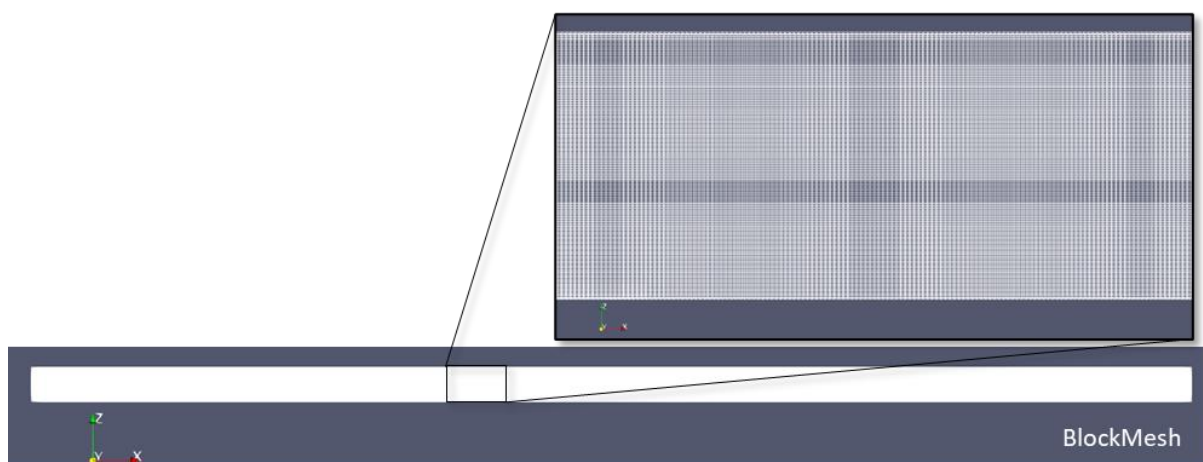
Figure 3.11. Mesh generation for the numerical wave flume

In order to obtain a reliable solution, a high-quality mesh generation was also verified in this study. A various set of mesh sizes was generated in the model. The 10 samples of Stoke second order wave generation were firstly simulated to find a proper mesh size, which was compared with the wave theory (Stokes 2nd order). The verification of mesh quality is shown in Figure 3.12.

Mesh	Average cell size in x-direction[m]	Average cell size in z-direction[m]
1	0.7	0.7
2	0.7	0.5
3	0.06	0.3
4	0.065	0.4
5	0.06	0.6
6	0.05	0.6
7	0.05	0.5
8	0.05	0.4
9	0.025	0.15
10	0.02	0.1
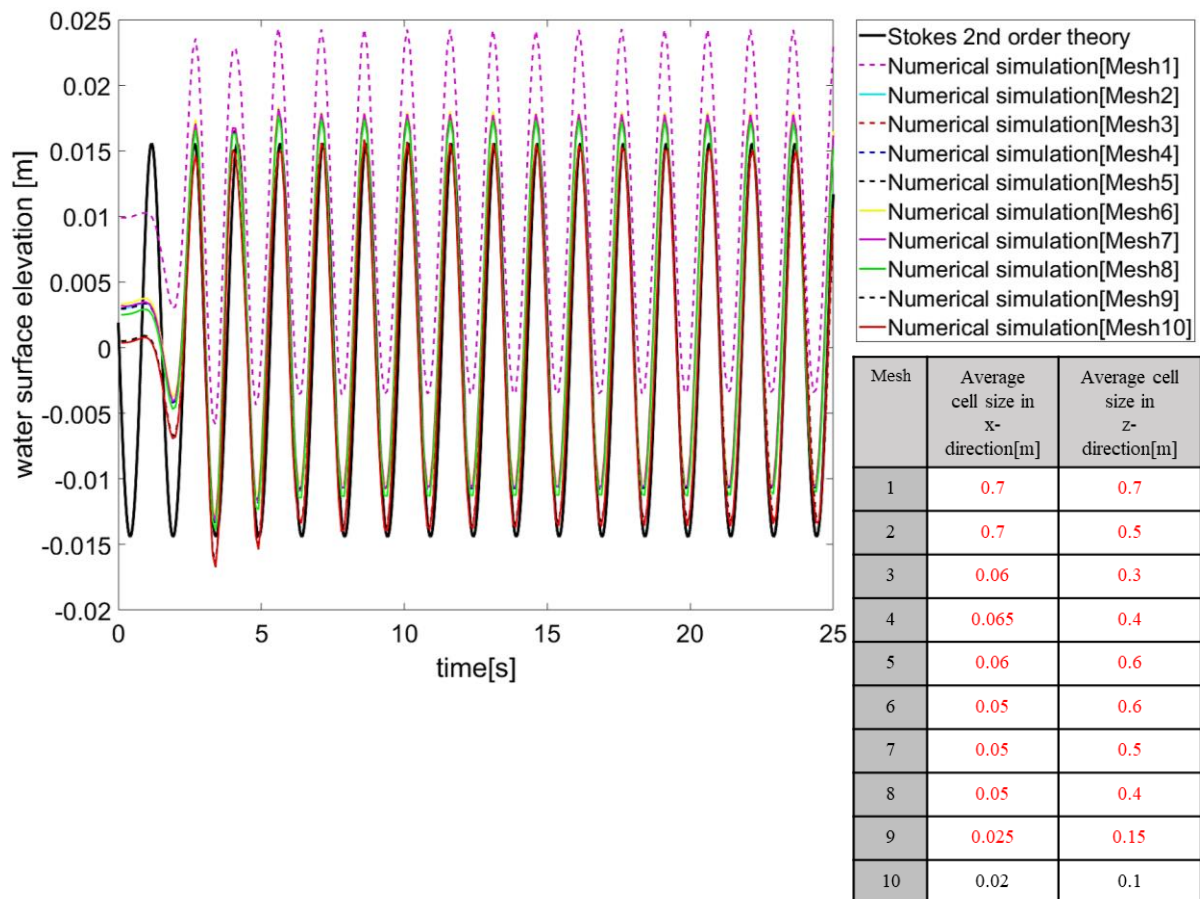
Figure 3.12. The verification of mesh quality

According to Figure 3.12, the high accuracy result based on the size of mesh generation properties was obtained from Mesh10, which was finally used to define the size of meshing in this study (Δx=0.02 m and Δz=0.1 m). However, even though it can be concluded that the fine mesh is better to provide a high-accuracy result, but the simulation also takes a lot of time to calculate in each grid cell. Therefore, the proper mesh size that can provide both reliable solutions and good time simulation is an important consideration.

3.6.2. SNAPPYHEXMESH

The snappyHexMesh utility generates high-quality meshes for a complex geometry, which modifies from a generated background mesh using the blockMesh utility. SnappyHexMesh creates a three-dimensional with high quality hexahedra mesh from triangulated geometries in STL format. A simple background mesh is morphed into a split-hex shape to the surface of object.

In this study, snappyHexMesh was used to create the model into a specific shape of submerged structures. The normal background mesh was decomposed into a complex cell along the object's surface. In order to improve the quality of mesh at boundary layer, three levels for nCellsBetweenLevels were used to set for a fine mesh creation on the structures. The materials can be cut with a smooth surface to reduce an error for calculation inside the mesh cells. The snappyHexMesh resulting in smooth slope (S_h= 0m), micro rough slope (S_h= 0.06m), macro rough slope (S_h= 0.09m), composite slope (S_h= 0.18m) and vertical structure (S_h= 0.54m) are presented in Figures 3.13, 3.14, 3.15, 3.16 and 3.17, respectively.
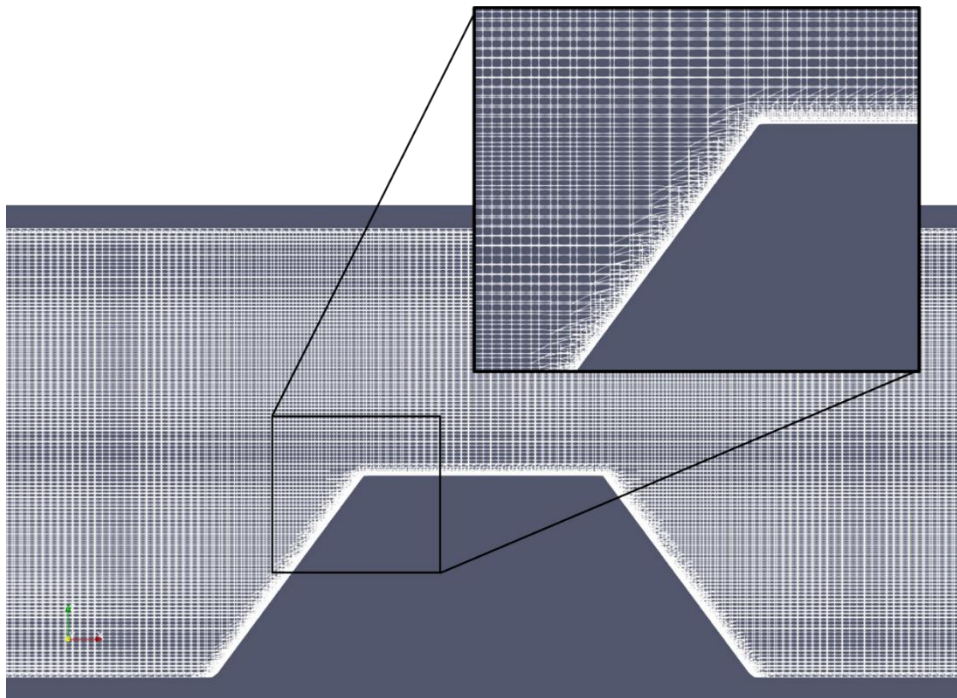
Figure 3.13. The snappyHexMesh resulting of a smooth slope structure (S_h= 0 m)

41
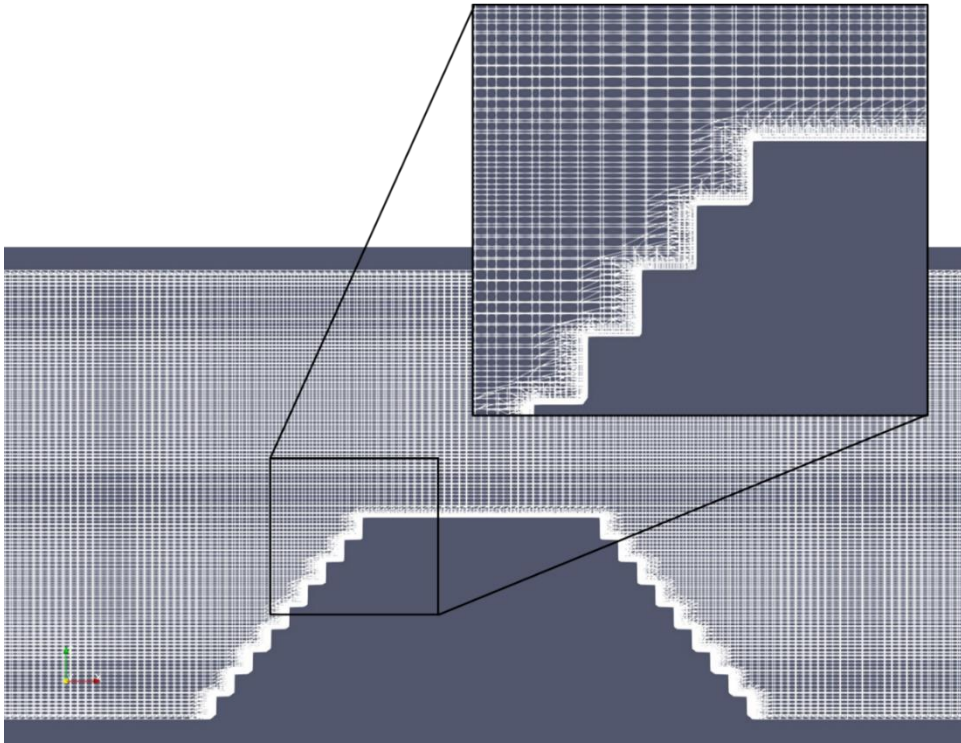
Figure 3.14. The snappyHexMesh resulting of a micro rough slope structure (S_h= 0.06 m)
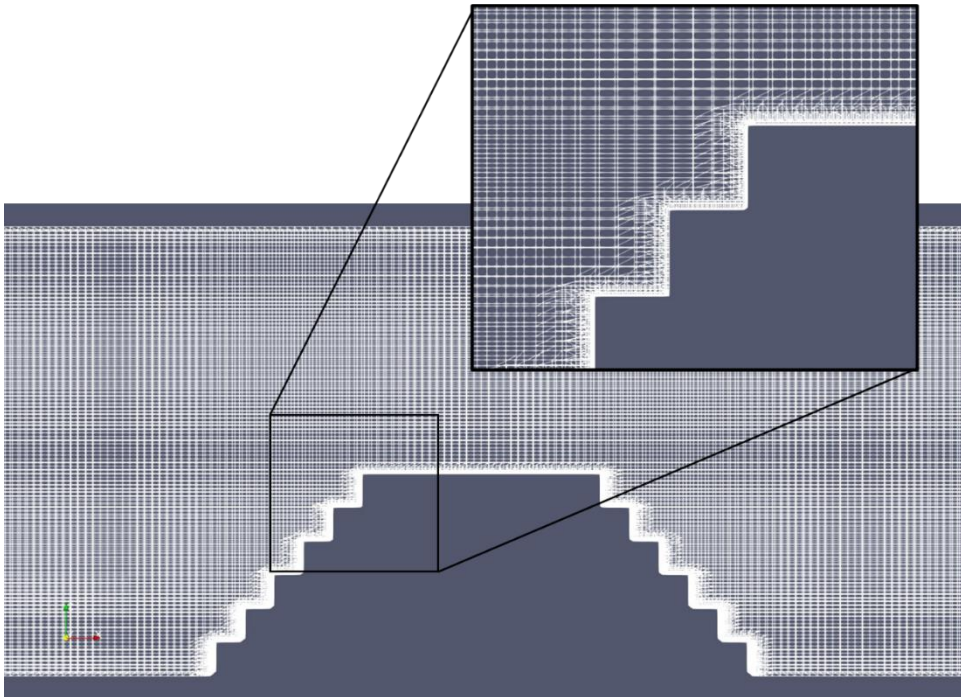
Figure 3.15. The snappyHexMesh resulting of a macro rough slope structure (S_h= 0.09 m)
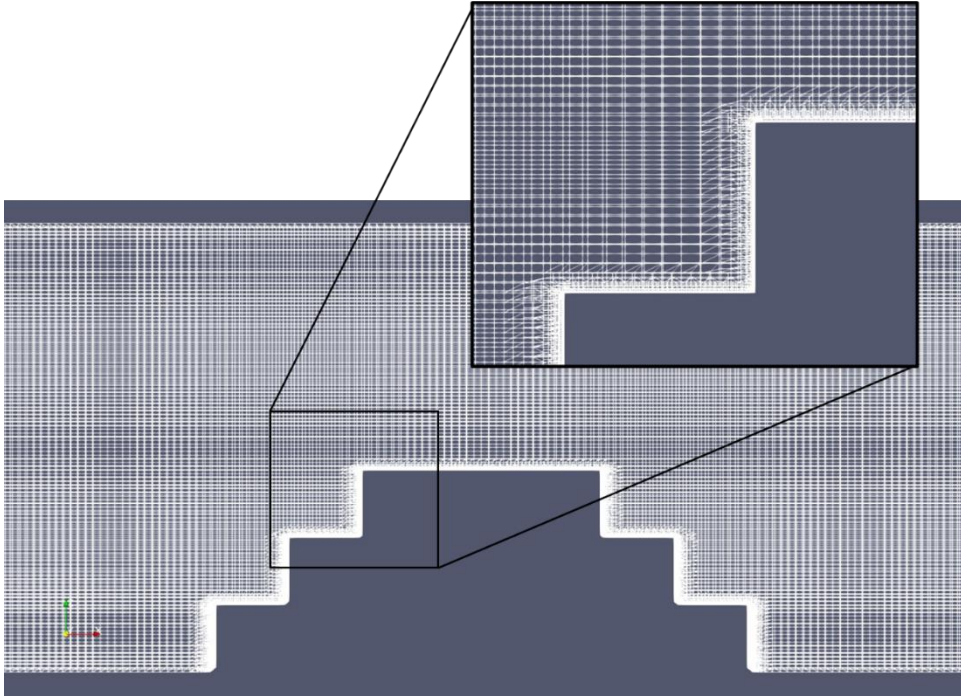
Figure 3.16. The snappyHexMesh resulting of a composite slope structure (S_h= 0.18 m)
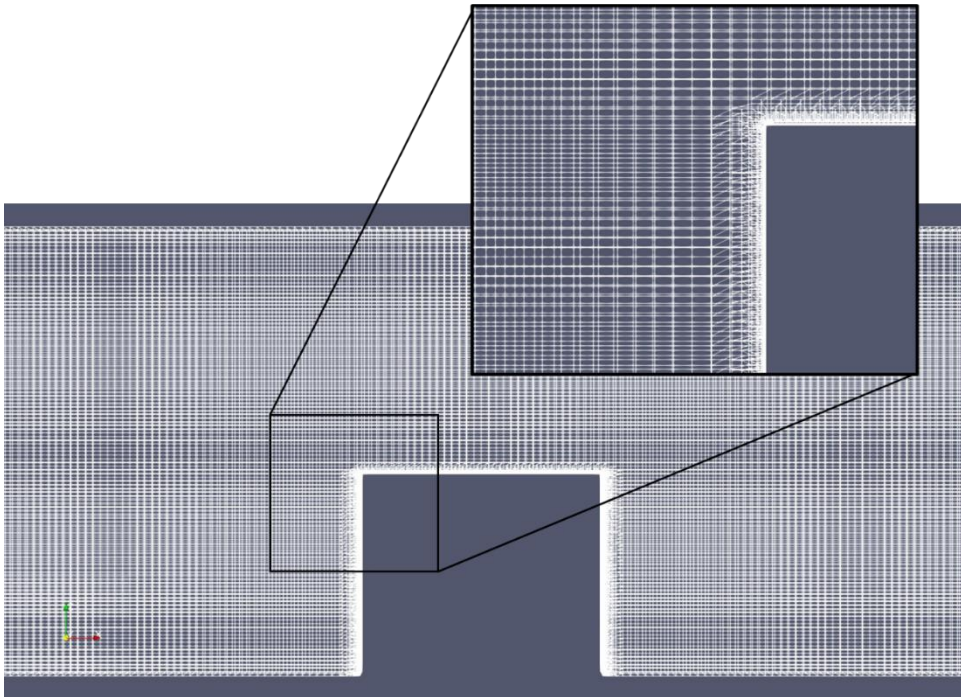
Figure 3.17. The snappyHexMesh resulting of vertical structure (S_h= 0.54m)

3.7. STRUCTURAL MODELING

The investigation of the effect of stepped slope on submerged structures was examined the performance on wave energy dissipation. Various stepped sizes and geometries were tested in this study, which is shown in Table 3.2. There were 30 models that were created for the different submergence depths, varied sizes of crest widths and steps. All of the structural modeling were created in FreeCAD software, which were exported as STL files. The models of different submerged breakwater crest widths for the smooth slope (S_h= 0m), micro rough slope (S_h= 0.06m), macro rough slope (S_h= 0.09m), composite slope (S_h= 0.18m) and vertical structure (S_h= 0.54m) are presented in Figures 3.18, 3.19, 3.20, 3.21 and 3.22, respectively.
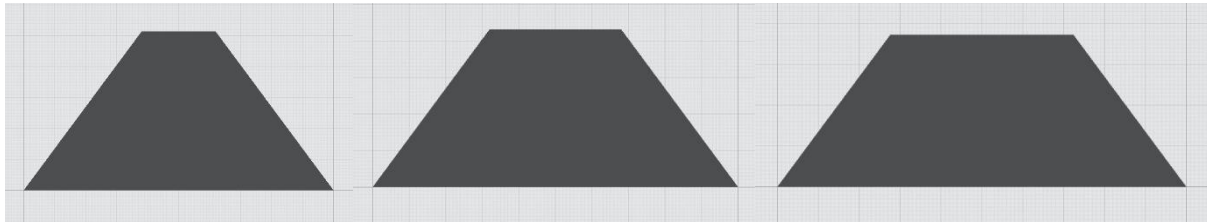
Figure 3.18. The submerged breakwater models with a smooth slope (S_h= 0 m)
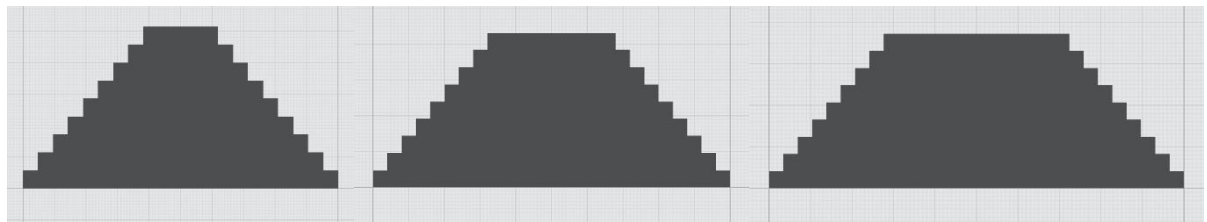
Figure 3.19. The submerged breakwater models with a micro rough slope (S_h= 0.06m)
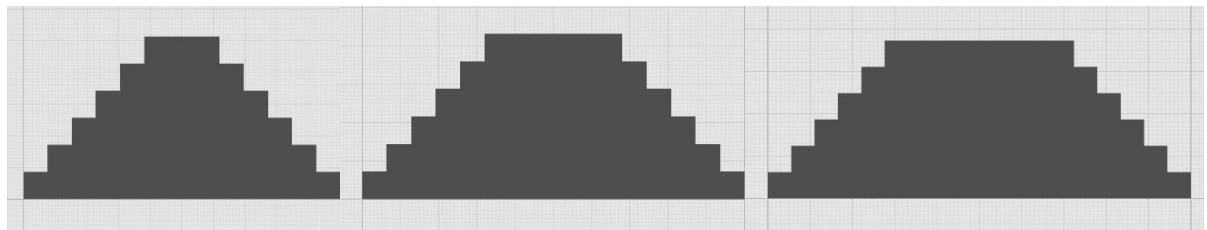
Figure 3.20. The submerged breakwater models with a macro rough slope (S_h= 0.09m)
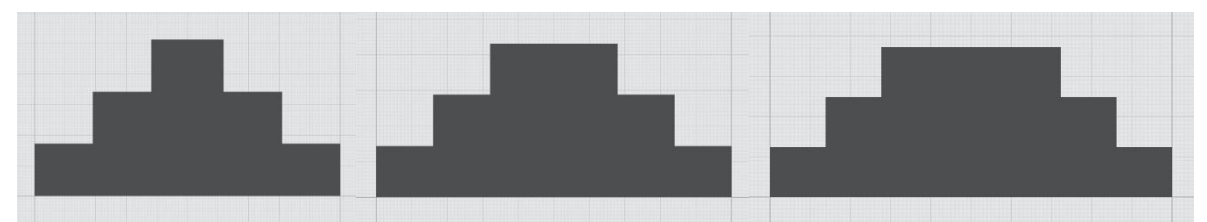
Figure 3.21. The submerged breakwater models with a composite slope (S_h= 0.18m)
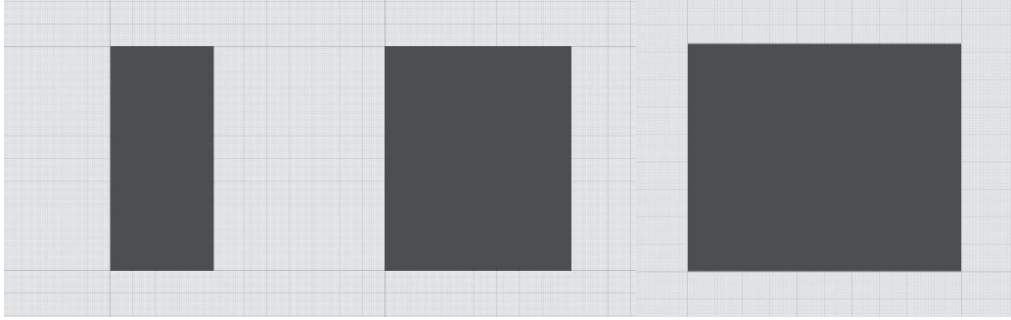
Figure 3.22. The submerged breakwater models with a vertical structure shape (S_h= 0.54m)

3.8. MODEL VALIDATION

To verify the developed numerical model, water-free surface data from the numerical simulation were compared with the theoretical free surface profile, which was given by Stokes second order wave theory in equation (3.9).

In this study, the varied wavelengths of simulation were generated in the range between 2.99 m to 4.85 m, which were computed from equation 3.16 for the intermediate water depth. The data of simulated wave conditions are shown in Table 3.2.

The examples of model validation for 2.9904 m and 4.36198 m wavelengths are shown in Figures 3.23 and 3.24, respectively. Figure 3.23 illustrates the comparison of wave surface elevations between numerical simulation and wave theory for 1.5 s of wave period, 0.03 m of wave height and 0.6 m of water depth. Wave was generated in an intermediate water depth with 1.26067 of relative depth (kh). In Figure 3.24, the wave model validation between numerical simulation and wave theory was compared in the case of 0.03 m wave height, 2 s of wave period, 0.6 m of water depth and 0.864266 of relative depth, which was simulated in an intermediate water depth.

$$L = \frac{gT^2}{2\pi} \tan h \left(\frac{2\pi d}{L}\right) \tag{3.16}$$
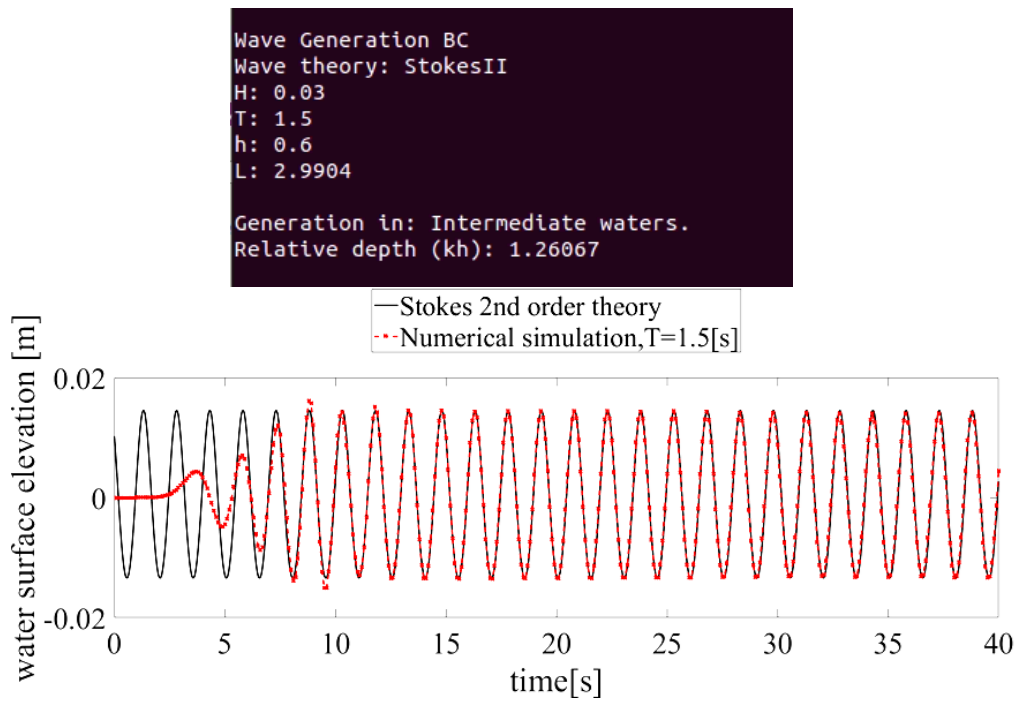
Figure 3.23. The comparison of simulated water surface elevation with wave theory, 2.9904 m of wavelength
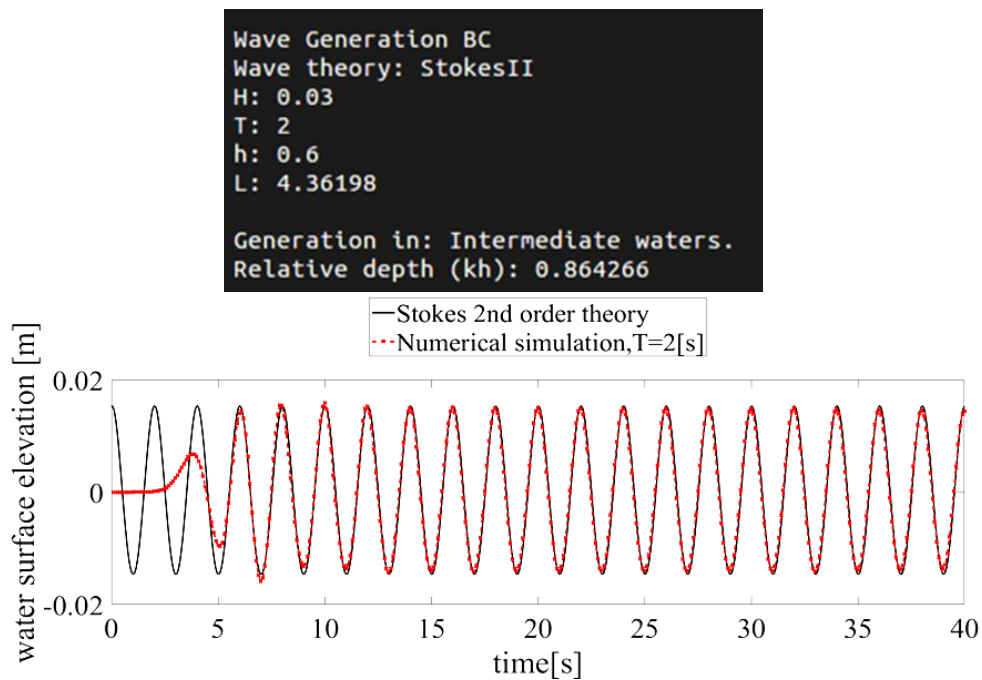
Figure 3.24. The comparison of simulated water surface elevation with wave theory, 4.36198m of wavelength

A set of waves was generated based on the OlaFlow solver. In order to verify the developed model, wave generations were first simulated in a numerical wave flume without any obstructions. Wave surface elevations were collected from a probe that was located in the middle of the model. Once the data of wave surface elevation were completely collected, the processes of model validation were computed by MATLAB code.

In model validation processes, the numerical results of wave generation show a good agreement with the wave theory. However, the results can confirm that the developed models in this study can simulate a certain wave. Therefore, the numerical models can be used to test with different cases of submerged structures. The numerical simulation of wave interaction with submerged structures are finally tested in the next step.

3.9. DURATION OF NUMERICAL SIMULATION

In this session, the records of duration in numerical calculation are described to compare the performance of simulation in each models. The chart of modeling duration is illustrated in case of d_s/d=0.1 and d_s/d=0.325, which are shown in Figure 3.25 and 3.26, respectively. In this study, there are four different wave conditions based on time periods and wave heights, which are considered under two different submergence depths. Fifteen geometries of submerged breakwaters are created in the model.

According to the data records, a smooth slope model spent the longest time in the simulation processes, which was two times longer than the others shapes. Moreover, the small submergence depth cases (d_s/d=0.1) took longer times in the calculation process, which was compared to the deeper submergence case (d_s/d=0.325).
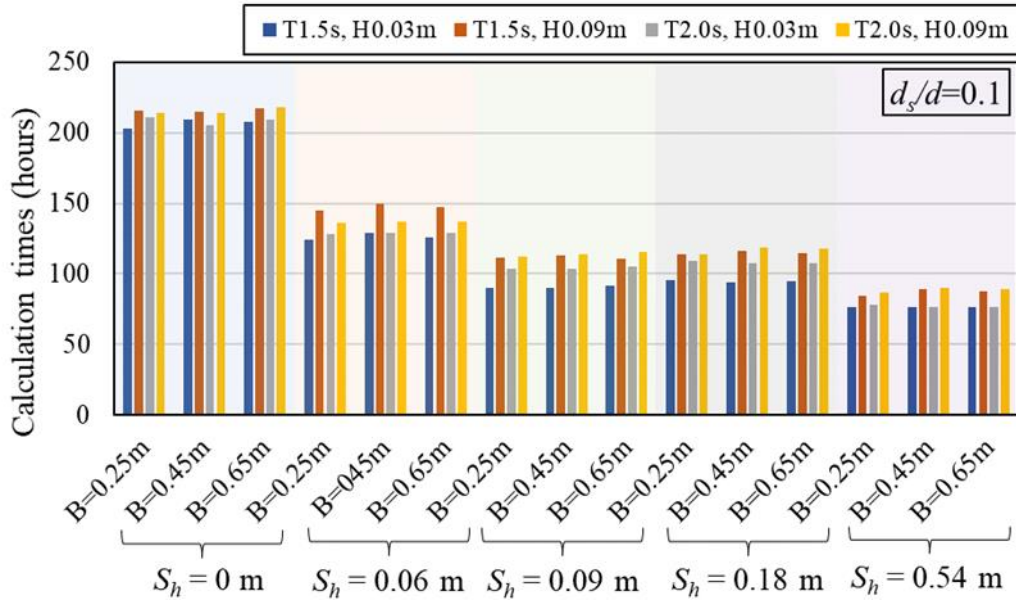
Figure 3.25. The records of modeling duration in case of d_s/d=0.1
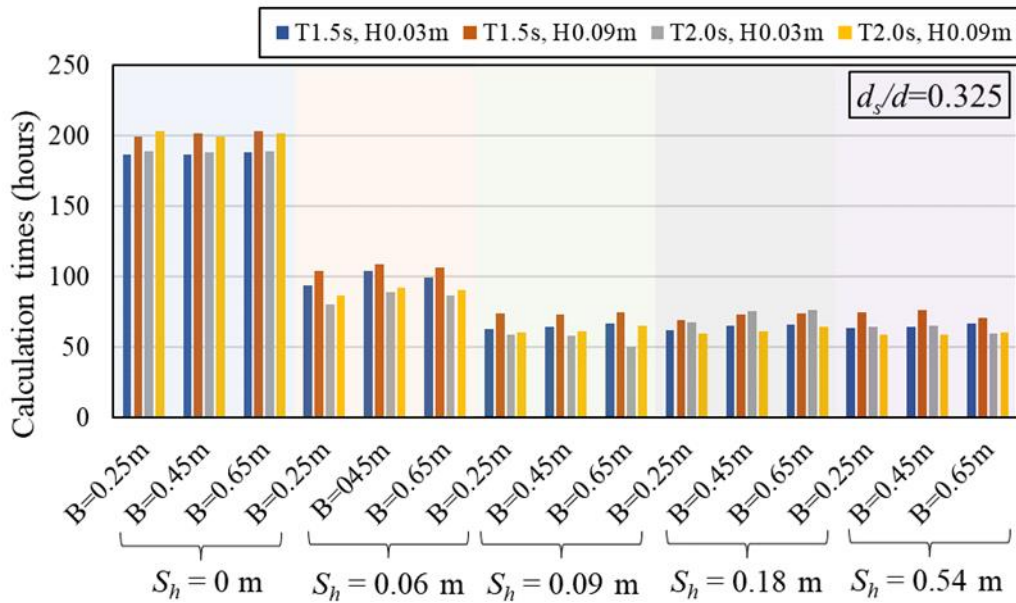
Figure 3.26. The records of modeling duration in case of d_s/d=0.325

CHAPTER 4

THE PERFORMANCE OF WAVE ENERGY

DISSIPATION

Chapter 4

THE PERFORMANCE OF WAVE ENERGY DISSIPATION

This chapter is mainly composed to discuss the performance of wave energy dissipation. The primary investigations on the effect of several geometries such as varying stepped heights, breakwater crest widths and submergence depths are analyzed with various dimensionless variables. This chapter focuses on the performance of wave dissipation, which was computed from a numerical simulation. The numerical results were also compared with several experimental studies. However, this study clearly shows that the geometries of the submerged structure affect the ability of wave attenuation.

This chapter consists of four main sections. Firstly, a brief introduction is given as the background of this study, which is followed by the theoretical background of the data analysis. Then, the results of the performance of wave energy dissipation are presented and discussed in detail with various comparisons. Finally, the summary of this chapter is concluded at the end of this chapter.

4.1.   INTRODUCTION

Based on the literature reviews of stepped submerged breakwaters, most of their studies were only focused on the performance of wave transmission. In order to consider for comprehensive data analysis, this chapter focuses on the ability of submerged breakwaters for wave energy dissipation that was considered on the properties of wave transmission coefficient, wave reflection coefficient and wave energy dissipation rate. The effects of a stepped slope on submerged structures were investigated under various wave conditions, which were also compared with conventional shapes such as smooth slopes and vertical shapes. There are five different stepped heights (S_h= 0 m, 0.06 m, 0.09 m, 0.18 m, 0.54 m), three different crest widths (B= 0.25m, 0.45m and 0.65m), and two submergence ratios (d_s/d= 0.1 and 0.325) of models that were conducted in this study.

A two-dimensional wave flume with a 40 m length (X-direction), 1.2 m height (Z-direction) and 0.05 m width (Y-direction) was created in the numerical model. The submerged breakwaters were located 10 m away from the inlet boundary. In order to collect the water surface elevation in the model, two wave probes were located in front of and behind the

structures, which were considered based on Goda and Suzuki's (1976) method. The distance between these two probes was denoted by Δl which is determined from the equation (4.1), where L is the wavelength.

$$0.05 \leq \Delta l/L \leq 0.45 \tag{4.1}$$

The snapshots of instantaneous wave propagation over the submerged breakwaters with a smooth slope (S_h= 0 m), a micro rough slope (S_h= 0.06 m), a macro rough slope (S_h= 0.09 m), a composite slope (S_h= 0.18 m) and a vertical shape (S_h= 0.54 m) are shown in Figures 4.1, 4.2, 4.3, 4.4 and 4.5, respectively. The samples of these instantaneous wave profiles were simulated from the cases of H_i=0.09 m, T =1.5s and d_s/d =0.1. The diagrams were captured at 24.7 s, 25.5 s and 26.2 s, which was 1 wave period of wave generation. The Volume of Fluid (VOF) technique was applied to represent two incompressible phases of water and air. The value of alpha.water=0 represents the air phase, while alpha.water=1 represents the water in the model. The water surface area is presented as 0 < alpha.water < 1, which are shown in the figures below.
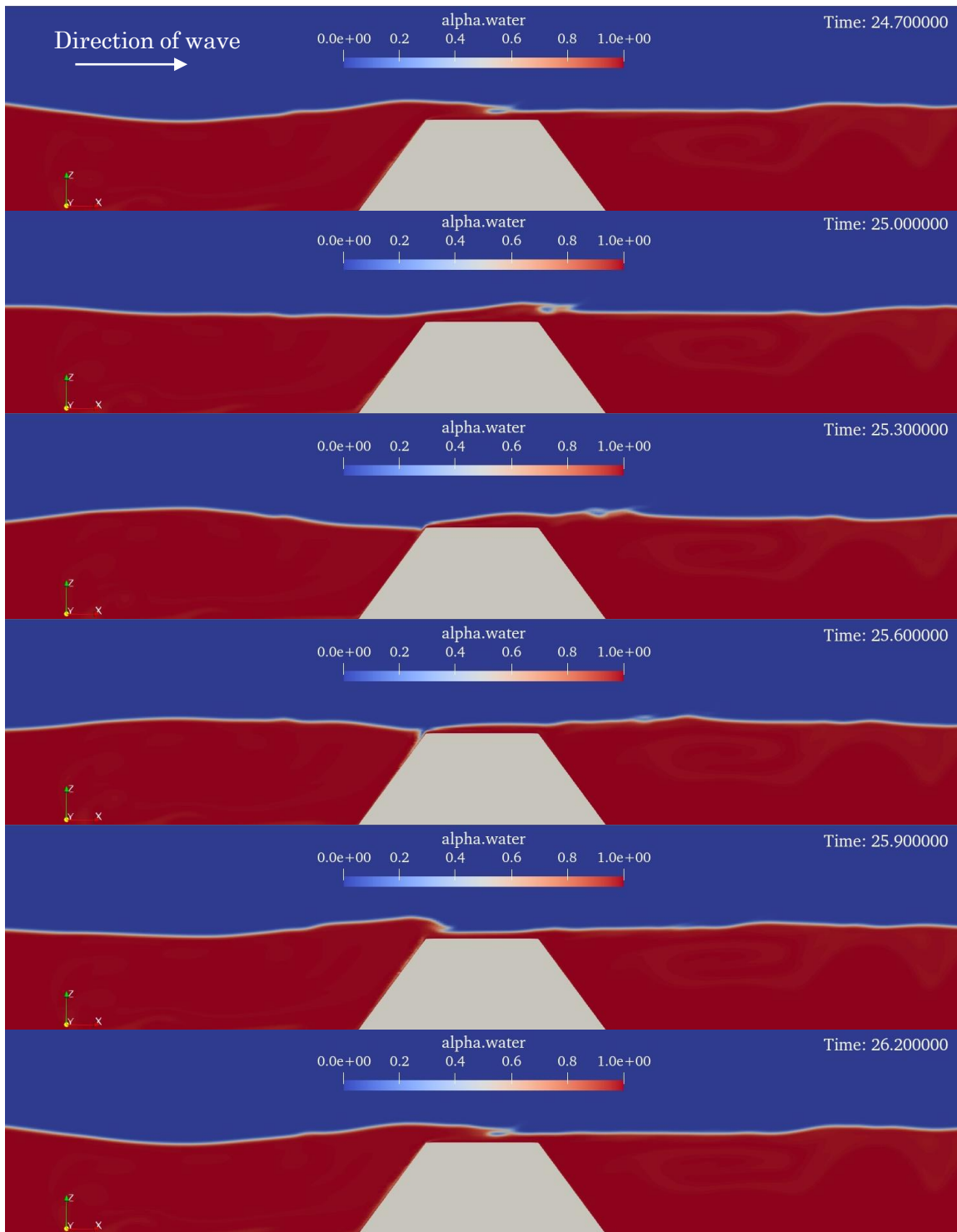
Figure 4.1. The evolution of the instantaneous wave propagation profile over a smooth slope breakwater ($S_h= 0$ m)
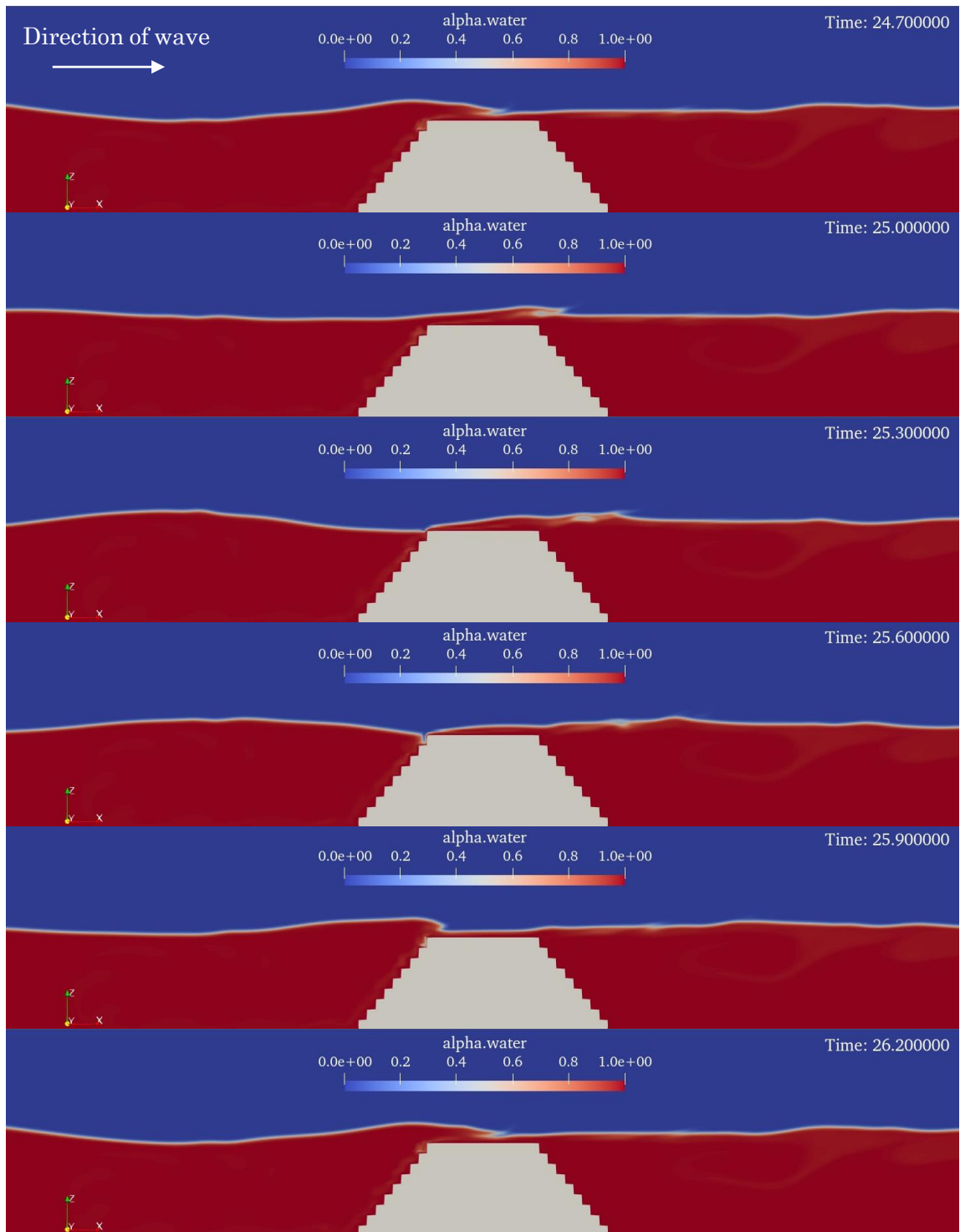
Figure 4.2. The evolution of the instantaneous wave propagation profile over a micro rough slope breakwater (S_h= 0.06 m)
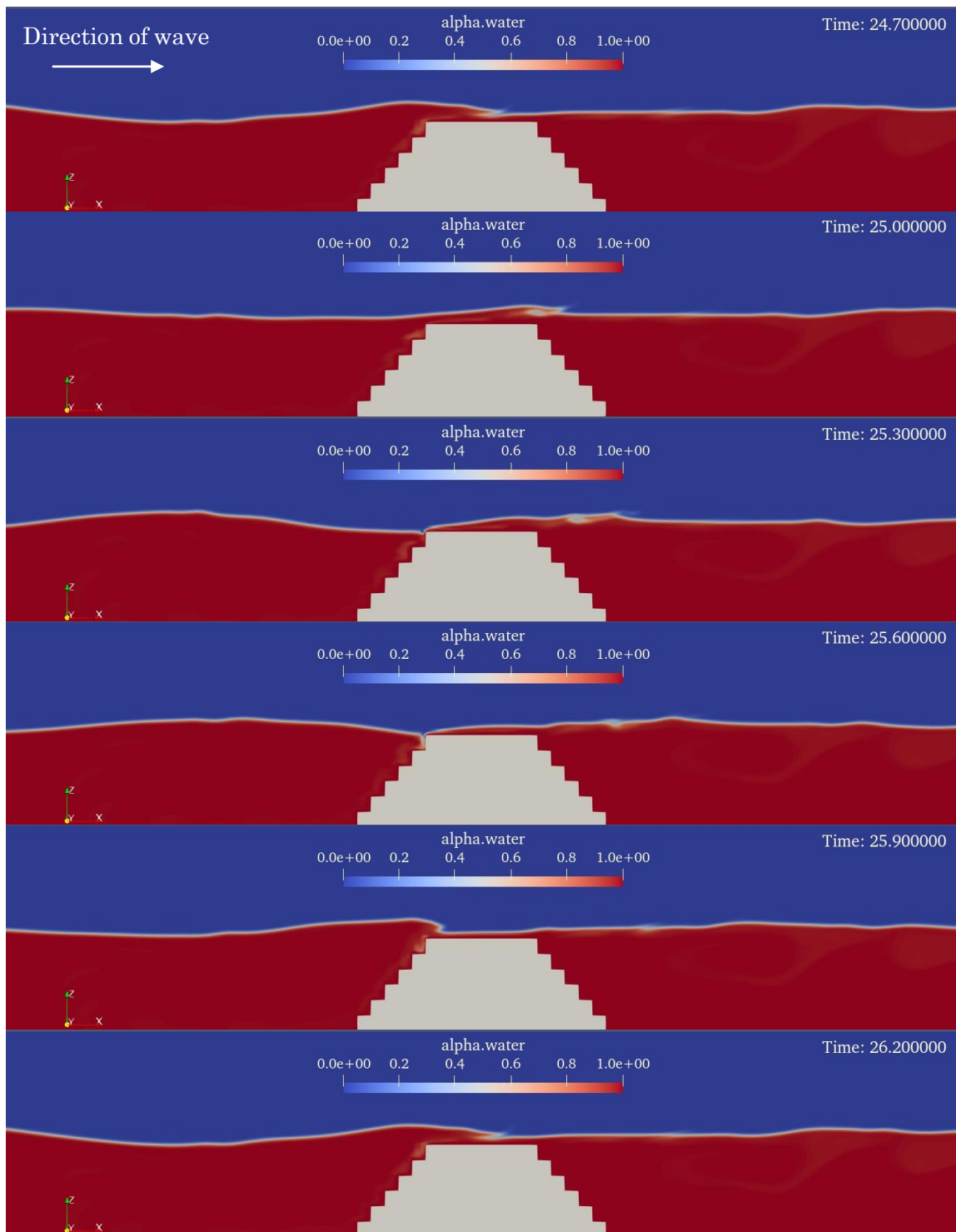
Figure 4.3. The evolution of the instantaneous wave propagation profile over a macro rough slope breakwater (S_h= 0.09 m)
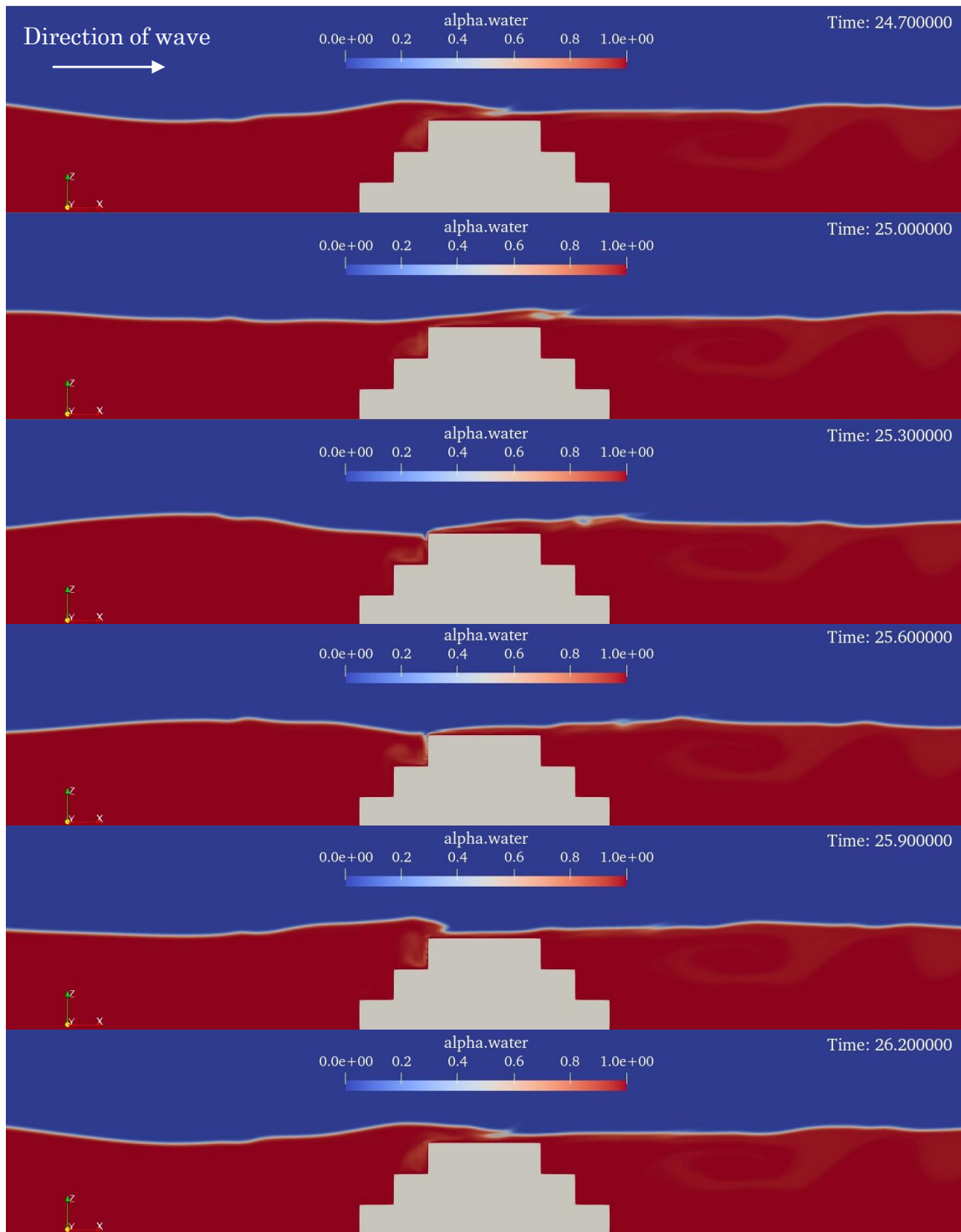
Figure 4.4. The evolution of the instantaneous wave propagation profile over a composite rough slope breakwater (S_h= 0.18 m)
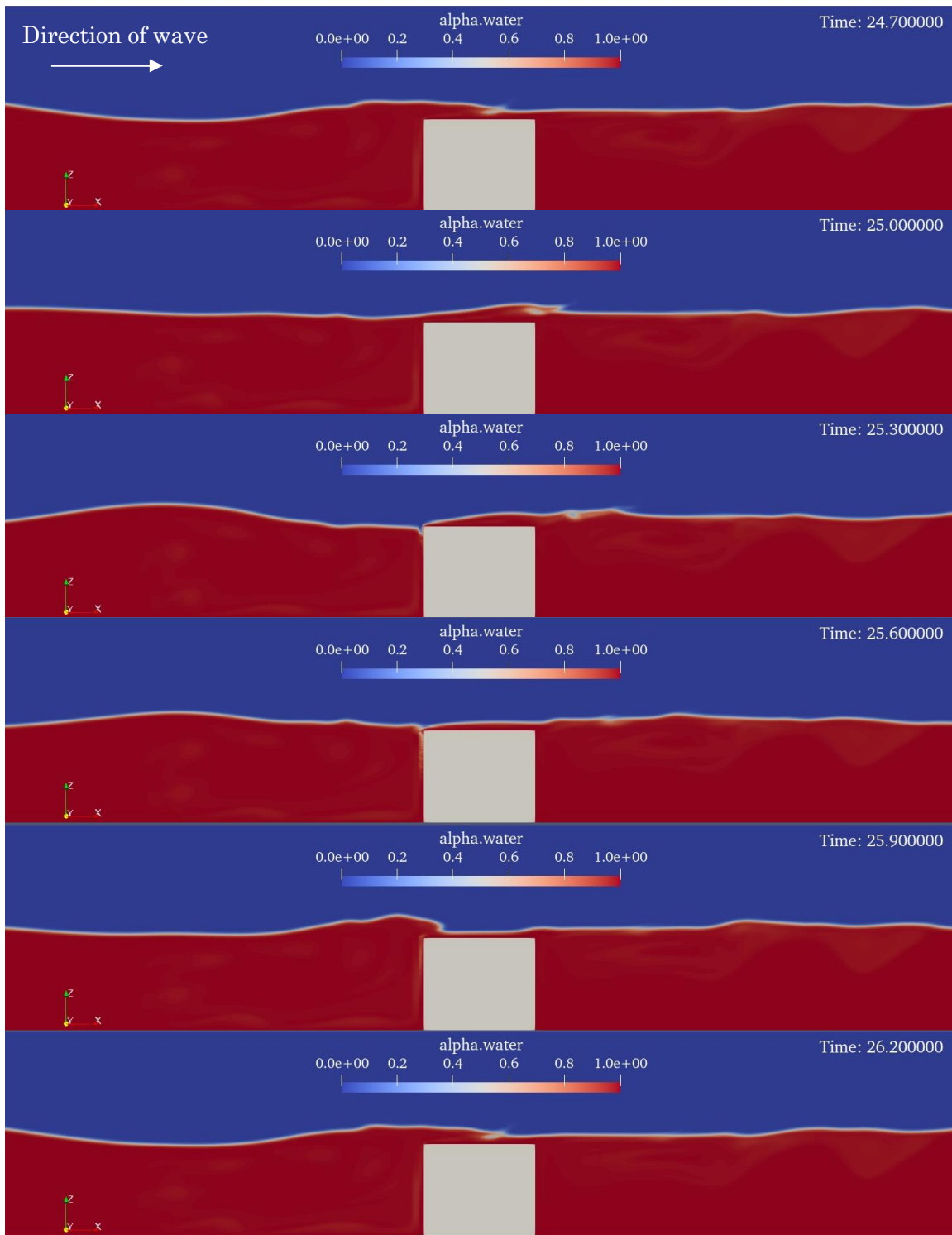
Figure 4.5. The evolution of the instantaneous wave propagation profile over a vertical breakwater (S_h= 0.54 m)

4.2. THEORETICAL BACKGROUND

The theoretical backgrounds for data analysis are presented in this section. In order to separate incident and reflected waves, the wave separation technique for regular waves was applied in the numerical model, which is described in the following subsection. The calculation method for the performance of wave transmission, wave reflection and wave energy dissipation are also introduced in this section.

4.2.1. WAVE SEPARATION

Goda and Suzuki (1976) revealed a well-known technique to resolve the incident and reflected waves that is applicable to both regular and irregular wave trains. The aim of wave separation is to analyze the distribution of wave energy into a potential wave train. In this study, the wave separation for a regular wave was applied in the numerical simulation.

Based on Goda and Suzuki's method (1976), a wave was generated by a wave paddle that propagates forward along the flume and reflects back by a structure on the other side of the wave generator. The wave propagation in the positive and negative directions were incident wave and reflection wave, respectively, which is shown in Figure 4.6. The water surface elevation of the incident wave is represented as η_I, and that of the reflected wave is η_R, which are described in the general form in equations (4.2) and (4.3). Two simultaneous wave records are taken at adjacent locations of x_1 and $x_2 = x_1 + \Delta l$.

Where a_I and a_R are the amplitude of incident and reflected waves, k_n is the wave number of $2\pi/L$, L is the wavelength, ω is the angular frequency of $2\pi/T$, T is the wave period, and ε_I and ε_R are the phase angles of incident and reflected waves.
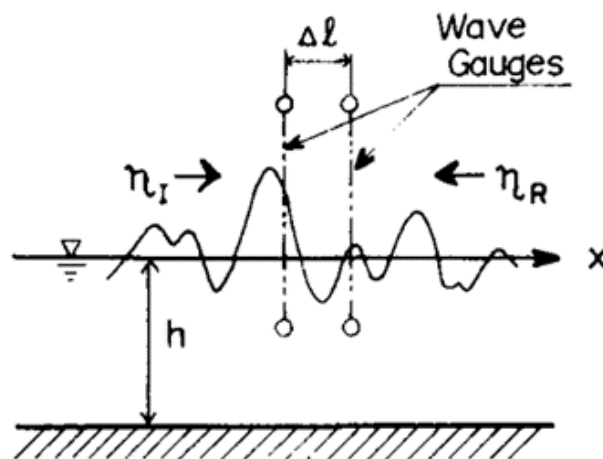
Figure 4.6. Definition sketch of the incident and reflected waves (Goda and Suzuki, 1976)

57

$$\eta_i = a_i \cos(kx - \omega t + \varepsilon_i) \tag{4.2}$$

$$\eta_r = a_r \cos(kx - \omega t + \varepsilon_r) \tag{4.3}$$

The surface elevations at two positions within a distance of x_1 and x_2 are measured in the direction of wave propagation that are presented in equations (4.4) and (4.5). A composite signal of a sine and cosine signal having different time-constant amplitudes can be obtained from Fourier analysis. The Fast Fourier Transform (FFT) technique is applied to estimate the amplitudes of A_1, B_1, A_2 and B_2.

$$\eta_1 = (\eta_i + \eta_r)_{x=x_1} = A_1 \cos\omega t + B_1 \sin\omega t \tag{4.4}$$

$$\eta_2 = (\eta_i + \eta_r)_{x=x_2} = A_2 \cos\omega t + B_2 \sin\omega t \tag{4.5}$$

where,

$$A_1 = a_i \cos\emptyset_i + a_r \cos\emptyset_r \tag{4.6}$$

$$B_1 = a_i \sin\emptyset_i - a_r \sin\emptyset_r \tag{4.7}$$

$$A_2 = a_i \cos(k_n \Delta l + \emptyset_i) + a_r \cos(k_n \Delta l + \emptyset_r) \tag{4.8}$$

$$B_2 = a_i \sin(k_n \Delta l + \emptyset_i) - a_r \sin(k_n \Delta l + \emptyset_r) \tag{4.9}$$

$$\emptyset_i = k_n \Delta l + \varepsilon_i \tag{4.10}$$

$$\emptyset_r = k_n \Delta l + \varepsilon_r \tag{4.11}$$

Finally, the amplitude of incident and reflected waves are expressed as in equations (4.12) and (4.13).

$$a_i = \frac{1}{2|\sin k_n \Delta l|}\sqrt{K_1^2 + K_2^2} \tag{4.12}$$

$$a_r = \frac{1}{2|\sin k_n \Delta l|}\sqrt{K_3^2 + K_4^2} \tag{4.13}$$

where,

$$K_1 = A_2 - A_1 cos k_n \Delta l - B_1 sin k_n \Delta l \qquad (4.14)$$

$$K_2 = B_2 + A_1 sin k_n \Delta l - B_1 cos k_n \Delta l \qquad (4.15)$$

$$K_3 = A_2 - A_1 cos k_n \Delta l + B_1 sin k_n \Delta l \qquad (4.16)$$

$$K_4 = B_2 - A_1 sin k_n \Delta l - B_1 cos k_n \Delta l \qquad (4.17)$$

4.2.2. WAVE TRANSMISSION

The wave transmission coefficient, K_t, is the ratio of the transmitted wave height, H_t, on onshore of the breakwater to the incident wave height, H_i, on offshore side, which is shown in equation (4.18). The definition diagram of numerical model is shown in Figure 4.7.

$$K_t = \frac{H_t}{H_i} \qquad (4.18)$$
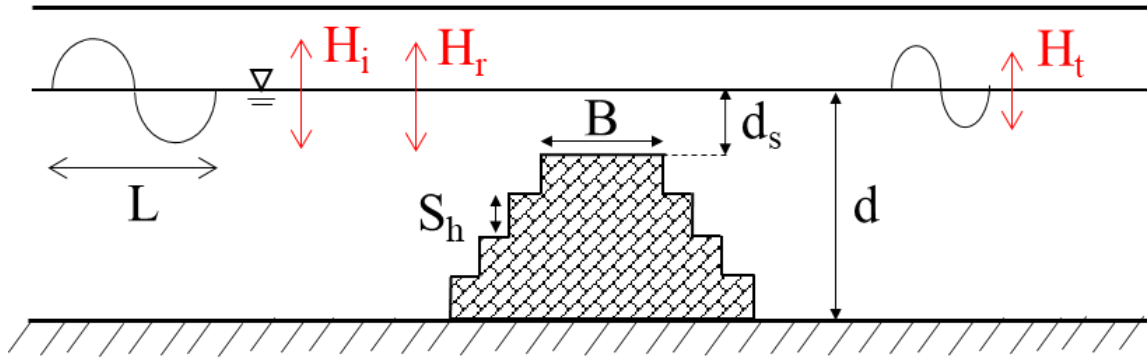
Figure 4.7. The diagram of model parameters in the numerical simulation

The transmitted wave is the energy of an approaching wave that is not reflected or attenuated through the process of wave breaking over a submerged structure. The ability of transmitted wave can be measured from the wave transmission coefficient, K_t. Therefore, the lower transmission coefficient means better wave dissipation of structures, which wave can be more safely transferred to the shoreline.

4.2.3. WAVE REFLECTION

The wave reflection coefficient, K_r, is used to define wave reflection characteristics, which is able to obtain from the ratio of reflected wave height, H_r, to the incident wave height, H_i. The wave reflection coefficient can be calculated from equation (4.19).

$$K_r = \frac{H_r}{H_i} \qquad (4.19)$$

The wave reflection coefficients identify the amount of energy that can be reflected from an approaching wave on the breakwater. However, the design associated with the reflection of incoming waves from coastal structures is also very important to recognize for the damage to surrounding areas, including the danger close to harbor entrances, influences on ship navigation and intensified sediment scour. Therefore, the consideration of wave reflection control also needs to be estimated in coastal engineering.

4.2.4. WAVE ENERGY DISSIPATION

The wave energy dissipation rate can be computed from wave transmission and reflection coefficients, which is given from the equation (4.20).

$$K_d = 1 - K_r^2 - K_t^2 \qquad (4.20)$$

The loss of wave energy due to wave breaking, turbulence, viscous effects and the effects of bottom friction can affect to the decrease in wave height. The results in higher wave energy loss mean better effective wave energy dissipation. Therefore, the total ability of wave energy loss can be estimated from the performance of wave transmission and reflection coefficients.

4.3. RESULTS AND DISCUSSION

In this section, the performance of submerged breakwaters with different stepped sizes were examined on wave transmission coefficient, wave reflection coefficient and wave energy dissipation rate. In order to investigate the efficiency of submerged structures, more than 120

sets of numerical simulations were tested in this study. There were five different stepped sizes (S_h= 0 m, 0.06 m, 0.09 m, 0.18 m, 0.54 m), three different crest widths (B= 0.25m, 0.45m and 0.65m), and two submergence depths (d_s= 0.06m and 0.26m) of models that were conducted with various wave conditions. A set of simulated results was analyzed with various dimensionless variables that were the relative structures' crest width, B/L, the relative submerged depth, d_s/H_i, and the wave steepness, λ.

4.3.1. WAVE TRANSMISSION

The abilities of wave transmission over submerged structures were analyzed on the effect of stepped slopes that were described with the various dimensionless variables in the following subtopics.

(a) Relative structures' crest width, B/L

Figures 4.8 and 4.9 show the relationship between wave transmission coefficient, K_t, and the relative crest width, B/L, in cases of d_s/d=0.1 and d_s/d=0.325, respectively.

The numerical results of five different step heights (S_h= 0 m, 0.06 m, 0.09 m, 0.18 m, 0.54 m) were also compared with the experimental results by Sarhan (2020). The experimental results were tested for wave transmission coefficient with S_h=0.075 m of the stepped submerged breakwater, which are shown as the solid line (H_i/L=0.01) and dash line (H_i/L=0.03) in case of d_s/d=0.1 and the dash line (H_i/L=0.02) in case of d_s/d=0.325. The empirical relations to estimate the transmission coefficient for impermeable model was also provided from the experimental study, which is presented in equation (4.21).

$$K_t = 0.005\lambda^{0.08}(B/d)^{-0.21}(1 - d_s/d)^{-2.24} \qquad (4.21)$$
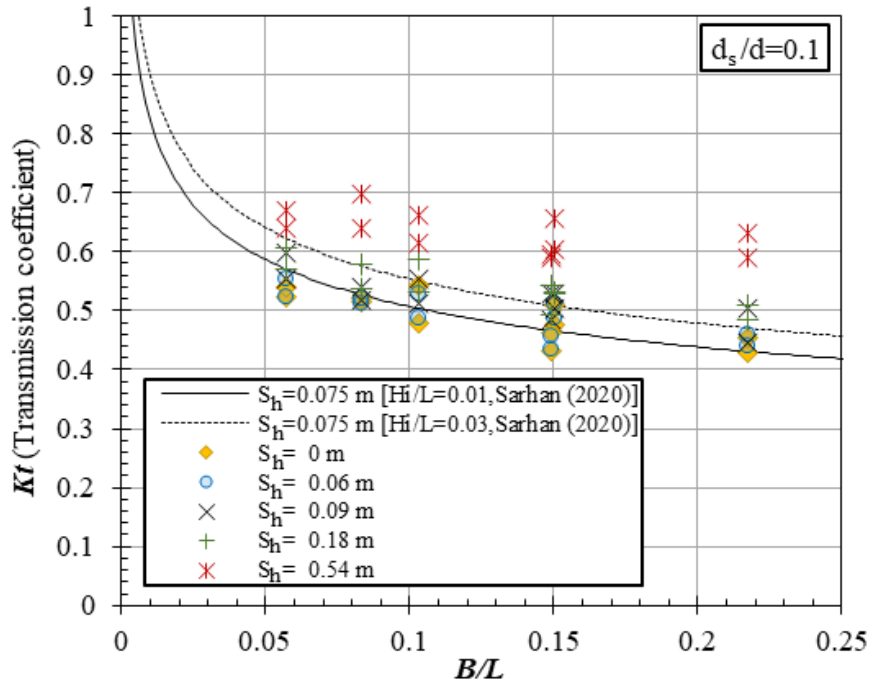
Figure. 4.8. The effect of relative crest width of d_s/d=0.1 on wave transmission coefficient
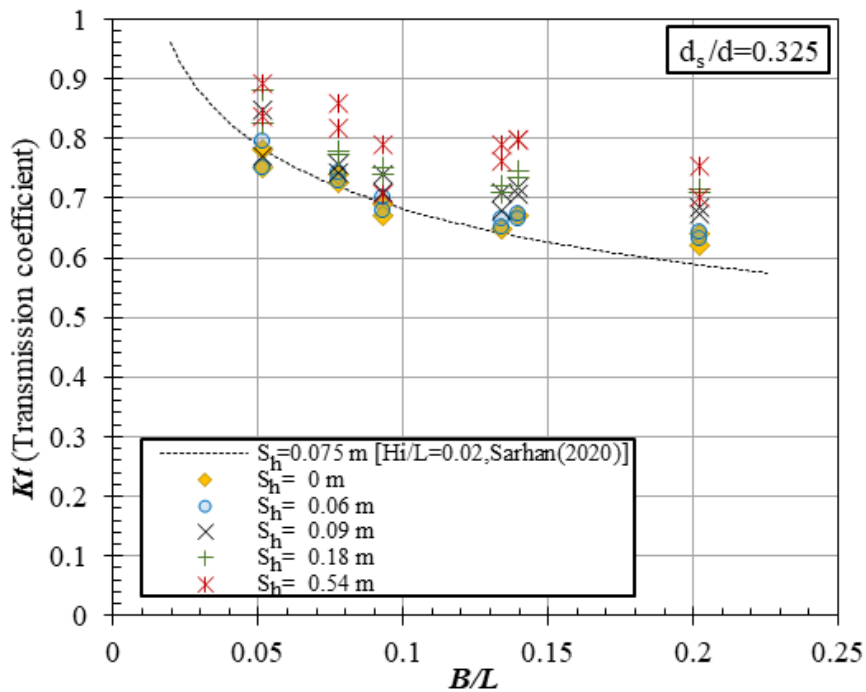
Figure. 4.9. The effect of relative crest width of d_s/d=0.325 on wave transmission coefficient

62

From the above Figures, the graphs showed a good agreement between numerical simulation results and experimental results (Sarhan, 2020). The increased relative crest width (*B/L*) provided an effective wave transmission coefficient.

In terms of the effect of varying stepped sizes on submerged structures, the smooth and small roughness surface slopes can provide an effective wave transmission. The difference between S_h=0 m (smooth slope) and S_h=0.06 m (micro rough slope) seemed to have negligible effect between these two cases, whereas the bigger stepped heights such as S_h=0.18 m (composite slope) or S_h= 0.54 m (vertical structure) have more apparently influence on transmission coefficient. However, the computational results showed that the bigger stepped heights had a lower ability on wave transmission.

For the comparison on different submergence depths, a smaller submergence ratio was better to reduce wave transmission than a larger submergence depth.

(b) Relative submerged depth, d_s/H_i

The relationship between wave transmission coefficient, K_t, and the relative submerged depth, d_s/H_i, is shown in Figure 4.10. The numerical results were compared with the experimental results by Bleck and Oumeraci (2001), which was showed as the solid line. The experiments were tested under various wave conditions with three different heights of the vertical submerged breakwaters (S_h= 0.4 m, 0.5 m and 0.6 m). The experimental study also presented the empirical equation to predict the relationship between wave transmission and the relative submerged depth, which is presented in equation (4.22).

$$K_t = 1 - 0.83 \exp(-0.72\frac{d_s}{H_i}) \tag{4.22}$$
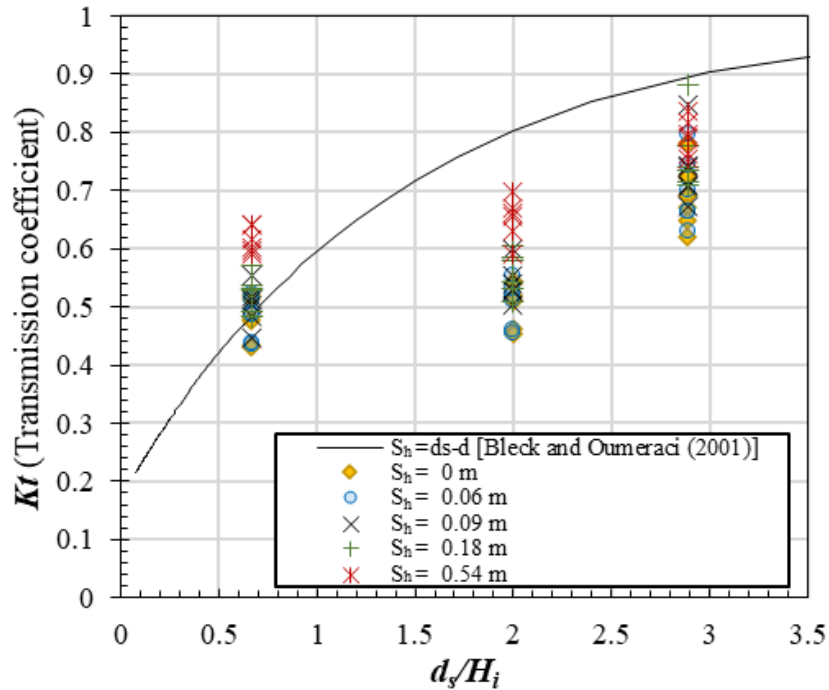
Figure. 4.10. The effect of relative submerged depth, d_s/H_i, on wave transmission coefficient

According to Figure 4.10, the results can be proposed that wave transmission coefficients increase with the increased relative submergence depth, d_s/H_i. The raising up of wave transmission coefficient means that the ability of wave transmission is dropped with the increased relative submerged depth, d_s/H_i. The gentler surface slopes on structures such as a smooth slope (S_h= 0 m) and a micro rough slope (S_h =0.06 m) provided the better results than a composite breakwater (S_h= 0.18 m) and vertical shape (S_h= 0.54 m).

(c) Wave steepness, λ

The relationship between wave transmission coefficient, K_t, and wave steepness, λ, in cases of d_s/d=0.1 and d_s/d=0.325 are presented in Figures 4.11 and 4.12, respectively.
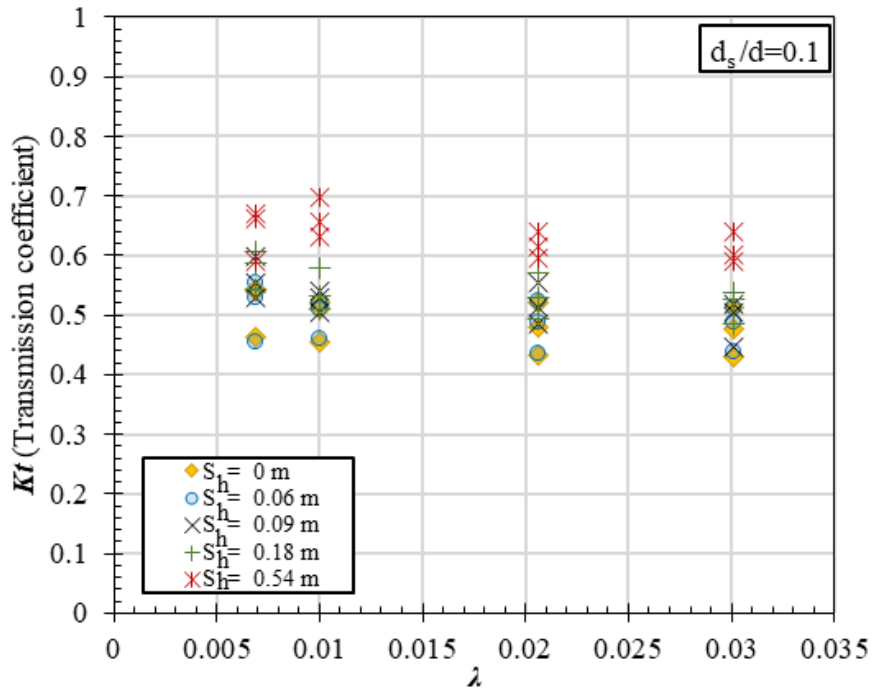
Figure. 4.11. The effect of wave steepness of d_s/d=0.1, on wave transmission coefficient
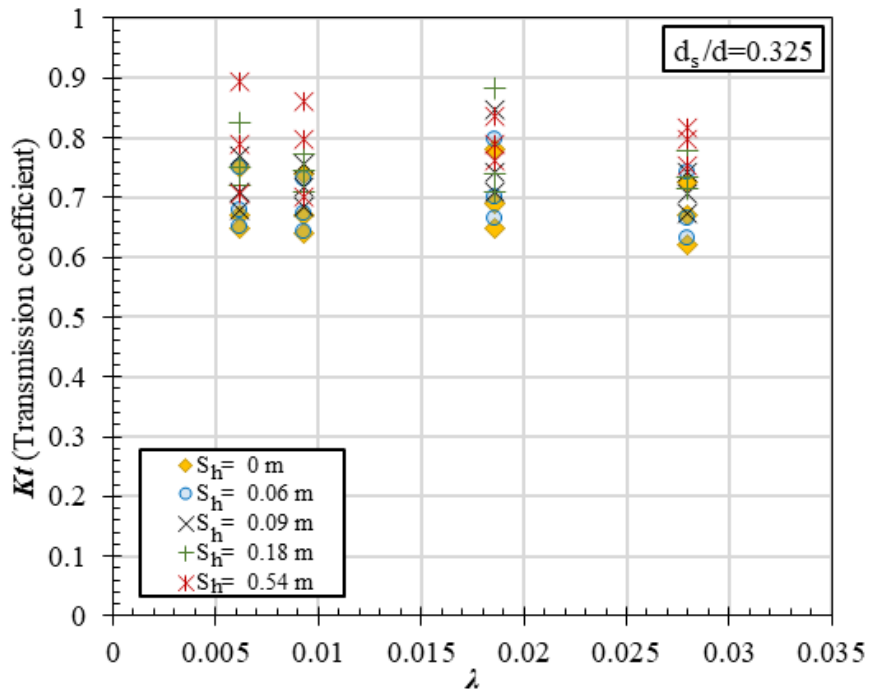
Figure. 4.12. The effect of wave steepness of d_s/d=0.325 on wave transmission coefficient

Figures 4.11 and 4.12 showed that the effective wave transmission can be obtained with the increased wave steepness, λ. For the comparison of different submergence ratios (d_s/d), wave was dissipated better in the shallow submerged depth than the deeper one. In terms of varying stepped sizes, the smooth (S_h=0 m) and micro stepped slope (S_h=0.06 m) were better to provide an effective transmitted wave than a composite slope (S_h=0.18 m) and a vertical shape (S_h=0.54 m).

4.3.2. WAVE REFLECTION

In this study, the incident wave and reflected wave were separated by using Goda and Suzuki (1976) method, which were solved by the Fast Fourier Transform technique. A data set of wave separation was collected from the two wave probes in front of the structures. Once the wave elevation data was collected in numerical simulation, the process of wave separation analysis was calculated by MATLAB code. The reflection coefficients identify the amount of energy that can be reflected from an approaching wave on the submerged structures.

In this subsection, the effects of various stepped sizes of submerged structures (S_h= 0 m, 0.06 m, 0.09 m, 0.18 m, 0.54 m) were examined on the performance of wave reflection, which were described with the relative structures' crest width, B/L, the relative submerged depth, d_s/H_i, and the wave steepness, λ.

(a) Relative structures' crest width, B/L

The relationship between wave reflection coefficient, K_r, and relative crest width, B/L, in cases of d_s/d=0.1 and d_s/d=0.325 are shown in Figs. 4.13 and 4.14, respectively. The numerical results were also plotted with a trend line for each case of stepped heights.
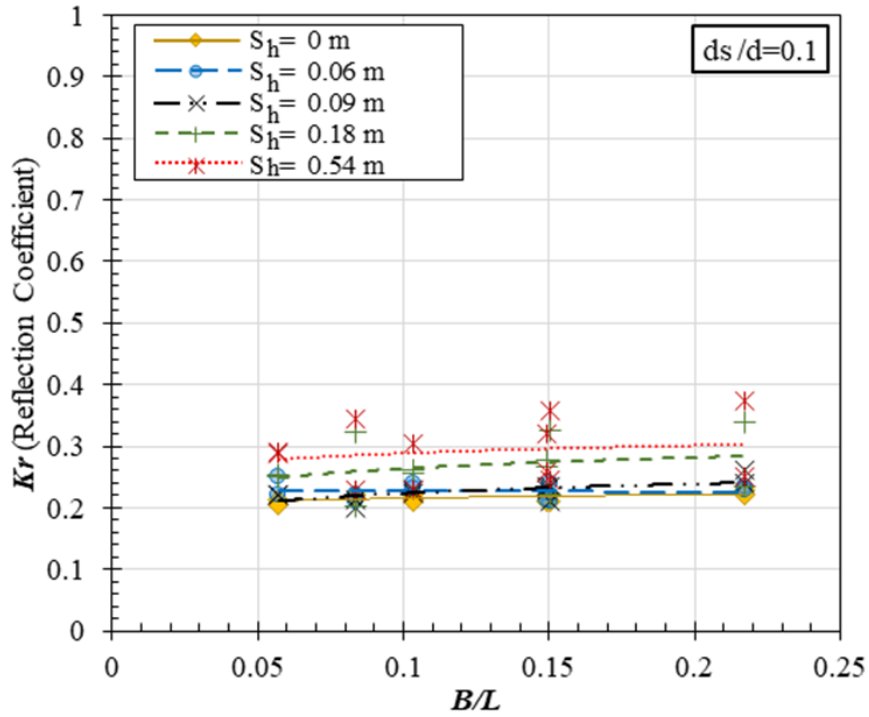
Figure. 4.13. The effect of relative crest width of d_s/d=0.1 on wave reflection coefficient
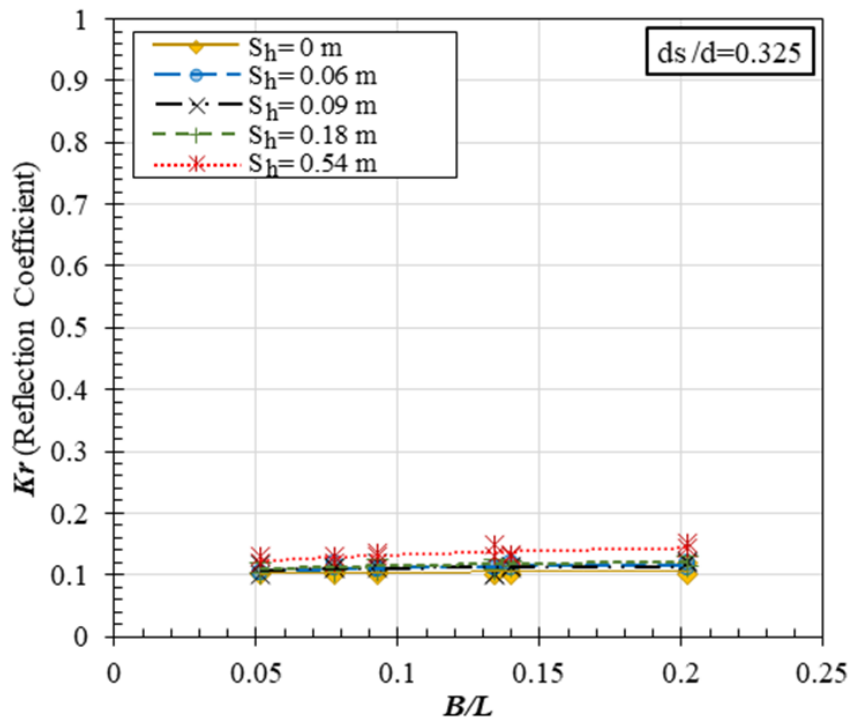
Figure. 4.14. The effect of relative crest width of d_s/d=0.325 on wave reflection coefficient

67

According to Figures 4.13 and 4.14, the wave reflection coefficient tended to slightly increase with the raised up relative crest width, *B/L*. In terms of the effect of stepped slope on structures, the large reflected wave was given from the bigger stepped height as shown in the case of S_h= 0.54m (vertical structure), which became smaller by the gentler surface slope such as smooth slope (S_h= 0 m) and micro rough slope *(S_h= 0.06 m)*. For the influence of submergence depth on the ability of wave reflection, a lower wave reflection was obtained with a deeper submergence ratio

(b) Relative submerged depth, d_s/H_i

Figure 4.15 presents the relationship between wave reflection coefficient, K_r, and the relative submerged depth, d_s/H_i. The numerical results of this study were also compared with the experimental results by Young and Testik (2011), which was represented as the solid line. Young and Testik (2011) revealed the experimental results of wave reflection on a vertical submerged breakwater. The experiments were tested under various wave conditions with S_h= 0.3 m height of the vertical submerged breakwaters. The experimental study also presented the empirical equation to predict the relationship between wave reflection and the relative submerged depth, which is shown in equation (4.23).

$$K_r = 0.53 \exp(-0.85 \frac{d_s}{H_i}) \tag{4.23}$$
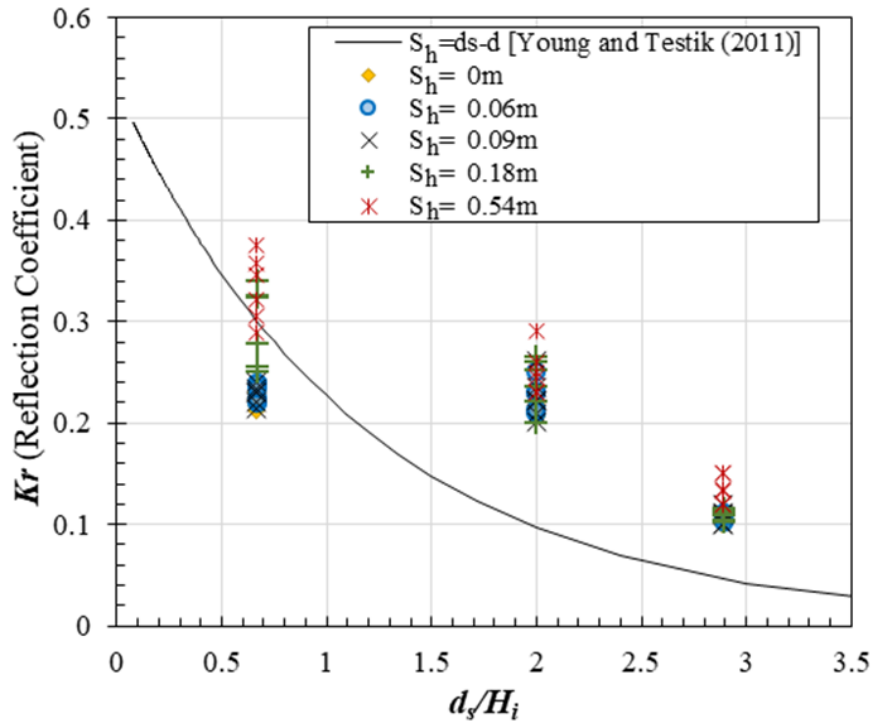
Figure. 4.15. The effect of relative submerged depth, d_s/H_i, on wave reflection coefficient

From the above figure, the performances of five different stepped heights on wave reflection were plotted against the relative submerged depth, d_s/H_i. The numerical and experimental results (Young and Testik, 2011) can be proposed that the wave reflection reduces with the increased relative submerged depth, d_s/H_i. In among of the cases study, the vertical shape of submerged structure reflected a larger wave in comparing with a gentler surface slope. Moreover, the performances of wave reflection were not obviously varied in deeper relative submerged depth.

(c) Wave steepness, λ

The relationship between wave reflection coefficient, K_r, and wave steepness, λ, in cases of $d_s/d=0.1$ and $d_s/d=0.325$ are shown in Figures 4.16 and 4.17, respectively.

Figures 4.16 and 4.17 show that a reflected wave slightly increases with the increased wave steepness, λ. It can be obviously noticed that a large reflected wave can be obtained from the vertical submerged breakwater ($S_h=0.54$ m). The reflected wave became smaller with the decreased stepped heights on the surface slopes. For the effect of submergence ratio (d_s/d), the deeper submerged depth provided a smaller reflected wave than in shallow submergence.

69
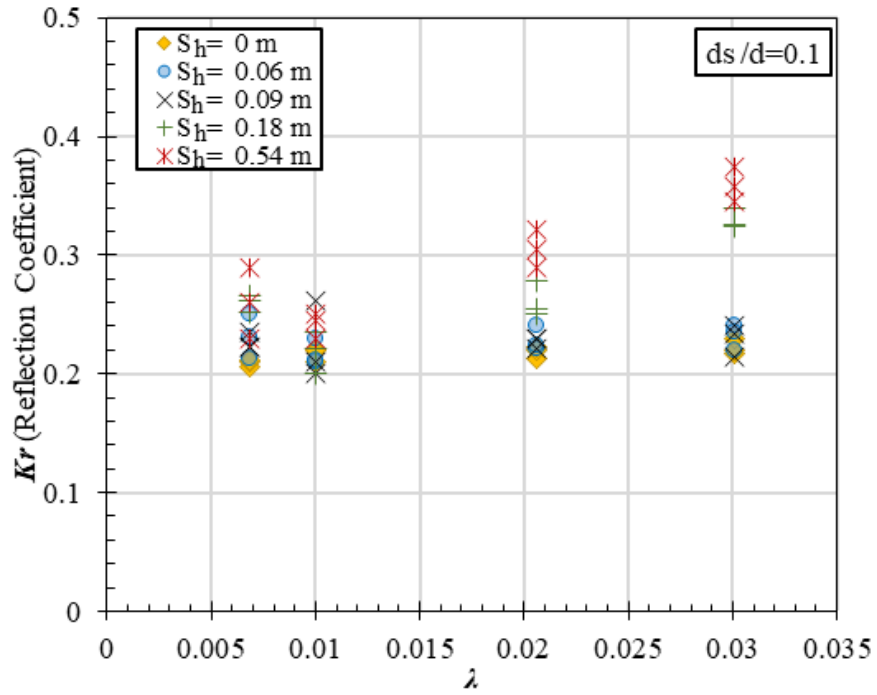
Figure. 4.16. The effect of wave steepness of d_s/d=0.1 on wave reflection coefficient
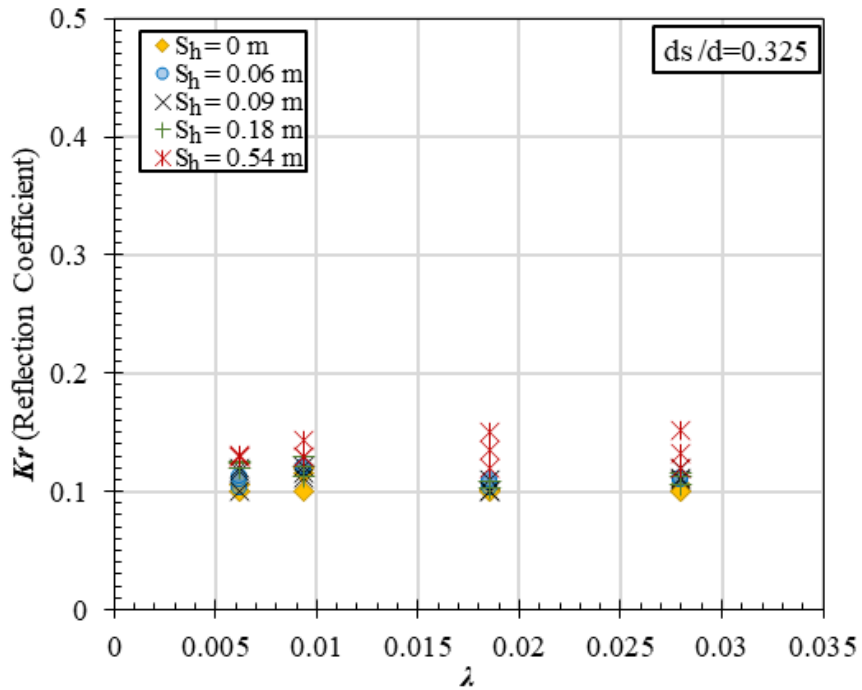
Figure. 4.17. The effect of wave steepness of d_s/d=0.325 on wave reflection coefficient

4.3.3. WAVE ENERGY DISSIPATION

The performance of wave energy dissipation can be computed from wave transmission coefficient and wave reflection coefficient, which is calculated from equation (4.20).

In this subsection, the ability of wave attenuation was described with the relative crest width, B/L, the relative submerged depth, d_s/H_i, and the wave steepness, λ, in the following.

(a) Relative structures' crest width, B/L

Figures 4.18 and 4.19 show the performances of the wave energy dissipation rate for a varying stepped height in the submergence ratio of $d_s/d=0.1$ and $d_s/d=0.325$, respectively. The differing stepped heights of $S_h=0$ m, $S_h=0.06$ m, $S_h=0.09$ m, $S_h=0.18$ m and $S_h=0.54$ m were plotted to compare the efficiency of wave energy dissipation rate, K_d, and related with the relative crest width, B/L.
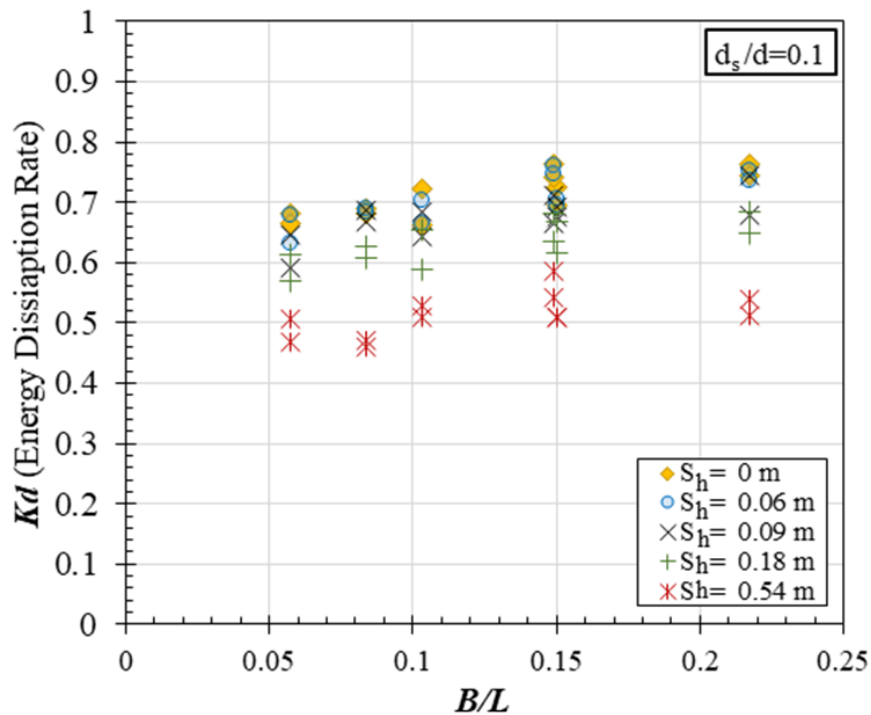
Figure. 4.18. The effect of relative crest width of $d_s/d=0.1$ on wave energy dissipation rate
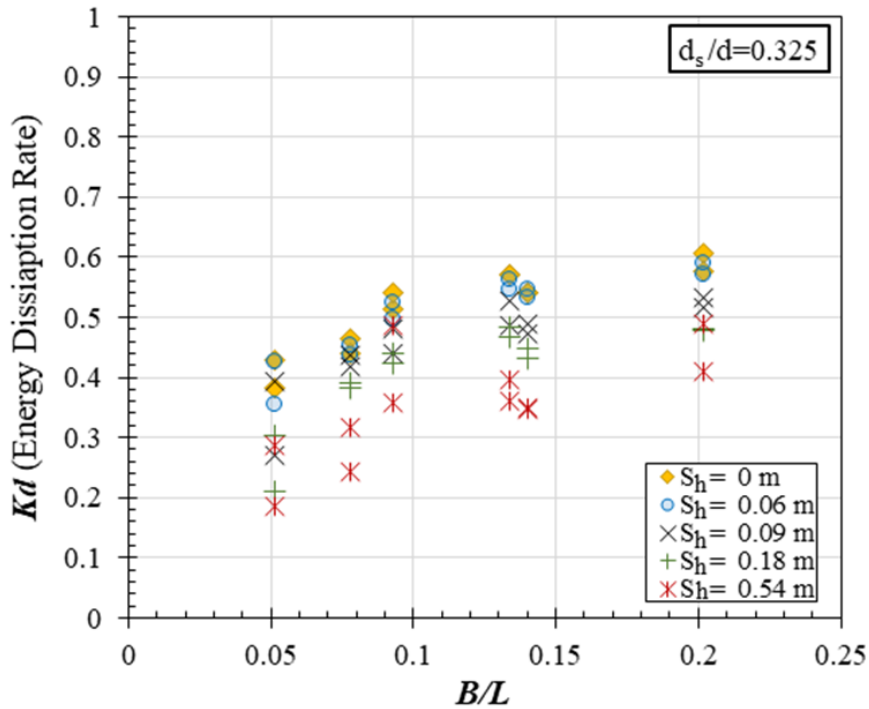
Figure. 4.19. The effect of relative crest width of d_s/d=0.325 on wave energy dissipation rate

According to Figures. 4.18 and 4.19, wave energy loss slightly gained with the increased relative crest width. The diagrams clearly showed that the gentler surface slope tended to provide an effective wave energy dissipation than the bigger stepped height. In terms of the influence due to the change of smooth to small stepped height, the results seemed to have a small effect. In the case of S_h= 0.54 m, the vertical structure evidently had the lowest efficiency on wave energy attenuation among these cases study. However, a better energy dissipation rate can be obtained in a shallow submergence depth.

(b) Relative submerged depth, d_s/H_i

The performance of wave energy dissipation on a varying stepped height versus the relative submerged depth, d_s/H_i that presents in Figure 4.20.
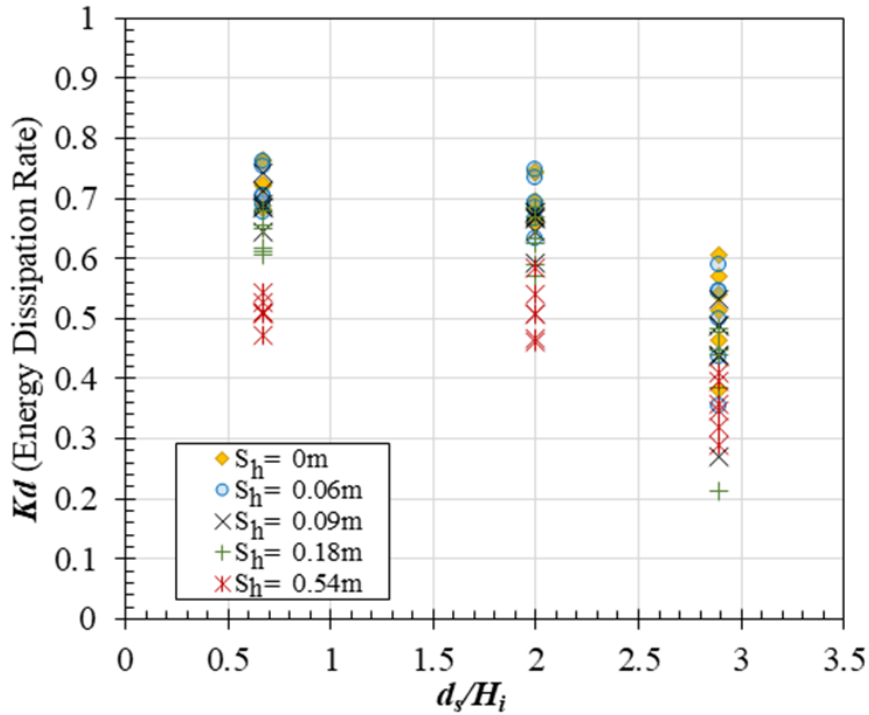
Figure 4.20. The effect of relative submerged depth, d_s/H_i, on wave energy dissipation rate

Figure 4.20 shows that the ability of energy dissipation rate drops down with the increased relative crest width, d_s/H_i. On the effect of structural geometries, the vertical shape ($S_h= 0.54$ m) of submerged breakwater provided a lowest energy dissipation rate, whereas the effective energy dissipation rate can be obtained from a gentler surface slope such as smooth ($S_h= 0$ m) and micro rough slope ($S_h= 0.06$ m).

(c) Wave steepness, λ

The ability of wave energy dissipation on a different stepped height was plotted against wave steepness, λ, which are shown in Figures 4.21 and 4.22 for $d_s/d=0.1$ and $d_s/d=0.325$, respectively.
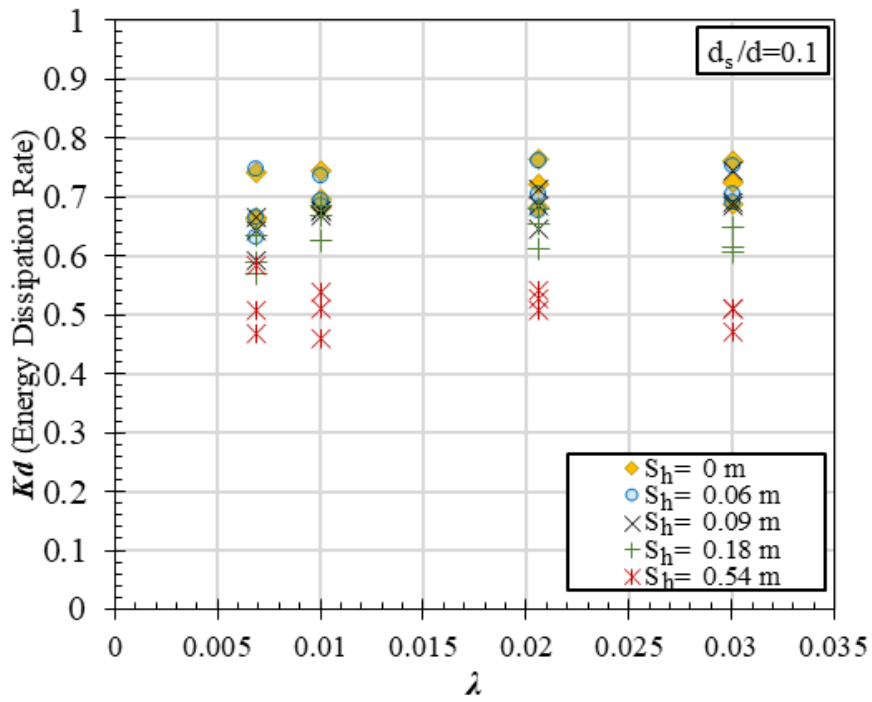
Figure 4.21. The effect of wave steepness of d_s/d=0.1 on wave energy dissipation rate
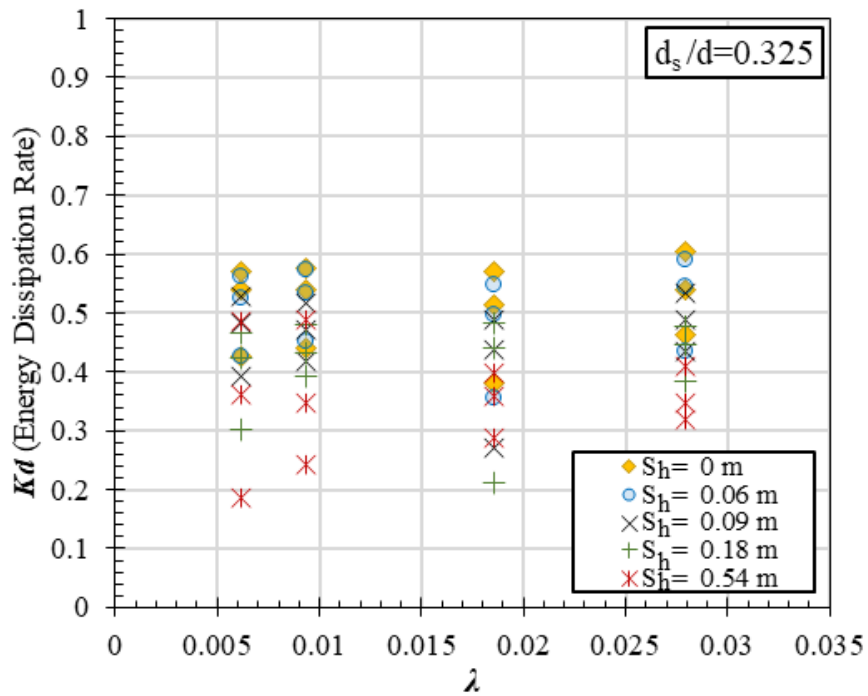
Figure 4.22. The effect of wave steepness of d_s/d=0.325 on wave energy dissipation rate

According to Figures 4.21 and 4.22, the smooth (S_h= 0 m) and micro rough slope (S_h= 0.06 m) were effective shapes in terms of wave energy dissipation. The results clearly showed that the lowest ability in energy dissipation was obtained from the vertical shape of the submerged structure. In terms of the comparison between different submergence ratios, the higher ability in energy dissipation was better to conduct in shallow submergence.

4.4. SUMMARY

This study examines the effects of stepped slope on wave energy dissipation. The efficiencies of a stepped slope were also compared with a smooth and a vertical conventional submerged breakwater, which were presented in a range of stepped heights, S_h, between $0 \leq d\text{-}d_s$. The performances of wave attenuation were analyzed based on the relative crest width, B/L, the relative submerged depth, d_s/H_i, and the wave steepness, λ, which were examined from the viewpoint of wave transmission, wave reflection and wave energy dissipation rate. This study was carried out in two-dimensional model, which was simulated in OpenFOAM software. Wave generation and absorption were applied by OlaFlow solver. In order to separate the incompressible phases of water and air and track the water surface in the model, the Volume of Fluid (VOF) method was applied in this numerical simulation. The processes of wave separation between incident and reflected wave were computed by Goda and Suzuki's (1976) method.

The assessment of wave transmission showed that effective wave transmission can be obtained with the increased relative crest width, B/L, the increased wave steepness, λ, the decreased submergence depth, d_s/H_i and the decreased submergence ratio, d_s/d. According to the effects of different stepped heights, the results can be concluded that wave transmission coefficients decrease with the gentler surface of slope on the submerged structures. In terms of the comparison between the effect of smooth and stepped slope, the change of smooth slope (S_h=0 m) and the small stepped height (S_h=0.06 m) seemed to have negligible effects, whereas an apparent change can be noticed from an expanded stepped height as S_h=0.18 m (composite slope) or S_h=0.54 m (vertical structure).

From the viewpoint of the wave reflection coefficient, a reflected wave slightly increased with the increase in relative crest width, B/L, the increased wave steepness, λ, the decreased submergence depth, d_s/H_i and the decrease in submergence ratio, d_s/d. The comparison between the different stepped heights on structures showed that the vertical structure (S_h= 0.54 m) provided the highest wave reflection among these case studies, which was slightly weakened with the gentler surface slope.

As the wave energy dissipation rates that were computed from wave transmission and reflection coefficients, the results can be concluded that the effective wave energy loss can be given with the increase in relative crest width, *B/L*, the increased wave steepness, λ, the decreased submergence depth, d_s/H_i and the decrease in submergence ratio, d_s/d. The full proficient wave energy attenuation was received from the structures with the intensive surface on the slope. The performance of wave energy loss tended to decrease with the expanded height of the step.

CHAPTER 5

THE BEHAVIOR OF WAVE ATTENUATION THROUGH SUBMERGED BREAKWATERS

Chapter 5

THE BEHAVIOR OF WAVE ATTENUATION THROUGH SUBMERGED BREAKWATERS

In order to observe the behavior of wave dissipation through submerged breakwaters, this chapter mainly describes the effects of structural geometries on the characteristic of wave breaking and the wave interaction with structures, which were analyzed based on turbulence modeling. The turbulence modeling was applied in OpenFOAM® software, which was solved by the OlaFlow solver package. The behaviors of waves were clearly visualized, which was able to analyze the hydrodynamic properties around submerged breakwaters.

This chapter consists of two main sections. The characteristics of wave breaking over different structural geometries are first illustrated with the results of numerical simulation, which are presented from the viewpoint of the instantaneous wave profile and turbulent kinetic energy. Then, it is followed by the behavior of interactive waves on the steps of submerged breakwaters.

5.1. WAVE BREAKING

The main purpose of submerged breakwaters is designed to attenuate the wave energy as coastal protection and beach control devices. The loss of wave energy can be processed due to wave breaking, turbulence and viscous effects, which are influenced by the shapes of structures, disturbance of the water surface, bottom configuration, etc. (Sawaragi, 1995a). The safely transferred waves to the shoreline are obtained where some of the waves are reflected and attenuated through the process of wave breaking over a submerged breakwater. Wave breaking is one of the most important energy transfer mechanisms, where the energy can be attenuated into turbulent kinetic energy, bubble formation, heat transfer, etc. (Lamarre and Melville, 1991; Melville, 1996).

As the analytical results of wave energy dissipation in Chapter 4, the results were mainly computed in terms of wave transmission, wave reflection and wave energy dissipation. Therefore, in order to have clearer visibility on wave energy dissipation due to wave-breaking processes, this section aims to present the behavior of wave breaking over submerged breakwaters. The properties of wave dissipation were presented in the following subsections

that were analyzed from the viewpoints of the instantaneous profiles of the water surface and the turbulent kinetic energy, k, on the water surface.

5.1.1. THE INSTANTANEOUS PROFILES OF WATER SURFACE

According to Chapter 4, the performances of wave energy dissipation were analyzed from the viewpoint of wave transmission coefficients, wave reflection coefficients and wave energy dissipation rates, which were computed from the water surface elevation data. In order to consider the behavior of energy dissipation from wave propagation in numerical simulation, the characteristic of energy loss due to wave breaking, and wave reflection can be primarily noticed from the tracking of water surface elevation.

The instantaneous profiles of the wave propagation over submerged breakwaters with different stepped heights are illustrated in Figures 5.1, 5.2, 5.3, 5.4 and 5.5, which were simulated from the case of T=1.5s of wave period, H_i=0.09m of wave heights and d_s/d=0.1 of submergence ratio. The positions of structures were set at x/L_i=0 in the diagrams. The seaward sides were presented in the negative direction (-) and the landward sides are in the positive direction (+) of the diagrams. The instantaneous wave profiles were captured at 24.7s, 25.5s and 26.2s, which was one of the complete vibrational cycles of the wave period. The diagrams illustrate the comparison of instantaneous profiles of the water surface caused by the effect of different crest widths (B=0.25 m, 0.45 m and 0.65 m) which were simultaneously compared with the case of without any obstructions.

Figure 5.1. Comparison of the instantaneous profiles of water surface elevation on the different crest widths of a smooth slope submerged breakwaters (S_h=0m)

Figure 5.2. Comparison of the instantaneous profiles of water surface elevation on the different crest widths of a micro rough slope submerged breakwaters (S_h=0.06m)

Figure 5.3. Comparison of the instantaneous profiles of water surface elevation on the different crest widths of a macro rough slope submerged breakwaters (S_h=0.09m)

Figure 5.4. Comparison of the instantaneous profiles of water surface elevation on the different crest widths of composite slope submerged breakwaters (S_h=0.18m)
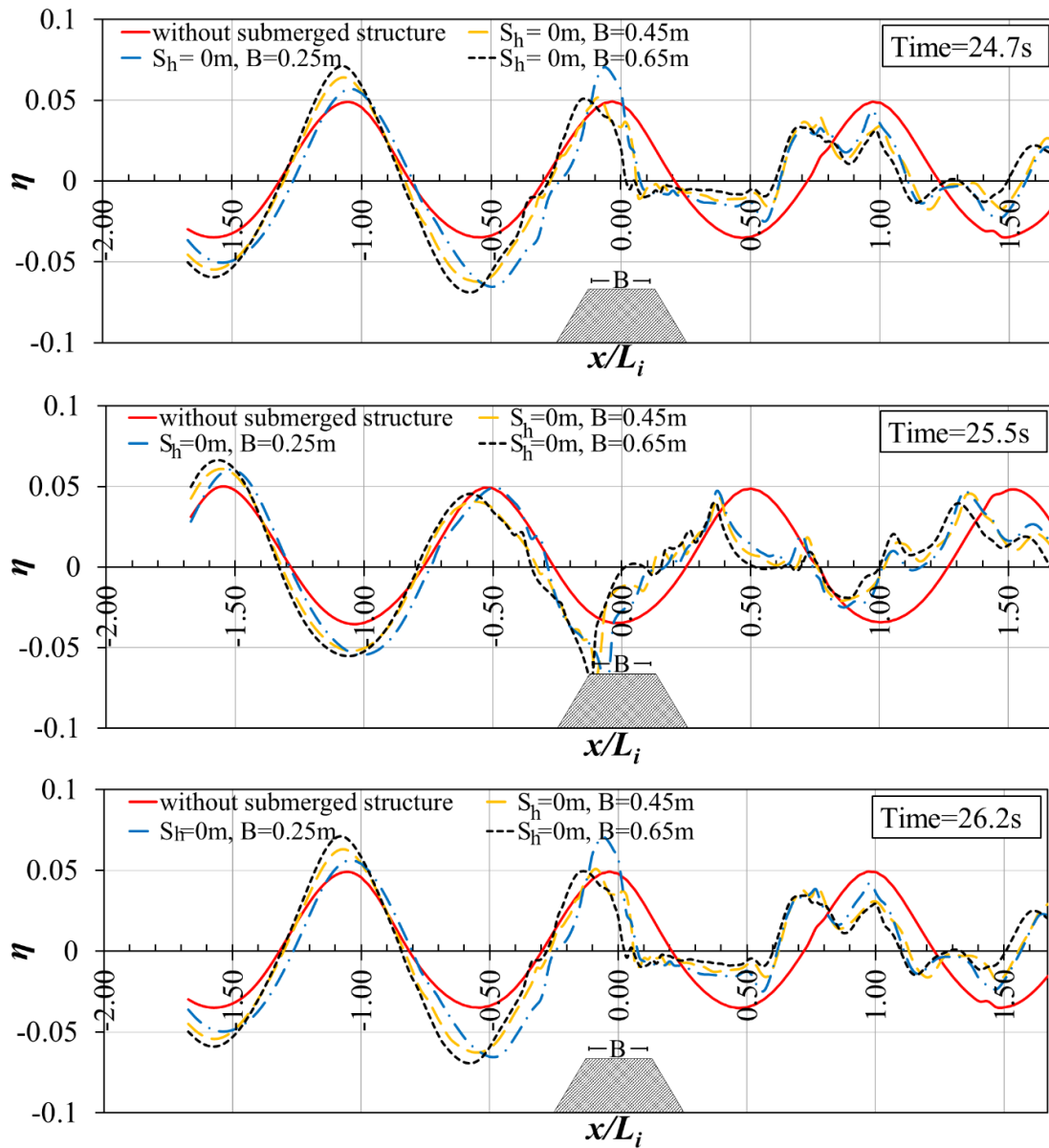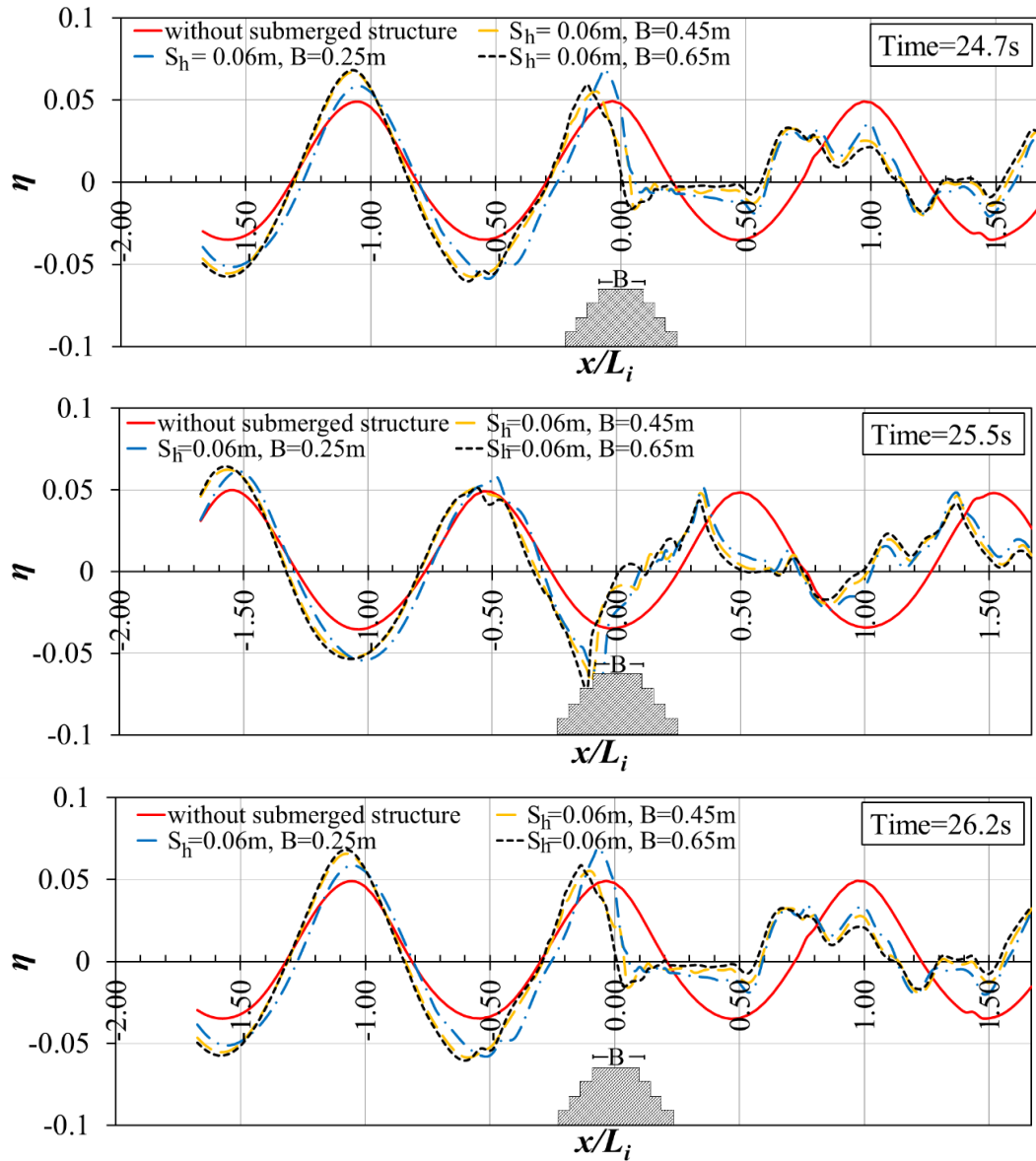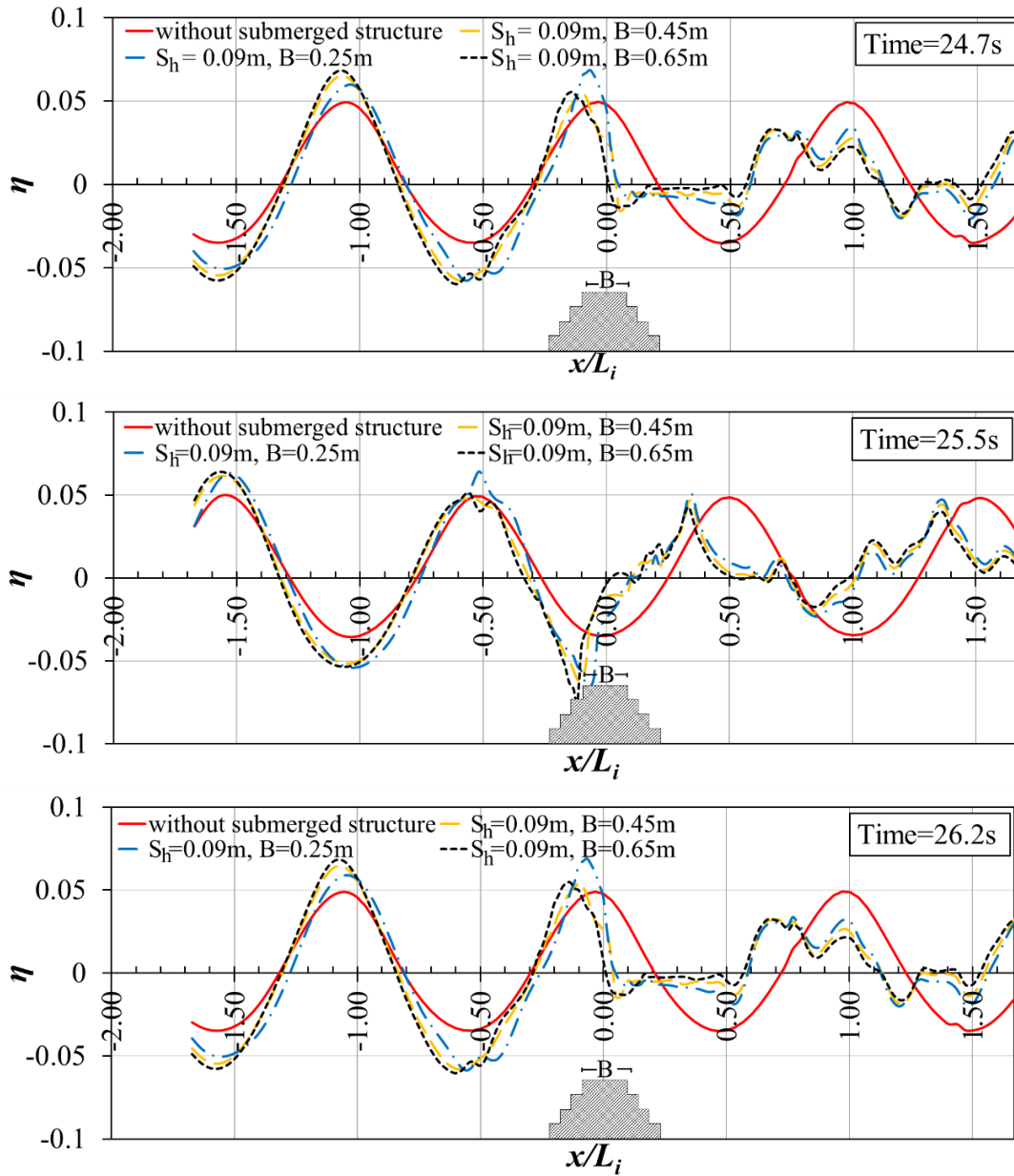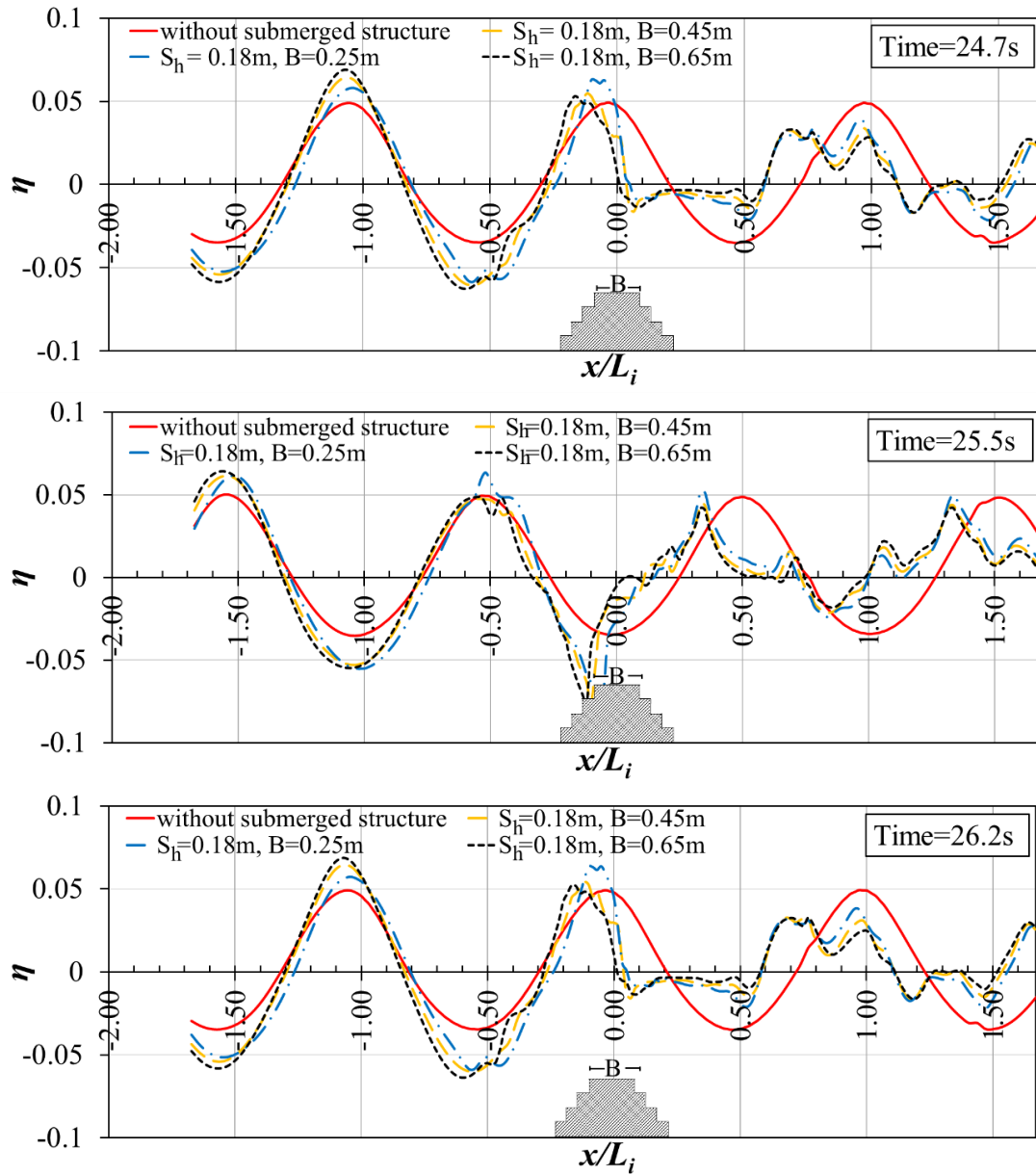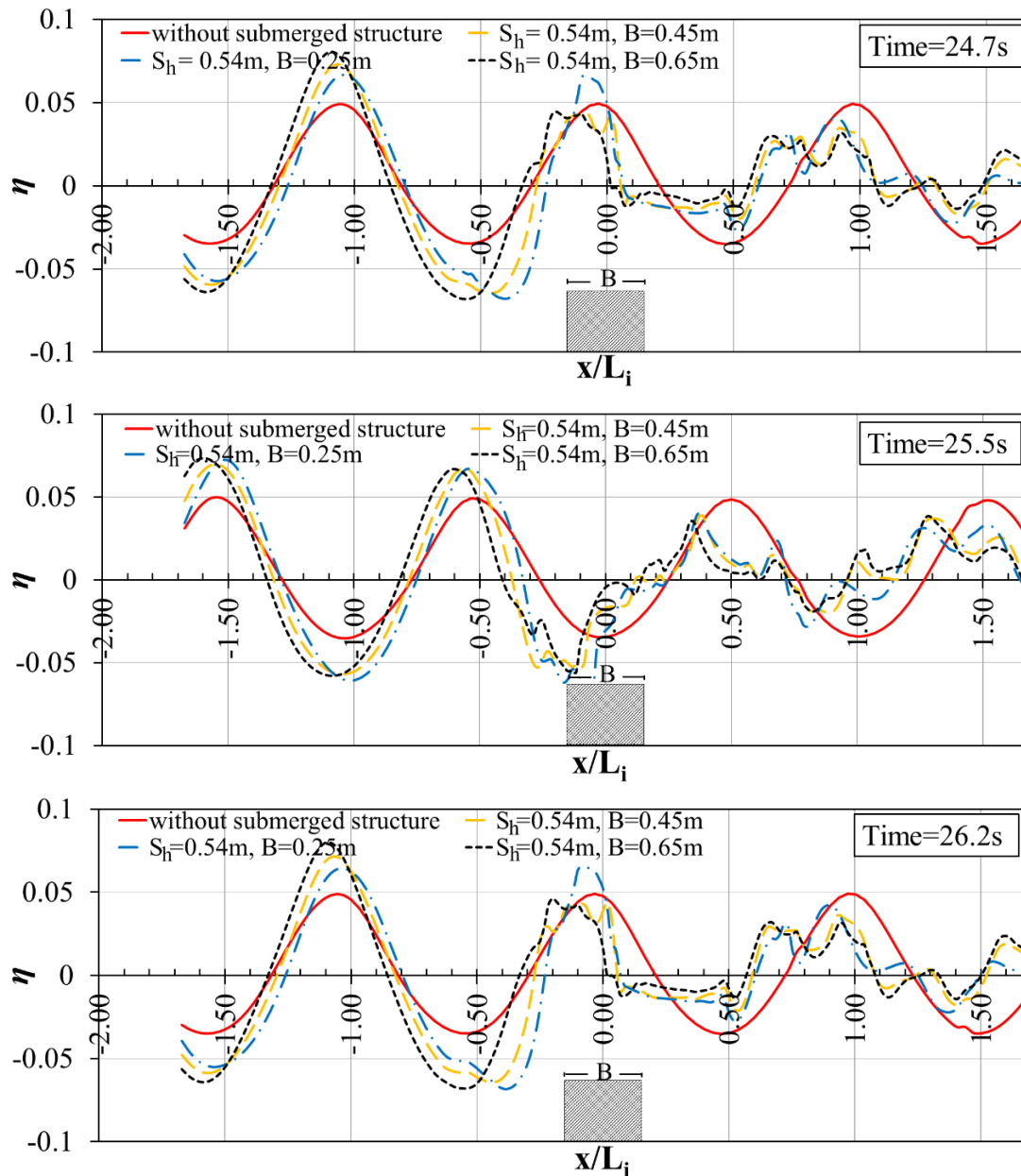
Figure 5.5. Comparison of the instantaneous profiles of water surface elevation on the different crest widths of vertical submerged breakwaters (S_h=0.54m)

According to the comparison of the instantaneous profiles of wave propagation through different crest widths of submerged breakwaters, it can be primarily noted that a reflected wave was presented in front of the structures (in the negative direction of x/L_i). A large reflected wave was obtained from the bigger crest width, which can be noticed in the case of B=0.65m as plotted as a black dot line. The reflected waves were gradually attenuated with the decreased crest widths, which were shown as the cases of B=0.45m (the yellow lines) and B=0.25m (the blue lines), respectively. In terms of the effect of stepped sizes on the wave reflection, it can be

noticed that the vertical shape obviously reflects more waves when it was compared with the gentler surface slope on the structures.

The instantaneous profiles of wave propagation also showed the location of wave breaking. The incoming waves broke over the structures, which were located above structures (at x/L_i=0). Therefore, the incoming wave was dissipated in the wave-breaking process and safely transferred to the landward side (in the positive direction of x/L_i), which caused the smaller transmitted wave height behind the structures.

In addition, the instantaneous wave profiles under different wave conditions are shown in Appendix A.

5.1.2. TURBULENT KINETIC ENERGY

In order to investigate the behavior of wave breaking, turbulent kinetic energy was also used to indicate the energy loss due to the wave breaking process over submerged breakwaters. Physically, turbulent kinetic energy (k) is a fundamental parameter indicative of the strength of turbulence, which is associated with energy dissipation rate. The turbulence model is required to simulate the turbulent characteristics. In this study, the turbulence model was simulated by the k-ω SST turbulence model (Menter, 1994), which was able to capture fluid flow separation. The turbulence kinetic energy is computed by equation (5.1).

$$\frac{d}{dt}(\rho k) = \nabla \cdot (\rho D_k \nabla k) + \rho G - \frac{2}{3}\rho k(\nabla \cdot u) - \rho \beta^* \omega k + S_k \tag{5.1}$$

The snapshots of turbulent kinetic energy (k) over different crest widths for a smooth slope (S_h=0m), a micro rough slope (S_h=0.06m), a macro rough slope (S_h=0.09m), a composite slope (S_h=0.18m) and a vertical shape (S_h=0.54m) of breakwaters are illustrated in Figures 5.6, 5.7, 5.8, 5.9 and 5.10, respectively. The range of turbulent kinetic energy was displayed between 0 and 0.3 m^2/s^2, which represented the intensity of turbulence as the shading color from blue to red. The snapshots of fluid motion were captured from the case of T=1.5s of wave period, H_i=0.09m of wave height and d_s/d=0.1 of the submergence ratio. The evolution of turbulent kinetic energy over submerged breakwaters was captured at Time=24.7s, 25.0s, 25.3s, 25.6s, 25.9s and 26.2s, which represented for the wave propagation for full wave cycle. The

influences of the various crest widths of submerged breakwaters ($B= 0.25$m, $B= 0.45$m and $B= 0.65$m) on the turbulent kinetic energy were also shown in each diagram accordingly.

Moreover, the comparisons of time average of the turbulent kinetic energy, k, on different crest widths for a smooth slope (S_h=0m), a micro rough slope (S_h=0.06m), a macro rough slope (S_h=0.09m), a composite slope (S_h=0.18m) and a vertical shape (S_h=0.54m) of breakwaters are also presented in Figure 5.11. The results were computed from 10 wave periods of wave generation through the submerged breakwaters.

In addition, the evolutions of turbulent kinetic energy (k) over submerged breakwaters in the case of T=1.5s of wave period, H_i=0.09m of wave height and d_s/d=0.325 of the submergence ratio are shown in Appendix B.

Figure 5.6a. The evolution of turbulent kinetic energy over a smooth slope breakwater (S_h=0m) in case of B=0.25m

Figure 5.6b. The evolution of turbulent kinetic energy over a smooth slope breakwater (S_h=0m) in case of B=0.45m
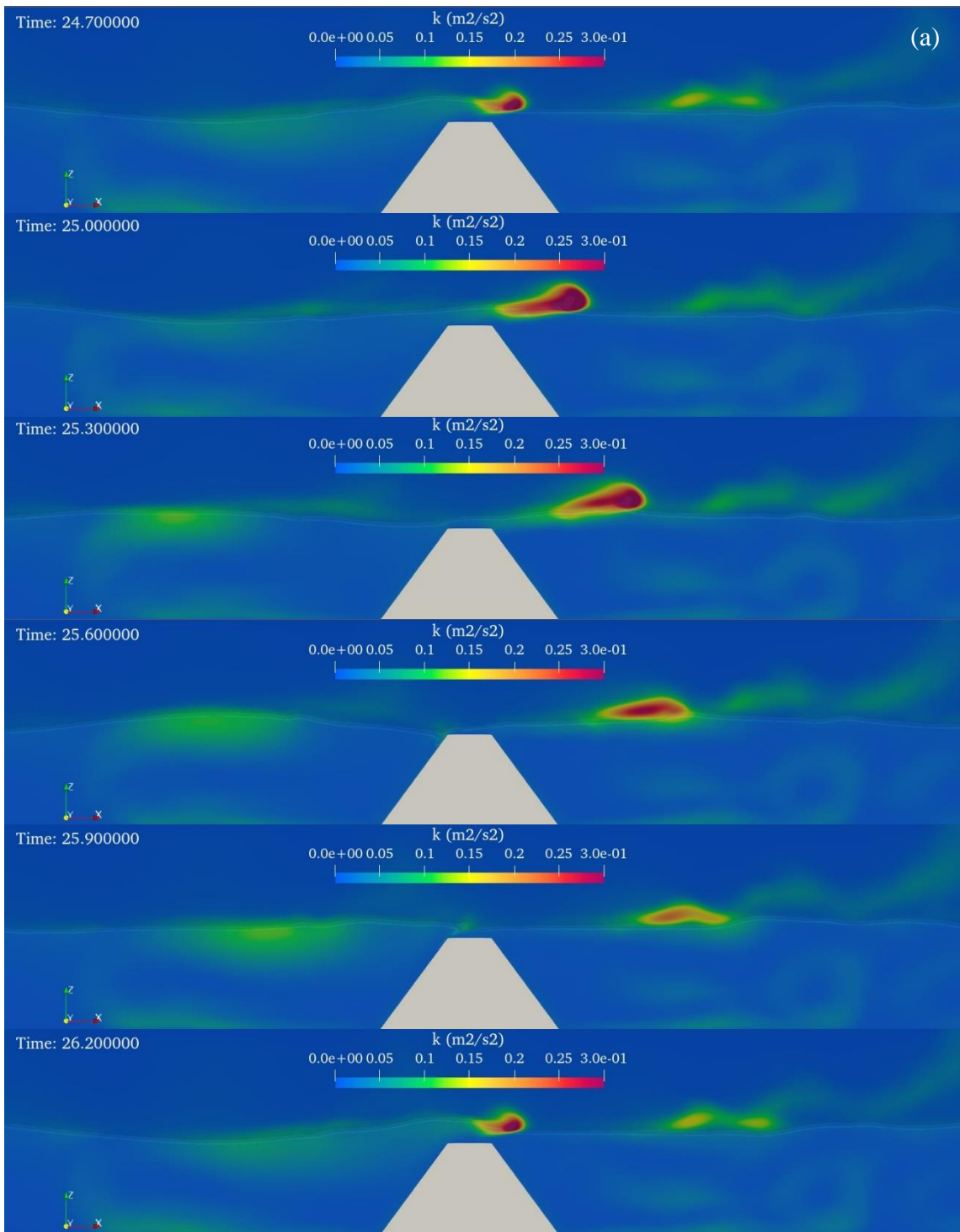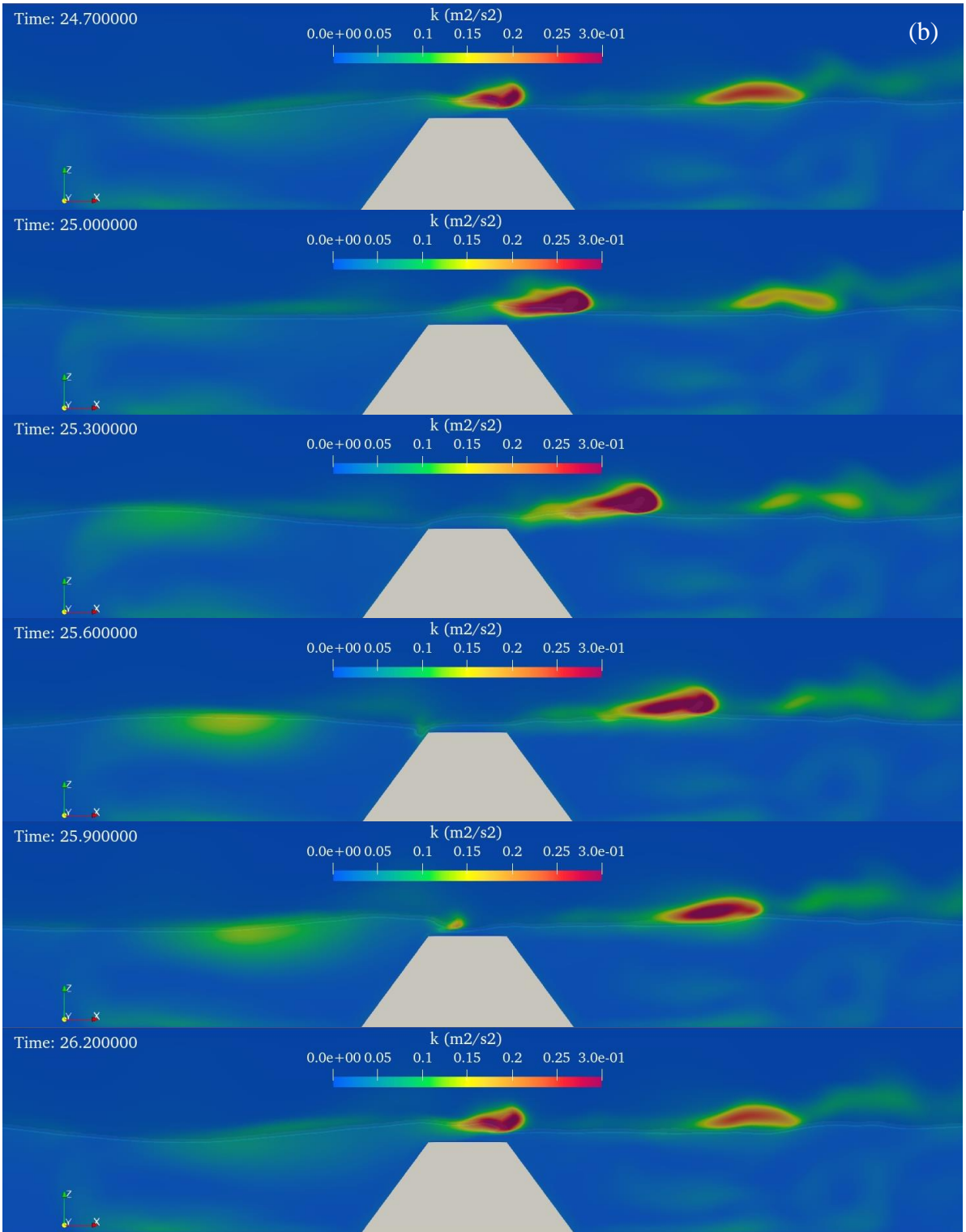
Figure 5.6c. The evolution of turbulent kinetic energy over a smooth slope breakwater (S_h=0m) in case of B=0.65m

Figure 5.7a. The evolution of turbulent kinetic energy over a micro rough slope breakwater (S_h=0.06m) in case of B=0.25m

Figure 5.7b. The evolution of turbulent kinetic energy over a micro rough slope breakwater (S_h=0.06m) in case of B=0.45m
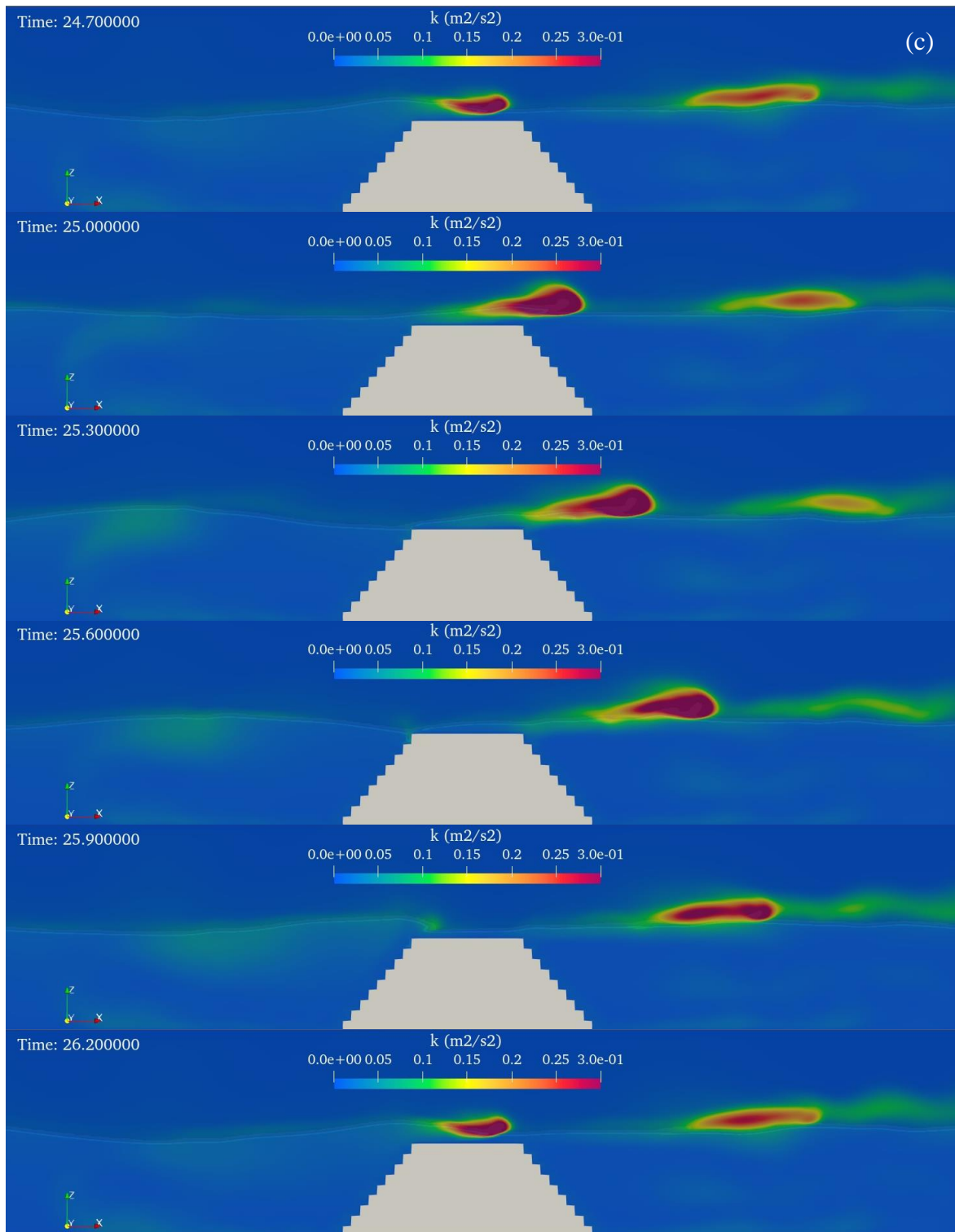
Figure 5.7c. The evolution of turbulent kinetic energy over a micro rough slope breakwater (S_h=0.06m) in case of B=0.65m
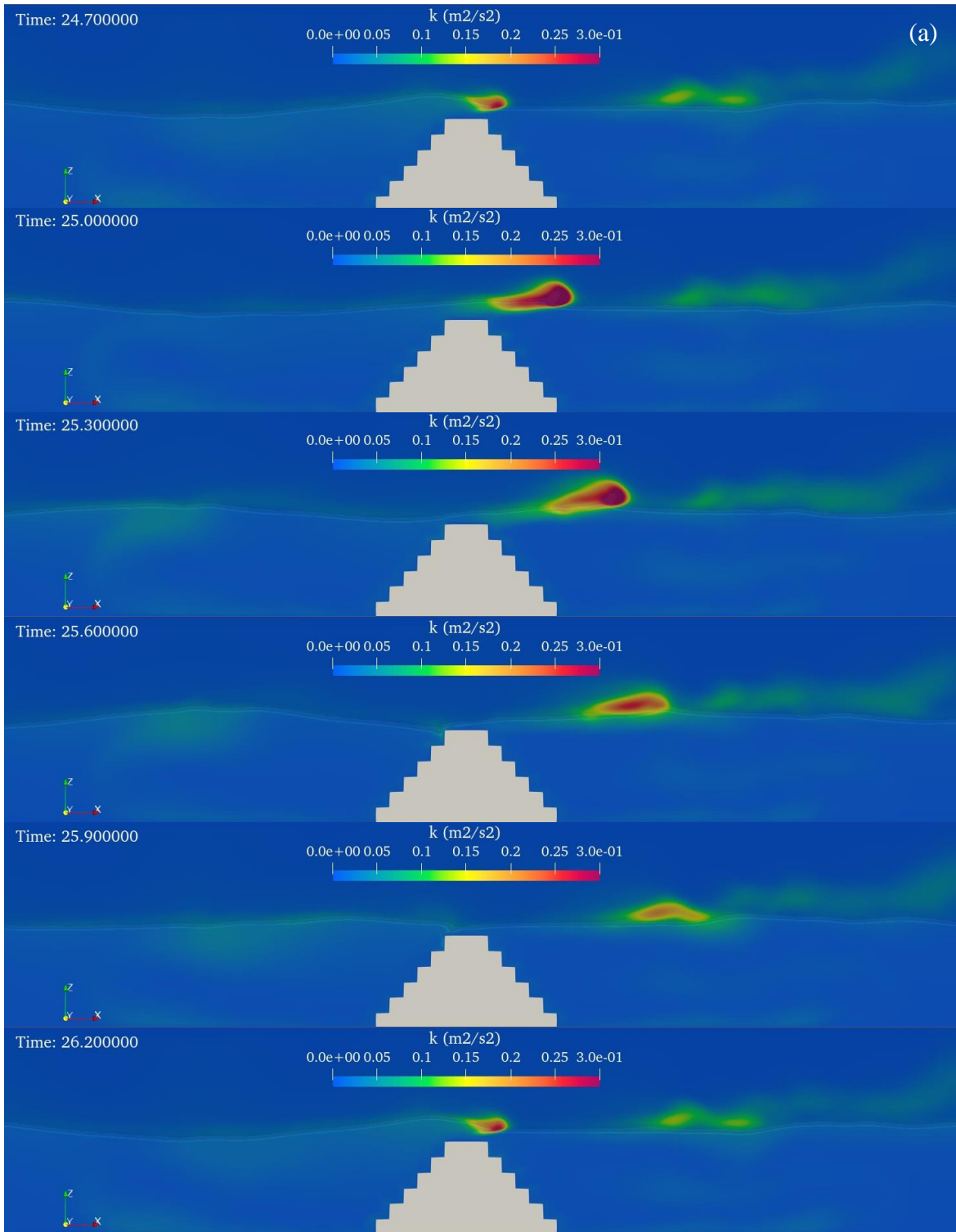
Figure 5.8a. The evolution of turbulent kinetic energy over a macro rough slope breakwater (S_h=0.09m) in case of B=0.25m
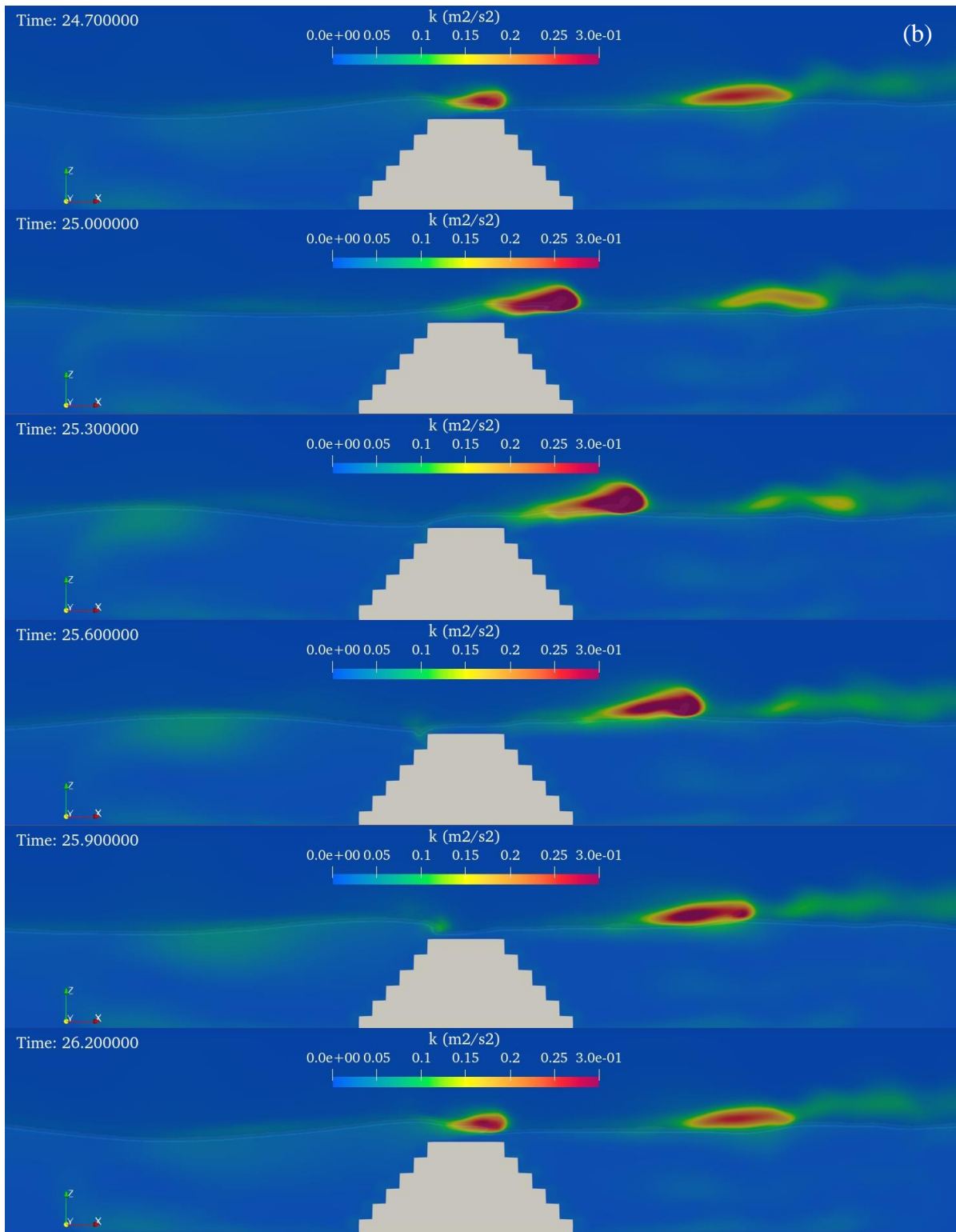
Figure 5.8b. The evolution of turbulent kinetic energy over a macro rough slope breakwater (S_h=0.09m) in case of B=0.45m
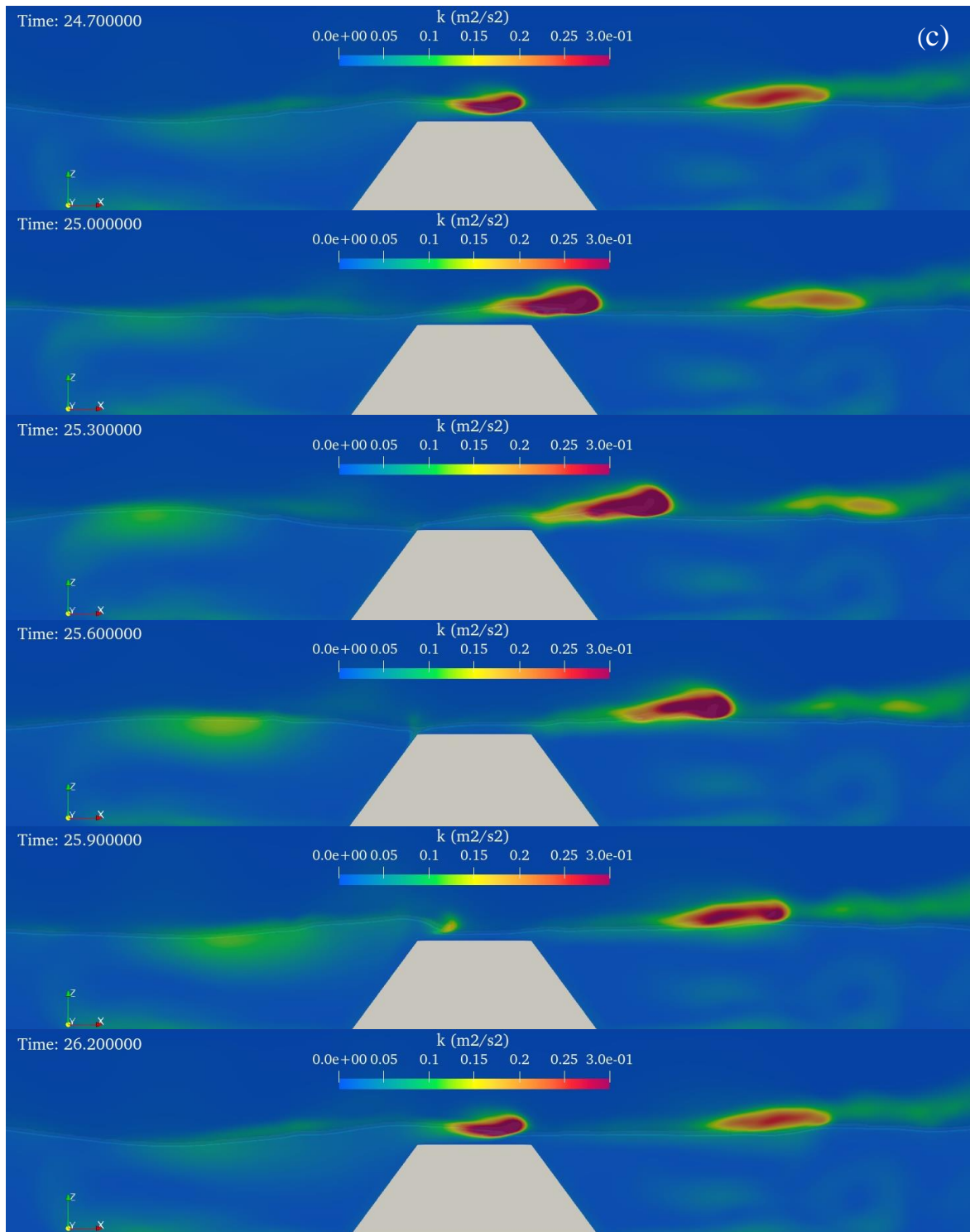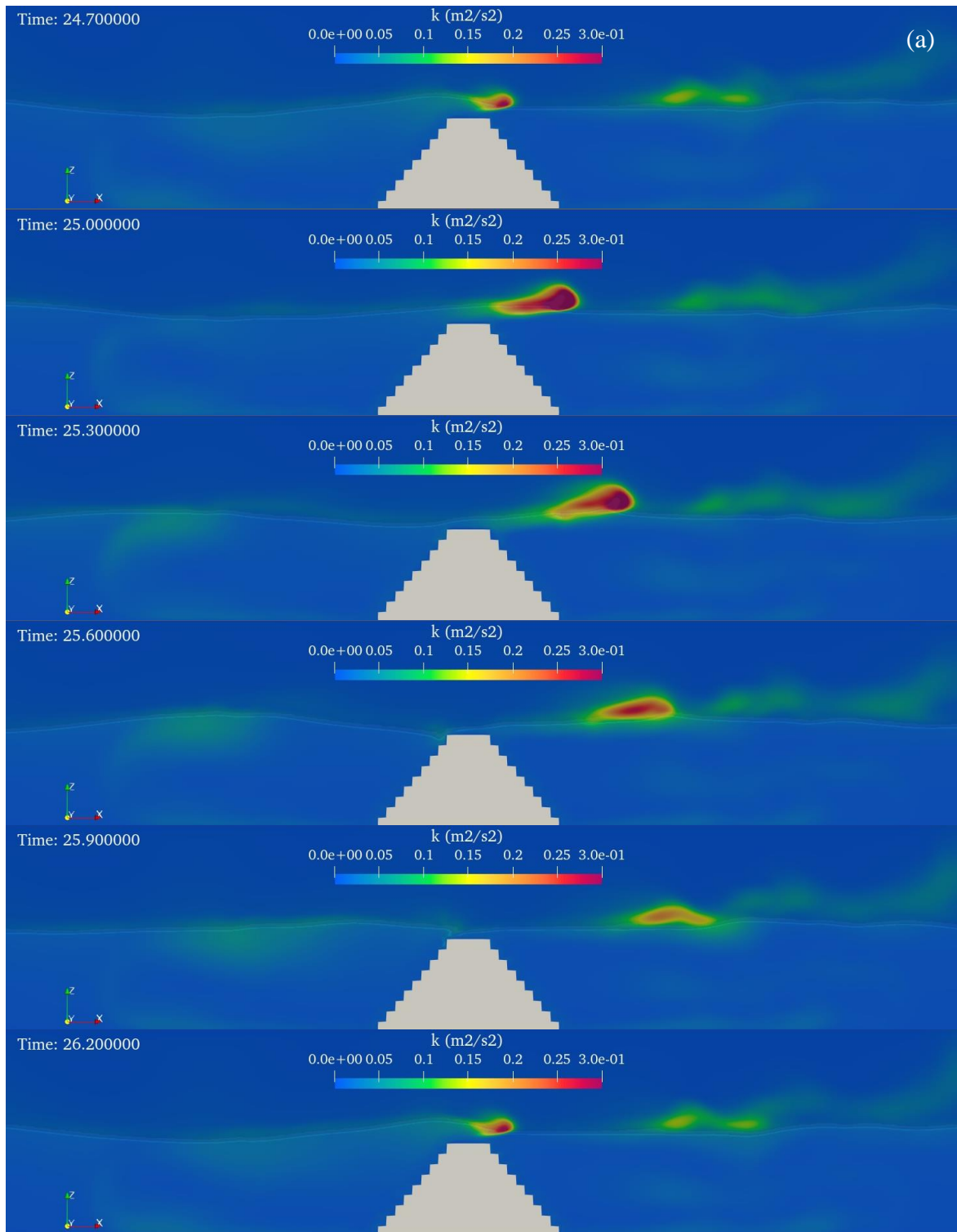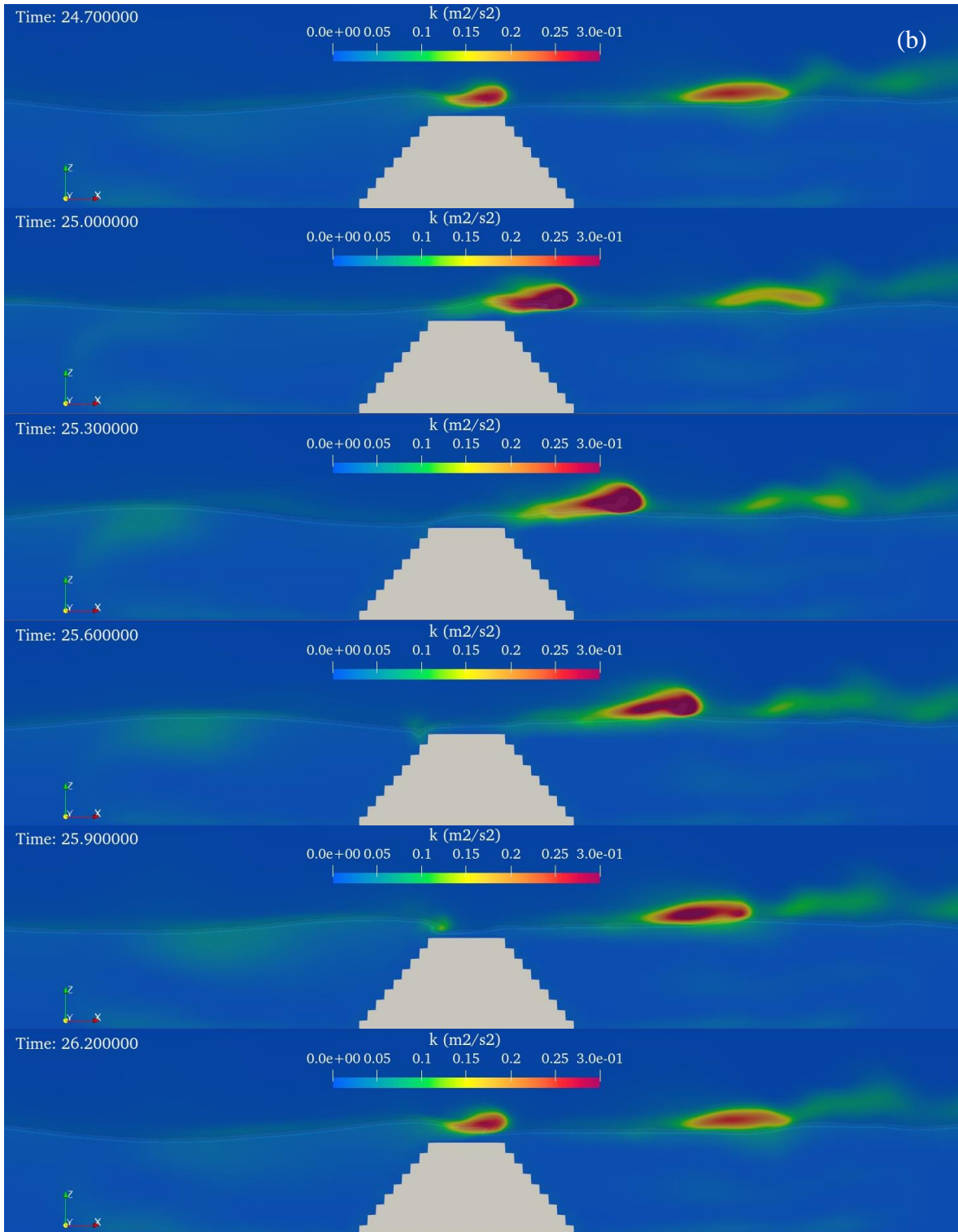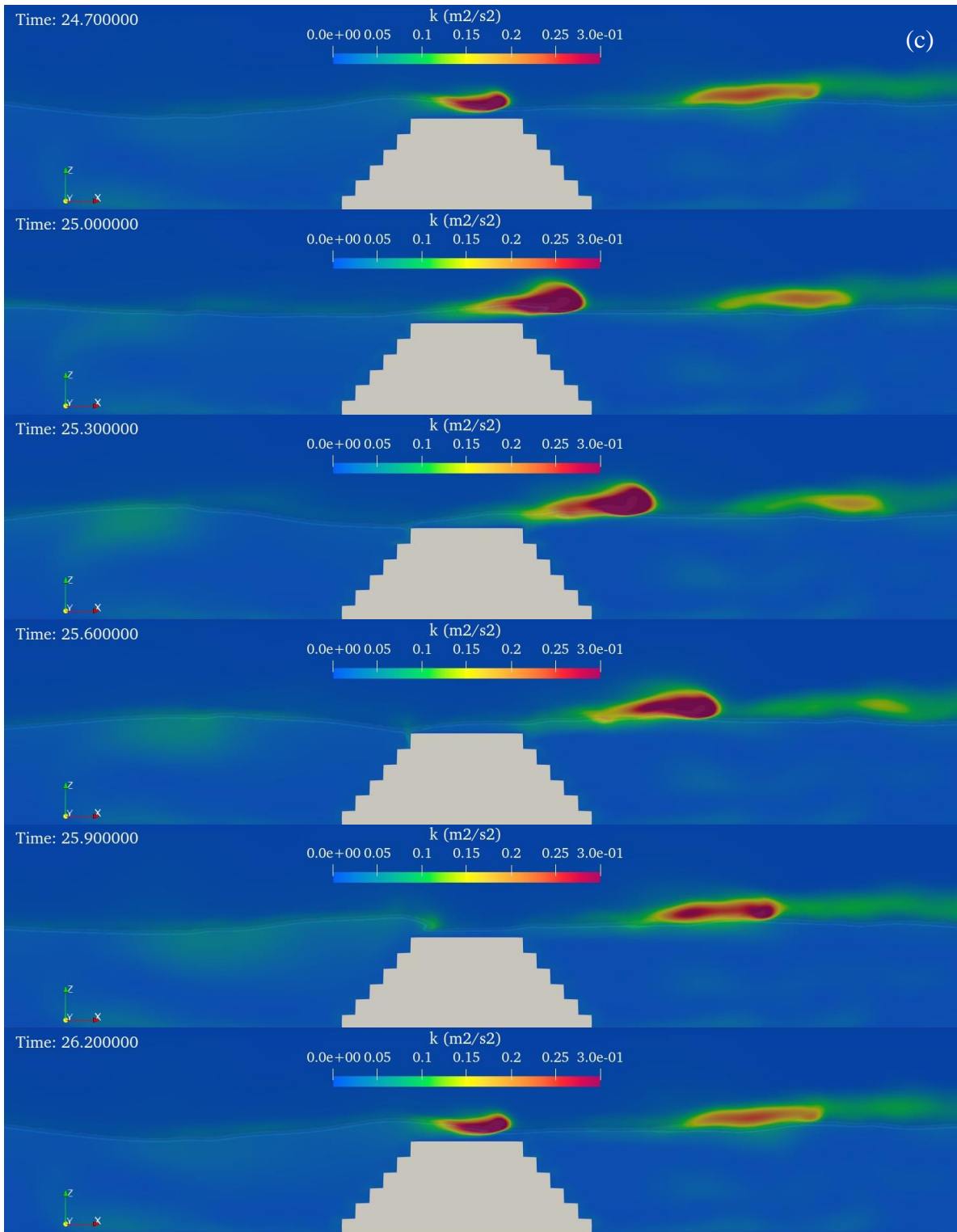
Figure 5.8c. The evolution of turbulent kinetic energy over a macro rough slope breakwater (S_h=0.09m) in case of B=0.65m
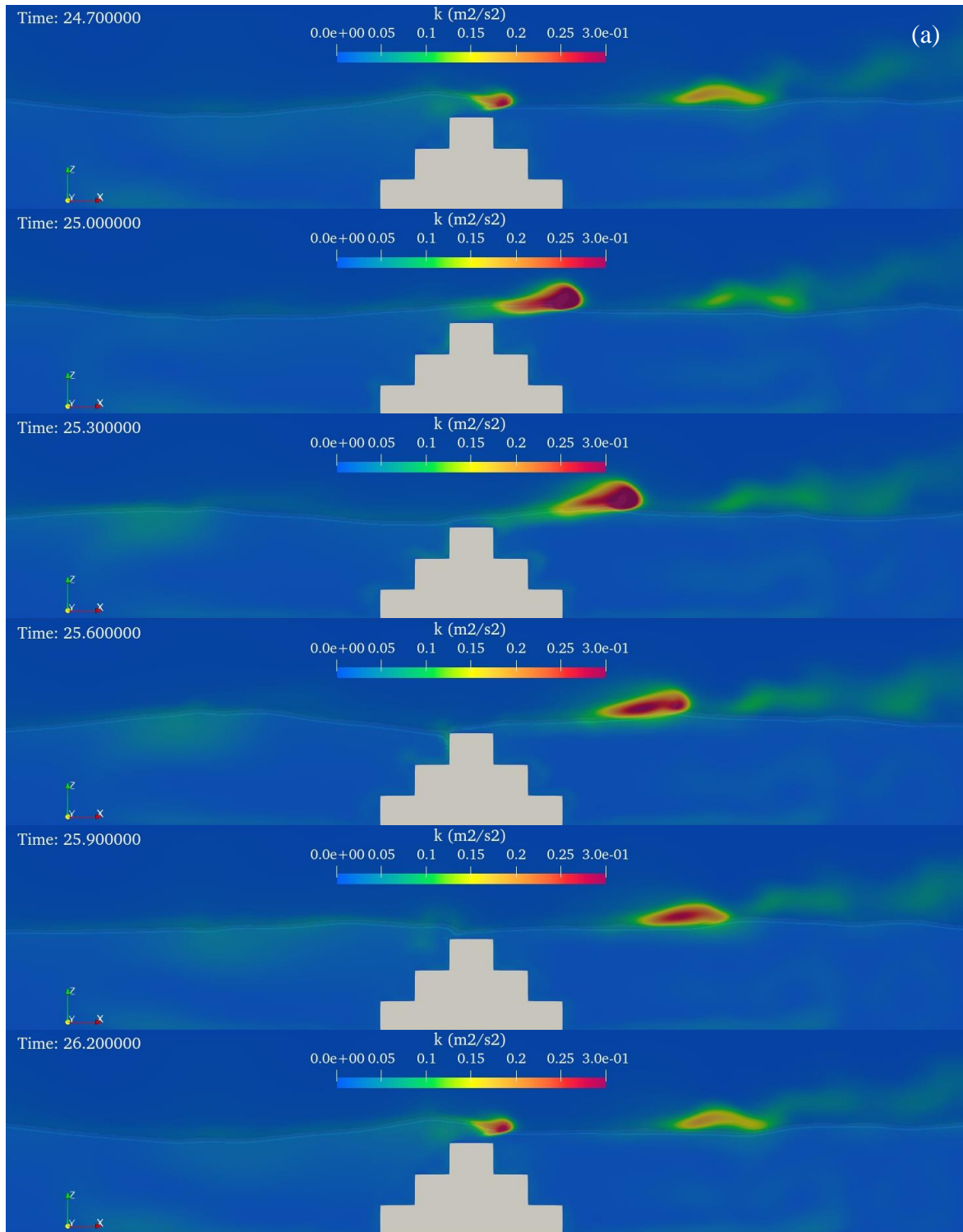
Figure 5.9a. The evolution of turbulent kinetic energy over a composite slope breakwater (S_h=0.18m) in case of B=0.25m
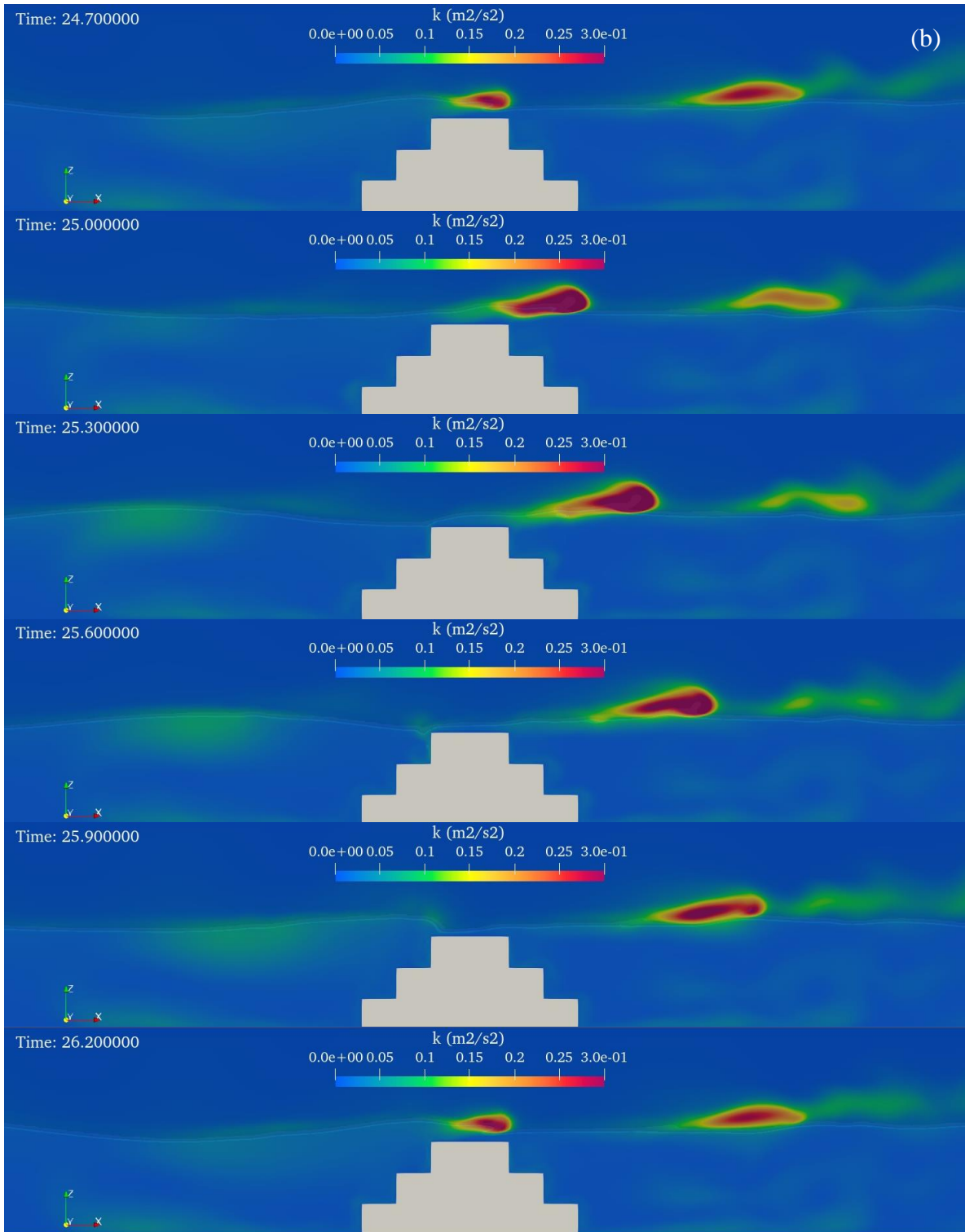
Figure 5.9b. The evolution of turbulent kinetic energy over a composite slope breakwater (S_h=0.18m) in case of B=0.45m
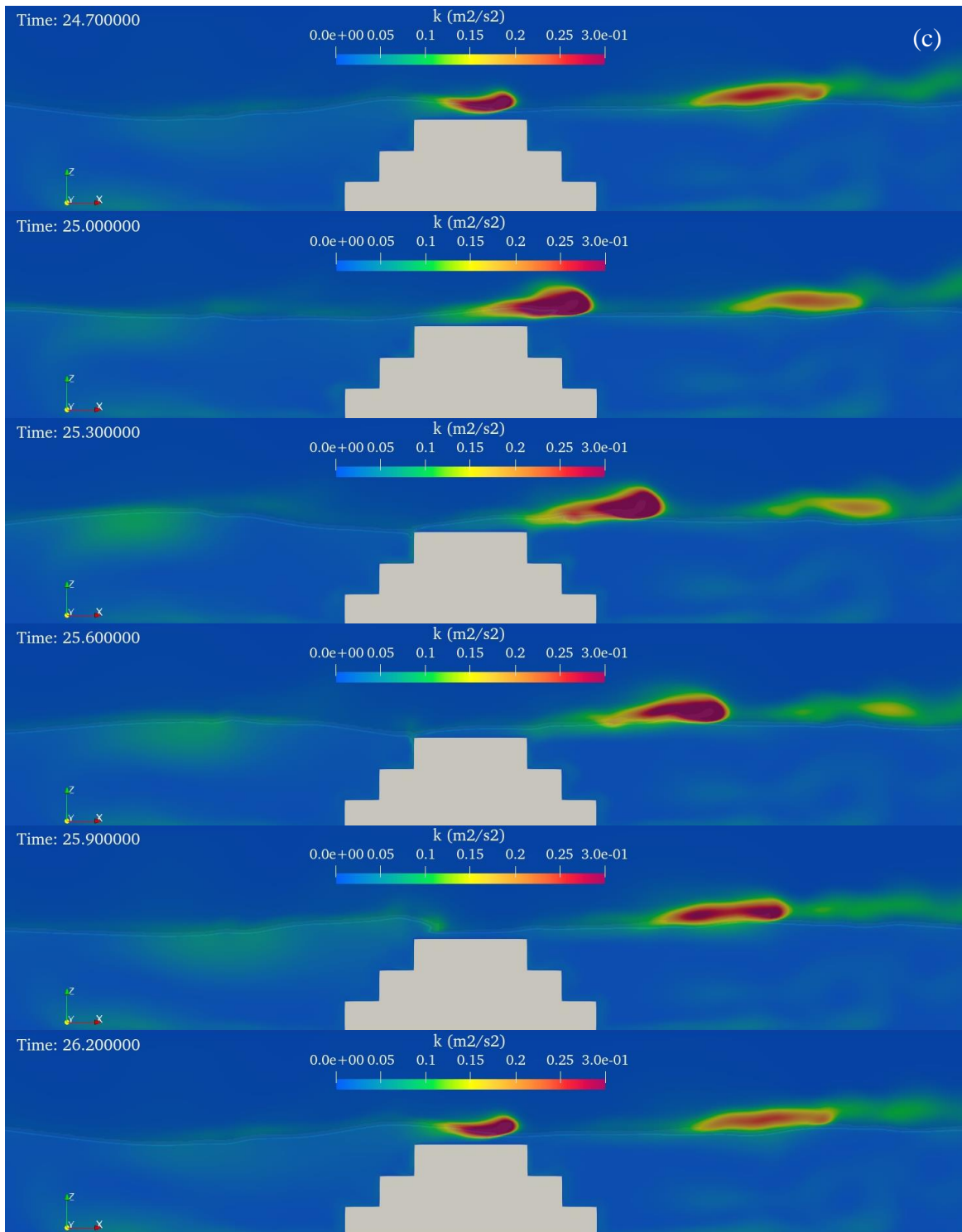
Figure 5.9c. The evolution of turbulent kinetic energy over a composite slope breakwater (S_h=0.18m) in case of B=0.65m

Figure 5.10a. The evolution of turbulent kinetic energy over a vertical breakwater (S_h=0.54m) in case of B=0.25m
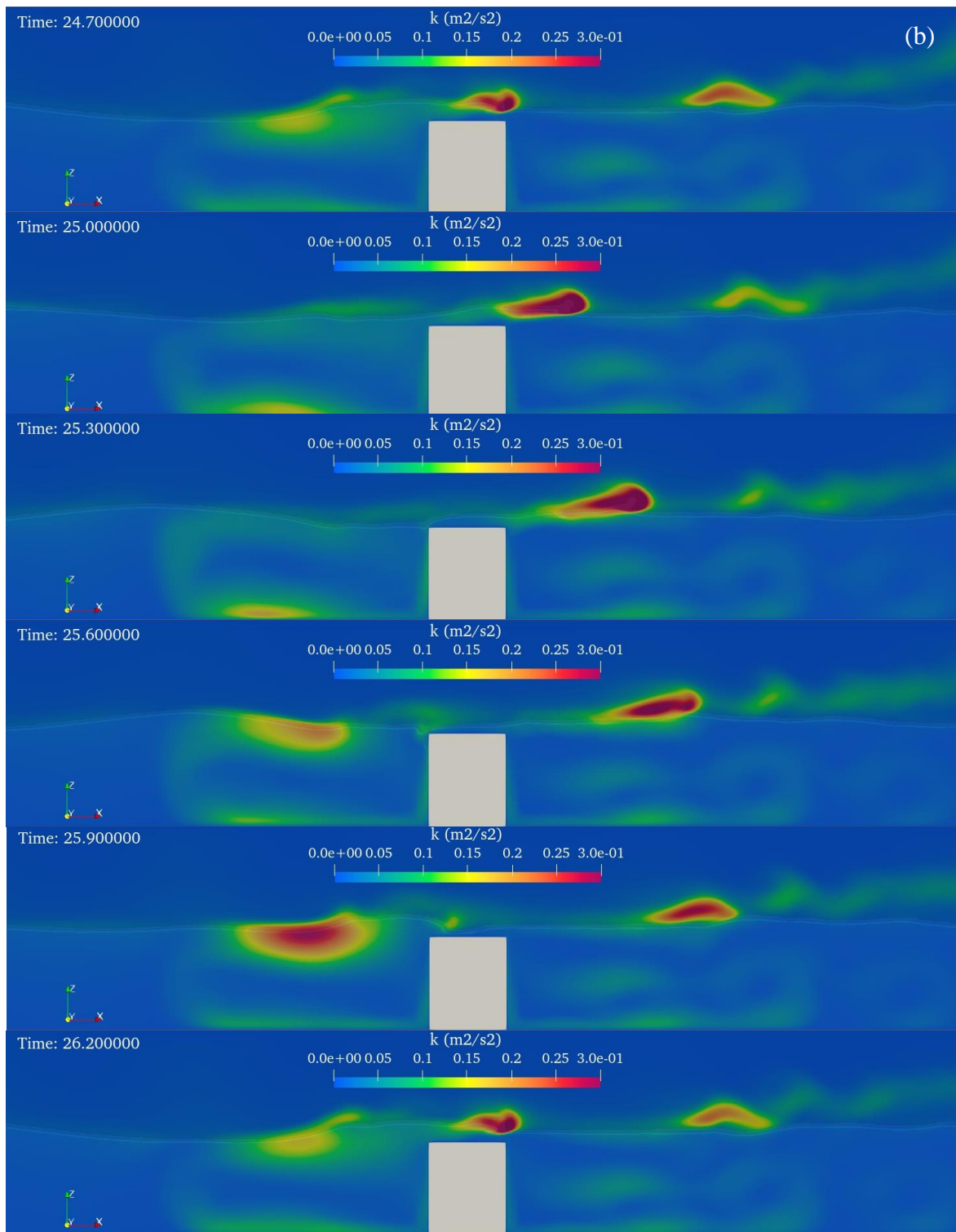
Figure 5.10b. The evolution of turbulent kinetic energy over a vertical breakwater (S_h=0.54m) in case of B=0.45m

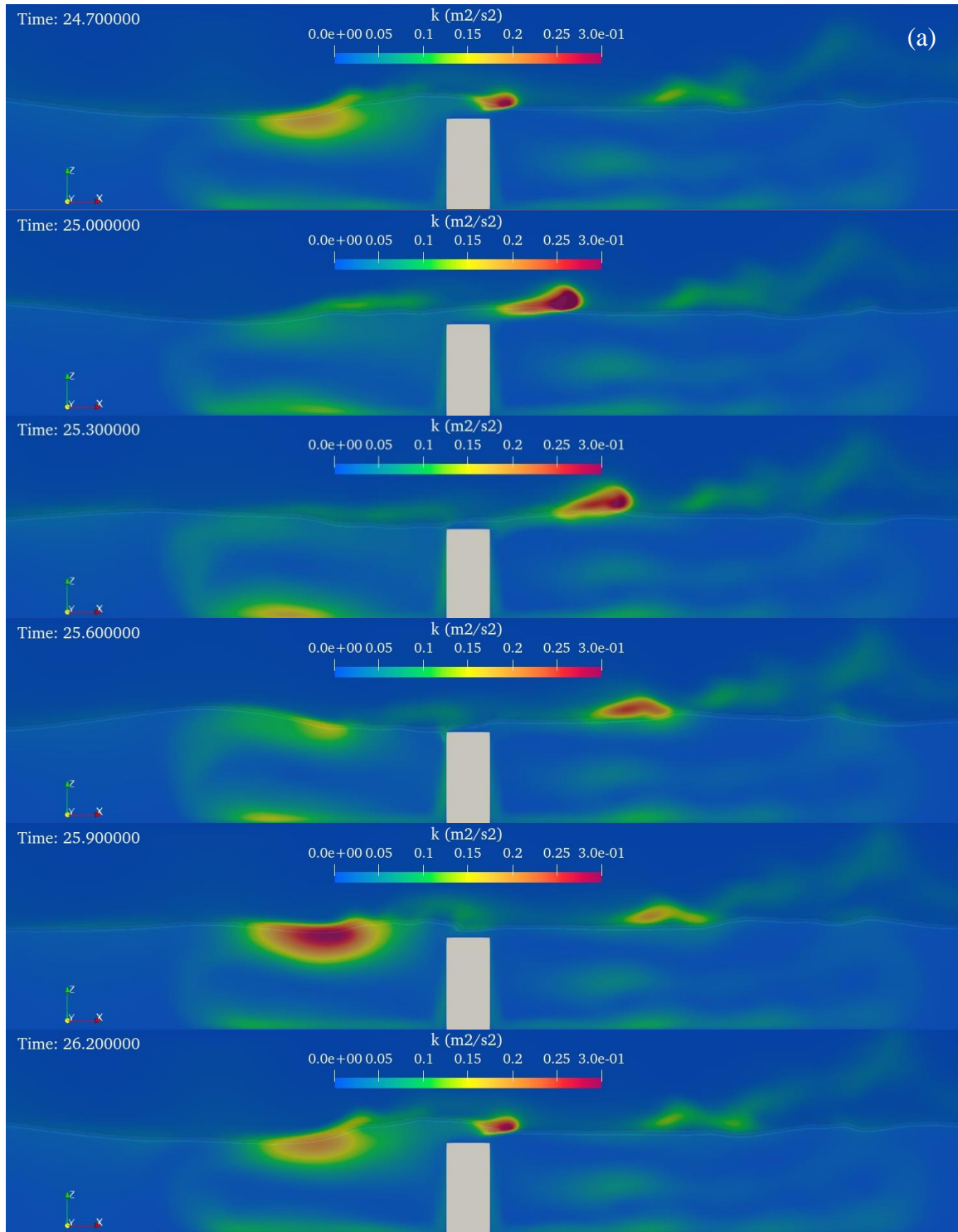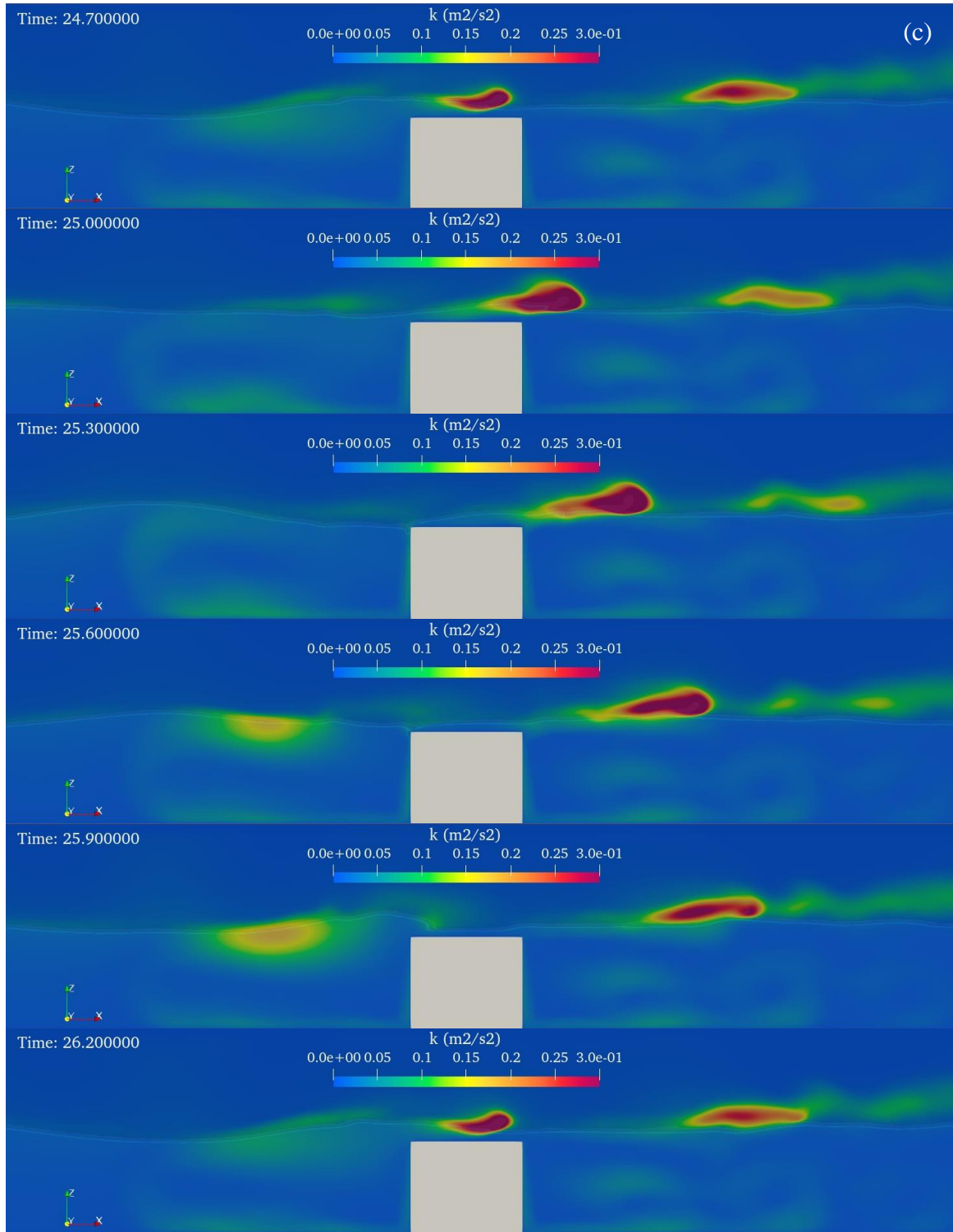Figure 5.10c. The evolution of turbulent kinetic energy over a vertical breakwater (S_h=0.54m) in case of B=0.65m
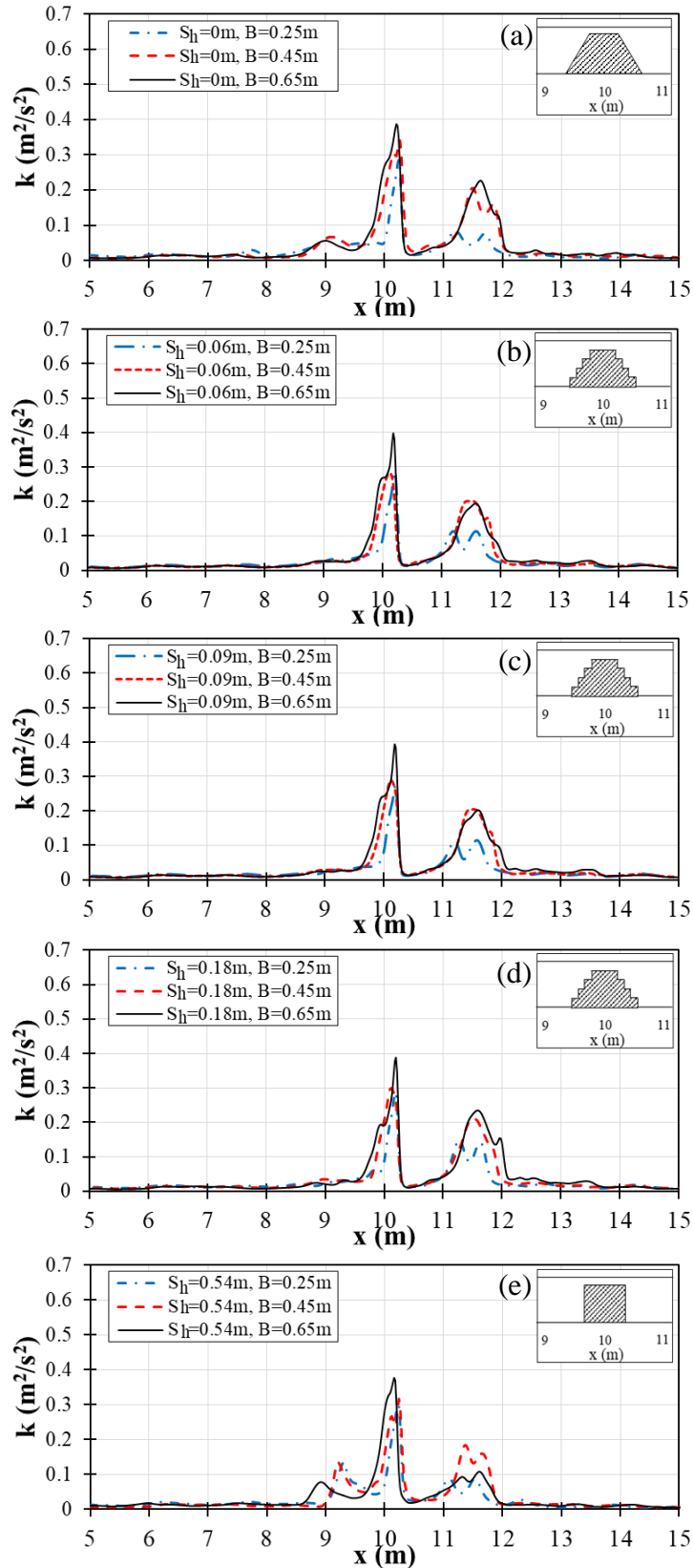
Figure 5.11. The comparison of the time average of turbulent kinetic energy over (a) a smooth slope, S_h=0m (b) a micro rough slope, S_h=0.06 (c) a macro rough slope, S_h=0.09 (d) a composite slope, S_h=0.18 (e) a vertical breakwater, S_h=0.54m with different crest widths

According to Figures 5.6, 5.7, 5.8, 5.9 and 5.10, the intense turbulent kinetic energy represented as a wave breaking on the water surface which appeared above and behind submerged structures. The results aim to compare the intensity of turbulence due to the energy loss in the wave breaking process over the different structural geometries.

Based on the comparison of the time average of TKE over different structure crest width, Figure 5.11 shows that the biggest crest width (B=0.65m) provided a larger turbulent kinetic energy, which was followed by the moderate (B=0.45m) and small (B=0.25m) crest width in every structural shapes. The time average of TKE showed two peaks of k, which was shown up above (at x=10m) and behind (at x=11.5m) submerged structures. Whereas, there was the turbulent kinetic energy that also presented in front of the vertical shape (at x=9m). Based on this result, the turbulent kinetic energy was noted as a reflected wave, which can be noticed from the magnitude of turbulent kinetic energy under the water surface in the Figure 5.10 and the computational results in Chapter 4.

Moreover, the comparison of the time average of TKE over submerged breakwaters with different stepped sizes is also illustrated in Figure 5.12. The effect of varying stepped size showed that the change of stepped sizes provided the smaller effect to the wave breaking process.
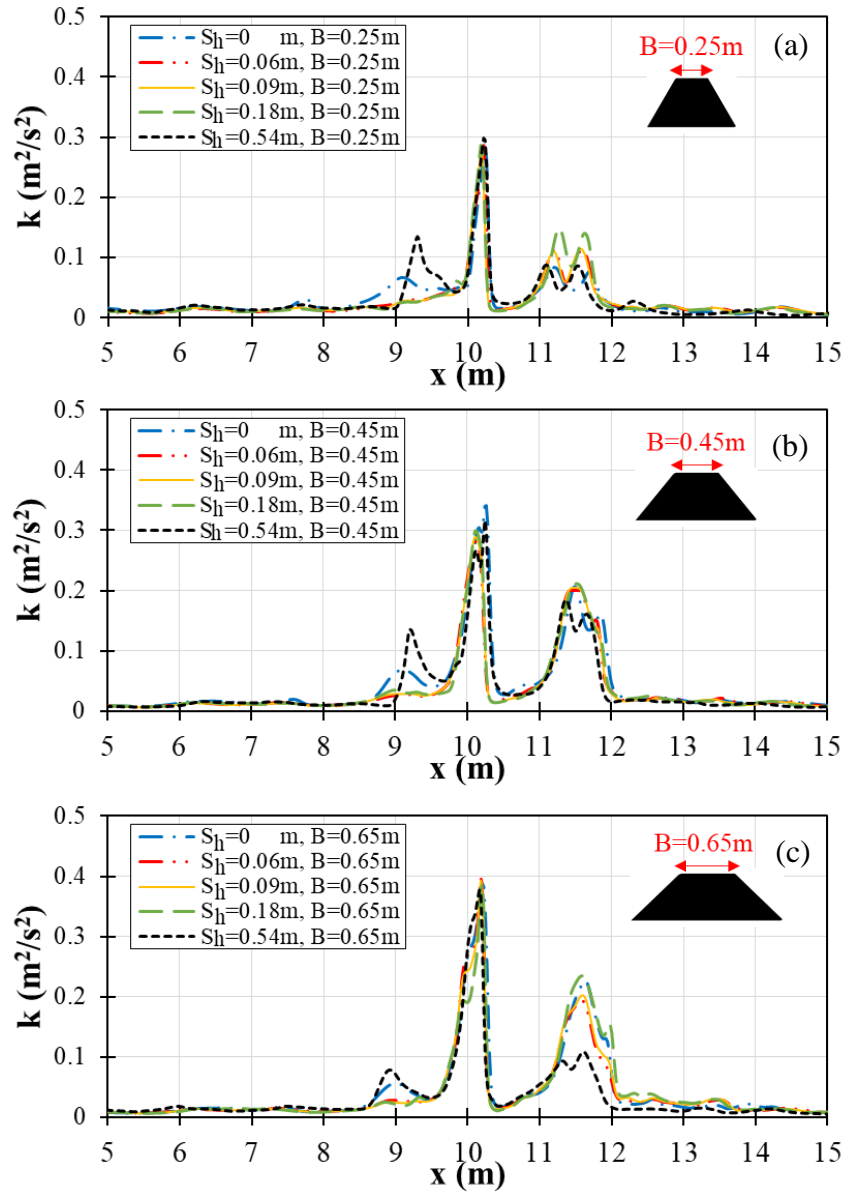
Figure 5.12. The comparison of the time average of turbulent kinetic energy over submerged breakwaters with different stepped sizes for (a) small size of crest width, B= 0.25m (b) moderate size of crest width, B= 0.45m (c) big size of crest width, B= 0.65m

5.2. WAVE INTERACTION WITH THE VARYING STRUCTURAL GEOMETRIES

This section aims to present the behavior of wave interaction with the differing stepped heights of submerged breakwaters. The results were simulated from the turbulence modeling. The behaviors of fluid motion were illustrated from the viewpoint of wave direction and the vorticity magnitude. The stop motion of wave interaction with submerged structures were captured at time=24.7s in the case of T=1.5s of wave period, H_i=0.09m of wave heights and

d_s/d=0.1 of submergence ratio, which was the moment of wave propagating over the structures. The captures of wave interaction with structures were presented for both of seaward side and landward side, which were mentioned in the following subsections.

5.2.1.   SEAWARD SIDE

The captured diagrams of fluid motion interactive with the smooth slope (S_h=0m), micro rough slope (S_h=0.06m), macro rough slope (S_h=0.09m), composite slope (S_h=0.18m) and vertical shape (S_h=0.54m) of breakwaters are shown in Figures 5.13, 5.14, 5.15, 5.16 and 5.17, respectively. The diagrams presented the behavior of wave at the seaward side of structures. In addition, the evolutions of fluid motion on seaward side are also presented in Appendix C1.

Figure 5.13. The snapshots of fluid motion on the smooth slope (S_h=0m) of breakwaters at seaward side (a) direction of flow (b) vorticity magnitude

Figure 5.14. The snapshots of fluid motion on the micro rough slope (S_h=0.06m) of breakwaters at seaward side (a) direction of flow (b) vorticity magnitude
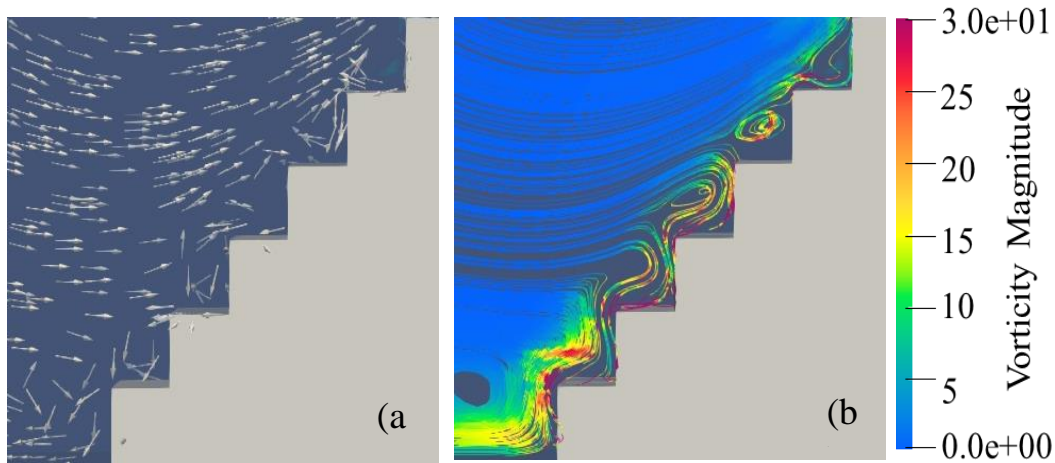
Figure 5.15. The snapshots of fluid motion on the macro rough slope (S_h=0.09m) of breakwaters at seaward side (a) direction of flow (b) vorticity magnitude
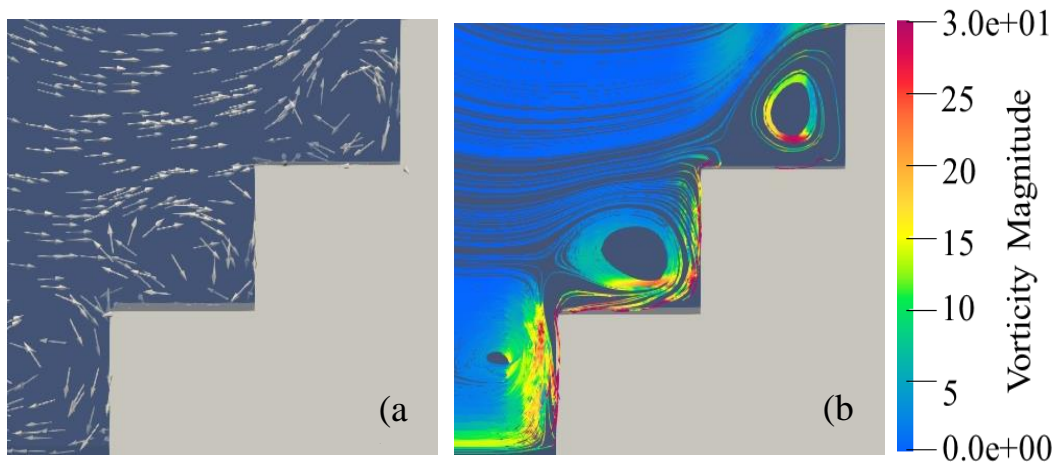
Figure 5.16. The snapshots of fluid motion on the composite slope (S_h=0.18m) of breakwaters at seaward side (a) direction of flow (b) vorticity magnitude
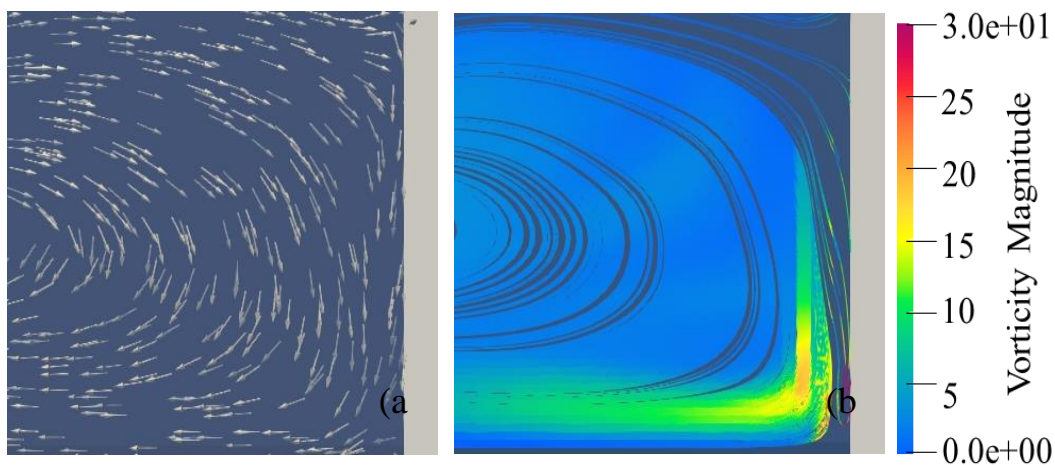
Figure 5.17. The snapshots of fluid motion on the vertical shape (S_h=0.54m) of breakwaters at seaward side (a) direction of flow (b) vorticity magnitude

5.2.2. LANDWARD SIDE

Figures 5.18, 5.19, 5.20, 5.21 and 5.22 showed the snapshot diagrams of fluid motion interactive with the smooth slope (S_h=0m), micro rough slope (S_h=0.06m), macro rough slope (S_h=0.09m), composite slope (S_h=0.18m) and vertical shape (S_h=0.54m) of breakwaters, respectively. The diagrams presented the behavior of wave at the landward side of structures, which were simulated based on the turbulence modeling. Moreover, the instantaneous fluid motion on landward side are also presented in Appendix C2.
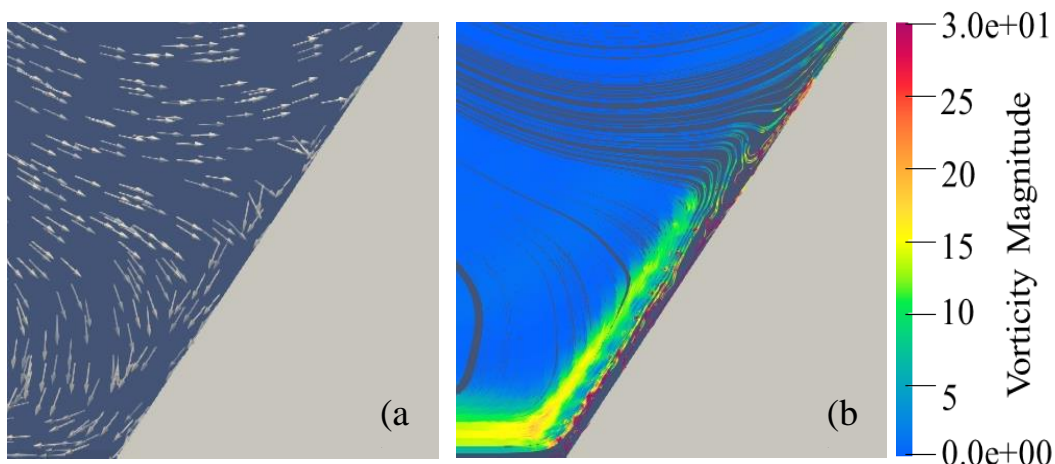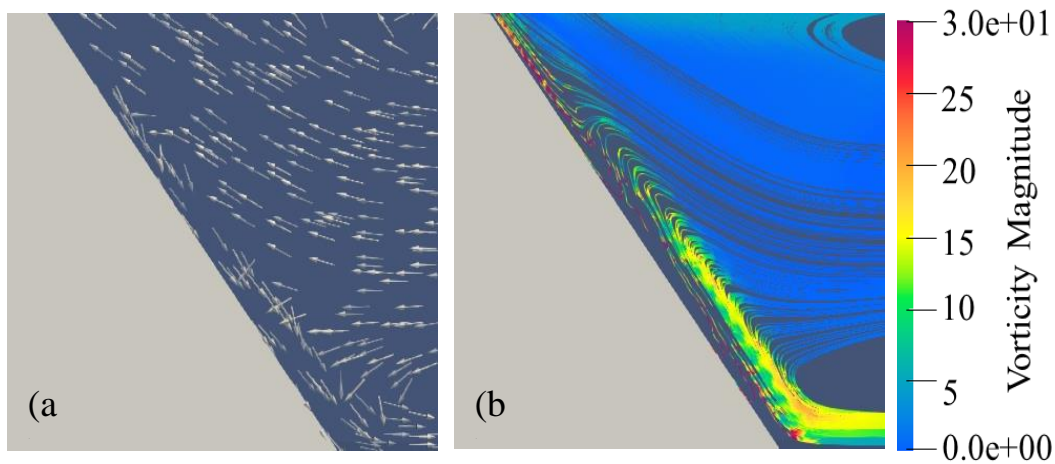

Figure 5.18. The snapshots of fluid motion on the smooth slope (S_h=0m) of breakwaters at landward side (a) direction of flow (b) vorticity magnitude
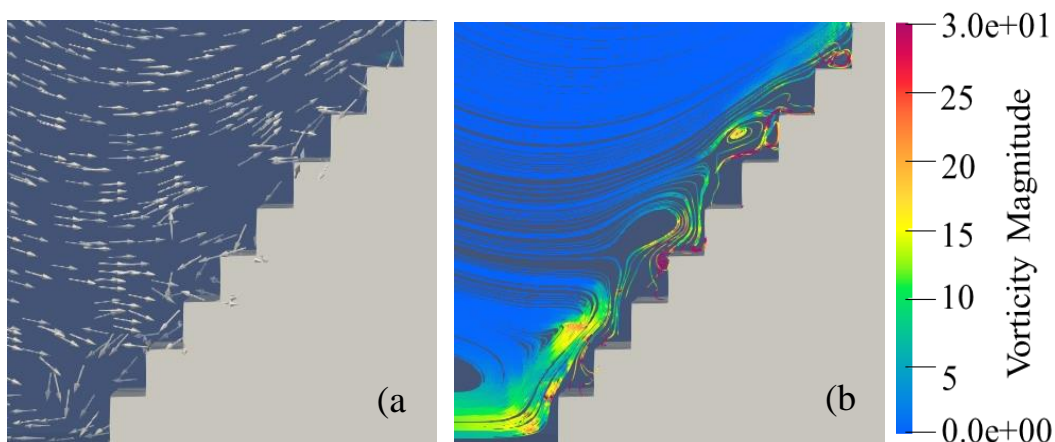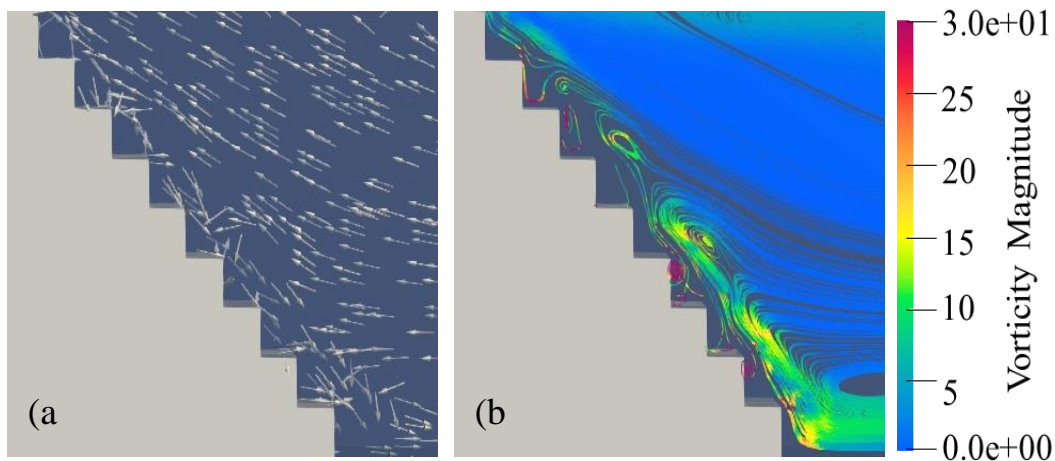

Figure 5.19. The snapshots of fluid motion on the micro rough slope (S_h=0.06m) of breakwaters at landward side (a) direction of flow (b) vorticity magnitude

Figure 5.20. The snapshots of fluid motion on the macro rough slope (S_h=0.09m) of breakwaters at landward side (a) direction of flow (b) vorticity magnitude
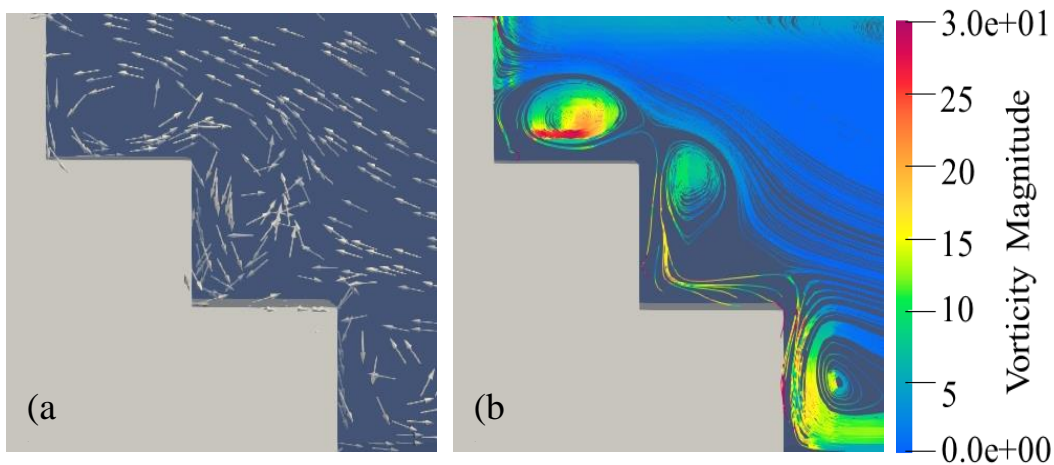
Figure 5.21. The snapshots of fluid motion on the composite slope (S_h=0.18m) of breakwaters at landward side (a) direction of flow (b) vorticity magnitude
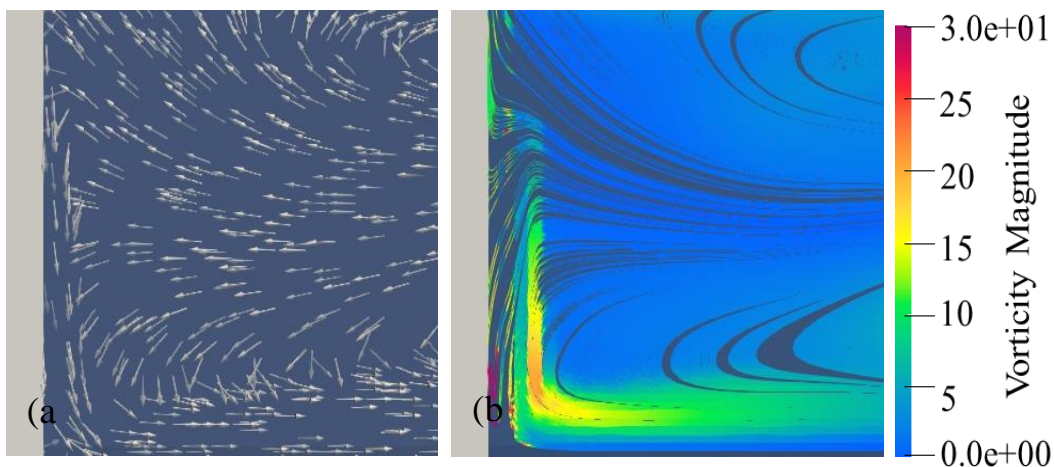
Figure 5.22. The snapshots of fluid motion on the vertical shape (S_h=0.54m) of breakwaters at landward side (a) direction of flow (b) vorticity magnitude

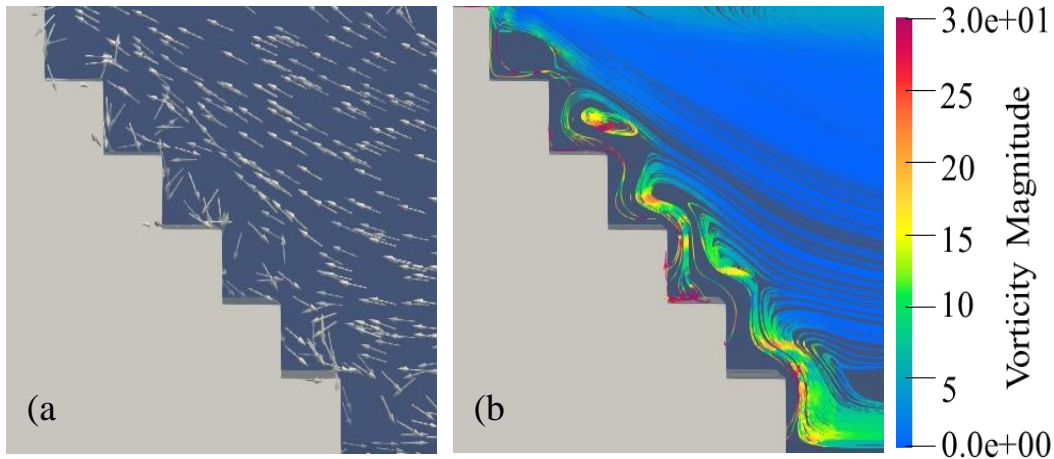According to the captured diagrams of wave interaction with structures at both sides of seaward and landward, it can be noticed that the fluid motion are captured as a flow along the smooth surface slope of breakwater (S_h=0m). A generation of turbulence slightly formed on the niches of the step. The directions of fluid motion were changed from the direction along the smooth surface slope (S_h=0m) to become a turbulence formimg with the increased stepped heights (S_h=0.06m, S_h=0.09m and S_h=0.18m). A re-direction of wave flow occured with the vertical shape of structures (S_h=0.54m), which was generated a large turbulence on the ground of the structures.

5.3. WAVE PROPAGATION OVER PERMEABLE AND IMPERMEABLE SUBMERGED BREAKWATERS

In this section, the porous effect was considered on the behavior of wave propagation over submerged breakwaters, which was mainly compared with the impermeable submerged structures. The case study of permeable breakwater was modeled based on the literature review (Srineash and Murali, 2019). The permeable models were set for 0.37 of porosity, 500 for friction factor and 3.3 for mean rock size, which were included in constant/porosityDict of OlaFlow solver.

The instantaneous profiles of wave propagation over a smooth slope (S_h=0 m), micro rough slope (S_h=0.06m), macro rough slope (S_h=0.09m), composite slope (S_h=0.18m) and vertical shape (S_h=0.54m) with B= 0.65m are illustrated in Figure 5.23, 5.24, 5.25, 5.26 and 5.27, respectively. The numerical models were simulated under T=1.5s of wave period, H_i=0.09m of wave heights and d_s/d=0.1 of submergence ratio. The structure was set at x/L_i=0 in the diagrams. The seaward sides were presented in the negative direction (-) and the landward sides were in the positive direction (+) of the diagrams. The instantaneous wave profiles were captured at 24.7s, 25.5s and 26.2s, which represented one cycle of wave period in this case. In each diagram, the instantaneous wave profiles over permeable structures were compared with the impermeable case, which were also evaluated with the case of wave propagation without any obstructions.
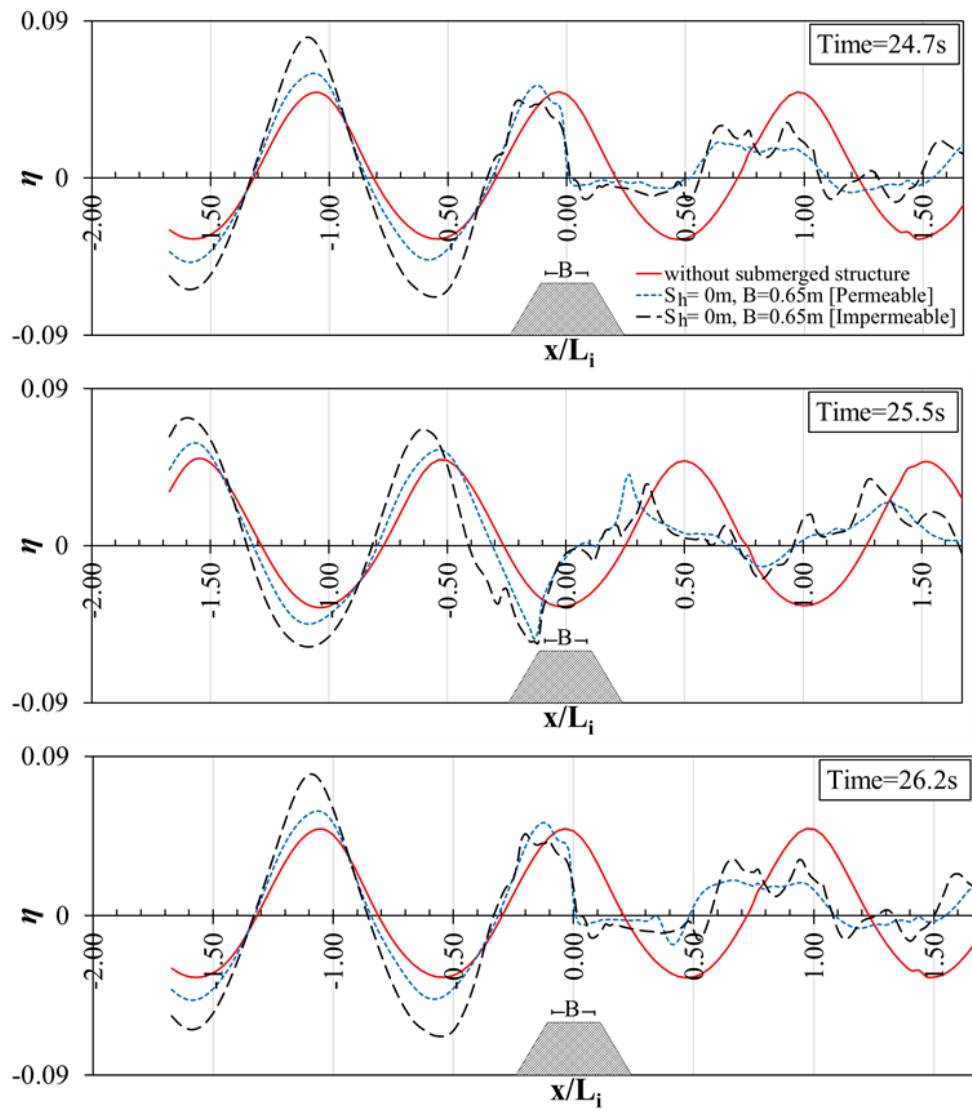
Figure 5.23. Comparison of the instantaneous wave profiles over permeable and impermeable with a smooth slope submerged breakwaters (S_h=0m)
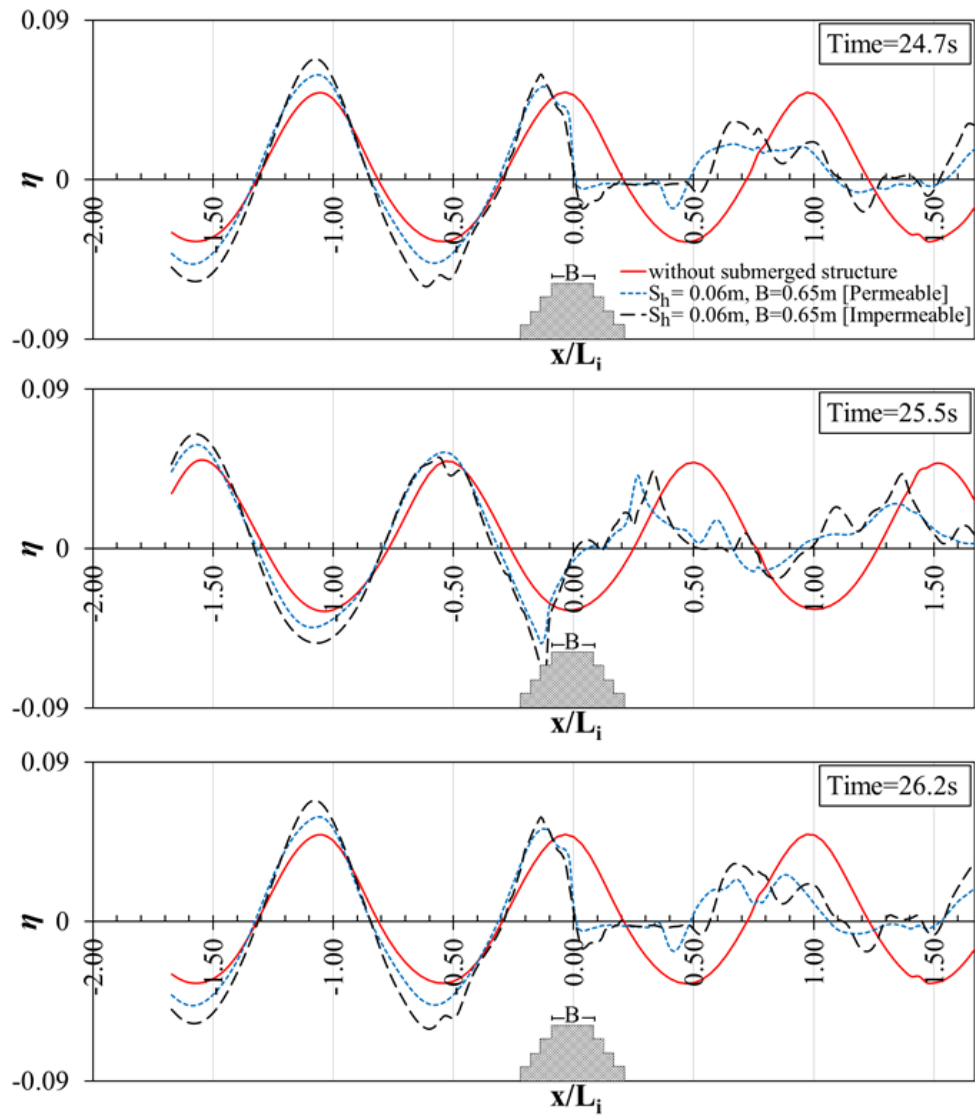
Figure 5.24. Comparison of the instantaneous wave profiles over permeable and impermeable with a micro rough slope submerged breakwaters (S_h=0.06m)
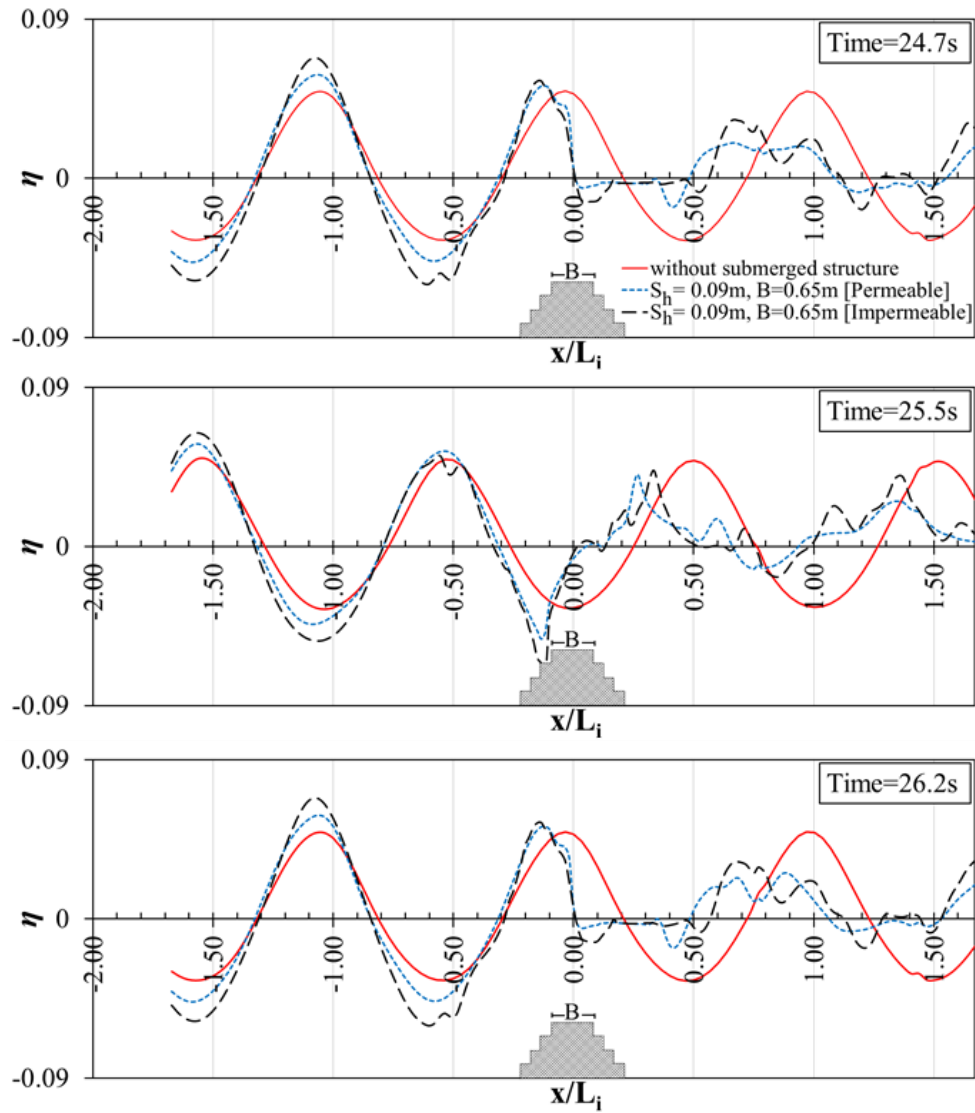
Figure 5.25. Comparison of the instantaneous wave profiles over permeable and impermeable with a macro rough slope submerged breakwaters (S_h=0.09m)
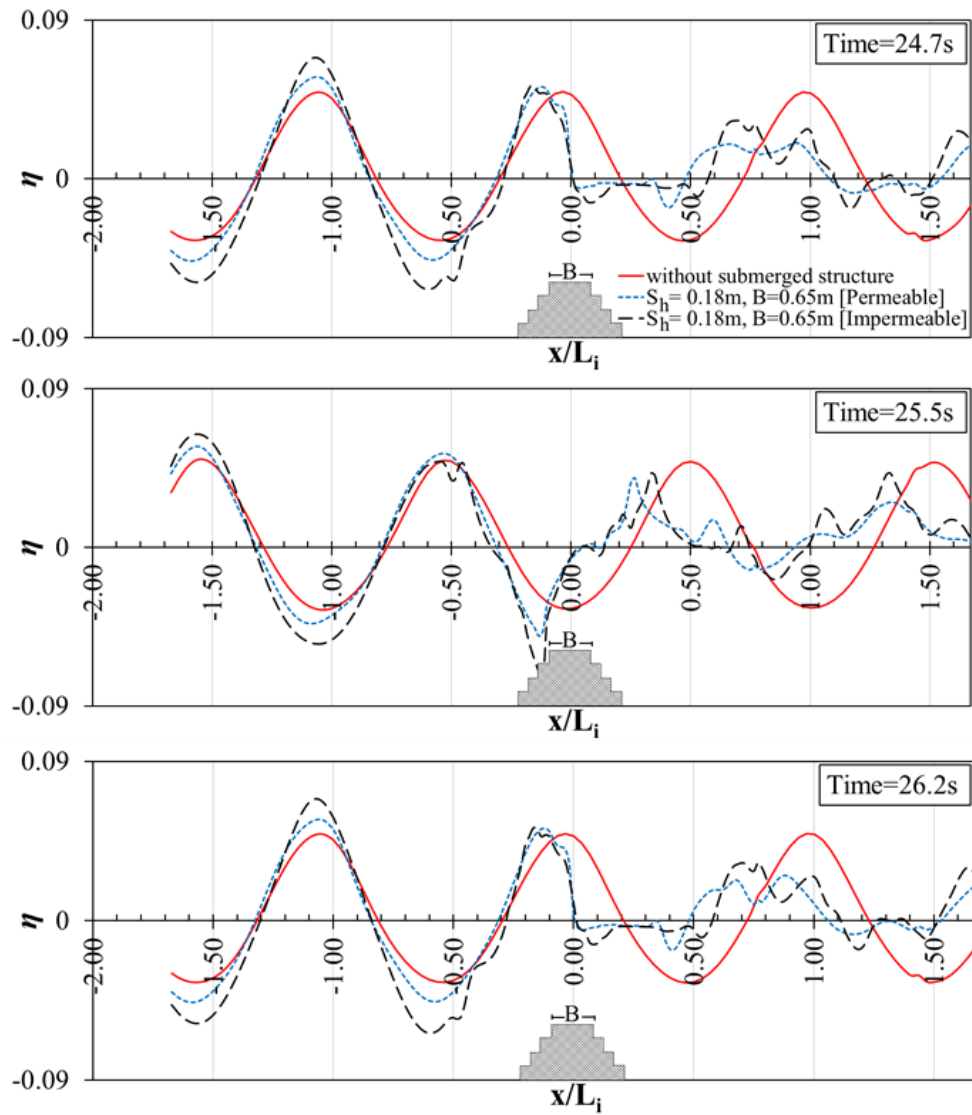
Figure 5.26. Comparison of the instantaneous wave profiles over permeable and impermeable with a composite slope submerged breakwaters (S_h=0.18m)

113
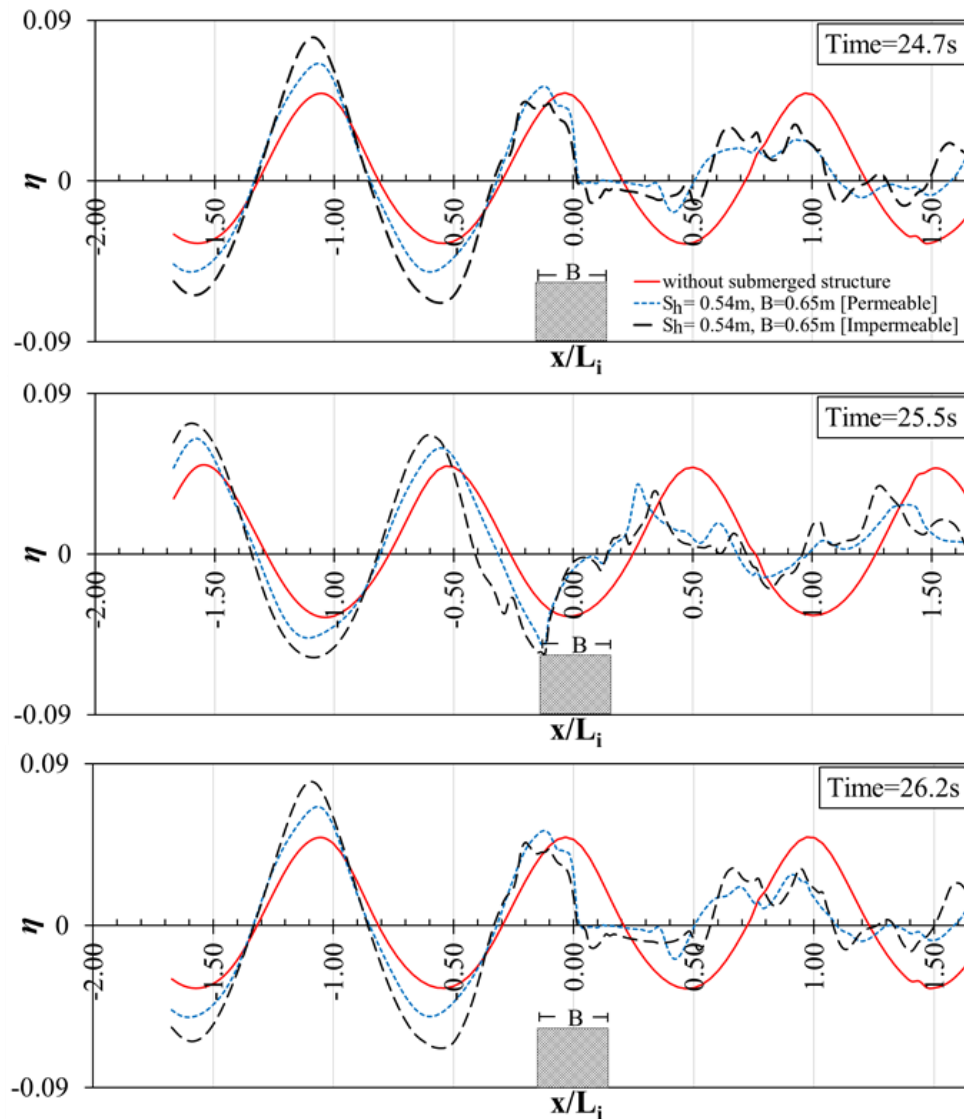
Figure 5.27. Comparison of the instantaneous wave profiles over permeable and impermeable with a vertical submerged breakwaters (S_h=0.54m)

The comparison of the instantaneous wave profiles over permeable and impermeable submerged structures were compared to consider the porous effects. According to the diagrams, the results showed that the permeable cases were capable to provide a lower reflected wave than the impermeable cases, which were presented in front of the structures (in the negative direction of x/L_i). Moreover, the propagated waves behind the permeable cases were gentler fluctuated due to the energy dissipation processes.

However, the comparison of permeable and impermeable models in this section can be used to provide the suggestion for the higher efficiency in the future study. In order to achieve and investigate the better ability of stepped submerged breakwaters, the porous parameters should be considered in the numerical simulation.

114

CHAPTER 6

THE RISK-BASED ASSESSMENT OF SCOUR

AROUND SUBMERGED BREAKWATERS

Chapter 6

THE RISK-BASED ASSESSMENT OF SCOUR AROUND SUBMERGED BREAKWATERS

According to the results in Chapter 5, the behaviors of wave propagation and turbulent kinetic energy around submerged breakwaters primarily show the risks of erosion on the ground that can be caused by a large reflected wave and the turbulence effects. In order to focus on the risk assessment of scour, this chapter aims to analyze this issue from the viewpoint of hydrodynamic characteristics, which are the shear stress properties and the turbulence characteristics at the seabed for both sides of seaward and landward.

This chapter consists of two main sections. Firstly, the characteristics of shear stress at seabed are analyzed for the different structural geometries. Then, the behaviors of the turbulence at the seabed are compared for the influence of different stepped heights and crest widths of submerged breakwaters.

6.1. BED SHEAR STRESS CHARACTERISTICS

In this section, the characteristics of bed shear stress are described on the influences of structural geometries. Firstly, the introduction of studying bottom shear stress is introduced in the first part. Then, the computational results based on the numerical simulation of bed shear stress around different structural shapes are presented and analyzed for the risk assessment of scour.

6.1.1. INTRODUCTION

Local scour around structure foundations can lead to partial failure or the collapse of structures. Studying bed shear stress is one of the hydrodynamic quantities that is directly associated to scour property. Coastal structures are mostly examined on the properties of shear stress and the effects of turbulence at the seabed around structures. The investigation of scour around various coastal structures (vertical cylinder, cone, vertical-wall breakwater and a rubble-mound breakwater) was examined by bed shear stress (Sumer et. al, 1994). The experimental studies of bed-shear stress measurements were conducted for both wave and steady current tests. The

damages of scour around these coastal structures were determined by the computational results of shear stress quantities and vortex shedding scales. The scour developments of offshore wind turbines were investigated by hydraulic model tests (Stahlmann and Schlurmann, 2012). The scour developments were examined by both wave model tests and field data collection, which considered the scour pattern and the assessment of bed shear stress around the tripod foundation of the wind turbine. Many kinds of research on scour development with various hydraulic model conditions were also examined from the viewpoints of bottom shear stress (Miedema, 2008; Ramos et. al., 2014; Wen et. al, 2020; Damme, 2021).

In this study, the effects of various geometries of submerged breakwaters on scour are investigated based on the characteristics of bottom shear stress. The different stepped heights of submerged breakwaters and crest widths are computed in numerical simulations to analyze the risk of erosion caused by scour. The study is carried out in a two-dimensional wave flume, which is conducted in the numerical model, OpenFOAM® software. The numerical wave flume is created with a size of 40 m in length, 1.2 m in height and 0.05 m in width. In this part, the model structures are exposed to wave tests in the intermediate depth waves (Le Méhauté, 1976), which is simulated in T=1.5s of wave periods, H_i=0.09m of wave height and d_s/d=0.1 of submergence ratio. The models are conducted with a smooth slope (S_h=0m), a micro rough slope (S_h=0.06m), a macro rough slope (S_h=0.09m), a composite slope (S_h=0.18m) and a vertical shape (S_h=0.54m) of breakwaters that are also created with three varying crest widths (B=0.25m, 0.45m and 0.65m). In order to directly focus on the effect of structural shapes on the hydraulic properties, the models are created by the impermeable structure.

Generally, shear stress is induced by the high velocity of water flows along the bottom surfaces, which affects erosion on the foundation at the seabed. The particles on the seabed are exposed to high-shear stresses associated velocity of flow that erode with the detachment and transport of individual particles. The classification of the flow layer according to shear stress characteristics is presented in Figure 6.1.
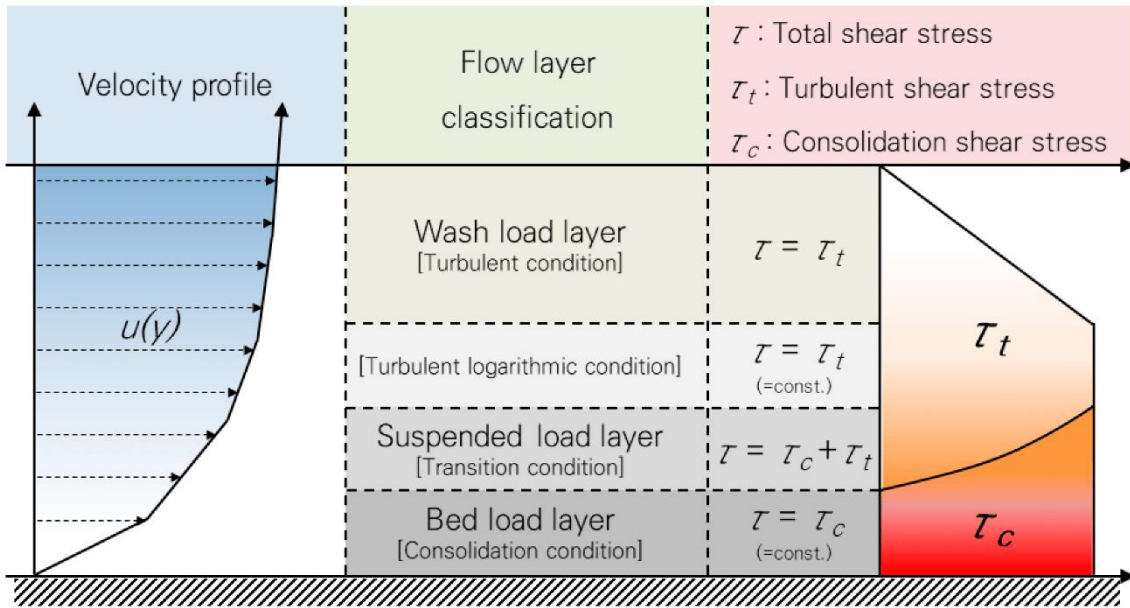
Figure 6.1. Classification of the flow layer according to shear stress characteristics

(Song et. al, 2020)

In order to consider the correlations between the hydrodynamics of wave and scour, the bed shear stress is analyzed in the wave process. The amplification factor (α) of the bed shear stress indicates the ratio of the local bed shear stresses (τ) to the shear stress without the presence of the structures (τ_0) that is imposed by the initial wave. The amplification of the bottom shear stress in wave cases is defined by equation 6.1 (Sumer et. al, 1994).

$$\alpha = \frac{Max\ |\tau|}{\tau_0} \tag{6.1}$$

6.1.2. RESULTS AND DISCUSSION

The influences of structural geometries on bed shear stress were analyzed for the risk of scouring around structures, which were considered in two-dimensional simulations. The computational results of bed shear stress were computed from the 10 wave periods of wave propagation in numerical simulations. In this part, the considerations of bed shear stress characteristics are described from the viewpoint of the effects of crest widths and the stepped sizes on submerged breakwaters, which are presented in the following topics.

6.1.2.1.   THE EFFECT OF VARYING CREST WIDTHS ON BED SHEAR STRESS
            CHARACTERISTICS

The influences of different crest widths of structures on bed shear stress were described in this part. Shear stress on the bottom of the numerical model was calculated in Paraview software, which was used to visualize the numerical results from OpenFOAM®. The magnitude of bed shear stress was computed based on the magnitude of velocity along the model, which was tracked at the seabed of numerical wave flumes.

The comparisons of average local bed shear stress with different crest widths of structures were plotted in the dimensionless positions (x/D) along the models, which are shown in Figures 6.2, 6.3, 6.4, 6.5 and 6.6 for a smooth slope (S_h=0m), a micro rough slope (S_h=0.06m), a macro rough slope (S_h=0.09m), a composite slope (S_h=0.18m) and a vertical shape (S_h=0.54m) of breakwaters, respectively. Where, D is the dimension of submerged breakwaters. The center of structural models was set at x/D=0. The computational results of bed shear stress around submerged breakwaters were computed from the edges of structures for both sides of seaward and landward, which were located from x/D= -0.5 for seaward and x/D= 0.5 for landward. The computational results of local bed shear stress were calculated from the time average of 10 wave periods in numerical wave generations.

Figure 6.2. The average local bed shear stress around a smooth slope (S_h=0m) of submerged breakwaters with different crest widths

Figure 6.3. The average local bed shear stress around a micro rough slope (S_h=0.06m) of submerged breakwaters with different crest widths
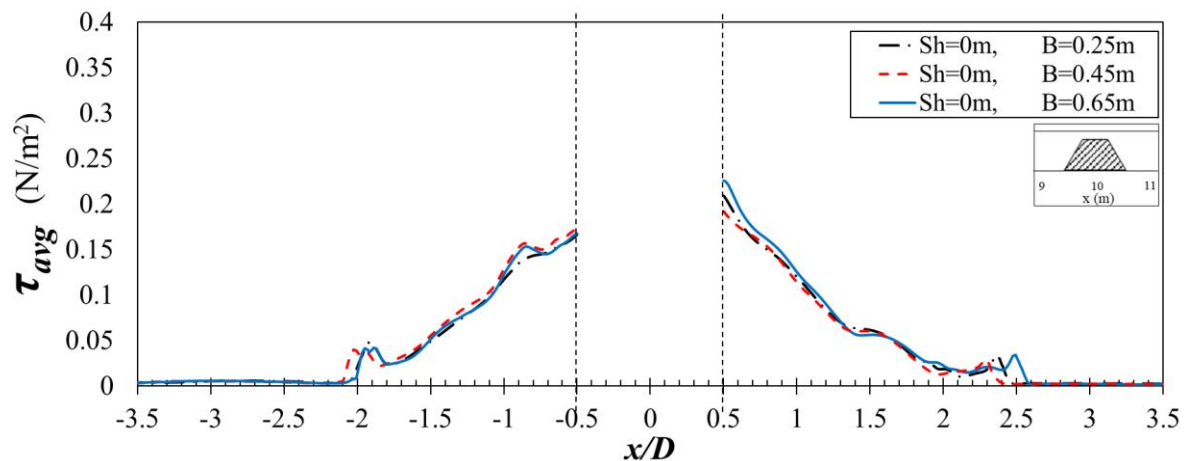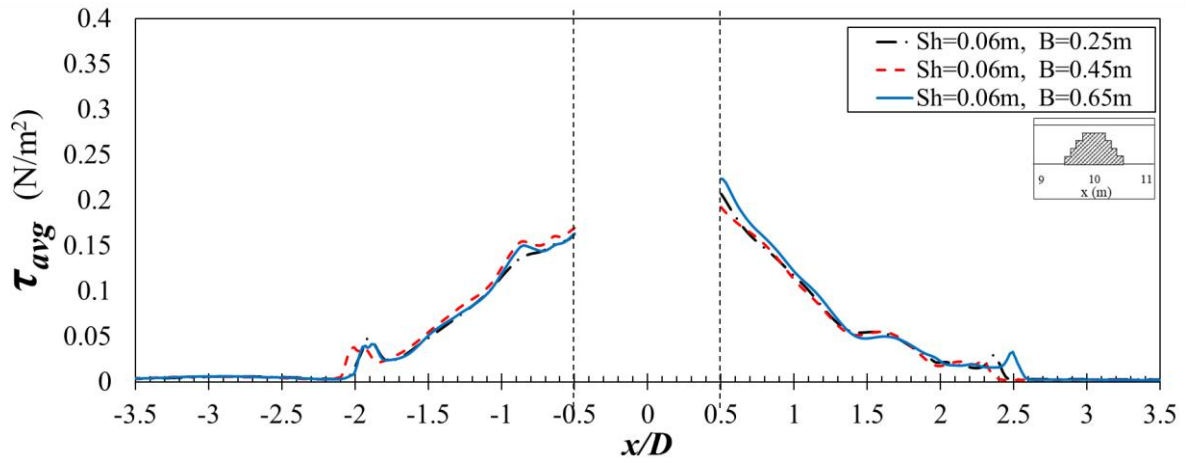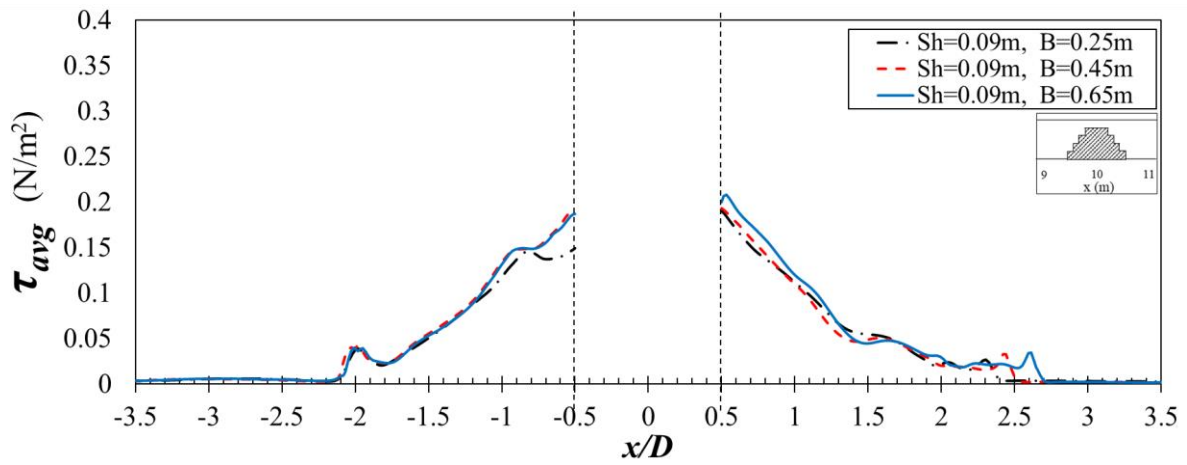

Figure 6.4. The average local bed shear stress around a macro rough slope (S_h=0.09m) of submerged breakwaters with different crest widths
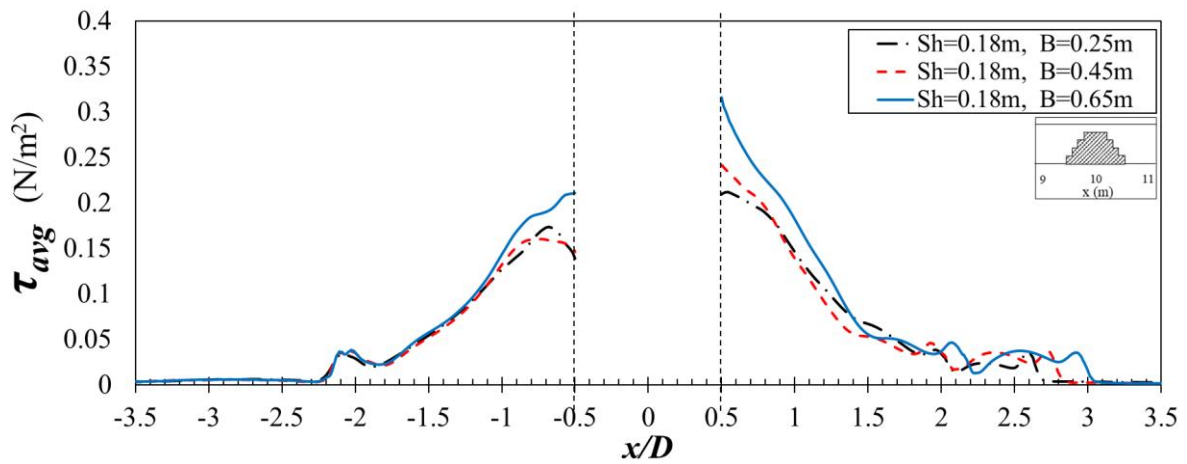

Figure 6.5. The average local bed shear stress around a composite slope (S_h=0.18m) of submerged breakwaters with different crest widths

120
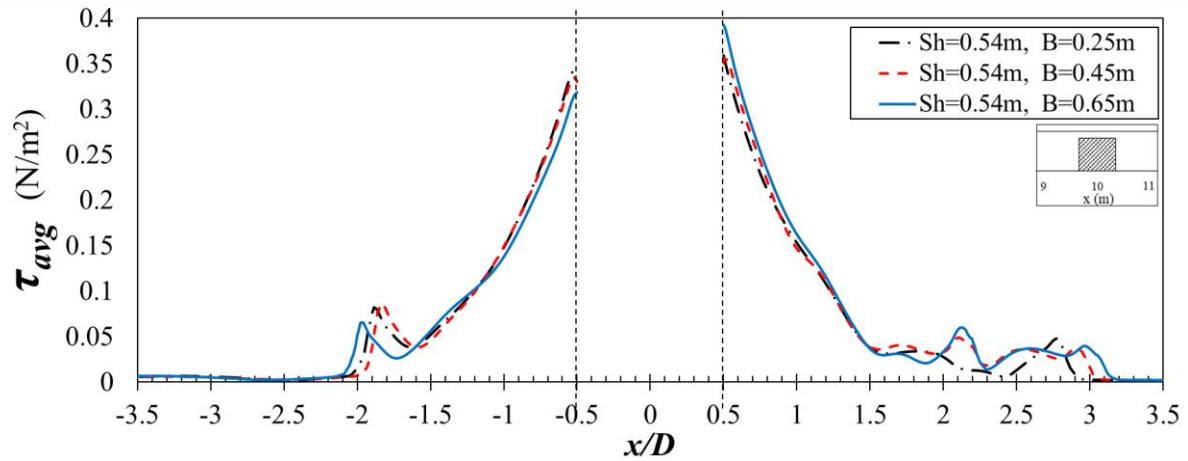
Figure 6.6. The average local bed shear stress around a vertical shape (S_h=0.54m) of submerged breakwaters with different crest widths

According to Figures 6.2, 6.3, 6.4, 6.5 and 6.6, the effects of different crest widths were compared from the viewpoint of shear stress at the seabed of submerged breakwaters. The results of time-average local bed shear stress around structures were plotted with the dimensionless position in the X-axis along the numerical wave flume. The influence of varying crest widths of submerged breakwaters showed that there was no significant effect on the bed shear stress characteristics. Whereas, the crest width of B=0.65m slightly provided a larger τ_{avg} behind the models, which was compared with a smaller crest width case in this study.

However, the influence of varying crest widths of submerged breakwaters seemed to have a negligible effect on the properties of bed shear stress. Whereas, according to these diagrams, the local bed shear stresses were significantly affected by the changes of stepped heights on structures. Therefore, the influence of different stepped sizes on submerged breakwaters is discussed in the next part.

6.1.2.2. THE EFFECT OF DIFFERING STEPPED HEIGHTS ON STRUCTURES TO BED SHEAR STRESS CHARACTERISTICS

In this part, the influences of various stepped heights on submerged breakwaters were considered on the properties of bed shear stress. The amplification factors of bed shear stress around different geometries of structures were plotted along the principal X-axis. The amplification factor was calculated from equation 6.1, which is the ratio of local shear stress to the shear stress with an undisturbed flow that is imposed by the incident wave. The evolutions

of amplification factors of bed shear stress for *B*=0.25m, 0.45m and 0.65m are illustrated in Figures 6.6, 6.7 and 6.8, respectively. The center of model structures was set at *x/D*=0 in the diagrams. The direction of the seaward side presented in the negative direction (-) and the landward side presents in the positive direction (+) of diagrams.

Figure 6.7. The amplification factor of bed shear stress along the principal X- axis around different geometries of submerged breakwaters with *B*=0.25m of crest width

Figure 6.8. The amplification factor of bed shear stress along the principal X- axis around different geometries of submerged breakwaters with *B*=0.45m of crest width
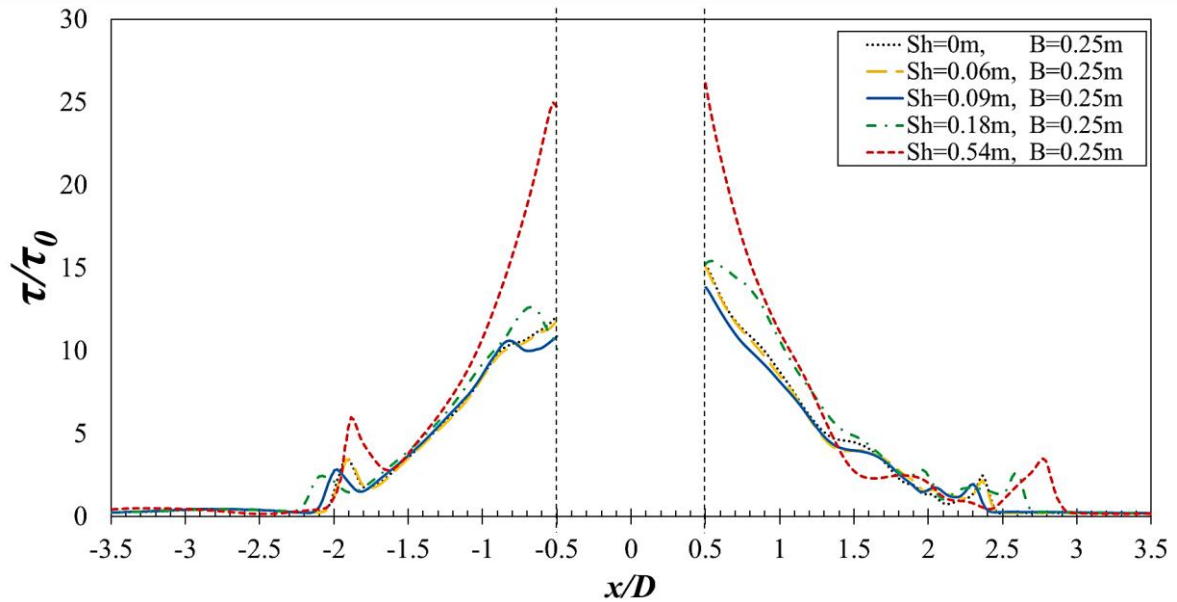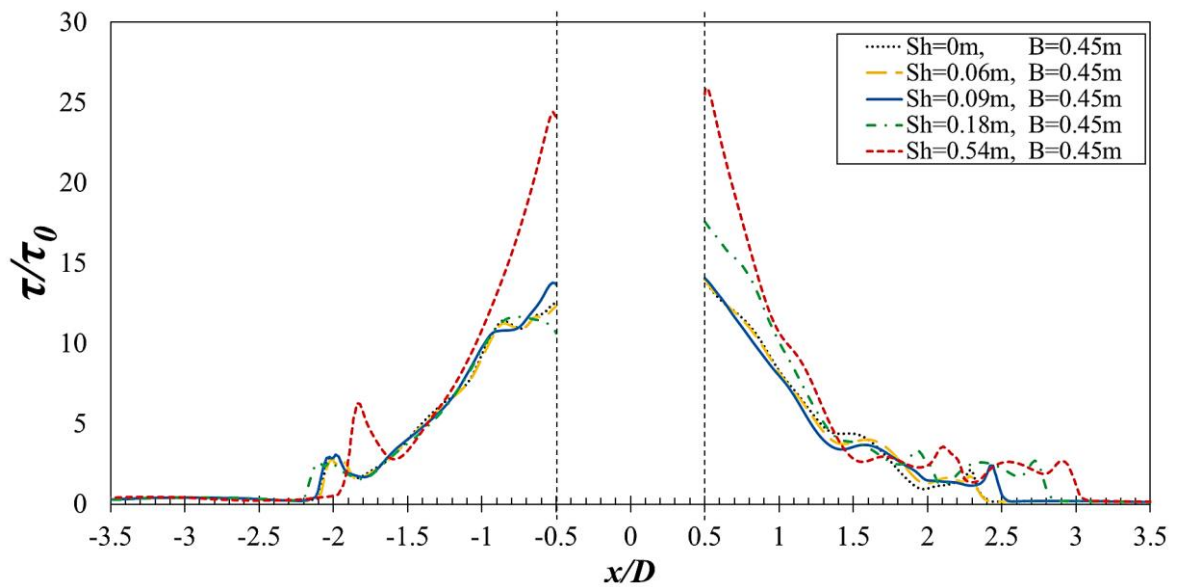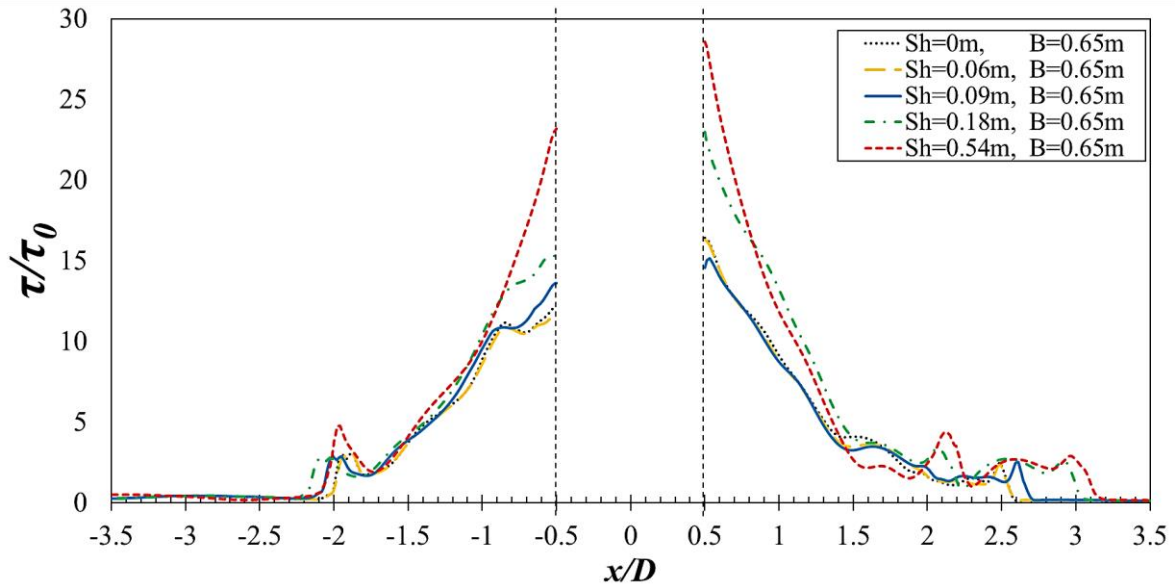
Figure 6.9. The amplification factor of bed shear stress along the principal X- axis around different geometries of submerged breakwaters with B=0.65m of crest width

According to Figures 6.7, 6.8 and 6.9, the comparison of bed shear stress amplification factors with differing stepped heights on structures was plotted with x/D along the numerical wave flume.

The influence of varying stepped sizes on structures showed that the vertical shape (S_h=0.54m) of breakwaters affected the largest amplification factor of bed shear stress among these several shapes in this study. The smooth slope (S_h=0m) and small stepped heights (S_h=0.06 and 0.09m) on structures showed a small effect between the change from a flat slope to a micro rough slope. Whereas, the changes obviously appeared in the composite slope (S_h=0.18m), which was larger in the forming of bed shear stress amplification factor. Then, the largest τ/τ_0 was developed in the vertical shape of submerged breakwaters.

In terms of τ/τ_0 distribution along the principal X-axis, the increased stepped heights of structures affected the increased developed areas in x/D on the landward side. The τ/τ_0 distribution of vertical shape (S_h=0.54m) was significantly wider developed behind the structure, which was compared with other geometries. The distribution of the amplification factor of bed shear stress along the principal X-axis decreased with the decreased stepped heights of structures.

6.2.   TURBULENCE CHARACTERISTIC AT SEABED

In this section, firstly the introduction of this study is explained with the objectives and the numerical setup for the analysis of turbulence properties, which is followed by the results and discussion. The results were analyzed from the viewpoint of the turbulent kinetic energy around the impermeable structures, which were considered by the effect of varying crest widths and the various stepped heights on submerged breakwaters.

6.2.1. INTRODUCTION

Generally, erosion consists of the detachment, entrainment and transport of sediment under coastal wave actions. During ground detachment, particles and water are exchanged with the turbulent flow. In order to investigate the erosion risk on coastal structures, turbulence property is also one of the hydrodynamic characteristics associated with sediment transportation. In the last few decades, computational fluid dynamic (CFD) models have been increasingly used to simulate and analyze the hydrodynamic models in coastal engineering, which can be gained considerable advantages of visualized results and clearly expressed graphic details. In order to observe the behavior of turbulent flow, the CFD models has been used to identify the turbulent characteristics under wave generation. Numerical and experimental studies of breakwater designs were carried out to investigate the turbulent flow characteristics and sediment transport (Wang et al., 2020). The influences of structural design on coastal erosion were identified based on the properties of turbulent flow and particle transportation. Many kinds of research on erosion assessment based on sediment transport were also analyzed from the viewpoint of turbulence characteristics, which were conducted with various conditions and coastal structures (Bridge and Demicco, 2008; Orencio et al., 2012; Rueda, 2015; Chang et al., 2020).

In this study, the risk-based assessment of erosion caused by various geometries of submerged breakwaters was observed by the turbulence characteristics at seabed. The different crest widths and the effects of various stepped heights of structures were analyzed in numerical simulation, OpenFOAM®. In this part, the aim of this study is to compare the quantity of turbulent kinetic energy around submerged breakwaters, which is presented both as computational results and the evolution diagrams of turbulence development based on the CFD modeling. The study was carried out in a two-dimensional numerical wave flume, which was created with a size of 40m in length, 1.2m in height and 0.1m in width. The models were exposed to wave tests in the intermediate depth waves (Le Méhauté, 1976), which were simulated in T=1.5s of wave periods, H_i=0.09m of wave height and d_s/d=0.1 of submergence

ratio. The models were tested with a smooth slope (S_h=0m), a micro rough slope (S_h=0.06m), a macro rough slope (S_h=0.09m), a composite slope (S_h=0.18m) and a vertical shape (S_h=0.54m) of breakwaters that were also created with three varying crest widths (B=0.25m, 0.45m and 0.65m). The k-ω SST model was used to define the turbulence simulation, which was computed from equations 3.10 and 3.11.

6.2.2. RESULTS AND DISCUSSION

In order to investigate the scour risks caused by turbulence effects, the turbulent kinetic energy was analyzed in the numerical simulation. The turbulence energy was tracked at the seabed for both seaward and landwards sides of submerged structures. The comparison of the time-average turbulent kinetic energy, k, on the different crest widths of structures was plotted with the dimensionless positions (x/D) in the X-direction, which D is the dimension of models. The model was set at x/D=0 for both sides of structures, which were presented as the seaward side in the negative direction (-) and the landward side in the positive direction (+) of the diagrams. The time-average turbulent kinetic energy was computed from 10 wave periods of wave generation through the impermeable breakwaters. The considerations of turbulence characteristics around submerged breakwaters were described from the viewpoint of the effects of crest widths and the stepped sizes on submerged breakwaters, which are presented in the following topics.

6.2.2.1. THE EFFECT OF VARYING CREST WIDTHS ON THE TURBULENCE CHARACTERISTIC

The comparison of the time-average turbulent kinetic energy with the different crest widths of a smooth slope (S_h=0m), a micro rough slope (S_h=0.06m), a macro rough slope (S_h=0.09m), a composite slope (S_h=0.18m) and a vertical shape (S_h=0.54m) of breakwaters are illustrated in Figures 6.10, 6.11, 6.12, 6.13 and 6.14, respectively, which were simulated in the case of T=1.5s of wave period, H_i=0.09m of wave height and d_s/d=0.1 of the submergence ratio. The snapshots of the evolution of turbulent kinetic energy were also included in each diagram. The snapshot diagrams were captured the developed turbulence energy at the seabed in one wave period.
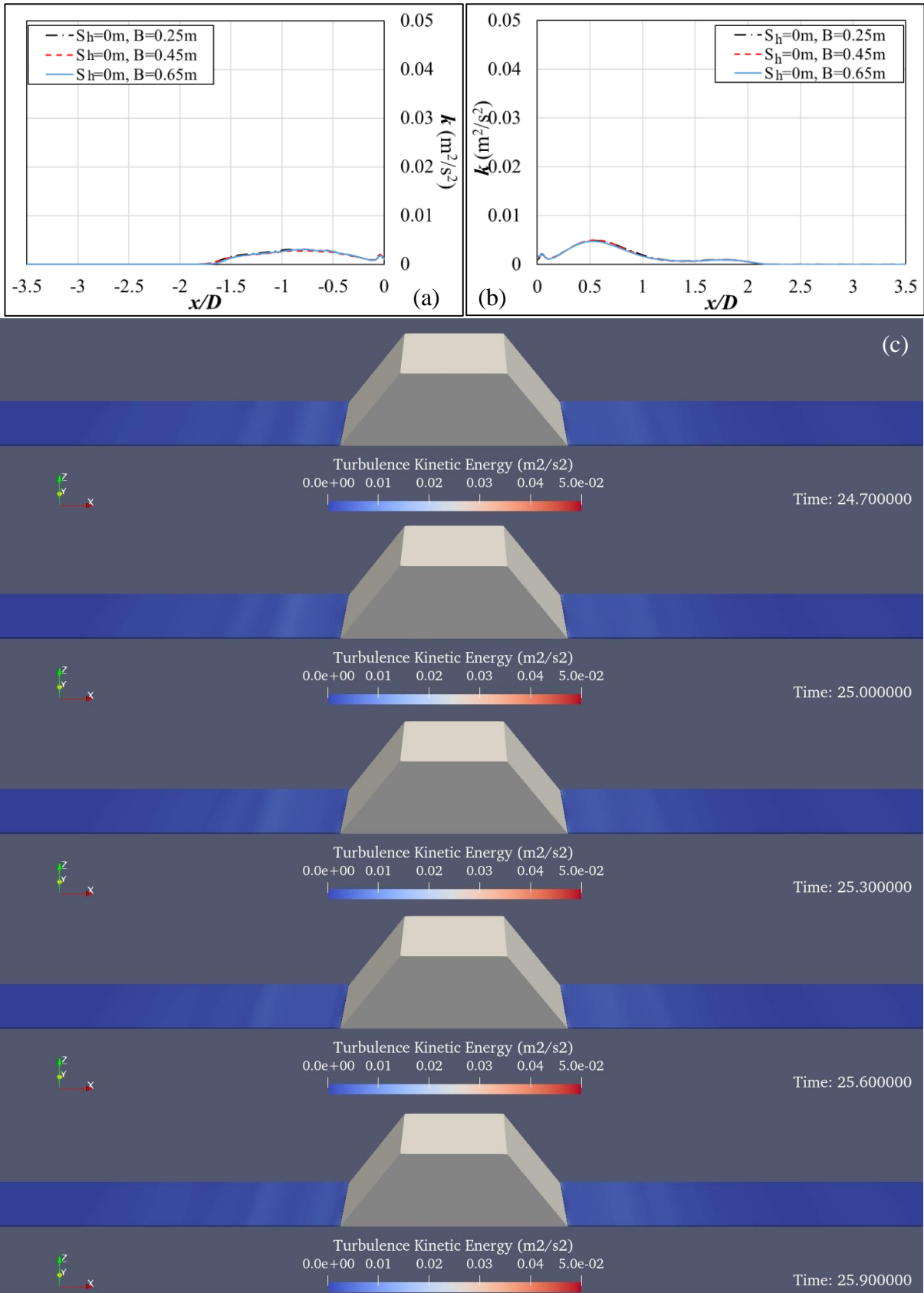
Figure 6.10. The turbulent kinetic energy, k, at the seabed of a smooth slope (S_h=0 m) on the submerged breakwater (a) the time-average TKE at the seaward side (b) the time-average TKE at the landward side (c) the evolution of TKE at the seabed of structure

126

Figure 6.11. The turbulent kinetic energy, k, at the seabed of a micro rough slope (S_h=0.06m) on the submerged breakwater (a) the time-average TKE at the seaward side (b) the time-average TKE at the landward side (c) the evolution of TKE at the seabed of structure
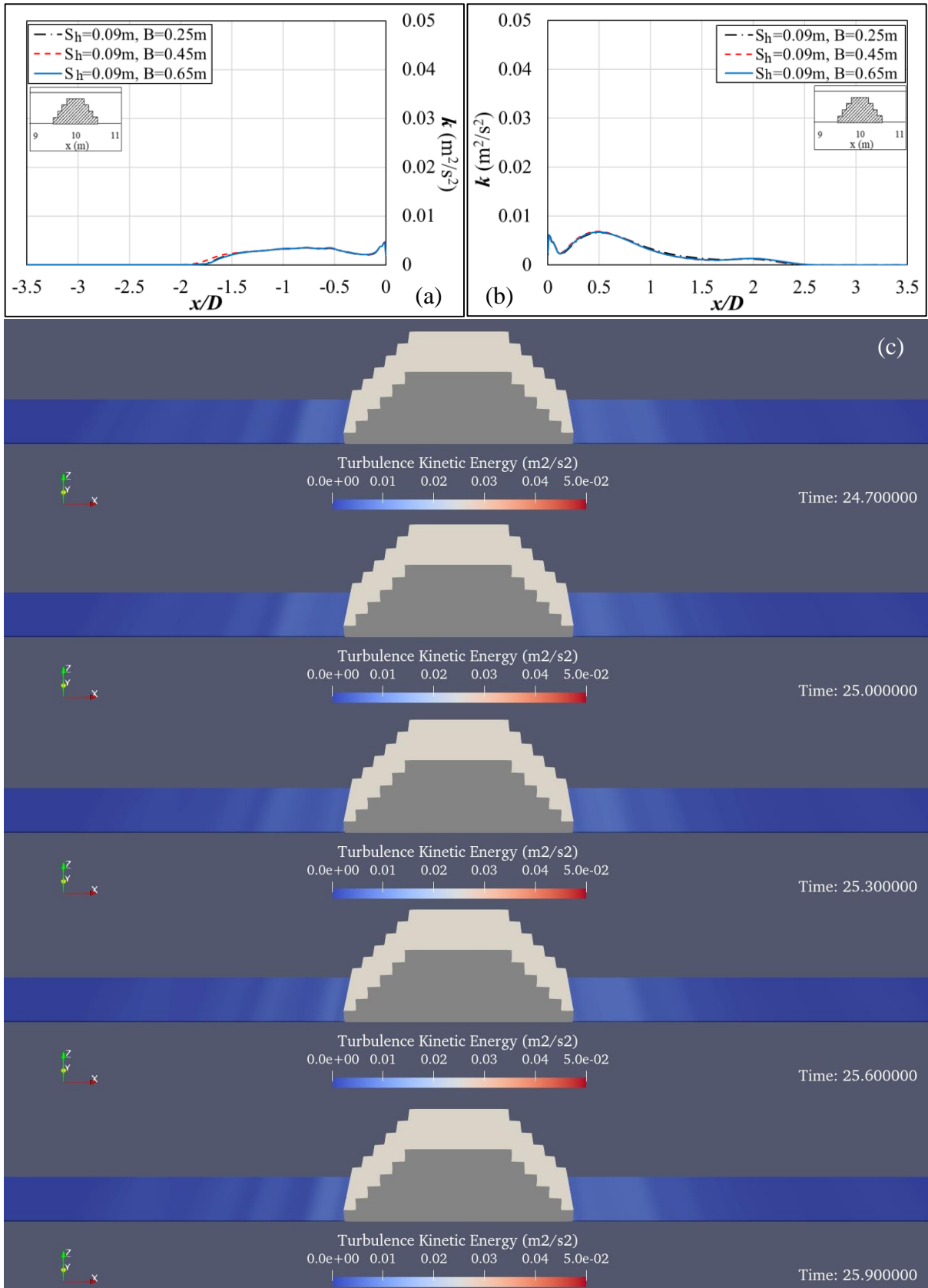
Figure 6.12. The turbulent kinetic energy, k, at the seabed of a macro rough slope (S_h=0.09m) on the submerged breakwater (a) the time-average TKE at the seaward side (b) the time-average TKE at the landward side (c) the evolution of TKE at the seabed of structure

Figure 6.13. The turbulent kinetic energy, k, at the seabed of a composite slope (S_h=0.18m) on the submerged breakwater (a) the time-average TKE at the seaward side (b) the time-average TKE at the landward side (c) the evolution of TKE at the seabed of structure
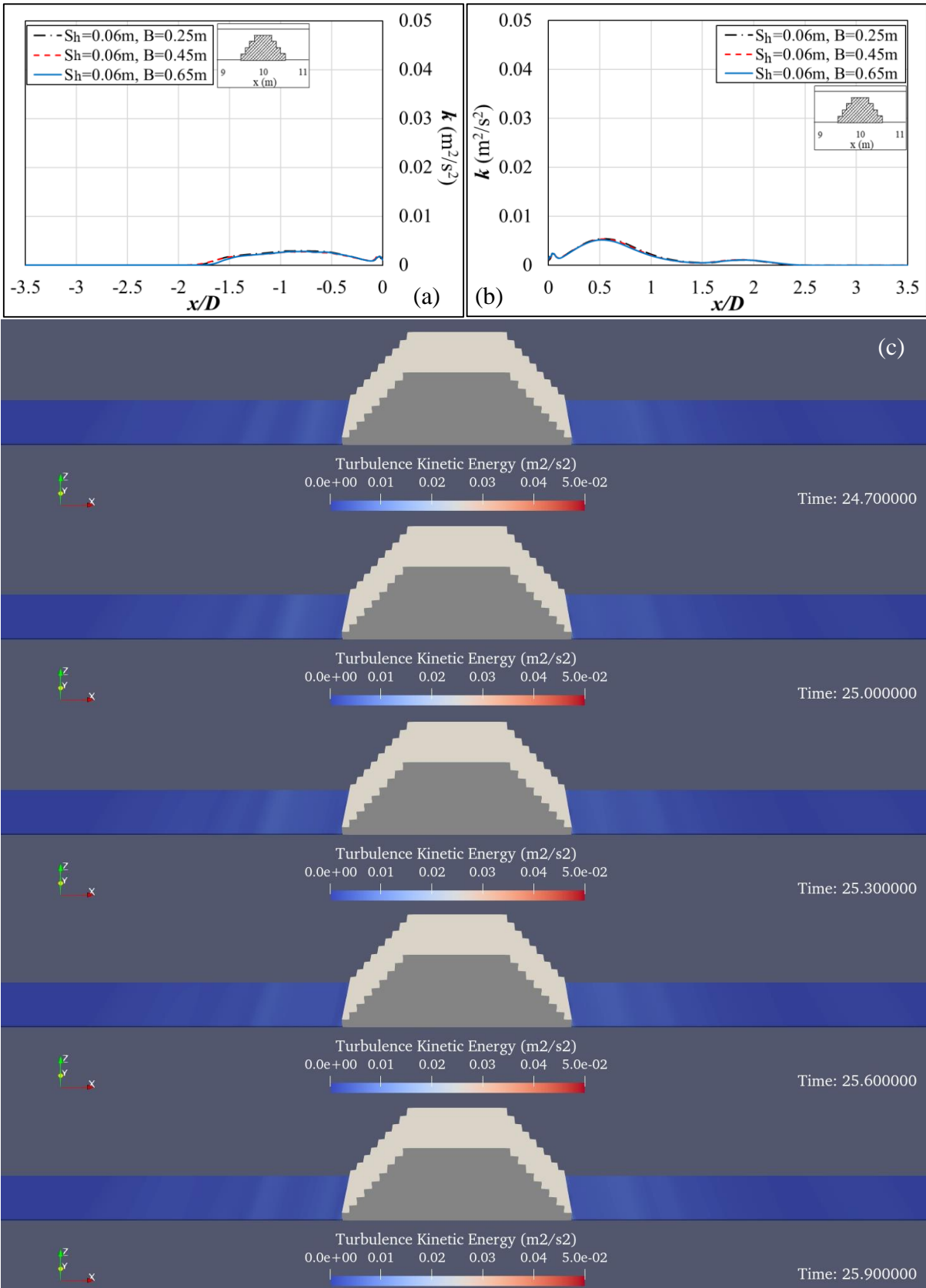
129

Figure 6.14. The turbulent kinetic energy, k, at the seabed of a vertical shape (S_h=0.54m) of the submerged breakwater (a) the time-average TKE at the seaward side (b) the time-average TKE at the landward side (c) the evolution of TKE at the seabed of structure
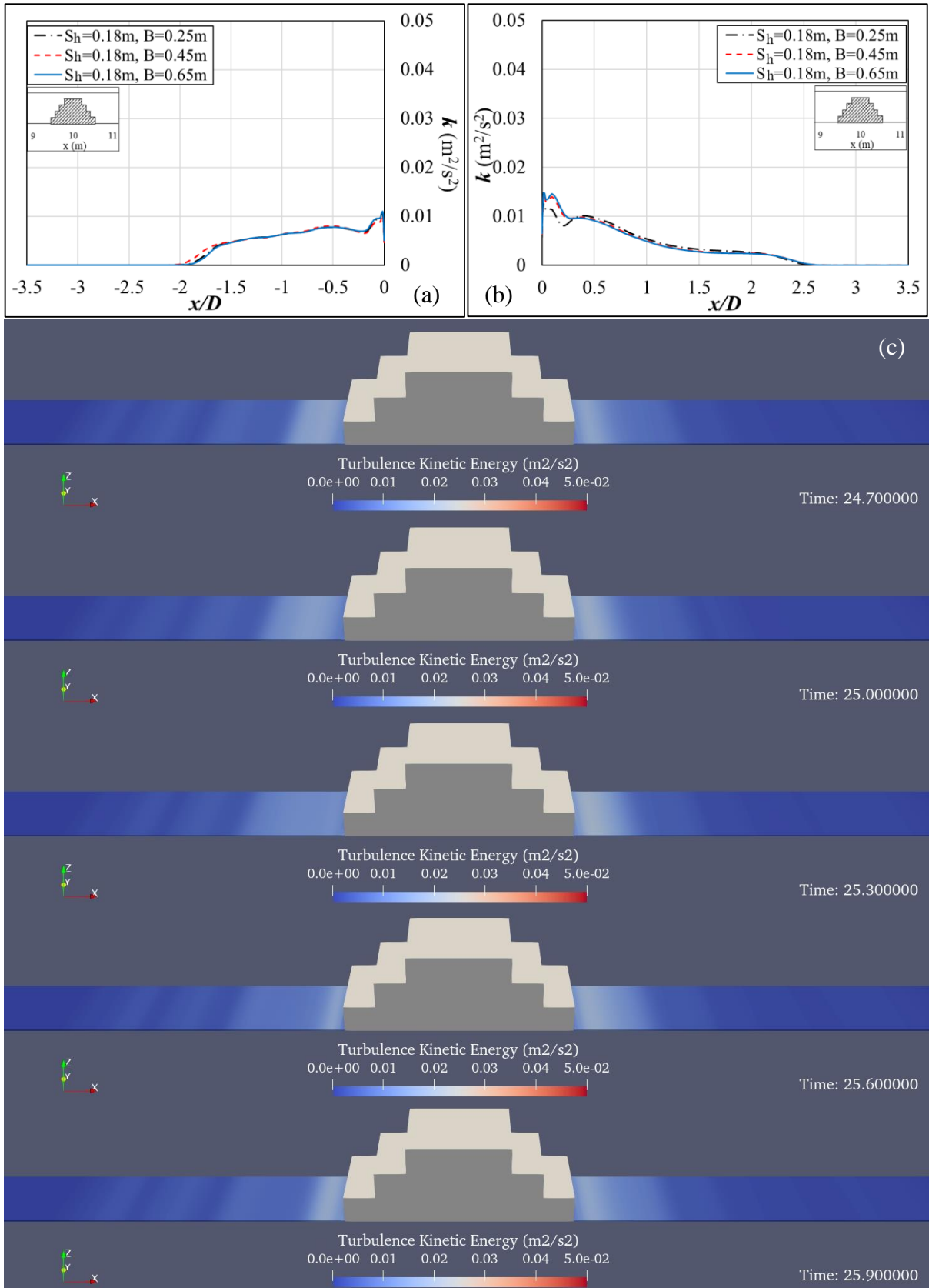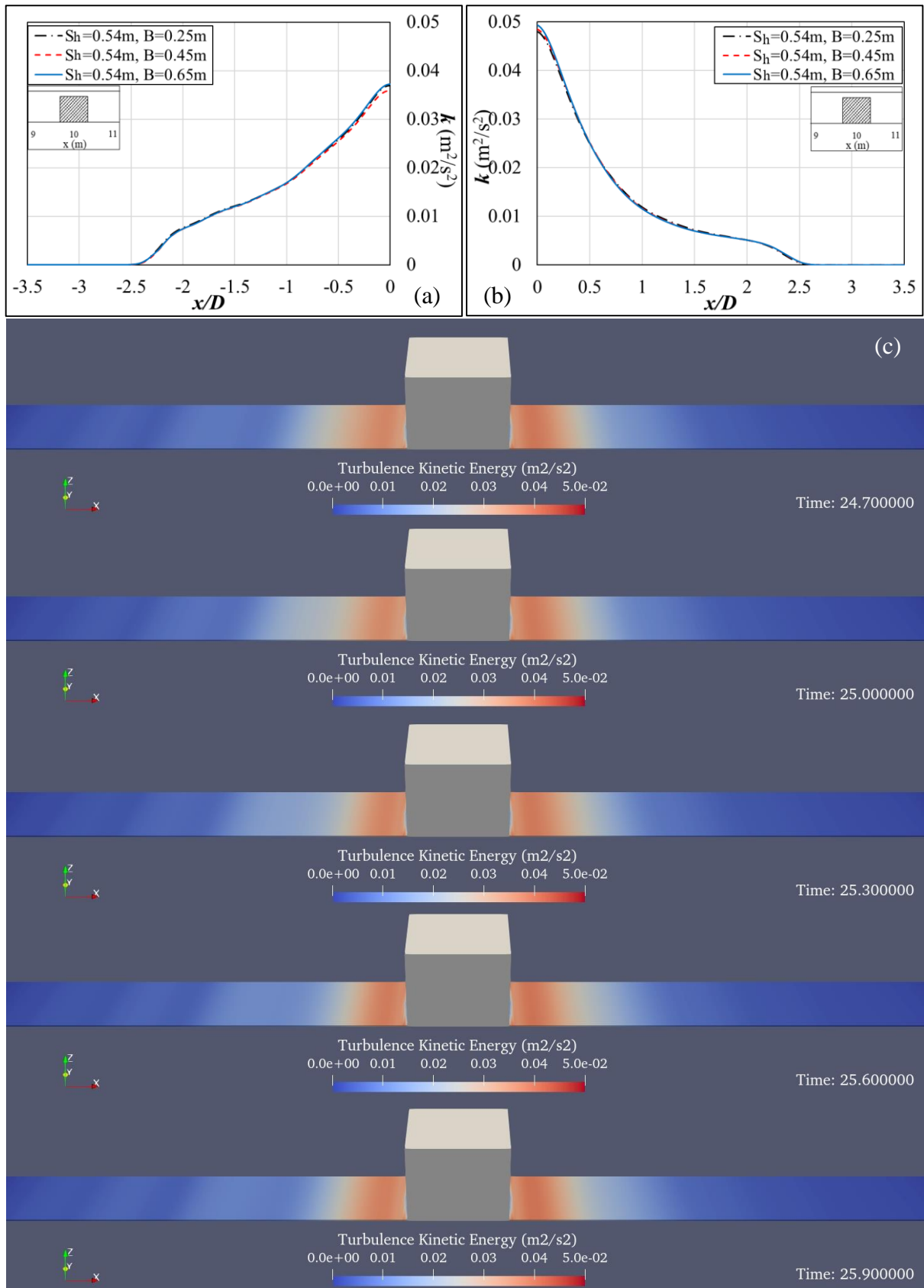
According to Figures 6.10, 6.11, 6.12, 6.13 and 6.14, the comparison of time-average turbulence kinetic energy with different stepped heights of submerged breakwaters was plotted with the dimensionless position in X-axis. In Figures 6.11 and 6.12, the diagrams for a smooth and micro rough slope (S_h=0m and 0.06m) showed that the turbulence kinetic energy on the landward side was slightly larger than the seaward side. The peaks of time-average TKE for different crest widths were located around x/D=0.5 behind the structures. Then, the higher TKE was developed in the case of the bigger stepped sizes such as a macro rough slope (S_h=0.09m) and a composite slope (S_h=0.18m) of structures. The peaks of average TKE were shifted to become closer to structures with the increased stepped heights. For the vertical shape (S_h=0.54m) of the submerged breakwater, the time-average TKE at the landward side was also slightly larger than the seaward side. The peaks of time-average TKE completely appeared at the structures on both sides of seaward and landward. For the effect of varying crest widths, the comparison showed a negligible impact on the turbulence property. Whereas, the influences of different stepped heights directly affected the forming of turbulence kinetic energy.

6.2.2.2. THE EFFECT OF DIFFERING STEPPED HEIGHTS ON STRUCTURES TO TURBULENCE CHARACTERISTICS

In order to consider the influences of differing stepped heights on the turbulence kinetic energy, the comparison of the time-average turbulent kinetic energy on the different crest widths (B=0.25m, B=0.45m and B=0.65m) are shown in Figures 6.15, 6.16 and 6.17, respectively. In each diagram, the turbulence kinetic energy was plotted against the dimensionless position in the X-direction for the seaward and landward sides. The different stepped sizes on submerged breakwaters for d_s/d=0.1 of the submergence ratio were all represented by the black lines. The red lines presented the cases of d_s/d=0.325 of the submergence ratio.
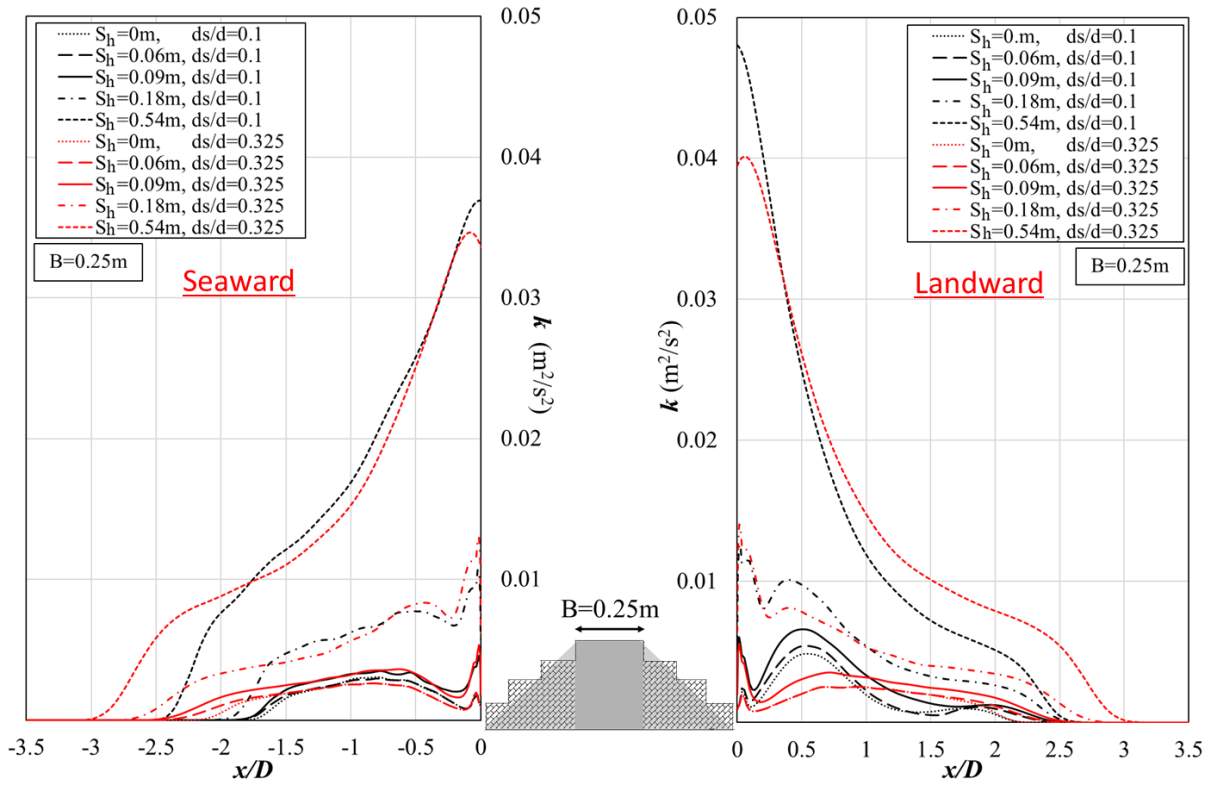
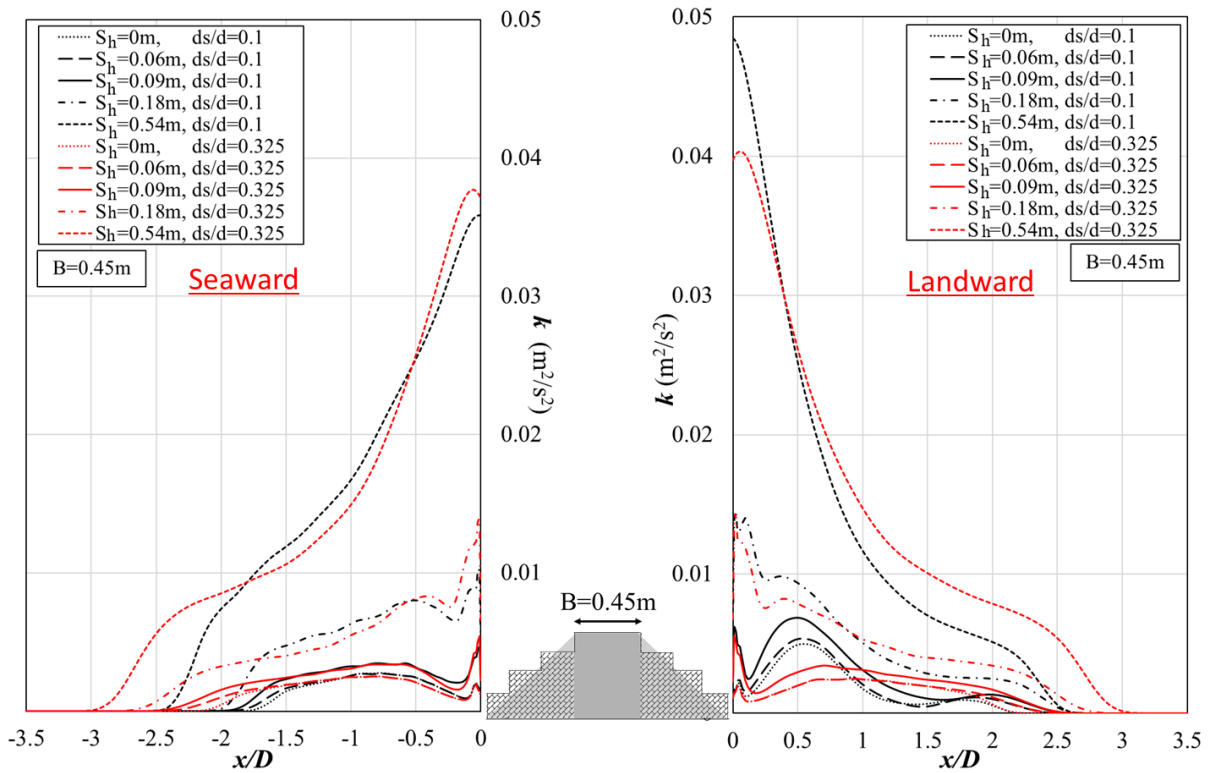Figure 6.15. The effect of different stepped heights of *B*=0.25 submerged breakwaters on the turbulent kinetic energy

Figure 6.16. The effect of different stepped heights of *B*=0.45 submerged breakwaters on the turbulent kinetic energy
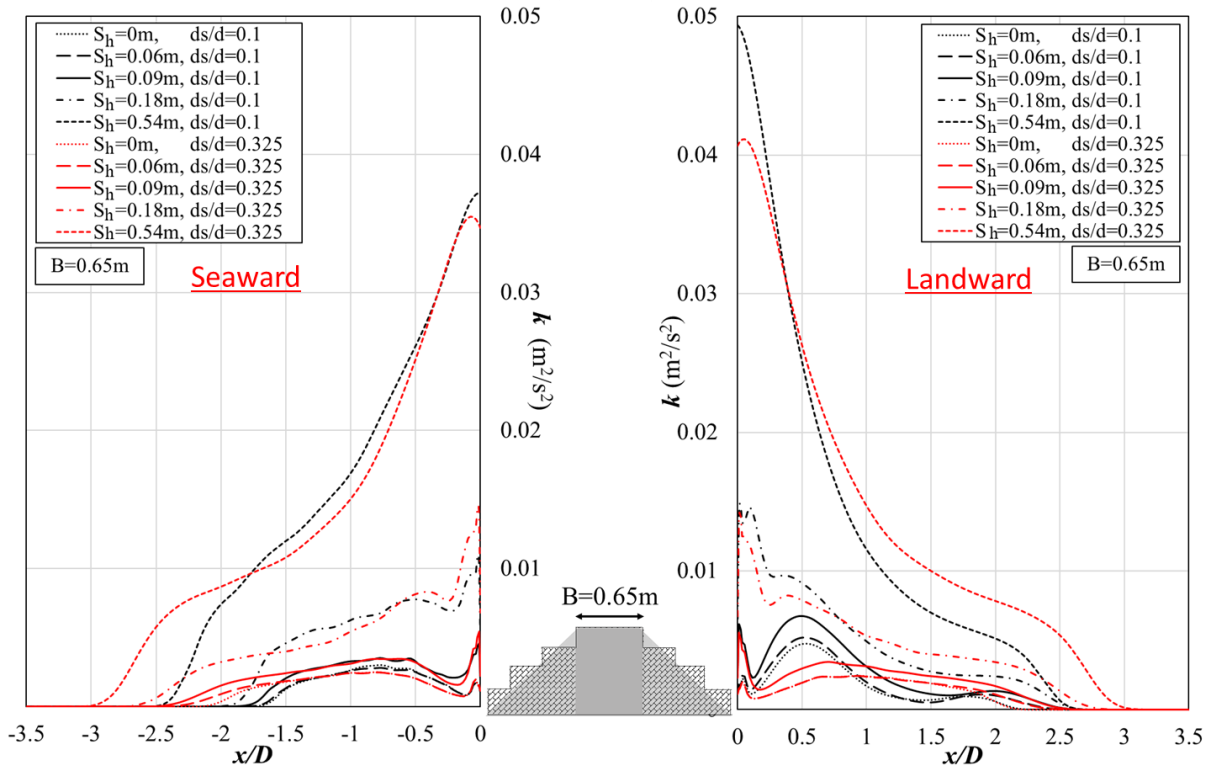
132

Figure 6.17. The effect of different stepped heights of *B*=0.65 submerged breakwaters on the turbulent kinetic energy

According to Figures 6.15, 6.16 and 6.17, the comparison of time-average TKE with the varying stepped heights was plotted with *x/D* for both seaward and landward sides of structures. For the effect of stepped sizes on structures, the results showed that the structures with a gentler surface slope provide a smaller turbulent kinetic energy. Whereas, the increased TKE can be directly obtained with the increased stepped heights on the structure. In this study, the results of time-average TKE for a vertical shape of structures obviously showed the largest turbulence among these several shapes, which was around four times higher than the other shapes. For the influence of the submergence ratio on the turbulence energy, the results showed that the magnitude of an average TKE between d_s/d=0.1 and d_s/d=0.325 had a small effect. Whereas, the effect of submergence ratio affected the scales of turbulence in the X-direction of the seaward side. The forming of TKE in d_s/d=0.325 was wider than the submergence ratio of d_s/d=0.1.

CHAPTER 7
CONCLUSIONS

Chapter 7

CONCLUSIONS

This chapter is allocated for the conclusions of all chapters in this thesis. Firstly, the introduction is introduced with the motivation and purposes of this research, which is followed by the literature reviews. Then, the processes of numerical simulation are summarized from the viewpoint of research methodology. The results and discussion of this thesis are divided into three topics, which are the performance of wave energy dissipation, the behavior of wave attenuation through submerged breakwaters and the risk-based assessment of scour around submerged breakwaters. The results of this thesis are also finally summarized and concluded in this chapter.

In this thesis, the studies on the influences of a stepped slope on submerged structures were conducted in a numerical model. A two-dimensional model was simulated by the open-source code fluid dynamics project, OlaFlow, which was developed within OpenFOAM® software. The effects of a stepped slope on submerged structures were investigated under several conditions of waves and structural geometries. Focusing on the ability of wave energy dissipation, the performances of stepped submerged breakwaters were analyzed from the viewpoint of the wave transmission coefficient (K_t), wave reflection coefficient (K_r) and wave energy dissipation rates (K_d). The abilities of stepped submerged structures were also compared with the conventional breakwaters (smooth slope and vertical shape of structures). In order to gain more insight into the hydraulic properties, the behaviors of wave propagation around submerged breakwaters were also investigated in this study. The characteristics of wave breaking over different structural geometries and the behavior of interactive waves on the steps of structures were analyzed by turbulent kinetic energy (k). In terms of the risk-based assessment of scour, the results were considered based on the shear stress (τ) properties and the turbulence characteristics at the seabed around structures.

In Chapter 1, the introduction of the research study is described in the first part. The motivation and the doubt of structural development are introduced with the general background of the research, which also briefly presents the causes of structural development and the ideas for problem solutions. Then, the purposes of this research are announced and described with the study plans.

In Chapter 2, the related theories and studies of this research are mentioned in the part of the literature review. Before presenting the ability of wave dissipation by coastal structures, the general theories are briefly presented for the property of wave, wave transformation and wave-breaking. Then, wave interactions with submerged breakwaters are described with the general background and the effects of structural geometry on wave energy dissipation. In order to develop an effective low-crest structure, various studies in the past are collected and reviewed for the effect of structural shapes on the ability of wave control. The idea of applying a stepped slope on the breakwater has been interesting in the last few decades and has been investigated in many studies. Whereas, most of the previous studies were only focused on the performance of wave transmission. Therefore, in order to have more understanding and comprehension of the ability of wave dissipation, comprehensive studies on the performance of wave reflection, wave transmission and wave energy dissipation are considered in this research. Moreover, the behaviors of wave interaction with structures are also illustrated by numerical simulations based on computational fluid dynamic (CFD) software. The effects of the various structural geometries are also investigated on the risk of erosion around the structure.

In Chapter 3, the main purpose of this chapter is to present the research methodology, which describes the outline processes in the numerical model. Firstly, the introductions of the related software, solver and simulation methods of this study are introduced with the description. This research was carried out in numerical simulations using open source CFD code package, OpenFOAM®. The problems were solved by the OlaFlow solver. The structural models were created in FreeCAD software and exported to calculate in OpenFOAM® software. In order to visualize the data sets of OpenFOAM®, the post-processing of numerical simulation was illustrated in ParaView software. For the numerical setup, the two-dimensional hydraulic model tests were conducted in a numerical wave flume with a length of 40 m, a depth of 1.2 m and a width of 0.05 m. To investigate the interaction between regular waves and specific obstruction, a stepped submerged breakwater model was fixed at 10 m away in the X-direction from the wave generation boundary. There were four points for wave surface elevation measuring based on the Volume of Fluid method, which was located in front of and behind the structure. The efficacies of the stepped slope on an impermeable structure were examined and compared with the conventional breakwaters (smooth trapezoidal and vertical breakwaters). The influences of stepped slope on submerged structures are presented in a range of stepped heights, S_h, from 0 $\leq d\text{-}d_s$. The structure with a non-stepped slope ($S_h= 0$ m) is represented as a smooth slope, which is followed by an expanded stepped height to the biggest stepped height as a vertical structure ($S_h=0.54$ m). The details of boundary conditions, numerical parameters and wave

maker are also explained in this part. For the processes of mesh generation, the details of BlockMesh and SnappyHexMesh are described in detail with the results of mesh creation. For the last process in this section, the model validation is included by comparing wave surface elevations between numerical simulation and wave theory. According to the range of wave conditions, the Stokes second-order wave theory was applicable to this study that was identified based on the relative water depth and wave steepness. The numerical results of wave generation show a good agreement with the wave theory. The model validation results confirm that the developed models can simulate a certain wave, therefore the models can test with different cases of submerged structures.

In Chapter 4, the numerical results of the study on the performance of wave energy dissipation were reported from the computation of wave transmission coefficient, wave reflection coefficient and wave energy loss rates. The computational data analysis was mainly computed from wave heights, which were collected by the water elevation tracking in the numerical model. Two wave probes method (Goda and Suzuki, 1967) was applied to separate the incident and reflected waves. According to the results of this study, the abilities of wave attenuation under various conditions of waves and structural geometries can be concluded and summarized in Figure 7.1. A small wave transmission, large reflected wave and effective wave energy loss were obtained with the increase in relative crest width, B/L, the increased wave steepness, λ, the decreased submergence depth, d_s/H_i and the decreased in submergence ratio, d_s/d. The full proficient wave energy attenuation was received from the structures with a smooth and small stepped slope. The performance of wave energy loss tended to decrease with the expanded height of the step. However, in terms of the comparison between the effect of smooth and stepped slope, the change of smooth slope (S_h=0 m) and the small stepped height (S_h =0.06 m) seemed to have negligible effects, whereas an apparent change can be noticed from an expanded stepped height as S_h =0.18 m (composite slope) or S_h =0.54 m (vertical structure).
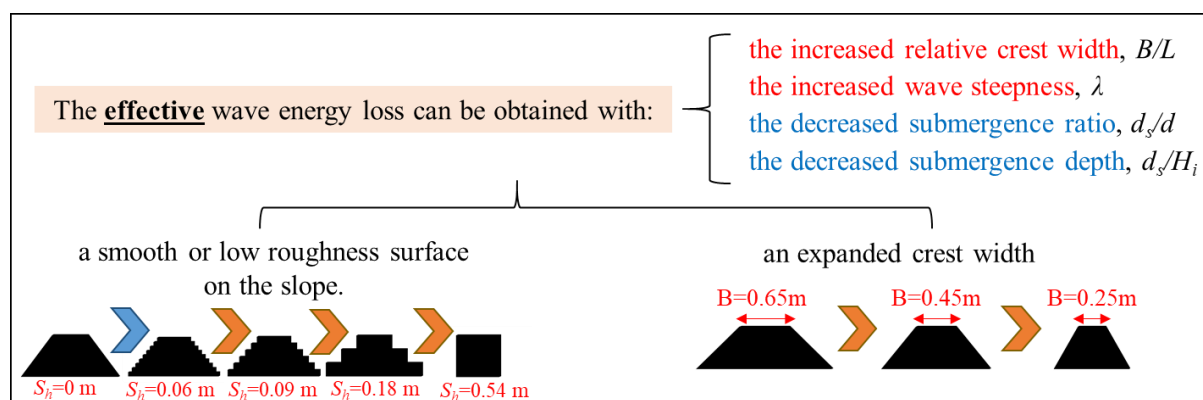

Figure 7.1. The summary of the performance of wave energy dissipation

In Chapter 5, this chapter aims to present the behavior of wave attenuation through submerged breakwaters, which was illustrated by the post-processing results of numerical simulation. The graphical diagrams and snapshots of the model simulation were used to indicate the processes of wave dissipation. The abilities of wave dissipation were analyzed based on wave breaking and turbulence models, which were illustrated from the viewpoint of wave propagation and the magnitude of turbulent kinetic energy. In this study, the numerical simulations were mainly developed from turbulence modeling, which was simulated by using the K-ω SST turbulence model (Menter, 1994). According to the observation of energy dissipation through wave breaking processes, the magnitude of turbulent kinetic energy was used to indicate the energy loss in the model simulation, which can be summarized in Figure 7.2. For the comparison of different stepped heights, the intense turbulent kinetic energy tended to form above a gentler surface slope, which was slightly pale with an expanded height of steps. Focusing on the effects of structure crest width, the turbulent kinetic energy consistently expanded with the larger crest width. However, the behavior of wave energy loss in this chapter provided a good agreement with the computational results in Chapter 4. For the behavior of wave attenuation through submerged breakwaters, the results of numerical simulations provide a summary in Figure 7.3. A smooth slope provided a low reflection of wave, which increased with the increased steps. Whereas, the pure wave reflection was obtained by the vertical shape with the re-direction particles of wave. Moreover, according to the comparison of permeable and impermeable structures, it can be summarized in Figure 7.4. The results showed that a permeable structure reflects a lower wave and provided a smaller wave height behind the structures, which was compared with the impermeable cases. Although, the main purpose of this research study is to focus on the performance of impermeable submerged breakwater, but in order to improve and suggest for the future study. The cases study of permeable simulations can be suggested for getting more effective results of submerged breakwater.
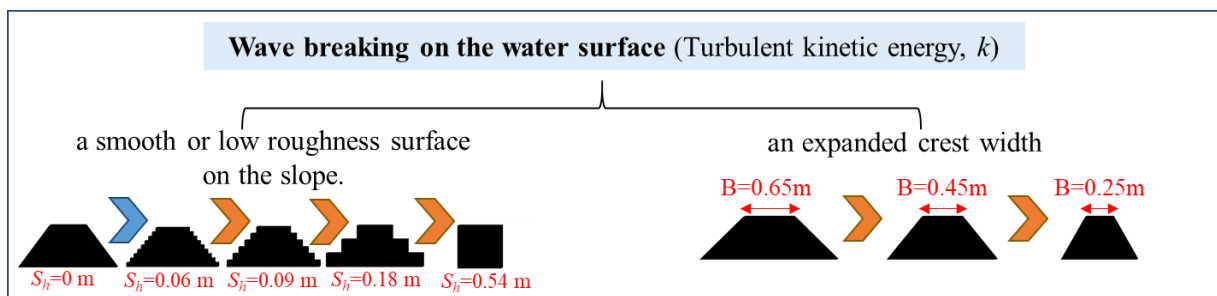

Figure 7.2. The summary of the wave breaking over submerged breakwaters

Smooth slope $S_h = 0$ m	Micro rough slope $S_h = 0.06$ m	Macro rough slope $S_h = 0.09$ m	Composite slope $S_h = 0.18$ m	Vertical structure $S_h = 0.54$ m
Move along smooth structure's surface	Turbulence in step niches	Major vortices in step niches	Vortex shedding at step edges	Re-direction of the flow
Low reflection	Low reflection	Moderate reflection	Reflection	Pure reflection

Figure 7.3. The summary of the behavior of wave attenuation through submerged breakwaters

The effect of porous structures

Impermeable   Permeable

Wave Reflection

Impermeable > Permeable

Wave height behind structures

Impermeable > Permeable
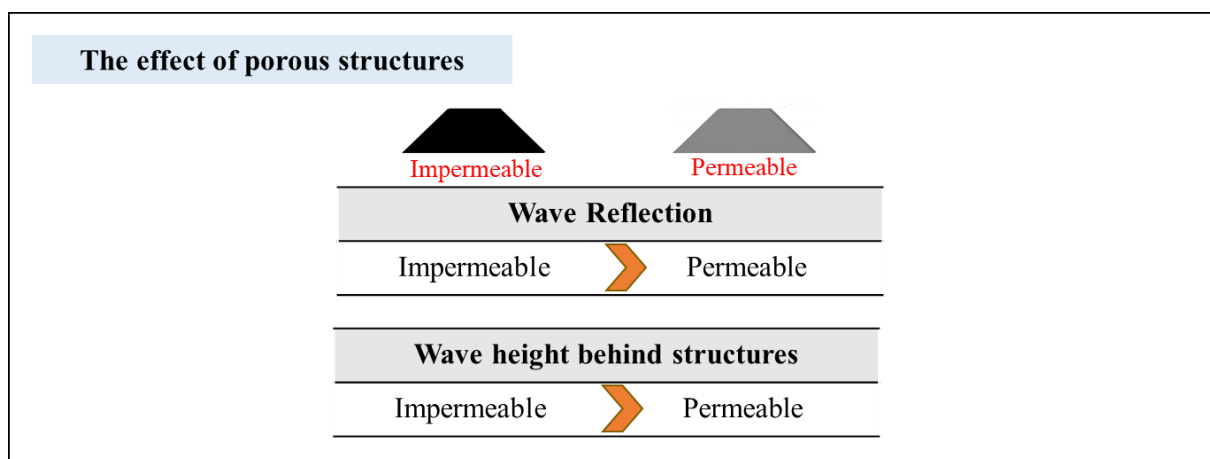
Figure 7.4. The summary of the effect of porous media on the performance of wave energy dissipation

In Chapter 6, the risk assessment of scour was mainly analyzed from the viewpoint of hydrodynamic characteristics, which were indicated by shear stress properties and turbulence characteristics at the seabed. In order to provide a clear simulated result, the computational results indicated the risk of scour, which can be concluded in Figure 7.5. Focusing on the risk assessment of scouring, the large amplification factor of bed shear stress (τ/τ_0) and turbulent kinetic energy (k) were developed around the vertical shape of submerged breakwaters. Bed shear stress (τ) and turbulent energy (k) tended to reduce with the decreased stepped heights on the structures. The smooth slope and a small stepped height on structures showed a small effect between the changes from a flat slope to a micro rough slope. Moreover, the changes of crest width also provided a small effect on the hydrodynamic characteristics. In terms of the influence of the submergence ratio on the turbulent energy, the results showed that the magnitude of an average TKE between d_s/d=0.1 and d_s/d=0.325 have a small effect. Whereas, the submergence ratio affected the area of turbulence formation in the X-direction. The forming of TKE in d_s/d=0.325 was wider than the submergence ratio of d_s/d=0.1.
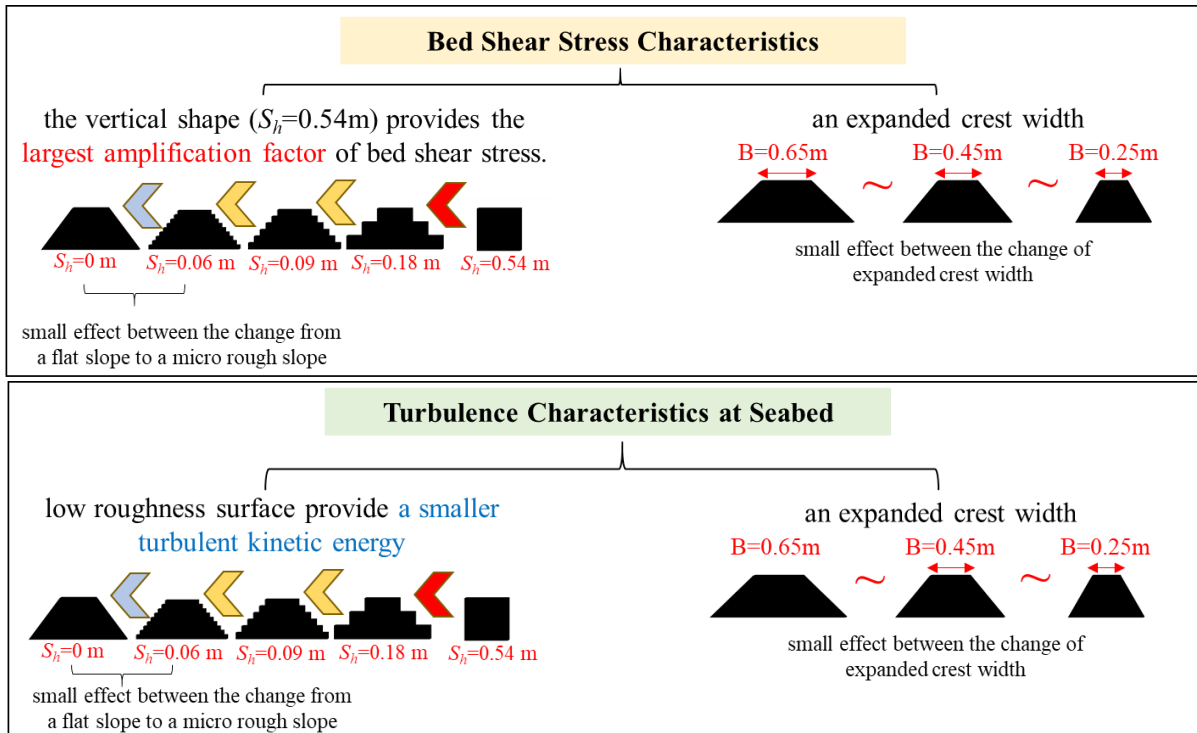
Figure 7.5. The summary of hydrodynamic characteristics on the risk assessment of scour

As the investigation on the performances of stepped submerged breakwaters, it can be concluded that effective wave energy attenuation can be obtained with a gentler surface slope (the smooth and micro rough slope), shallow submergence depth and expanded crest widths of submerged breakwaters.

However, it should be noted that the impermeable structures were mainly considered in this study. The range of parameters in the numerical simulation was designed based on the finding of previous research studies. In order to have a comprehension of submerged breakwater development, it is necessary to consider the wider range of parameter sets and the influence of permeable models, which are also better to validate with a physical experiment.

In addition, as the simulation process in the numerical model suggests, the models with a flat slope and micro rough slope had a negligible effect on the analytical hydraulic performances. Whereas, the duration of the model simulation for a smooth slope spent longer times in the simulation process, which was two times longer than the simulation with a micro rough slope case and the other structural shapes. However, it would be beneficial to consider a micro rough slope of the submerged breakwater in the numerical model, which can represent the trapezoidal shape of a conventional breakwater and reduce the simulation time in a numerical model.

REFFERENCES

Abdullah, S.F., Fitriadhy, A. and Desa, S.M. (2021) "Numerical and experimental investigations of wave transmission behind a submerged WABCORE breakwater in low wave regime" J. Ocean Eng. Mar. Energy 7, pp.405–420. doi: 10.1007/s40722-021-00209-8.

Ahmed A. R., Hossam M. M., Iskander M.M. and Ahmed M. A. (2022) "Performance assessment of corrugated semi-circular breakwaters for coastal protection," Alexandria Engineering Journal, Volume 61, Issue 5,2022, pp. 3587-3598. doi: 10.1016/j.aej.2021.08.086.

Bascom W. (1980) "Waves and Beaches: The dynamics of the ocean surface," Anchor Book, Garden city, New York.

Bay I. (2005) "Measurement and analysis of wave overtopping," European University of Lefke, Ph.D. thesis, pp. 16.

Bleck, M. and Oumeraci, H. (2001) "Wave Damping and Spectral Evolution at Artificial Reefs," Proc. 4th International Symposium on Ocean Wave Measurement and Analysis, San Francisco, California, USA.

Bosboom J. and Stive M. J. F. (2023) "Coastal dynamics," Open Education Resource (OER) LibreTexts Project: https://geo.libretexts.org/Bookshelves/Oceanography/Coastal_Dynamics _%28Bosboom_and_Stive%29/08%3A_Coastal_protection/8.05%3A_Structures_influencing _longshore_transport_rates/10.5.4%3A_Detached_shore_parallel_offshore_breakwaters, pp.10.5.4.1. (Accessed 6 June 2023).

Bridge, J., and Demicco, R. (2008) "Unidirectional turbulent water flow, sediment transport, erosion, and deposition," In Earth Surface Processes, Landforms and Sediment Deposits (pp. 121-194). Cambridge: Cambridge University Press. doi:10.1017/CBO9780511805516.006.

Carevic , D, Prsic , M, and Ocvirk, E. (2009), "Modelling of Wave Interaction with Submerged Breakwater Using MIKE 21 BW," International Symposium on Water Management and Hydraulic Engineering ,Ohrid Macedonia.

Chang, Y.S., Do, J.D. and Jeong, W.M. (2020) "Comparison of Turbulent Flows and Suspended Sediment Particle Motions Simulated around a Submerged Breakwater Using RANS and LES," Ocean Sci. J. 55, pp. 1–16. doi: 10.1007/s12601-020-0009-7.

Cho, Y. S., Yoon, S. B., Lee, J.I. and Yoon, T. H. (2001) "A Concept of Beach Protection with Submerged Breakwaters," Journal of Coastal Research, pp. 671–678.

Conde, J. M. P. (2019) "Comparison of Different Methods for Generation and Absorption of Water Waves." Revista de Engenharia Térmica, 18(1), pp. 71-77.

Damme M. V. (2021) "Detachment of dilatant soil due to high hydraulic shear stresses explained," Journal of Hydraulic Research, 59:1, pp. 51-60, DOI: 10.1080/00221686.2020.1714758.

Dean R.G. and Dalrymple R.A. (1991) "Water wave mechanics for engineers and scientist," World scientific, Singapore.

Department of Marine and Coastal Resources (2013) Status of coastal environment in Thailand, Available: https://km.dmcr.go.th/c_55/d_1210 (Accessed 24 January 2021).

Department of mineral resources (2016) Types of Coastal Zone in Thailand, Available: http://www.dmr.go.th/main.php?filename=coastal_En (Accessed 22 January 2021).

Dong S. H., Kwang H. L. and Dong S. C. (2011) "Effect of the Slope Gradient of Submerged Breakwaters on Wave Energy Dissipation, Engineering," Applications of Computational Fluid Mechanics, Vol.5, No.1, pp.83-98, doi: 10.1080/19942060.2011.11015354.

El Saie Yasser Mohamed (2018) "Effect of using submerged rectangular stepped breakwater for the defence of the shore line," International Journal of Architecture, IJA, pp. 41-53.

Goda Y, Suzuki Y. (1976) "Estimation of incident and reflected waves in random wave experiments," Proc. 15th Costal Eng. Conf., ASCE, Honolulu, pp. 828-845.

Gomes, A., Pinho, J.L.S., Valente, T., Antunes do Carmo, J.S. and V. Hegde (2020) "A Performance Assessment of a Semi-Circular Breakwater through CFD Modelling," J. Mar. Sci. Eng. 2020, 8, 226. doi: 10.3390/jmse8030226.

Higuera P. (2015) "Application of computational fluid dynamics to wave action on structures," University of Cantabria, Ph.D. thesis.

Higuera, P. C., Lara, J. L., and Losada, I. J. (2013) "Realistic Wave Generation and Active Wave Absorption for Navier–Stokes Models: Application to OpenFOAM", Coastal Engineering, Vol. 71, pp. 102-118.

Hirt, C.W. and Nichols, B.D. (1981) "Volume of fluid (VOF) method for the dynamics of free boundaries", Journal of Computational Physics. 39 (1), pp. 201–225, doi:10.1016/0021-9991(81)90145-5.

Ibrahim, I. N., Ab Razak, M.S., and Safari, M. D. (2018) "A Short Review of Submerged Breakwaters," MATEC Web Conf. 203(2018): 01005.

Issa, R. I. (1986) "Solution of the implicitly discretised fluid flow equations by operator splitting", Journal of Computational Physics, 62(1), pp. 40–65.

Jiang X.L., Zou Q.P. and Zhang N. (2017) "Wave load on submerged quarter-circular and semicircular breakwaters under irregular waves" Coastal Engineering, Vol.121, pp.265-277.

Johnson, H.K., Karambas, T.V., Avgeries, I., Zanuttigh, B., Gonzalez-Marco, D., and Caceres, I. (2005) "Modelling of waves and currents around submerged breakwaters," Coastal Engineering, Vol 52, pp. 949-969.

Karpen, N.B. and Schlurmann, T. (2016) "Stepped Revetments-Revisited", In Proceedings of the 6th International Conference on the Application of Physical Modelling in Coastal and Port Engineering and Science, Ottawa, Canada, 10-13 May 2016, pp.10.

Kishi, T. (1959) "The possible highest gravity waves in shallow waters," Coastal Eng. In Japan, JSCE, Vol.2, pp.9-16.

Lachmi SM, Hee MT and Chai HL (2017) "Wave transmission of submerged breakwaters consisting multiple pipes," ARPN J of Eng. and Applied Sci., Vol.12 (20), pp. 5807-5810.

Lamarre E, Melville WK., (1991) "Air entrainment and dissipation in breaking waves," Nat 351(6326), pp.469–472. doi: 10.1038/351469a0.

Le Mehaute, B. (1976) "An Introduction to Hydrodynamics & Water Waves," Springer-Verlag, New York, pp. 315.

Li, C.-Y.; Shih, R.-S.; Weng, W.-K. (2020) "Visualization investigation of energy dissipation induced by eddy currents for a solitary-like wave passing over submerged breakwater sets" J. Mar. Sci. Eng., pp.834. doi: 10.3390/jmse8110834.

Lokesha, Kerpen, N.B., Sannasiraj, S.A., Sundar, V. and Schlurmann, T. (2015) "Experimental investigations on wave transmission at submerged breakwater with smooth and stepped slopes," Proc. of the 8th Int. Conf. on Asian and Pacific Coasts, APAC, Procedia Eng. 116, pp. 713-719.

Manun T. (2023) Coastal Erosion in Southern Thailand, Available: https://www.shutterstock.com/image-photo/coastal-erosion-waves-southern-thailand-picture-677980792 (Accessed 3 June 2023).

Mahmoudi, A., Hakimzadeh, H., Ketabdari, M.J., Cartwright, N. and Vaghefi, M. (2017) "Experimental Study on Wave Transmission and Reflection at Impermeable Submerged Breakwaters," Int. J. Coast. Offshore Eng, Vol.1, pp.19–27.

Melville W. (1996) "The role of surface-wave breaking in Air-Sea interaction," Annu Rev Fluid Mech 28(1):279–321. doi:10.1146/annurev.fl.28.010196.001431.

Menter, F. (1994) "Two-equation eddy viscosity turbulence models for engineering applications," AIAA J, Vol. 32, pp. 1598–1605.

Miche, A. (1944) "Mouvements ondulatories de la mer en profendeur constante ou decroissante, Forme limit de la houle lors de som déferlement: Application aux digues maritimes," Ann. Ponts et Chausees, Tome 114.

Michell, J. H. (1983) "The highest waves in water, Phill. Mag. (5), Vol.36, pp.430-437.

Miedema, S. A. (2008) "An analytical method to determine scour," WEDA XXVIII &Te x as A &MUniv.39, 8–11.

Nguyen-Thi, LQ., Nguyen, VD., Pierens, X. et al. (2021) "An experimental and numerical study of the influence of viscosity on the behavior of dam-break flow", Theor. Comput. Fluid Dyn. 35, pp. 345–362, doi: 10.1007/s00162-021-00562-2.

OpenCFD, Ltd. (2023) Overview of OpenFOAM® structure, Available: https://www.openfoam.com/documentation/user-guide/1-introduction (Accessed 22 May 2023).

OpenCFD, Ltd. (2023a) The dissection of domain geometry in blockMesh utility, Available: https://www.openfoam.com/documentation/user-guide/4-mesh-generation-and-conversion/4.3-mesh-generation-with-the-blockmesh-utility (Accessed 22 May 2023).

Orencio D., Bruno A.and Philippe C. (2012) "Numerical simulation of turbulent sediment transport, from bed load to saltation," Physics of Fluids 24 (10): 103306. doi: 10.1063/1.4757662.

Pattaya Mail (2021) The damage of waves on the shoreline in Thailand, Available: https://www.pattayamail.com/thailandnews/thailand-retains-balance-between-economic-development-and-natural-resources-conservation-373834 (Accessed 24 May 2023).

Penny, W. G. and Price A. T. (1952) "Finite periodic stationary gravity waves in a perfect fluid," Phill. Trans., Roy. Soc. London, A244, pp.254-284.

Ramos, P., Pêgo, J.P., and Maia, R. (2014) "Numerical simulation of the flow around a pier using openfoam", 3rd. IAHR Europe Congress, Book of Proceedings, Porto – Portugal.

Rueda L. V. A. (2015) "Turbulence, sediment transport, erosion, and sandbar beach failure processes in Grand Canyon," Arizona State University, Ph.D. thesis.

Sarhan Th.E (2020) "Stepped submerged offshore breakwaters for wave energy dissipation," Int J Oceans and Oceanography, Vol.14, pp. 125-137.

Sawaragi, T., (1995) "Coastal Engineering-Waves, Beaches, Wave-Structure Interactions," Elsevier, Developments in Geotechnical Engineering Series, No. 78, Amsterdam, The Netherlands, pp. 1-12.

Sawaragi, T. (1995a) "Coastal Engineering - Waves, Beaches, Wave-Structure Interactions," Elsevier, Developments in Geotechnical Engineering Series, No. 78, Amsterdam, The Netherlands, pp. 42-44.

SimCenter, (2020) Case directory structure, Available: https://nheri-simcenter.github.io/CFD-Notebooks/lectures/beginner/lecture02.html (Accessed 22 May 2023).

Song, Y.H., Joo, J.G., Lee, J.H. and Yoo, D.G. (2020) "Numerical assessment of shear boundary layer formation in sewer systems with fluid-sediment phases," Water 2020, 12, 1332. doi: 10.3390/w12051332.

Sorensen, R.M. (1993) Basic Wave Mechanics for Coastal and Ocean Engineers, John Wiley, New York.

Srineash, V.K. and Murali, K. (2019) "Effects of seaward slope on wave transmission of porous and non-porous reef breakwaters with smooth and stepped slopes," Hydraulic Engineering Repository, pp.275.

Stahlmann, A., & Schlurmann, T. (2012) "Investigations on scour development at tripod foundations for offshore wind turbines: modeling and application," Coastal Engineering Proceedings, 1(33), sediment.90. doi: 10.9753/icce.v33.sediment.90.

Sumer B.M., Fredsoe J., Christiansen N. and Hansen S.B. (1994) "Bed Shear Stress and Scour Around Coastal Structures," Proceedings of 24th International Coastal Engineering Conference ASCE, Kobe, Japan, vol. 2, pp. 1595-1609.

Wang, H., Foltz, W., Zhang, N., and Dermisis, D. (2020) "Numerical and experimental Analyses of breakwater designs for turbulent flow characteristics and sediment transport under coastal wave actions." ASME. J. Fluids Eng. July 2020; 142(7): 071207.

Wen, J., Chen, Y., Liu, Z. and Li, M. (2022) "Numerical Study on the Shear Stress Characteristics of Open-Channel Flow over Rough Beds", Water 2022, 14, 1752. doi: 10.3390/w14111752.

Wiegel, R.L. (1964) "Oceanographical Engineering", Prentice Hall, pp.523.

Yamada, H. (1957) "On the highest solitary wave", Rept. Res. Inst. Appl. Mech. Kyushu Univ., 5, pp.53-67.

Young, D. M. and Testik, F. Y. (2011) "Wave reflection by submerged vertical and semicircular breakwaters," Ocean Engineering, Vol.38, pp. 1269-1276, doi: https://doi.org/10.1016/j.oceaneng.2011.05.003.

Appendix A

Appendix A shows the samples of the comparison of the instantaneous wave profiles over the different crest widths under various wave conditions.

A1. The instantaneous profile of water surface in the case of T=1.5s of wave period, H_i=0.03m of wave heights and d_s/d=0.1 of submergence ratio
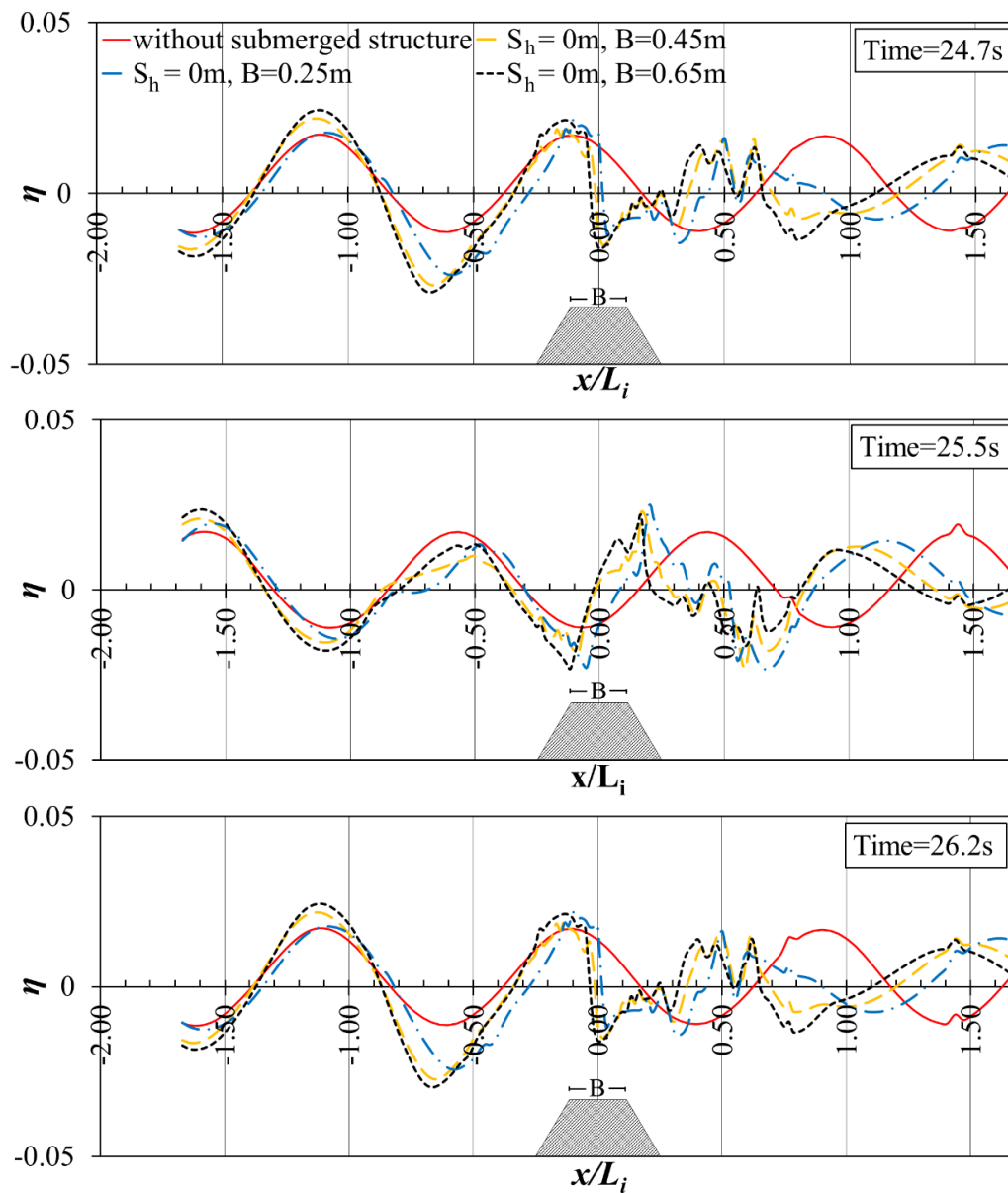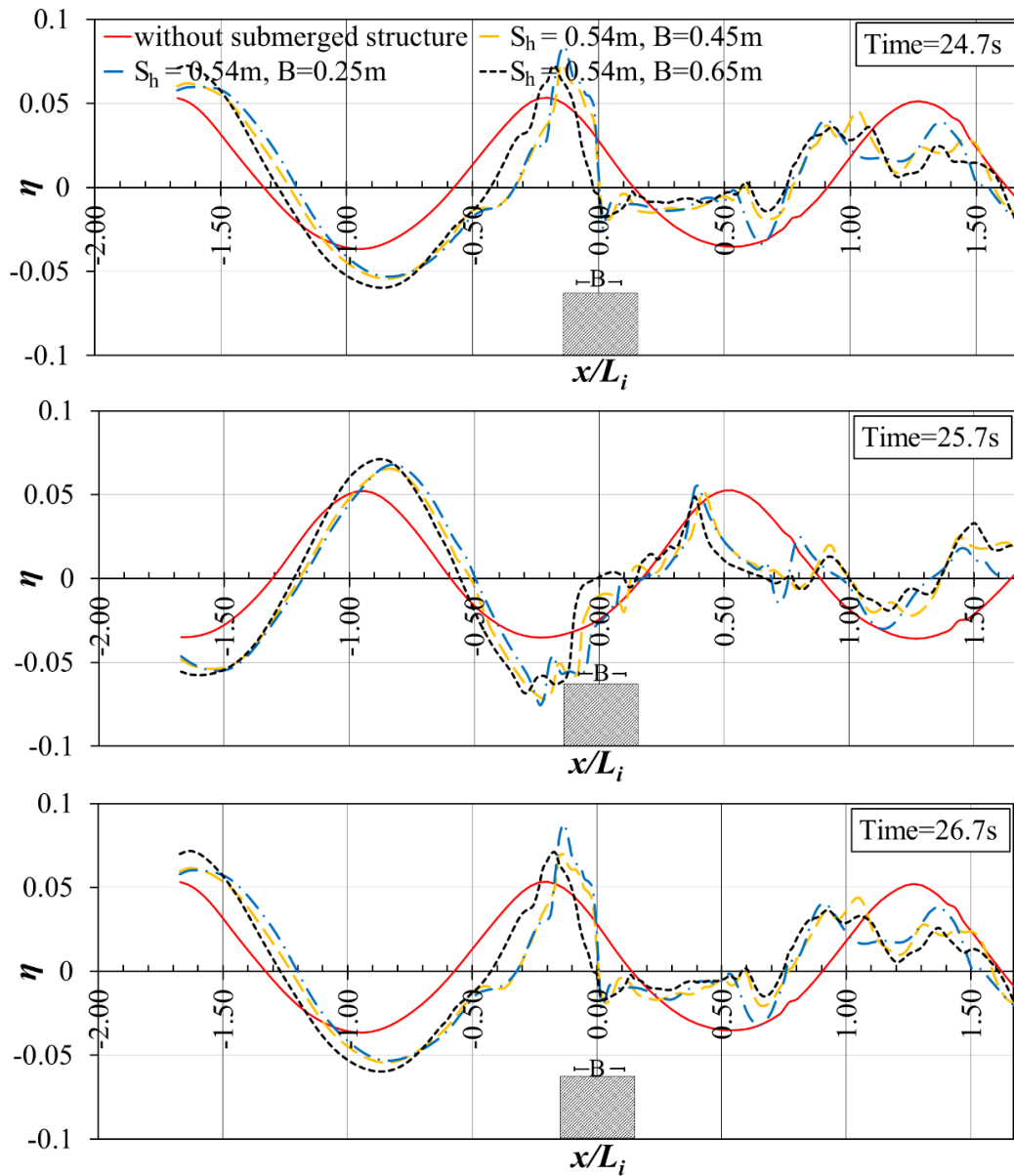

Figure A1.1. Comparison of the instantaneous profiles of water surface elevation on the different crest widths of a smooth slope (S_h=0m) in case of T=1.5s and H_i=0.03m

147
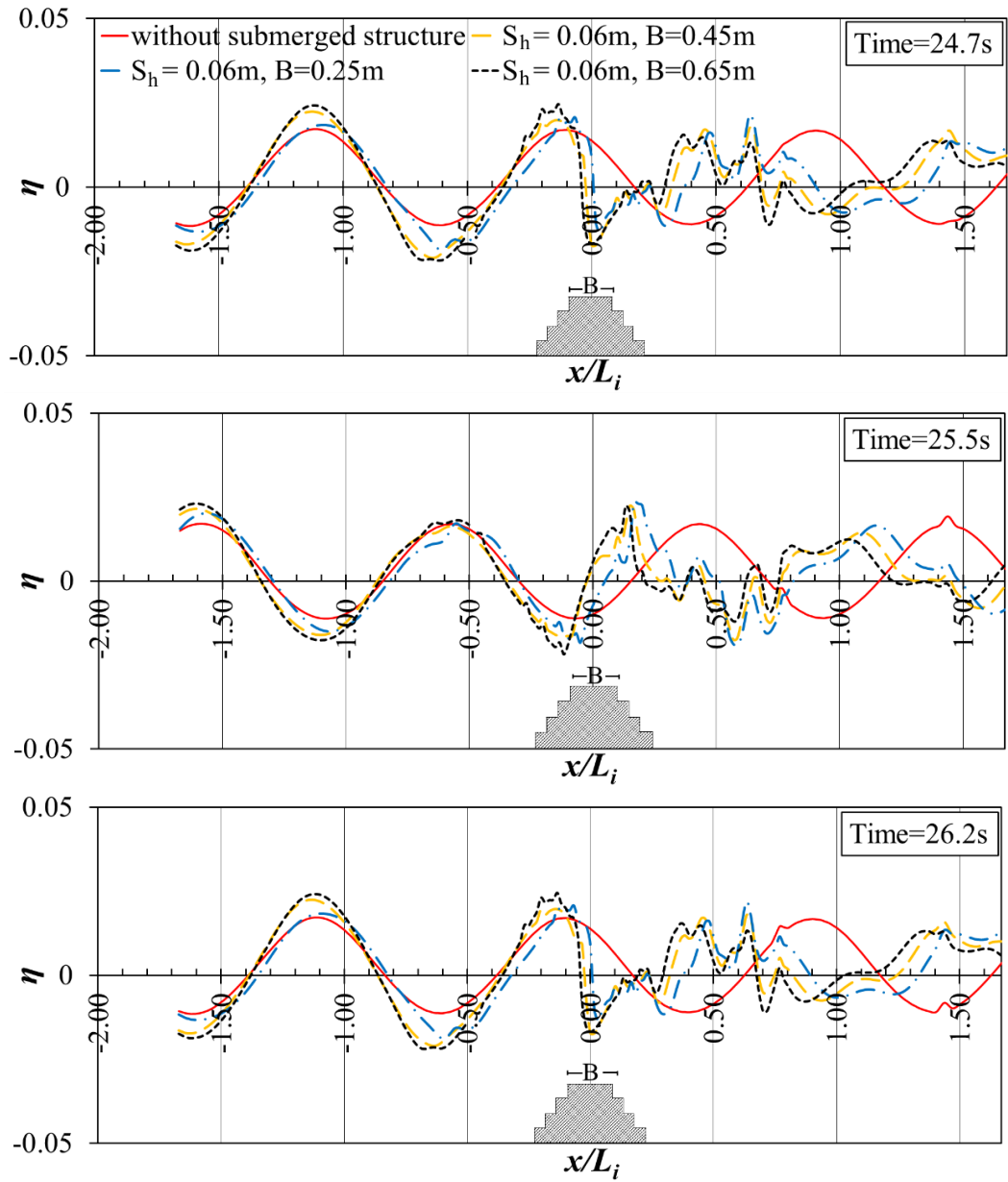
Figure A1.2. Comparison of the instantaneous profiles of water surface elevation on the different crest widths of a micro rough slope (S_h=0.06m) in case of T=1.5s and H_i=0.03m
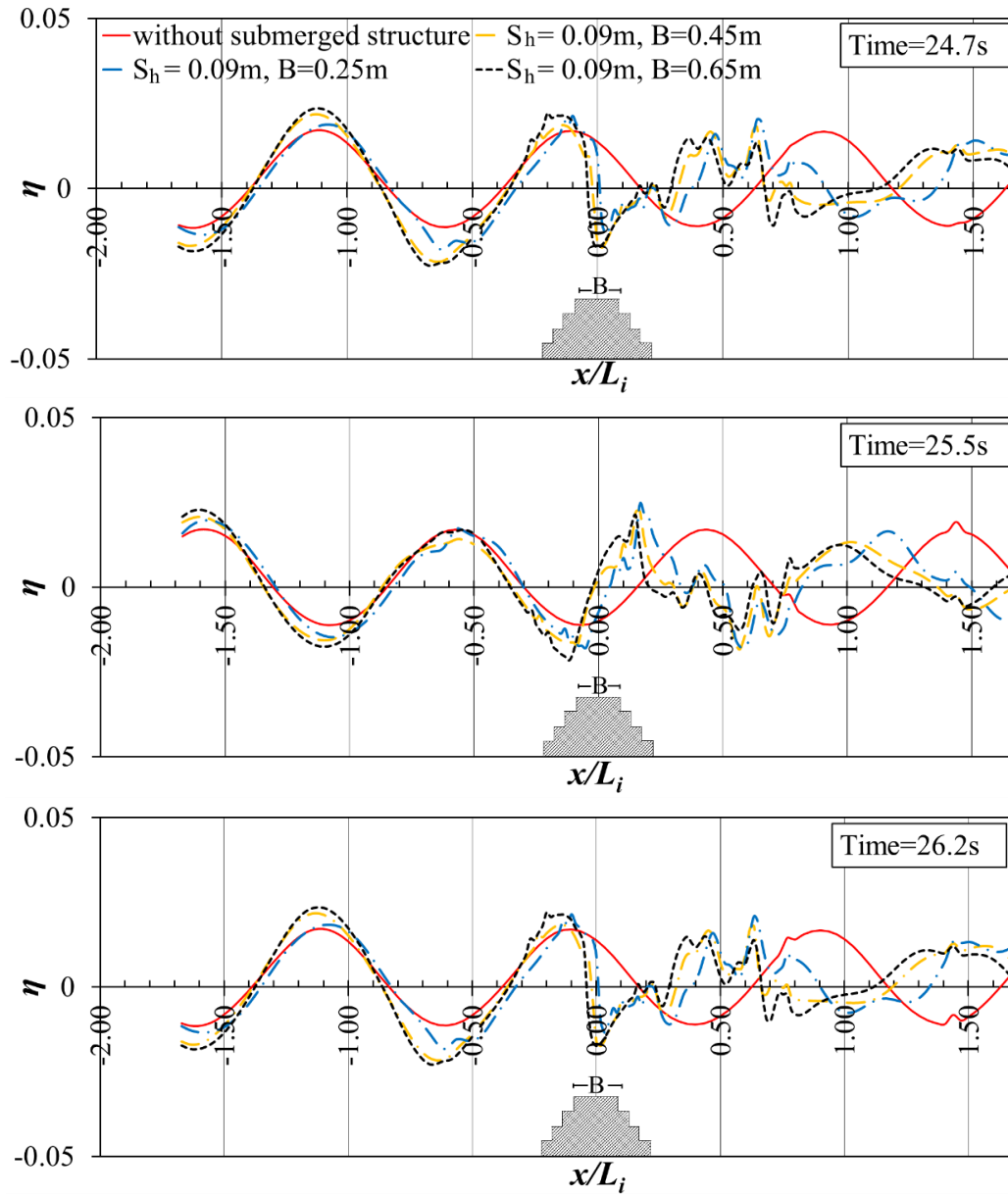
Figure A1.3. Comparison of the instantaneous profiles of water surface elevation on the different crest widths of a macro rough slope (S_h=0.09m) in case of T=1.5s and H_i=0.03m
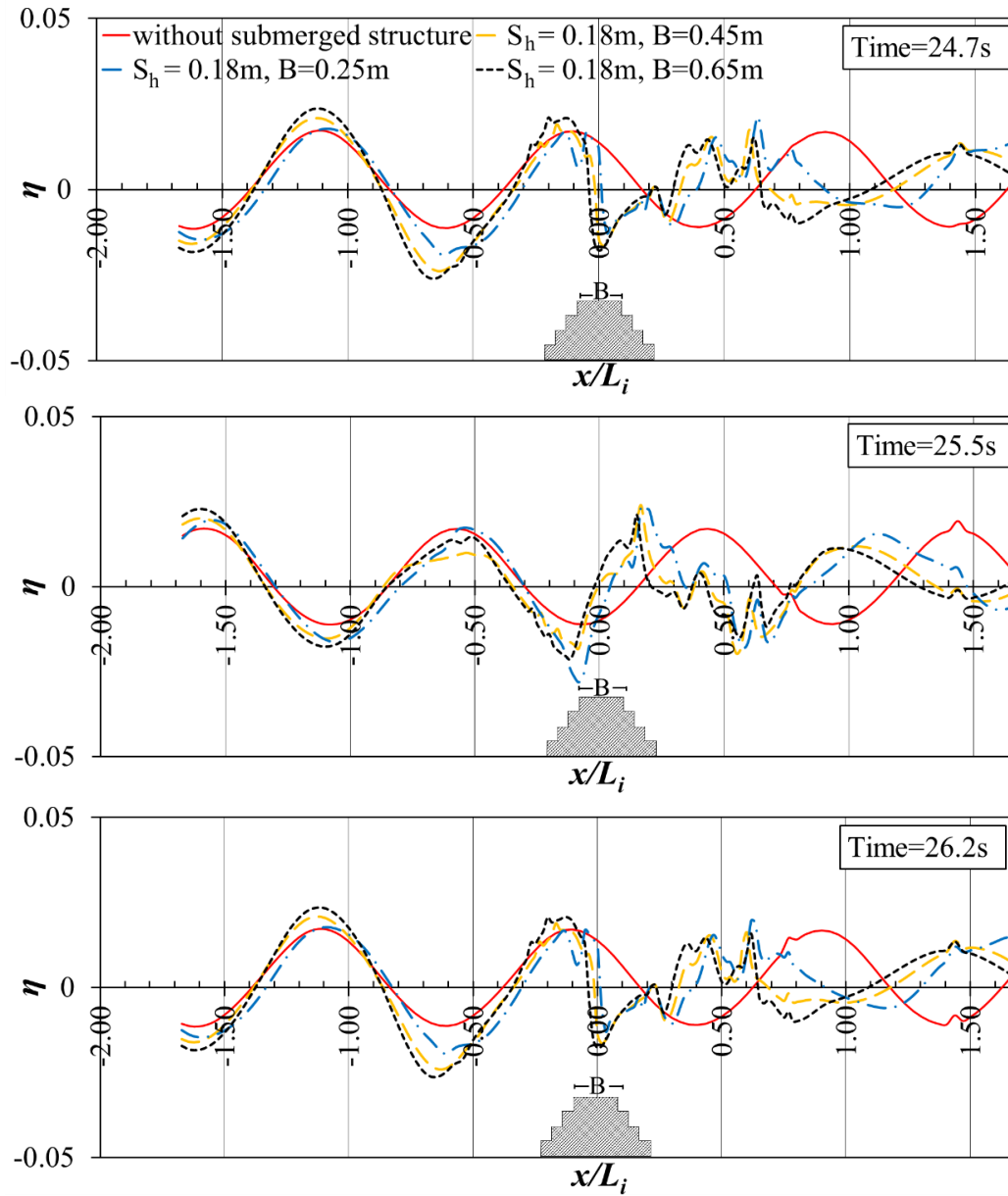
Figure A1.4. Comparison of the instantaneous profiles of water surface elevation on the different crest widths of a composite slope (S_h=0.18m) in case of T=1.5s and H_i=0.03m
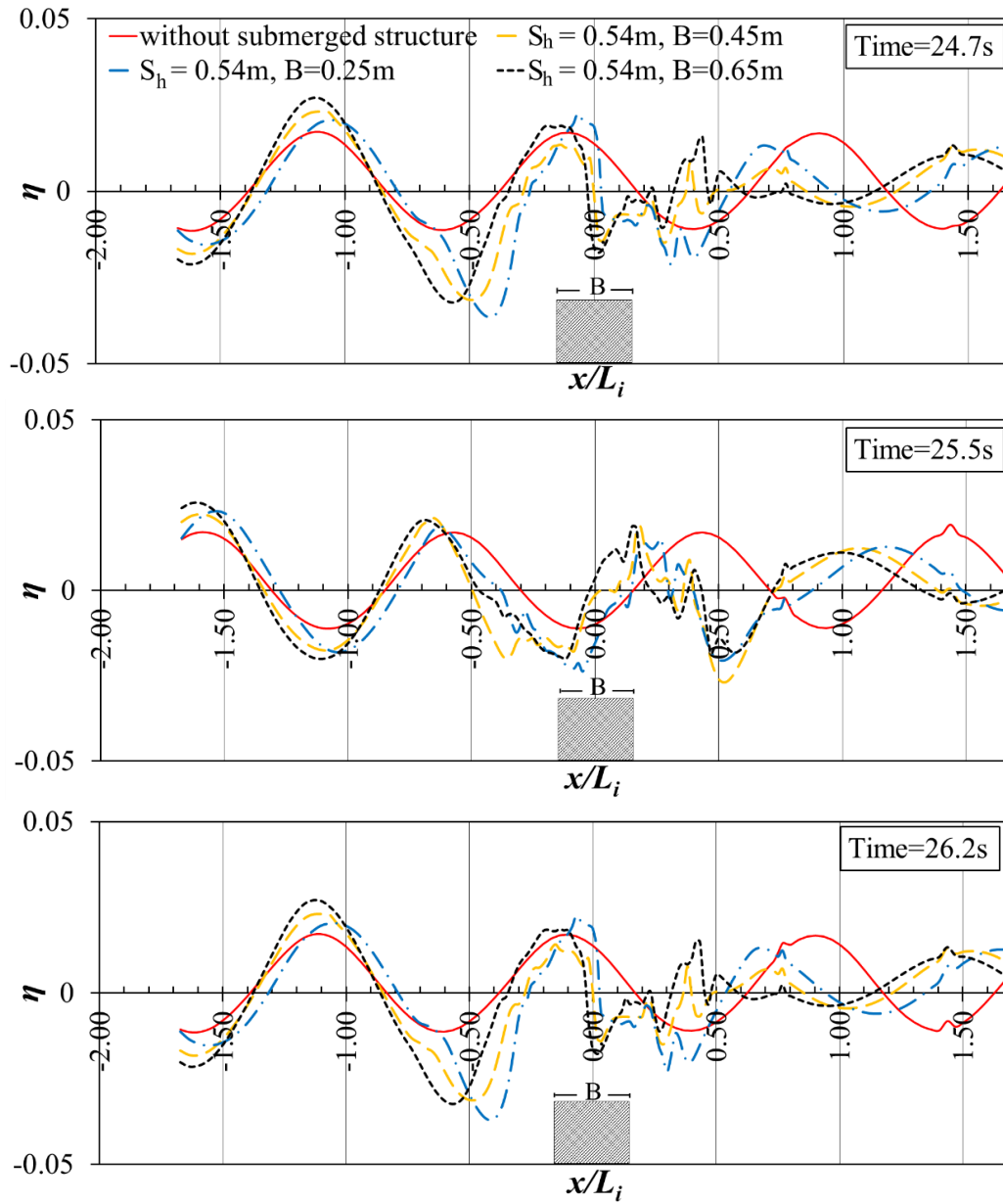
Figure A1.5. Comparison of the instantaneous profiles of water surface elevation on the different crest widths of a vertical shape (S_h=0.54m) in case of T=1.5s and H_i=0.03m

Figure A2.1. Comparison of the instantaneous profiles of water surface elevation on the different crest widths of a smooth slope (S_h=0m) in case of T=2s and H_i=0.03m
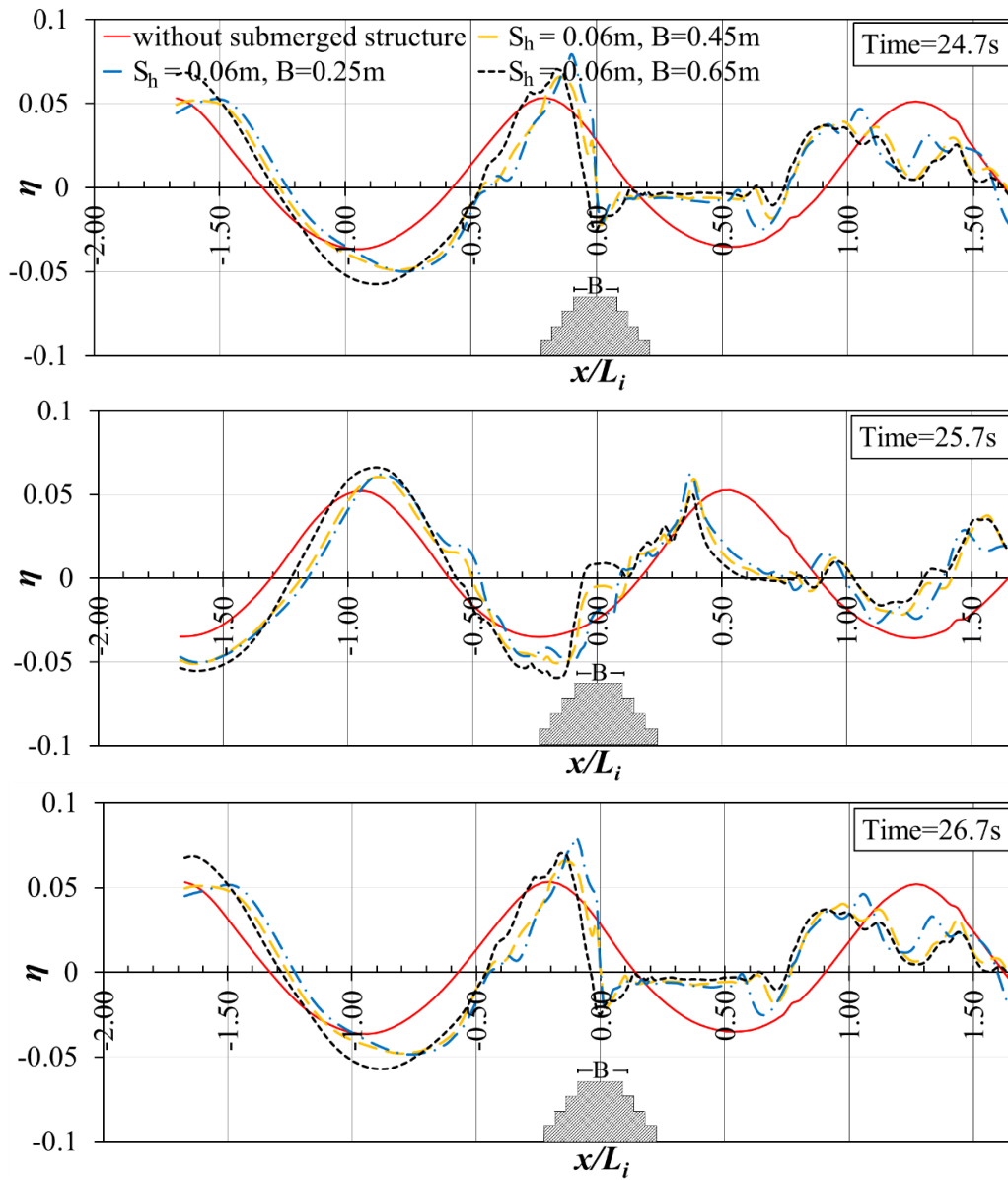
Figure A2.2. Comparison of the instantaneous profiles of water surface elevation on the different crest widths of a micro rough slope (S_h=0.06m) in case of T=2s and H_i=0.03m
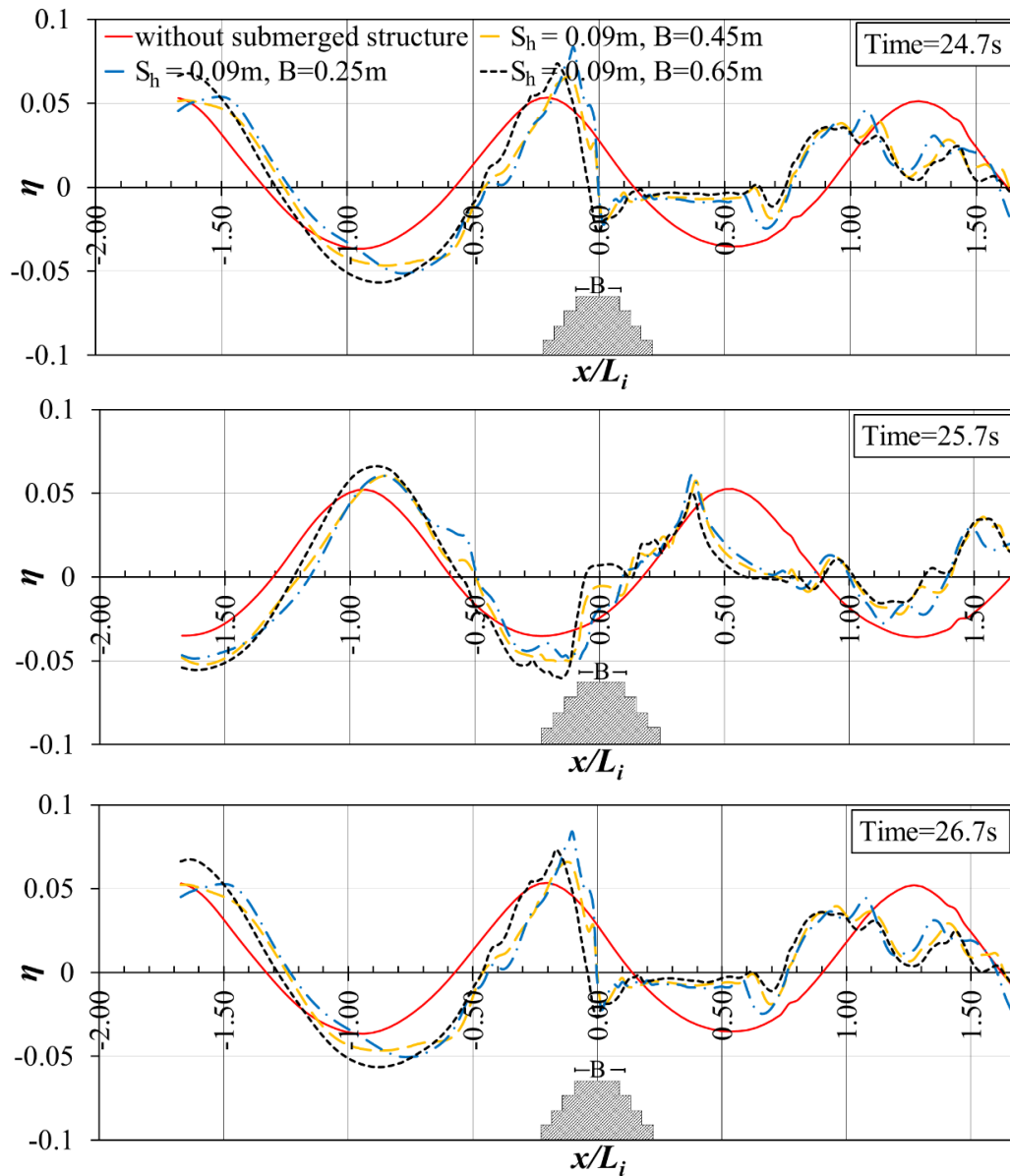
Figure A2.3. Comparison of the instantaneous profiles of water surface elevation on the different crest widths of a macro rough slope (S_h=0.09m) in case of T=2s and H_i=0.03m
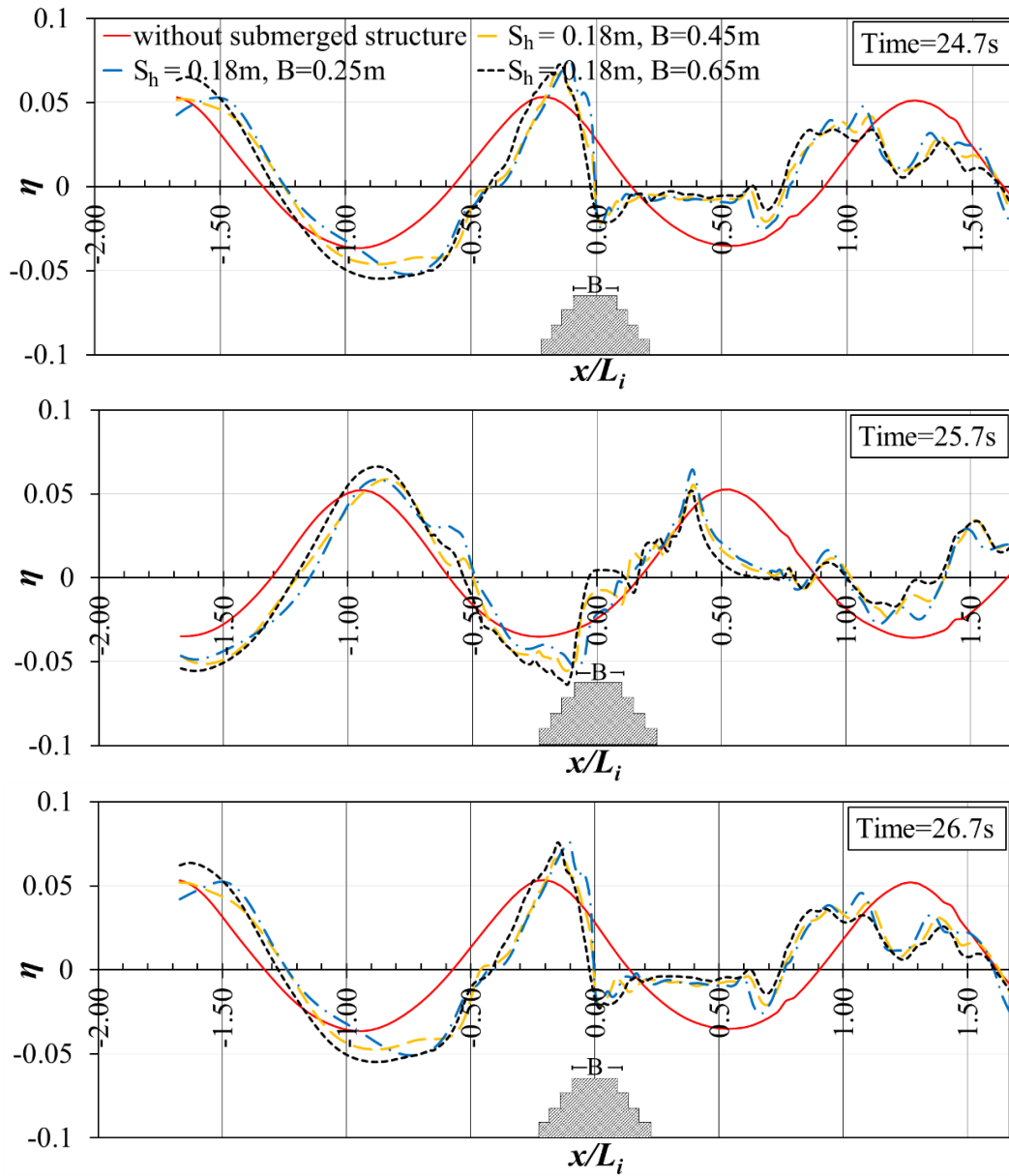
Figure A2.4. Comparison of the instantaneous profiles of water surface elevation on the different crest widths of a composite slope (S_h=0.18m) in case of T=2s and H_i=0.03m

Figure A2.5. Comparison of the instantaneous profiles of water surface elevation on the different crest widths of a vertical shape (S_h=0.54m) in case of T=2s and H_i=0.03m

Appendix B

Appendix B shows the samples of the evolutions of turbulent kinetic energy (k) over submerged breakwaters in the case of $T=1.5$s of wave period, $H_i=0.09$m of wave height and $d_s/d=0.325$ of the submergence ratio. The snapshots were captured for one cycle of wave period, which are illustrated in the following diagrams.

Figure B.1a. The evolution of turbulent kinetic energy over a smooth slope breakwater ($S_h=0$m) in case of $B=0.25$m
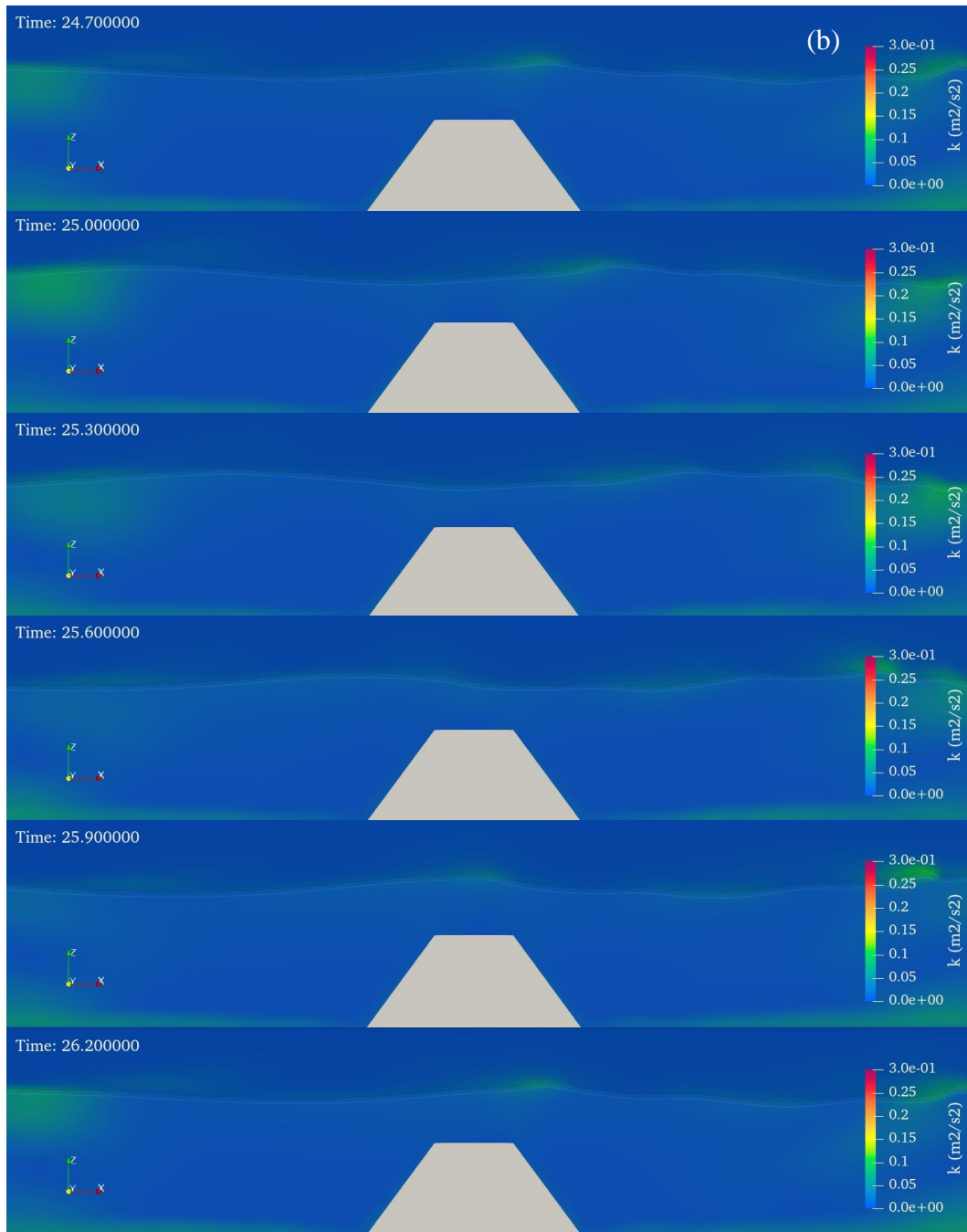
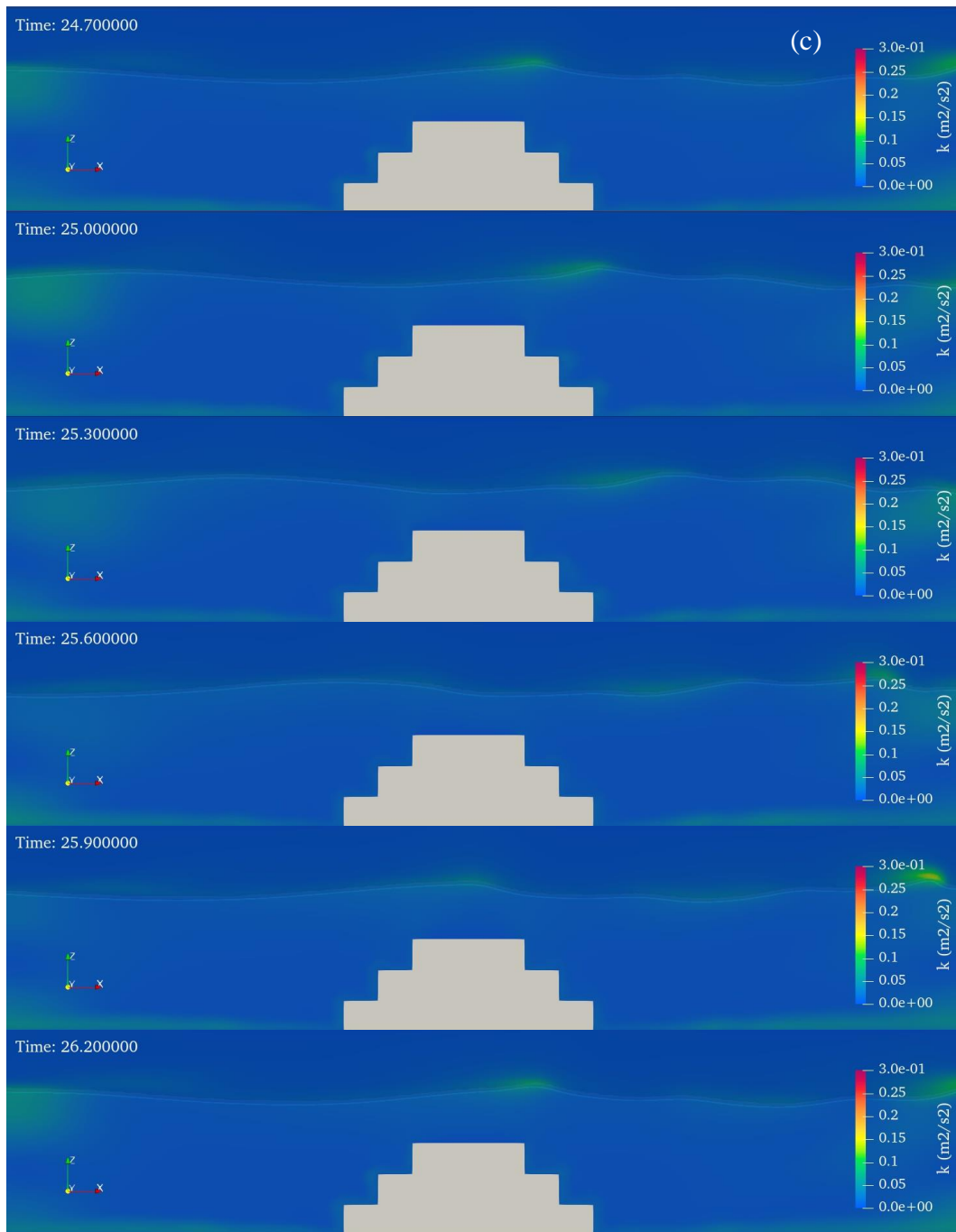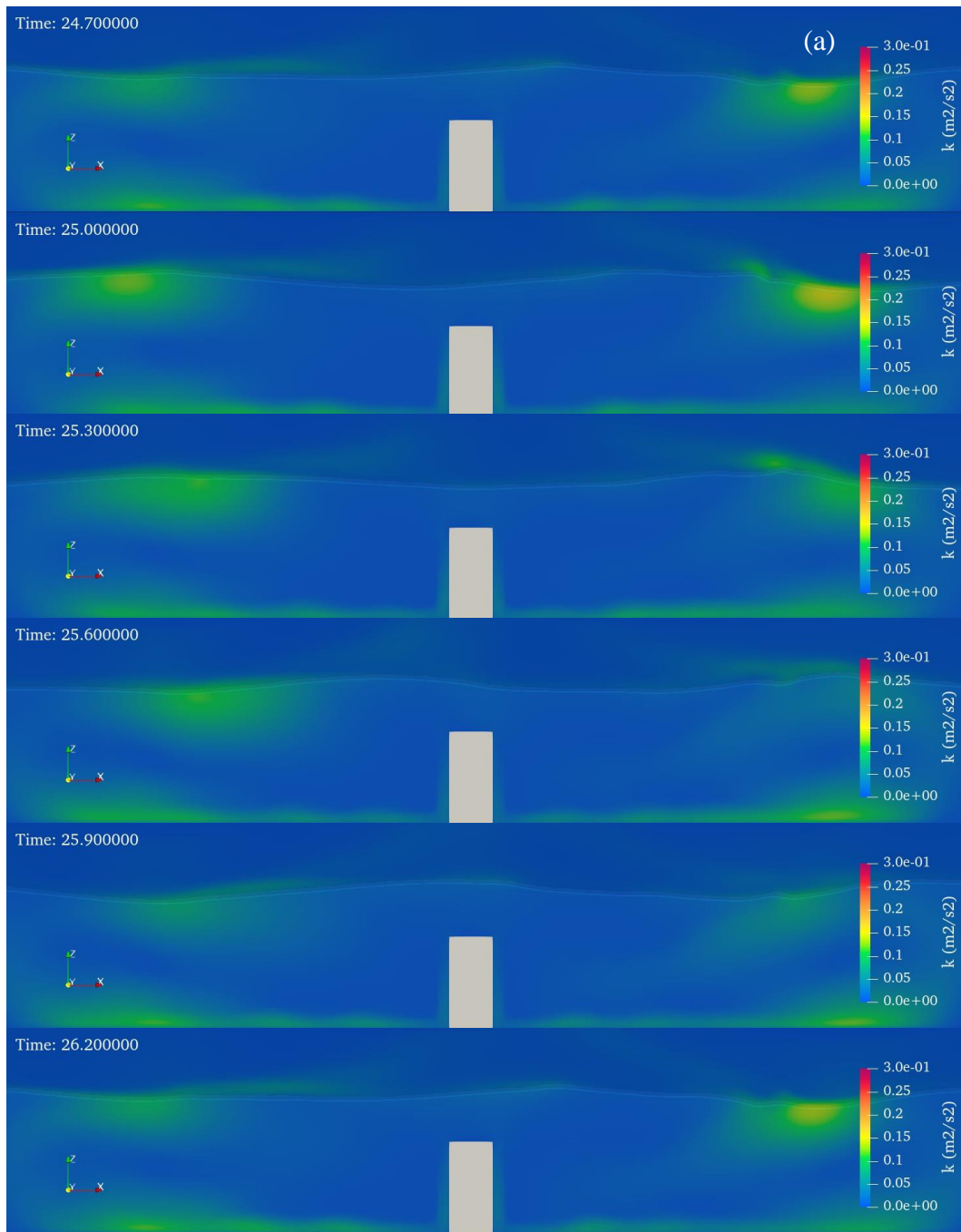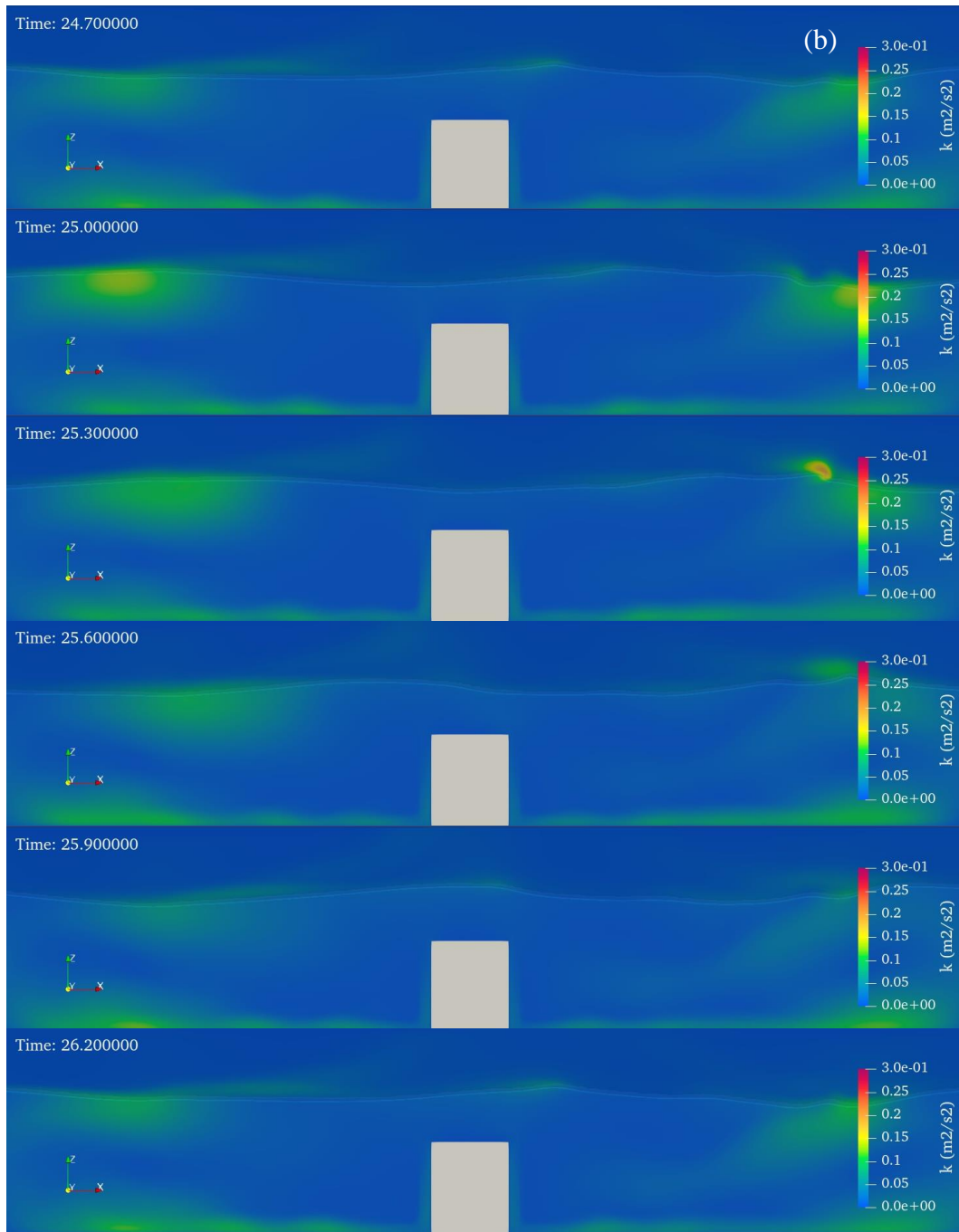Figure B.1b. The evolution of turbulent kinetic energy over a smooth slope breakwater
(S_h=0m) in case of B=0.45m
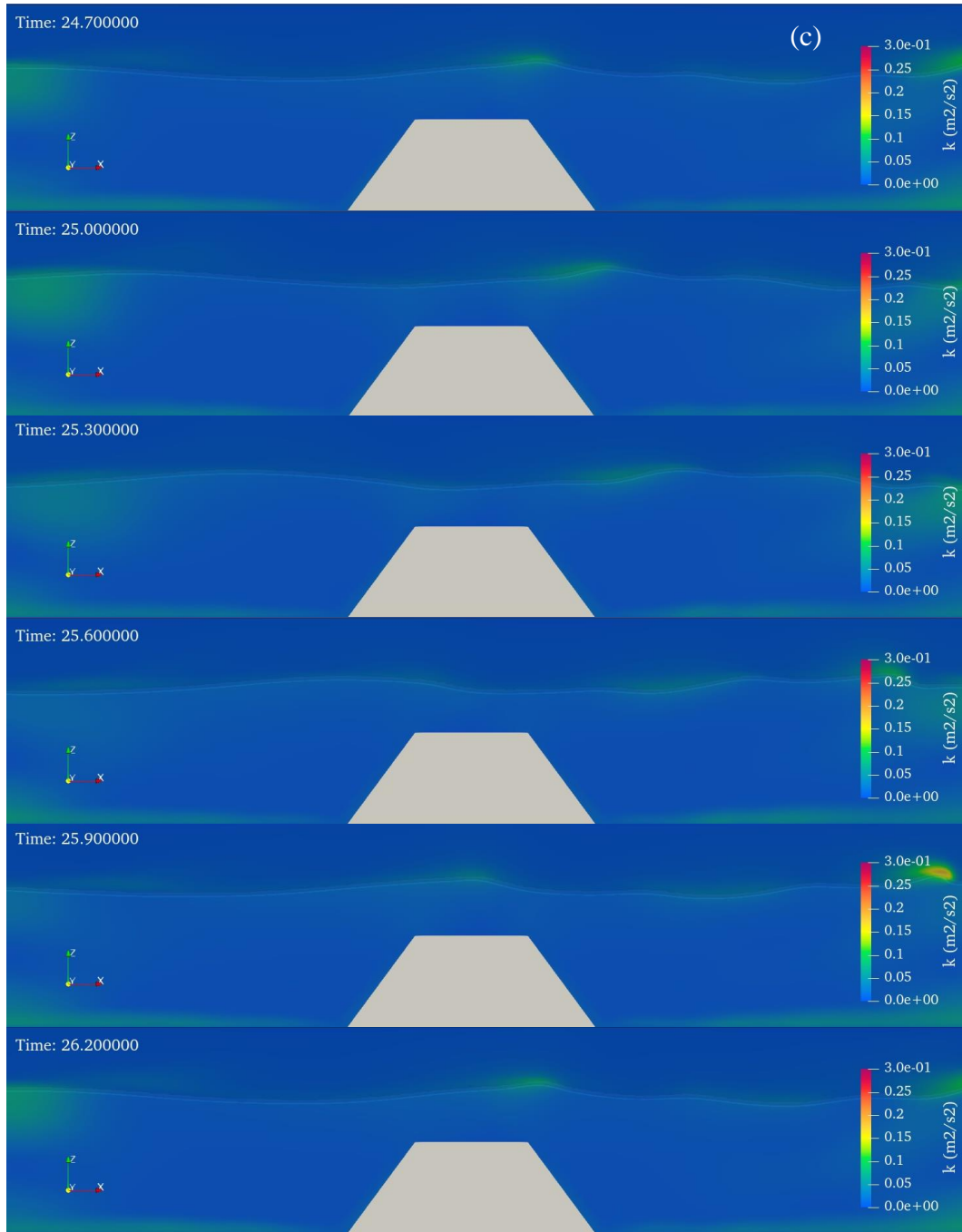
Figure B.1c. The evolution of turbulent kinetic energy over a smooth slope breakwater (S_h=0m) in case of B=0.65m

Figure B.2a. The evolution of turbulent kinetic energy over a micro rough slope breakwater (S_h=0.06m) in case of B=0.25m
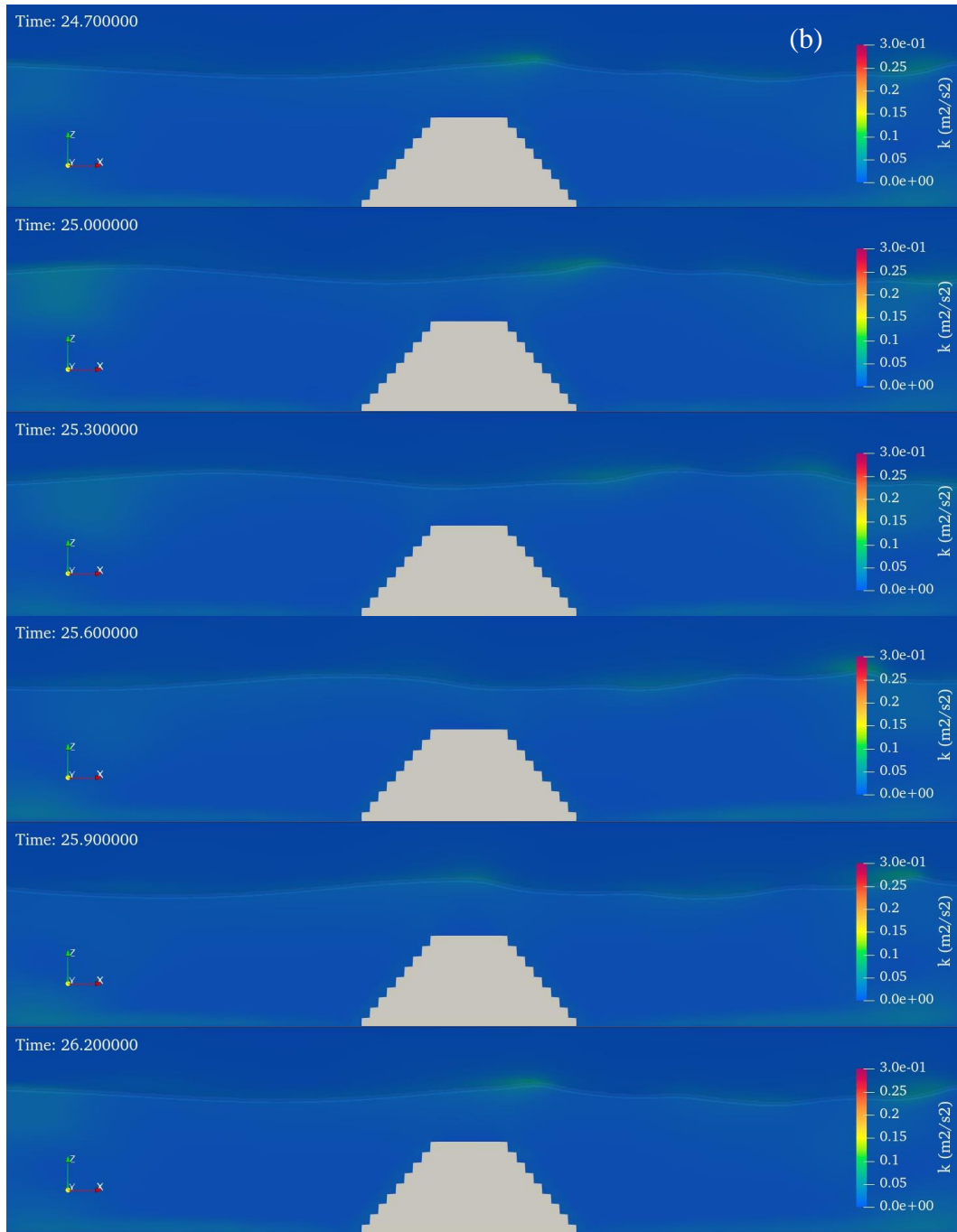
Figure B.2b. The evolution of turbulent kinetic energy over a micro rough slope breakwater (S_h=0.06m) in case of B=0.45m
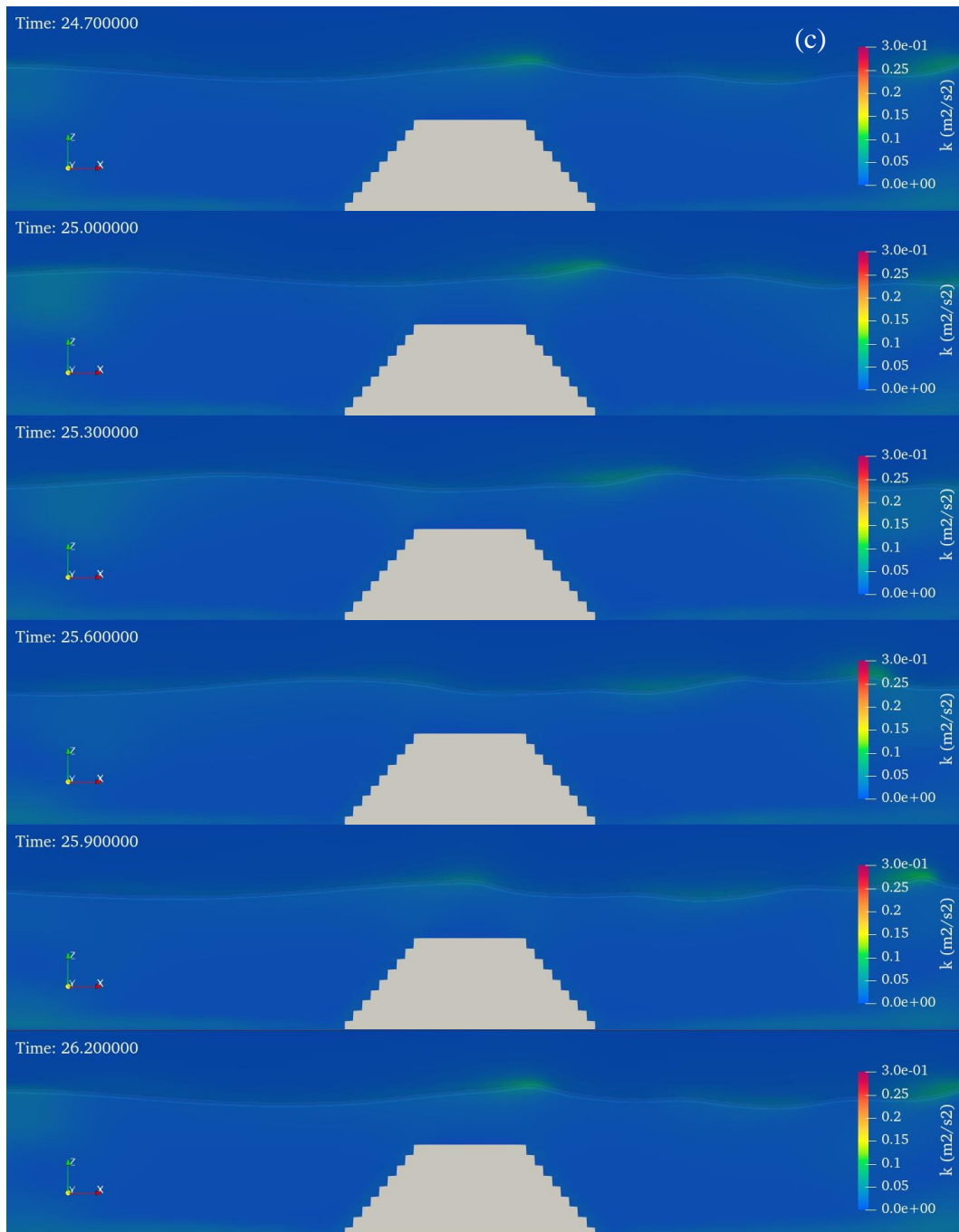
Figure B.2c. The evolution of turbulent kinetic energy over a micro rough slope breakwater (S_h=0.06m) in case of B=0.65m

Figure B.3a. The evolution of turbulent kinetic energy over a macro rough slope breakwater (S_h=0.09m) in case of B=0.25m
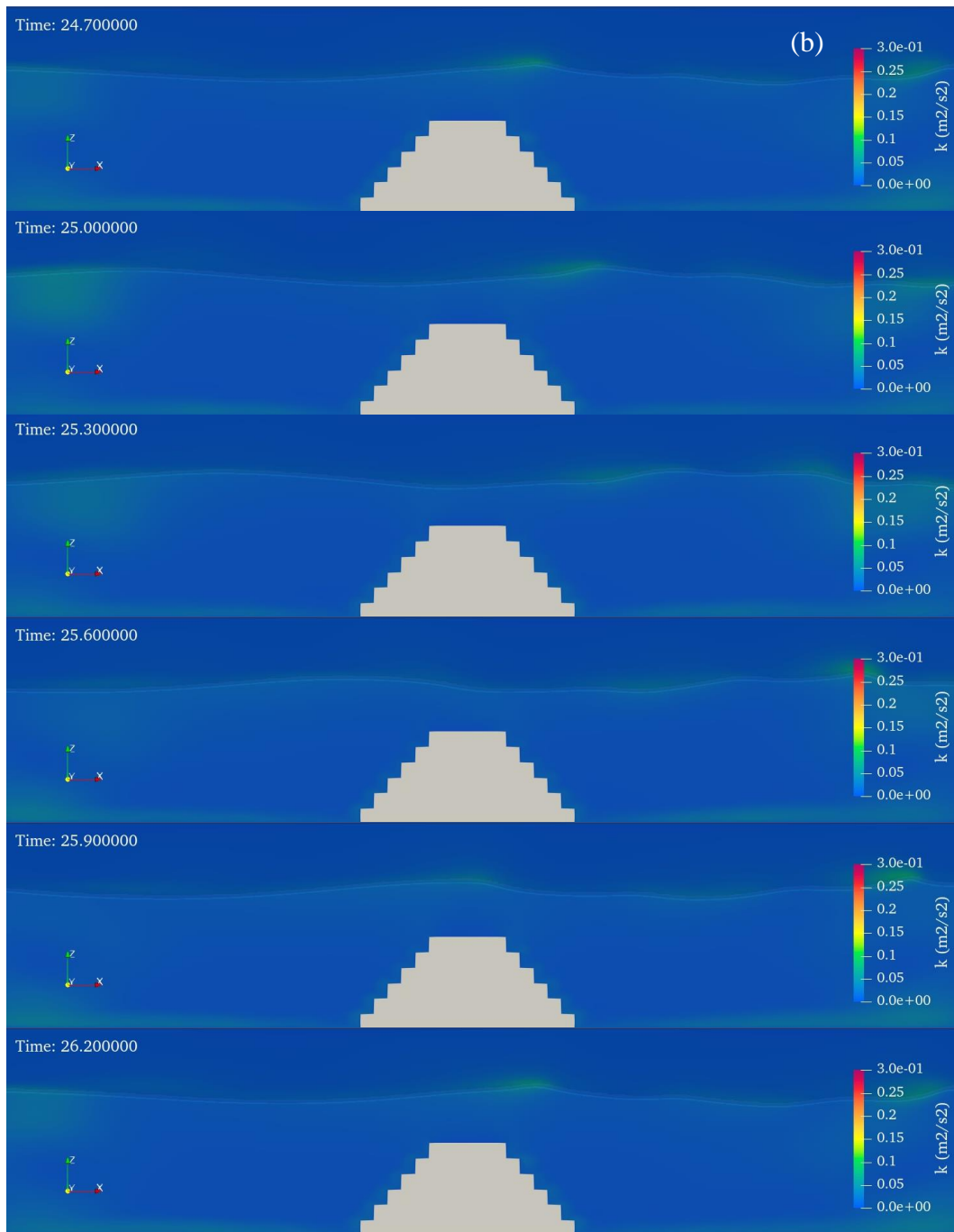
Figure B.3b. The evolution of turbulent kinetic energy over a macro rough slope breakwater (S_h=0.09m) in case of B=0.45m
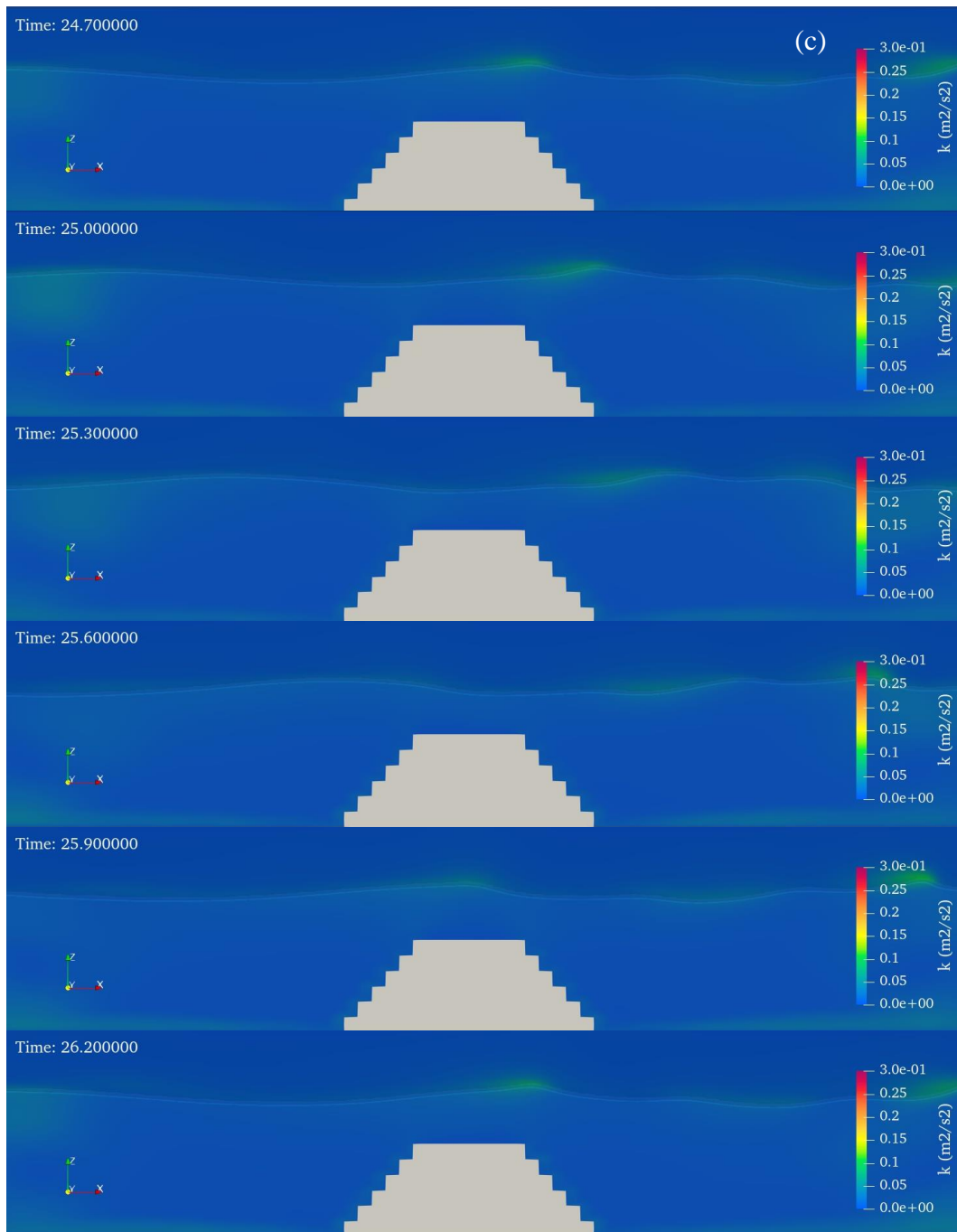
Figure B.3c. The evolution of turbulent kinetic energy over a macro rough slope breakwater (S_h=0.09m) in case of B=0.65m
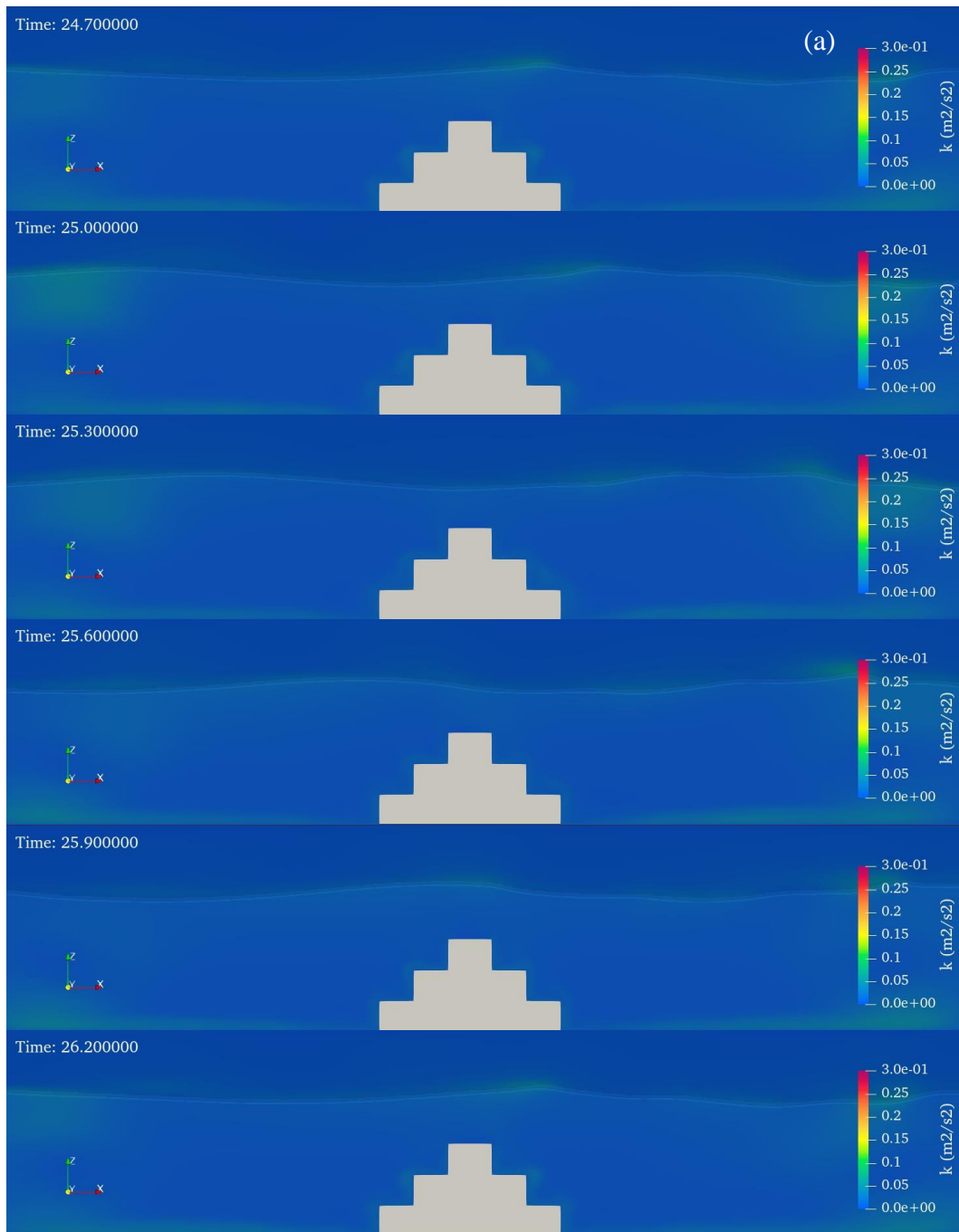
Figure B.4a. The evolution of turbulent kinetic energy over a composite slope breakwater (S_h=0.18m) in case of B=0.25m
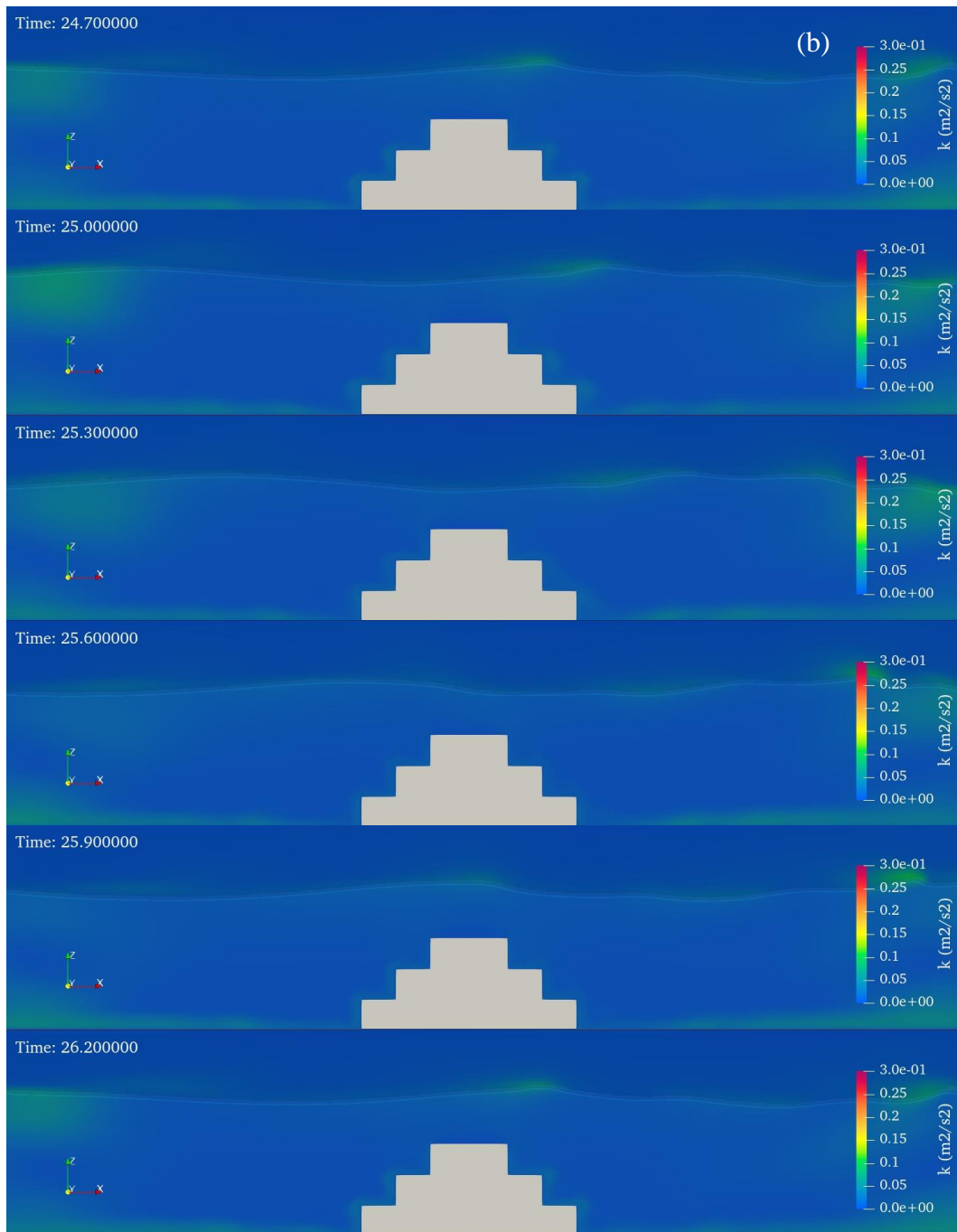
Figure B.4b. The evolution of turbulent kinetic energy over a composite slope breakwater (S_h=0.18m) in case of B=0.45m

Figure B.4c. The evolution of turbulent kinetic energy over a composite slope breakwater (S_h=0.18m) in case of B=0.65m

Figure B.5a. The evolution of turbulent kinetic energy over a vertical breakwater (S_h=0.54m) in case of *B*=0.25m

Figure B.5b. The evolution of turbulent kinetic energy over a vertical breakwater (S_h=0.54m) in case of B=0.45m
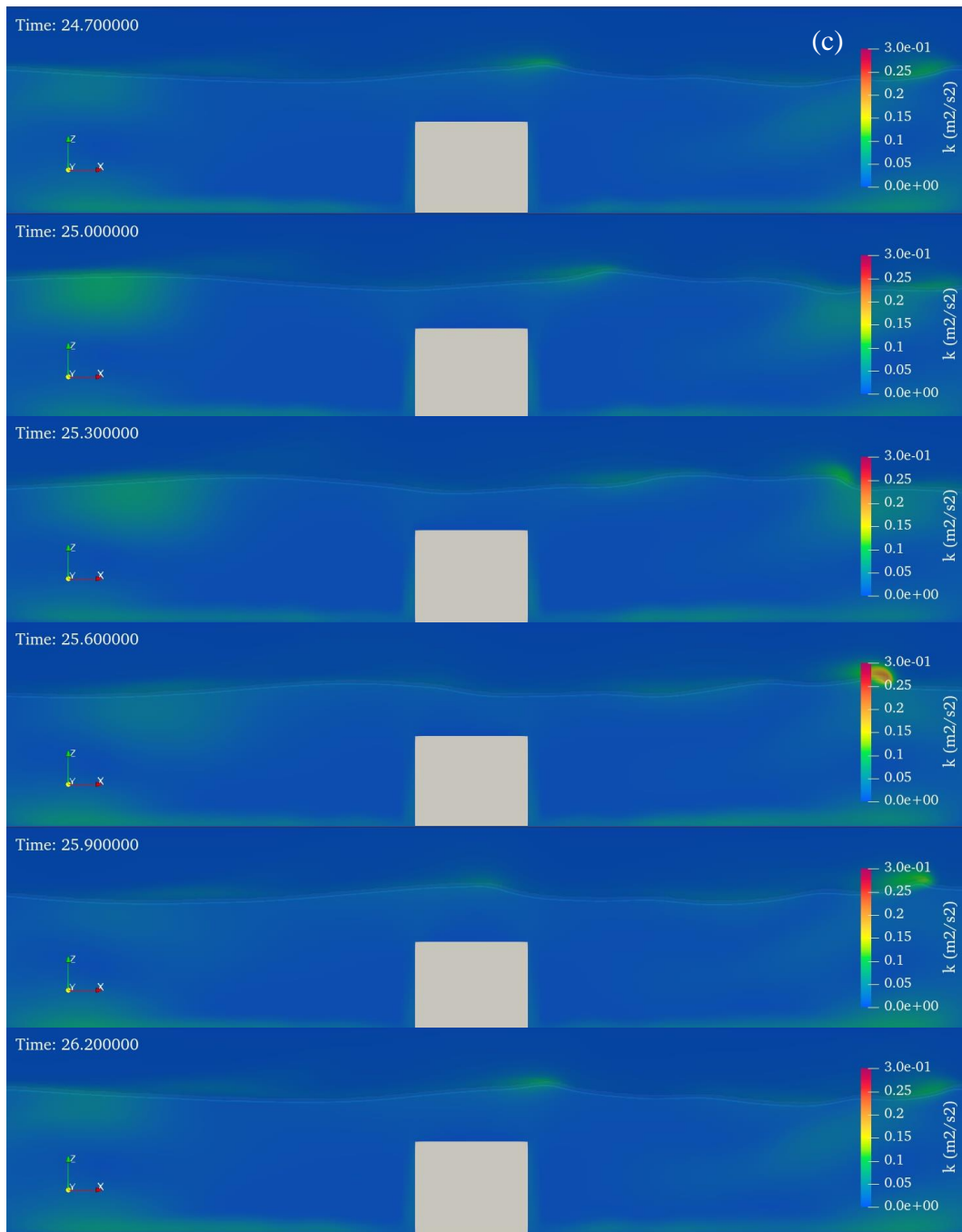
Figure B.5c. The evolution of turbulent kinetic energy over a vertical breakwater (S_h=0.54m) in case of B=0.65m

Appendix C

Appendix C shows the evolution of wave interaction with submerged breakwaters in the case of $T=1.5$s of wave period, $H_i=0.09$m of wave heights and $d_s/d=0.1$ of submergence ratio

C1. Seaward side
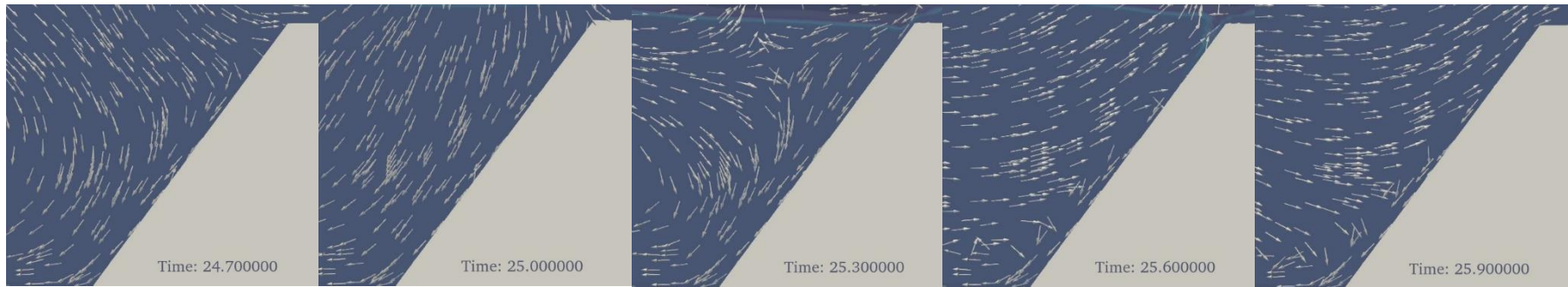
Figure C1.1. The evolution of fluid motion on a smooth slope ($S_h=0$m) breakwater at seaward side
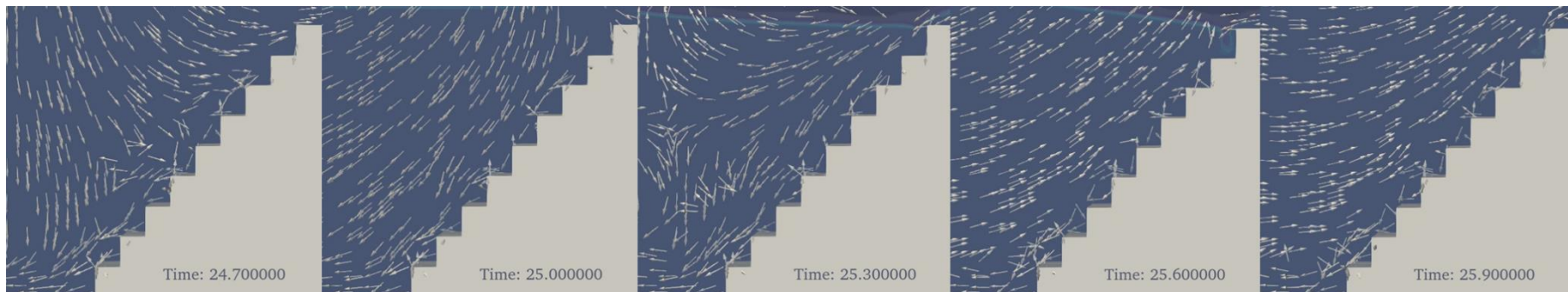
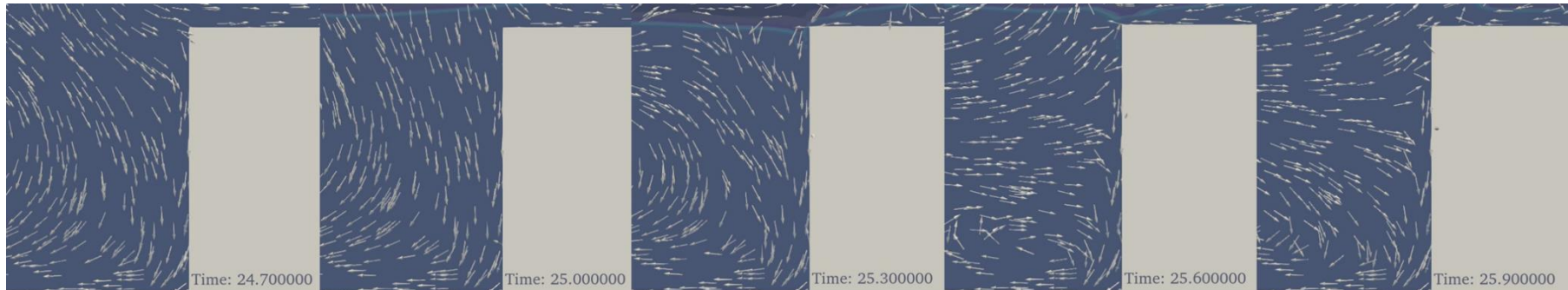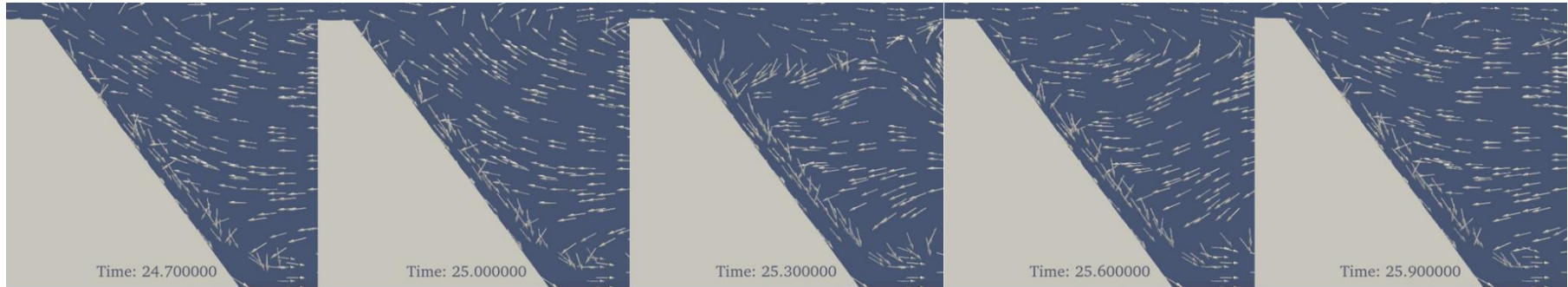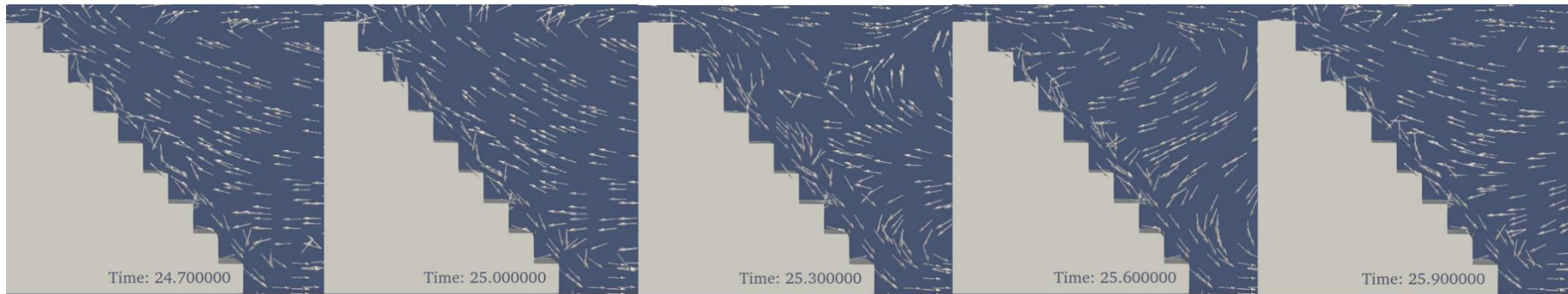Figure C1.2. The evolution of fluid motion on a micro rough slope ($S_h=0.06$m) breakwater at seaward side
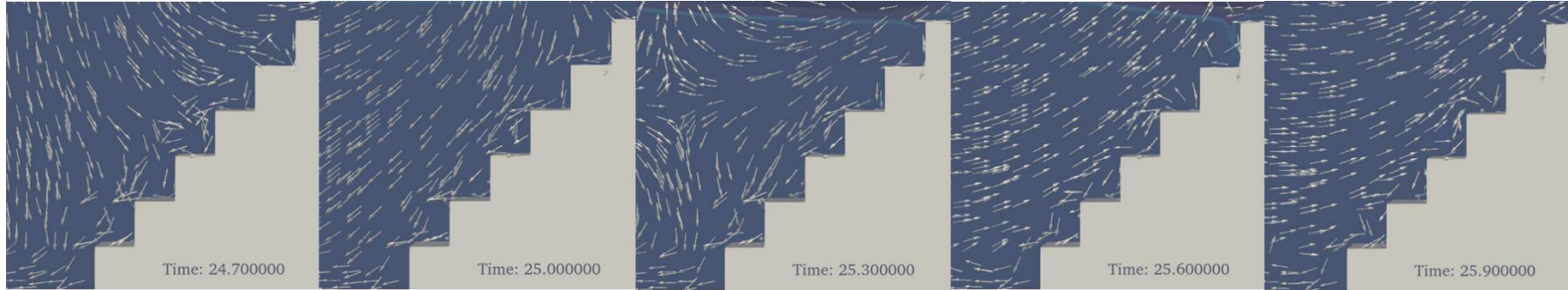
Figure C1.3. The evolution of fluid motion on a macro rough slope (S_h=0.09m) breakwater at seaward side
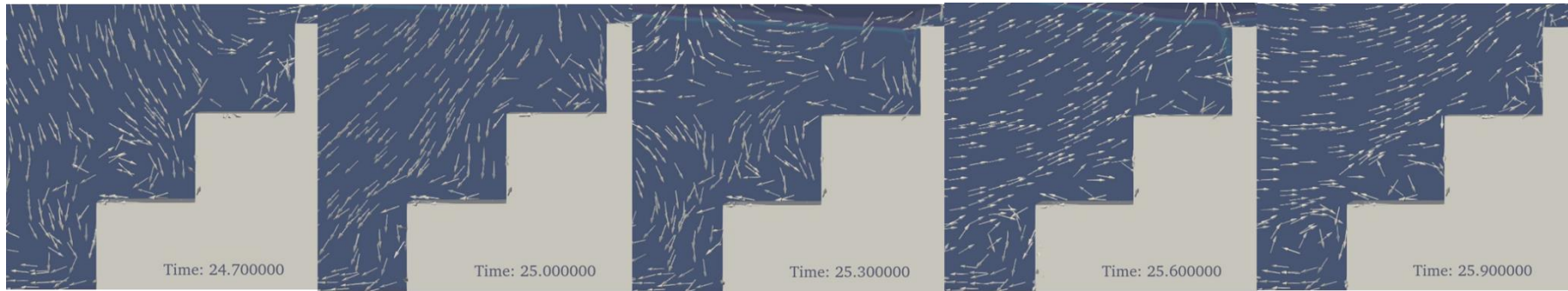
Figure C1.4. The evolution of fluid motion on a composite slope (S_h=0.18m) breakwater at seaward side

Figure C1.5. The evolution of fluid motion on a vertical (S_h=0.54m) breakwater at seaward side

173

Figure C2.1. The evolution of fluid motion on a smooth slope (S_h=0m) breakwater at landward side

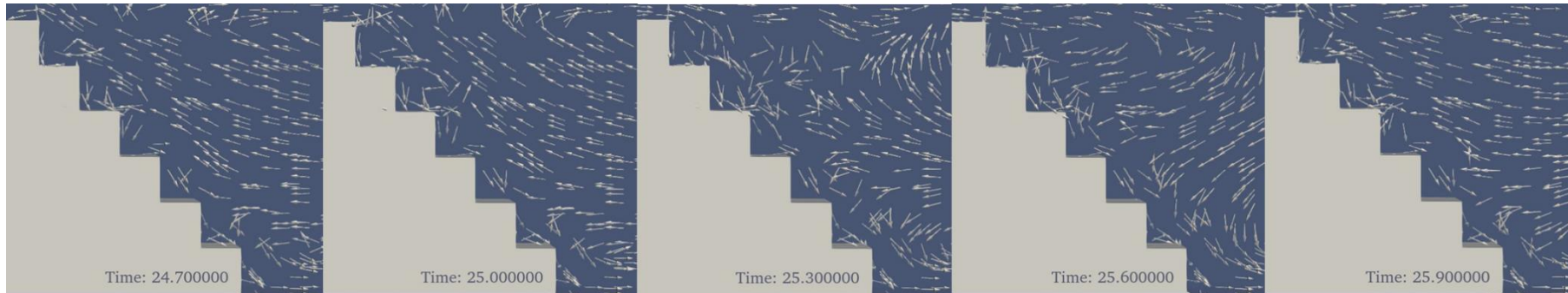Figure C2.2. The evolution of fluid motion on a micro rough slope (S_h=0.06m) breakwater at landward side

Figure C2.3. The evolution of fluid motion on a macro rough slope (S_h=0.09m) breakwater at landward side

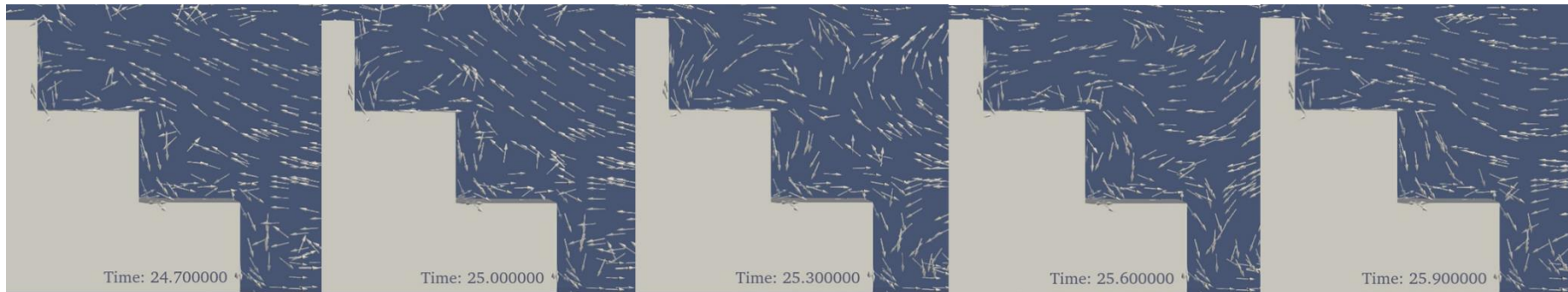

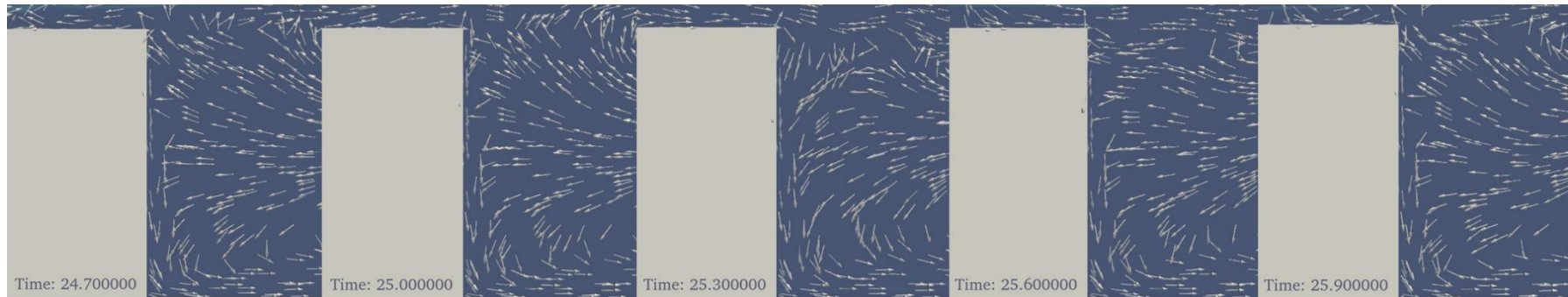Figure C2.4. The evolution of fluid motion on a composite slope (S_h=0.18m) breakwater at landward side

Figure C2.5. The evolution of fluid motion on a vertical (S_h=0.54m) breakwater at landward side

175